The dynamical properties of the cell cycle control network

Calin-Mihai Dragoi
Trinity College
University of Oxford

A thesis submitted for the degree of
D.Phil.

January 2025

Abstract

The eukaryotic cell cycle is the physiological process by which cells divide and proliferate. Normally, it consists of four phases (G1, S, G2 and M) necessary for carrying out DNA replication, chromosome segregation and division. Under special circumstances, cells bypass some of the canonical phases, giving rise to endocycles, which drive a diversity of developmental processes, such as growth, multi-nucleation, or germ cell generation. Despite ample characterisation of cell cycle biochemistry, the mechanistic requirements for endocycle emergence remain poorly understood. To address this knowledge gap, the work presented here proposes a mechanistic model of the mammalian cell cycle control network which predicts the emergence of endoreplication and mitotic endocycles (Cdc20 endocycles) following molecular perturbations. These predictions are verified experimentally.

Using a control systems approach and analytical tools from the field of nonlinear dynamics, I show that the cell cycle can be framed as a complex oscillatory system, analogous to mechanical devices, such as “Newton’s cradle” or a “Wheel of fortune”, to explain endocycles. Such minimal models explain the organisational principles of the cell cycle in terms of hierarchies of dynamical control motifs. This approach provides general, broadly applicable frameworks, which can guide the experimental dissection of cell cycle regulation, regardless of the model organism choice. Further, the frameworks presented herein provide a scaffold for building tailored mechanistic models for specific organisms and cell types.

Acknowledgements

I am grateful to my supervisor, Prof. Bela Novak who has provided so much invaluable support over the past five years, helping me develop my scientific ideas and teaching me all the technical skills that went into producing this thesis.

I would like to thank Dr. Alexis Barr and her group, for their eagerness to test our hypotheses experimentally and their consistent reliability. I equally appreciate the opportunity they have given me to contribute to some of the exciting projects they have been working on.

I am also thankful to Prof. John Tyson, whose expert advice has so much improved our joint papers.

I thank Prof. Ulrike Gruneberg and Prof. Omer Dushek, who have provided much useful feedback on my research and how to present it.

I extend my thanks to Trinity College for the “Elizabeth Murphy” Scholarship, which has provided the financial support to carry out this research.

I am grateful to Oriel college, which has been my academic home for 4 terms, for having given me the chance to teach their brilliant Biochemistry undergraduate students, and for the many friends I have made in the SCR.

I thank Miles Pattenden for encouragement, many interesting discussions and proofreading several chapters.

I am thankful to my parents for supporting me unconditionally and for motivating me.

Table of Contents

List of Abbreviations

Cyclin-Dependent Kinases (CDKs)

Abbreviation	Full Name	Function
CDK1	Cyclin-Dependent Kinase 1 (Cdc2 in fission yeast, Cdc28 in budding yeast)	Mitotic entry (G2/M transition)
CDK2	Cyclin-Dependent Kinase 2	G1/S transition and S-phase progression
CDK4	Cyclin-Dependent Kinase 4	Regulates G1 phase with cyclin D
CDK6	Cyclin-Dependent Kinase 6	Similar to CDK4, controls G1 phase

Cyclins

Abbreviation	Full Name	Function
CycA	Cyclin A	Regulates both S-phase and mitosis (partners with CDK2 and CDK1)
CycB	Cyclin B	Controls mitotic entry (partners with CDK1)
CycD	Cyclin D	Controls G1 phase (partners with CDK4/6)
CycE	Cyclin E	Drives G1/S transition (partners with CDK2)

Ubiquitin Ligases

Abbreviation	Full Name	Function
SCF	Skp, Cullin, F-box Complex	Ubiquitin ligase that targets G1/S regulators for degradation
CRL4	Cullin-RING Ligase	Ubiquitin ligase family involved in protein degradation
APC/C	Anaphase-Promoting Complex/Cyclosome	Ubiquitin ligase that degrades mitotic cyclins and securin
Cdc20	Cell Division Cycle 20	APC/C activator at mitotic exit
Cdh1	Cdc20 Homolog 1	APC/C activator in G1 phase

Mitotic Checkpoint Regulators

Abbreviation	Full Name	Function

Mad1	Mitotic Arrest Deficient 1	Spindle assembly checkpoint component
Mad2	Mitotic Arrest Deficient 2	Inhibits Cdc20 to delay anaphase
Bub1	Budding Uninhibited by Benzimidazoles 1	Spindle assembly checkpoint kinase
BubR1	Bub-related 1 (Bub1b)	Ensures proper kinetochore-microtubule attachment
Bub3	Budding Uninhibited by Benzimidazoles 3	Checkpoint protein that binds BubR1

Cell Cycle Inhibitors (CDK Inhibitors - CKIs)

Abbreviation	Full Name	Function
Rb	Retinoblastoma Protein	Suppresses E2F to prevent premature S-phase entry
p16	Cyclin-Dependent Kinase Inhibitor 2A (CDKN2A)	Inhibits CDK4/6 to prevent G1 progression
p21	Cyclin-Dependent Kinase Inhibitor 1 (CDKN1A)	Universal CDK inhibitor, regulated by p53
p27	Cyclin-Dependent Kinase Inhibitor 1B (CDKN1B)	Inhibits CDK2 to regulate G1 length

Mitotic Regulators

Abbreviation	Full Name	Function
Wee1	Wee1 Protein Kinase	Inhibits CDK1 to control mitotic entry
Myt1	Membrane-associated tyrosine/threonine 1 kinase	CDK1 inhibitor similar to Wee1
Cdc25	Cell Division Cycle 25 Phosphatase	Removes inhibitory phosphorylation on CDK1
Plk1	Polo-like Kinase 1	Regulates mitotic progression and spindle assembly
Aurora A	Aurora Kinase A	Centrosome maturation and mitotic spindle assembly
Aurora B	Aurora Kinase B	Spindle-chromosome attachment sensing
CENP-A	Centromere Protein A	Histone H3 variant in centromeres

DNA Damage Response Regulators

Abbreviation	Full Name	Function
ATM	Ataxia Telangiectasia Mutated Kinase	Responds to DNA double-strand breaks
ATR	Ataxia Telangiectasia and Rad3 Related Kinase	Responds to single-strand DNA

Chk1	Checkpoint Kinase 1	Pauses cell cycle in response to DNA damage
Chk2	Checkpoint Kinase 2	Works with ATM to mediate DNA repair
53BP1	p53 Binding Protein 1	Regulates double-strand break repair
MRE11	MRE11 Homolog	Part of MRN complex (doudble strand break detection)
RAD50	Radiation sensitive 50	Component of the MRN complex
NBS1	Nijmegen Breakage Syndrome 1	Component of the MRN complex
RPA	Replication Protein A	Binds single-stranded DNA to prevent degradation
ATRIP	ATR-Interacting Protein	ATR recruitment and activation
RAD9	Radiation sensitive 9	Component of the 9-1-1 complex for DNA damage sensing
HUS1	Hydroxyurea sensitive 1	Part of the 9-1-1 complex, recruited to damage sites
RAD1	Radiation sensitive 1	Third component of the 9-1-1 DNA damage checkpoint complex

DNA Replication & Licensing Factors

Abbreviation	Full Name	Function
MCM	Minichromosome Maintenance Complex	Helicase required for DNA replication
ORC	Origin Recognition Complex	DNA replication initiation complex
Cdc6	Cell Division Cycle 6	Licensing factor for replication origins
Cdt1	Chromatin Licensing and DNA Replication Factor 1	Essential for loading MCM helicase
Geminin	Geminin DNA Replication Inhibitor	Inhibits licensing to prevent re-replication
Pol α	DNA Polymerase Alpha	Initiates DNA replication by synthesizing primers
Pol δ	DNA Polymerase Delta	Synthesizes the lagging strand during replication
Pol ε	DNA Polymerase Epsilon	Synthesizes the leading strand during replication
PCNA	Proliferating Cell Nuclear Antigen	Sliding clamp for DNA polymerases
CDC45	Cell Division Cycle 45	Essential for helicase activation

GINS	GINS Complex	Essential for DNA helicase activity during replication
CDC7	Cell Division Cycle 7	Kinase that phosphorylates MCM for replication initiation
DBF4	DBF4 Regulatory Subunit	Activates CDC7 kinase for replication firing
Sld2/3/7	Synthetic Lethal with Dpb11	DNA replication firing factors
TopBP1	Topoisomerase II Binding Protein 1	Facilitates replication origin activation
GINS	Go-Ichi-Ni-San Complex	Essential for CMG helicase activation during replication
MCM10	Minichromosome Maintenance Protein 10	Stabilizes MCM helicase complex

Transcription Factors in Cell Cycle Control

Abbreviation	Full Name	Function
E2F	E2 promoter-binding Factor	Regulates expression of S-phase genes
FoxM1	Forkhead Box Protein M1	Regulates G2/M transition and mitotic progression
B-MYB	B-Myeloblastosis Oncogene	Regulates G2/M transition and mitotic progression
MuvB	Multi-vulval class B	Transcriptional coregulator – forms a complex with FoxM1 and B-Myb to regulate CycB transcription
c-Myc	Myelocytomatosis	Regulates cell cycle entry and proliferation

Preface

This thesis aims to develop an understanding of the organisation of cell cycle events through the means of mathematical modelling. Here, I hope to position the work of the chapters that follow within a broader modelling landscape, explain where my approach differs from the common practice, the challenges it addresses, and why it is legitimate by referring to examples from the history of the physical and biological sciences. In broad terms, a model is a mental construction resting on a number of statements about the laws of nature, assumed to be true. Subsequently, through logical deduction, the outcome of an experiment can be either predicted or explained to an arbitrary level of accuracy. Models vary widely in their aims, form and construction. They can be as simple as intuitively understood conditional or probabilistic statements (e.g. "if an object is released from a hight it will drop to the ground and it might brake"). Models may also take the form of verbal descriptions of phenomena, highlighting cause and effect relations. In their most complex form, models prescribe some formalism for encoding objects in the real world and their relations, as well as a well-defined algorithm for computing some outcome that might follow from the natural evolution of the system or its perturbation.

Given this great diversity of models, some criteria by which to categorise models ought to be introduced in order to appropriately circumscribe the nature and purpose of the work presented in the subsequent chapters. For the purposes of the current argument, I analyse models from the perspective of two dichotomies: predictive/explanatory and abstract/concrete.

Explanatory and predictive models

I distinguish explanatory and predictive models based on the extent to which the aim of the model is to identify causal forces that underpin a phenomenon. A chiefly predictive model is not necessarily concerned with the causes of phenomena – simple correlations may suffice. In other words, the relation between a system's inputs and outputs need not be mediated by mechanistic assumptions – empirical links may be enough (e.g. in the

choice of a regression function). Such models play important roles in epidemiology, for instance. A physiological explanation for why saturated fat consumption increases the risk of developing coronary heart disease may be lacking, but observing a correlation may warrant introducing new public health advice. In contrast, explanatory models aim to determine the causes of phenomena/experimental observations. The two approaches can be delimited methodologically: purely empirical connections are sufficient for making predictions (be they poor), whereas there is no empirical methodology for determining causality. All one can hope to record in an experiment, or more generally *a posteriori*, is strictly speaking a series of events that follow each other in time. Thus, experience alone may establish correlations between phenomena. Causality, on the other hand, is inferred when a mental model can be generated to explain why a particular set of outcomes will *necessarily* follow a given event*. Thus, explanations involve a certain level of fact interpretation, of introducing some subjective assumptions about the way nature works, whereas predictions, understood in the narrow frequentist statistical sense can dispense with that.

Distinguishing between explanatory and predictive aims as the two opposite ends of a spectrum appears as a misguided approach. No doubt, any good model provides both accurate predictions and satisfying explanations for why specific outcomes occur. A model that makes predictions without identifying appropriate causal forces is only accurate by chance and in limited contexts. A model that proposes an explanation without making correct predictions is just wrong. Despite this, it is rare that an investigative approach can reach both goals simultaneously without a great deal of effort. Historically, both approaches have had legitimate contributions to scientific development and were indeed necessary steps towards the emergence of successful theories.

An interesting example of chiefly predictive models is encountered in ancient astronomy. The best-known model is that of Claudius Ptolemy, which provided predictions of the

* This can be a particular outcome in a deterministic system, or a probability distribution in a truly stochastic system (e.g. in quantum mechanics)

positions of astronomical bodies, the dates of eclipses and other events. Although this model is not entirely free of mechanistic assumptions, unlike earlier ones, which merely identified approximate arithmetic rules for determining the dates of relevant events, these assumptions were not primarily under the remit of the astronomer. The common assumption that the Earth lies at the centre of the universe and the planets move along concentric circular orbits was a dogma imposed by ancient philosophers. The astronomers worked within the constraints of these assumption, which are not altogether unreasonable, as from a terrestrial perspective, the planets, moon, sun and stars do superficially appear to orbit the Earth. Nevertheless, when the principles of Euclidean geometry are applied to calculate the trajectory of planets based on these assumptions, little agreement with observation can be found, because the assumptions are, of course, wrong. One of the most striking inconsistencies is that of retrograde motion (the apparent temporary change of a planet's direction of movement), which is characteristic for a number of planets, the most notable of which is Mercury. Clearly, such behaviour cannot be accounted for through uniform circular motion around the Earth. Instead, to account for this, it was proposed that the planet also moves on the circumference of a second circle of smaller radius, termed *epicycle*, independently of the main orbit around the Earth, termed *deferent*. However, even with this adjustment, the predictions of the model were still poor. Satisfying solutions were only found after the introduction of multiple tiers of epicycles or other devices. In essence, this approach bears resemblance to that of series expansions in empirical model fitting, and it is a paradigmatic example of a type of scientific practice with important practical applications that is employed in the absence of a suitable explanatory framework.

The counterpoint to this approach is that of the Copernican revolution. Copernicus' revolutionary idea of the heliocentric universe was spurred by the exceedingly complicated computational algorithm of the Ptolemaic system. Copernicus noticed that a great deal of complexity can be done away with if it is assumed that all planets, including the Earth, orbited the sun. Nevertheless, clear evidence that the model yielded better predictions was not forthcoming for several decades. Despite this, the new perspective gained traction because it appeared to yield better insight into organisation of the Solar System. Following the careful measurements of Tycho Brahe, it became

apparent that only the predictions made for some of the planets were indeed more accurate relative to those of Ptolemy[1]. In addition, the slight predictive improvement over the other planets was likely thanks to the availability of better astronomical measurements and of a better fitting procedure. Further, the Copernican system did not do away with epicycles either, which remained necessary due to the incorrect assumption of circular, rather than elliptical, orbits. The conclusion is that the value of Copernicus' work lay in providing a more satisfying (or 'aesthetically pleasing') explanation for the causes of the observed planetary motion, until Kepler produced a model that was strong from the perspective of both explanation and prediction.

There is an additional sense in which explanatory models contribute to scientific development. In order to design and interpret an experiment, a conceptual framework of how the system is organised is necessary for its rational interrogation. A complex biological or physical system can be dissected experimentally in so many ways as to be impractical to test in a reasonable time frame. Therefore, some preconceived idea of how the system operates is necessary to limit the number of experiments to be performed to a practicable extent and to enable the interpretation of findings in terms of causes and effects. A paradigmatic example of how exploratory models have led to scientific advancement is in the development of atomic structure understanding.

Modern atomic theory started with Dalton's postulate that matter is composed of *indivisible* units, whose mass determines their chemical identity. The idea of atom indivisibility was challenged in 1897 by J.J. Thomson[2] whose experiments on cathode rays showed that they consisted of negatively charged particles (electrons), which were thousands of times less massive than the hydrogen atom[3]. This discovery opened the way for the study of subatomic structure and gave rise to an iterative process of model development and experimentation. Thomson's first proposal was the plum pudding model of the atom, where the positive charge is dispersed over a large volume, while smaller negative charges are scattered throughout[4]. This model was disproved in 1909 by Geiger and Marsden, under the guidance of Rutherford, who showed that, when fired against a thin gold sheet, α particles are scattered in a manner that is inconsistent with Thomson's model[5]. While it was expected that virtually all particles would experience a

very small angle deflection, a small but significant proportion were scattered at an angle greater than 90 degrees. Subsequently, Rutherford proposed that the positive charge of the atom is condensed in a nucleus that is confined to a small volume of the overall atom[6]. Thus, the pattern of α particle scattering would be explained by the (improbable) collision with a gold atom's positive nucleus. Despite being a significant advancement, this model again failed to explain some atomic properties, such as absorption and emission spectra, or to propose a stable configuration of the charges within the atom. Some of these issues were addressed by Bohr's 'planetary' model of the atom, which incorporated Planck's ideas about the quantisation of emission spectra[7]. As with early modern astronomy, models that were both explanatory and predictive of atomic properties emerged only after decades of research, with Schrodinger's description of electrons as wavefunctions.

This example illustrates the value of speculative models in the development of scientific theories even when these models fail to account for all known properties of a system under study and are quickly discounted in favour of more complex models which make more accurate predictions. Together with the example from astronomy, this validates the idea that during the early stages of scientific theory development, models tend to be either predictive or exploratory. An additional conclusion of this argument is that although on the short-term predictive models can have important practical applications, they tend to be supplanted by theoretical descriptions which aim to identify the 'internal logic' of a process or system by proposing the necessary and sufficient conditions that underpin phenomena. This approach is the more enduring one on the long term and the one I choose to take throughout this thesis.

Although producing models that both predict and explain natural phenomena is the goal of the scientific practice, no theory or model has reached finality, in the sense that no further improvement in explanatory or predictive power can be made. This is especially true in the context of cellular physiology. This is largely because biological systems are characterised by a very high degree of complexity: many components, unknown interactions, non-linearity and feedback. While the cell cycle regulatory pathways have been extensively dissected biochemically and genetically, many high-level cell cycle

properties remain poorly explained. Consequently, the experimental exploration of cell cycle regulation that is not guided by the appropriate explanatory models is akin to groping in the dark. In this case, the appropriate level of precision can only be reached by resorting to mathematical descriptions and computations. The unaided intuition fails to account for minutiae of the systems under study. As such, the work herein aims to explore the behaviour of the cell cycle in response to various perturbations, from a dynamical lens, to propose conceptual frameworks that may aid the further dissection of this system from a systems level perspective. The methods available for this and their limitations are discussed in the next section.

Abstract and concrete models

Concrete models encode directly measurable physical quantities, such as mass, charge, position, volume. In contrast, abstract models operate with derivative concepts, which may not have a directly measurable physical equivalent, but from which some observable quantity or qualitative effect may be computed. One example is that of the wavefunction in quantum mechanics. In molecular systems biology, concrete models describing the quantities and interactions of molecules predominate overwhelmingly and are seen as the gold standard approach. The justification for this is that these models can be correlated to experiments directly and unequivocally, and thus they are ideally suited to making and testing predictions. This approach can simultaneously offer a wealth of theoretical insight, balancing out both predictive and explanatory aspects. In contrast, in abstract models, a knowledge gap may exist between experimental findings and model construction. For this reason, it is occasionally difficult to establish whether the agreement between predictions and experimental findings is simply accidental. For instance, it has been previously argued that Physarum polycephalum can be induced to anticipate periodic changes in their environment thanks to the existence of a large number of incoherent oscillators with different natural frequency, which can be synchronised by some external forcing[8]. Although this is a thought-provoking idea, it is difficult to imagine what the chemical nature of these many oscillators is. Although a few chemical oscillators have been characterised in Physarum[9], the natural frequency of

biochemical oscillators tends to be restricted to a narrow range, imposed by fixed kinetic constants, rather than the wide range presupposed by the model. Therefore, it is difficult to see how such a model could be implemented mechanistically. This example speaks to a more general view that abstraction in biological sciences is often an inconvenience stemming from a lack of proper physiological understanding.

And yet, the concrete route to molecular modelling is not without challenges. Although the contributing factors are complex, they boil down to the idea that the gap between biochemistry and physiological function is often very large. This means that linking biochemical causes to phenotypic effects through a series of necessary and sufficient mechanistic steps is a remarkably difficult task, for which no universally successful algorithm is available.

The objections to biochemical reductionism

In cell biology, the prevailing assumption for nearly a century has been that biological properties are best explained with reference to molecular processes. This approach has been unquestionably fruitful in uncovering fundamental biological principles, including the central dogma of molecular biology[10], gene regulation in bacteria[11] and a remarkably vast array of metabolic pathways. In each of these cases, structural and biochemical analysis coupled with in vitro reconstitution have led to virtually complete mechanistic explanations of the phenomena under question. Following such success, biochemists have attempted to dissect, catalogue and analyse every cellular process at molecular level. And yet, for many biological processes, explaining how phenotypes emerge from biochemical interactions is not at all straightforward. For instance, developmental biology appears as collections of case studies, rather than as a fully systematic theory. There is no sense yet in which one can meaningfully reconstruct embryogenesis either *in vitro* or *in silico*, despite ample characterisation of the molecular players[12].

This suggests that either the molecular processes underpinning development are not known in sufficient detail, or that development is not appropriately reduced to the

molecular level and should instead be explained with reference to a higher organisational level. Although the former is no doubt true, in this section I will argue for the latter position in the broader cell biology context. Compiling increasingly complex molecular details under one model becomes intractable from an explanatory perspective. Thus, exploring the latter hypothesis might lead to more fruitful approaches in understanding cell biology. Consider how metabolism is not explained at quantum mechanical level (with very few exceptions, e.g. electron transfer in some redox reactions[13]), but rather with reference to organic chemistry in its conventional understanding. To pursue a similar line of inquiry, in this section I investigate why reducing complex cellular pathways to their constituent molecular components may fail to provide appropriate insight into the emergence of physiological properties.

One of the primary methodological issues with biochemical reductionism is the fact there is no one-to-one relationship between genes (understood in molecular terms) and functions. On the one hand, various degrees of redundancy exist between many genes in higher eukaryotes. These genes often have overlapping, but not identical, functions, such that knocking out one or more isoforms in one context can have different effects from knocking out the same gene(s) in a different context. In addition, different genes may carry out multiple different roles, occasionally within different pathways[14]. One textbook example is that of cytochrome c, which plays distinct roles in the electron transport chain and apoptosis, and potentially in other pathways[15]. In cell cycle context, the p27 CKI has a canonical role in inhibiting CDK2 and CDK1, but it also aids the formation of active CDK4:CycD complexes[16]. This gives rise to pleiotropy, which makes disentangling a protein from its phenotypic effect challenging, as the relationship between genes and functions is many-to-many. In other words, biochemical reduction may be difficult to implement as an explanatory device, insofar as determining causal relations in cell biology is concerned.

A further problem with biochemical reductionism has to do with the high degree of pathway and parameter uncertainty. It is practically impossible to determine the constants that characterise a vast array of biochemical reactions, especially with great accuracy. Even assuming that elementary reactions could be accurately assayed *in vitro*,

it is nevertheless difficult to determine whether or not the measured parameters apply to the same reactions in vivo, because additional, possibly unknown, regulatory processes may affect the parameter of interest. Even effects as simple as the local substrate concentration and chemical environment may affect the biological outcome. In addition, the lack of pathway conservation may confound results. This does not exclusively apply to comparisons of the same biological processes in different model organisms; it is also a problem with comparing results between different cell lines originating from the same species, as different tissues will express different ratios of isoforms or other regulators. Indeed, even cell culturing methodology or circadian effects may impact cell cycle progression in ways that are potentially difficult to quantify and control for.

The effect of such uncertainties may be negligible when attempting to understand elementary biochemical processes, such as the expression of one particular gene. However, the potential errors compound when considering large biochemical systems underpinning complex processes, such as the cell cycle. The large number of degrees of freedom these models must operate with imply that even if these models make accurate predictions, they may still misrepresent the underlying process in some respects. Thus, the general problem of underdetermination[17] becomes more and more pressing with highly complex pathways having many degrees of freedom. In broad terms, underdetermination is a situation that occurs when different underlying models can predict the outcome on an experiment equally well (i.e. the data goodness of fit is similar). When this happens, it is customary to select the model the uses the fewest assumptions, so as to avoid overfitting (a principle otherwise known as Occam's razor). A typical information theoretical tool that allows balancing model complexity and accuracy is the Akaike Information Criterion[18].

Such sophisticated statistical tools are not customarily used in biology. Moreover, even if they are used, model selection may still remain equivocal. Thus, the underlying model structure becomes a matter of situational judgement for the researchers. In the particular context of cell cycle modelling, it is typical to ask which of the known cell cycle regulatory interactions ought to be included in explaining some given experimental observations: should we attempt a maximalist description of the known facts, or do away

with any redundancy in the network and focus on the interactions that are likely to have the greatest contribution to the process/phenotype of interest, tacitly 'absorbing' the other variables into empirical constants and parameters that simply make the model *work*, rather than represent actual biologically meaningful values? Even if such considerations are nominally agreed upon, the mechanistic description of even relatively simple biochemical reactions can become the subject of much debate. For instance, one may consider the description of the phosphorylation kinetics of one site of a CDK substrate: should mass action or Michaelis-Menten kinetics be used? Or perhaps even more complex (but presumably more accurate)[19] reaction schemes are appropriate. Even if the quandary were somehow resolved, one could begin to consider whether competition between CDK substrates ought to be considered. Further, CDKs phosphorylate multiple sites on the same substrate and the order in which this happens (if there is a predetermined one at all), as well as the effect of each combination of phosphor-sites has on activity/function is largely unknown, even for well-studied regulators[20]. Whatever the case, such questions cannot be answered practically. In fact, the problem of underdetermination goes even deeper, because the statistical algorithms, such as the AIC, typically employed in model selection are themselves not free from bias[21].

Thus, the complexity of the biochemical networks that underpin cellular phenomena, such as signalling and proliferation, poses a very significant methodological barrier to the reduction of these processes to pathways of enzyme catalysed reactions. Nevertheless, other types of objections can be put forward to biochemical reduction as a means to explain cell biology.

The reduction of biological processes to physico-chemical phenomena may also not be warranted from an ontological perspective. One possible issue is that a varied array of biochemical mechanisms may underpin the same function. In other words, biochemical details may be dispensable for explaining higher level biological function. For instance, a negative feedback loop may underpin homeostasis just as well, regardless of whether it is implemented through a transcriptional network, protein phosphorylation, stoichiometric binding, or some other regulatory strategy. In the philosophy of science,

this many-to-one relationship between 'fundamental' and emergent phenomena is known as *multiple realisability*[22]. This property may imply that, since no *specific* biochemical mechanism is necessary for explaining a particular process, some other functional unit ought to be considered the necessary cause of the process. For instance, the function of a transcription factor may be understood as the combination of a DNA binding motif, a transcriptional activator domain, and potentially one or more coregulator binding regions. The validity of this is illustrated by the successful use of modular biochemical units in synthetic biology[23]. The exact amino acid sequence of the transcription factor, in contrast, does not uniquely determine function, because numerous amino acids can be mutated, added or deleted without a measurable effect on physiology.

This kind of description of transcription factors is practically trivial in the context of simple gene regulatory processes, such as might occur in the control of bacterial metabolic genes. However, the simplicity of this approach becomes a necessity when considering the far more complex context of gene regulation in multicellular organisms. Not only are there multiple transcription factors which fine tune the expression of specific genes, but they also synergise, compete or antagonise in complex and potentially non-linear ways[24], facilitating the computation of cellular decisions in response to vast arrays of physiological inputs. Indeed, further information is encoded in the dynamical patterns of transcription factor availability[25]. Therefore, abstracting certain properties, like the regulatory motifs in which the transcription factors are engaged, allows the investigation of biological phenomena at the conceptual level at which they emerge, rather a purely biochemical level, which, though fundamental, can be equivocal with respect to the functional level. By analogy, the meaning of words does not emerge from a juxtaposition of letters (c.f. amino acids) and so to attempt to translate a foreign language on the basis of the properties of the symbols which make up an alphabet is bound to be fruitless. Quite obviously then, to begin to understand a new language one should focus on establishing syntactical rules and the meaning of individual words. Similarly, to understand complex cellular processes, one must figure out what the relevant informational units are and how they are assembled into functional programs.

Thus, abstraction also serves an epistemological role, beyond the methodological and the ontological ones.

The cell cycle and dynamical reductionism

So far, I have argued that attempting to reduce cellular phenotypes to molecular processes may fail to capture the essential causal forces that underpin biological function. It is then reasonable to ask what abstract units cellular pathways should be framed in relation to in order to reach the explanatory goal put forward. Arguably, cell biological phenomena can be framed at different levels of organisation or complexity, as exemplified by the following scheme: Biochemistry > Regulatory interactions > Control units/motifs > Function. For instance, biochemical properties of macromolecules explain how interactions take place and may lead to the modulation of activity of proteins and nucleic acids. Taken together, subsets of these interactions give rise to control motifs, such as feedback loops, which, in their own right, display novel emergent properties that cannot be reduced to those of the individual molecules. Further, such motifs can be assembled into complex dynamical units, such as bistable switches and oscillators, which form the basis of physiological function. Notice how each level of complexity is most appropriately explained by the level immediately below it, because identifying cause-effect relations requires the least number of logical steps. Further, while the problem of multiple realisability exists between any two adjacent levels, the issue compounds as the distance in explanatory levels increases. Thus, it is sensible to aim to explain functional programs, like the cell cycle, in terms of dynamical units, like bistable switches and oscillators.

The main advantage of taking higher-order abstract dynamical units as building blocks in biological modelling is that it facilitates the scrutiny of internal mechanistic coherence. This stands in contrast with the requirement of accounting for numerous biochemical assumptions, which can be computationally cumbersome and occasionally difficult to falsify. In some circumstances, abstraction coupled with mathematical modelling and logical reasoning may reveal more about a physical process than an experiment could.

As an example, in the late 19th century, one problem in theoretical physics was accounting for the properties of black body radiation (the spectrum of electromagnetic radiation emitted by matter when heated to a certain temperature). The problem, until Max Planck's daring proposal of 1900, was that all models which were continuous predicted the amount of light released by an object would increase rapidly with the frequency. This implied that matter would release infinite amounts of energy in the form of light. This paradox was known as the ultraviolet catastrophe. Purely as a way of avoiding this issue, Planck postulated that only specific quantised wavelengths of light are emitted by matter, such that the total energy released is finite. At the time, no experimental verification of this assumption was available. However, as is well known, this postulate, which aimed at producing a coherent theory, rather than one that was consistent with the 'common sense' of the time, turned out to be correct and led to the development of quantum mechanics.

Another important role of abstraction is generalisability. The aim of scientific research is to make statements about the world that apply as broadly as possible, rather than just to a specific experimental system. When Geiger, Marsden and Rutherford fired alpha particles at a gold sheet, they hoped that their findings would apply to the structure of all atoms, not just to gold. In molecular biology, researchers likewise hope to find broadly applicable principles, which hold across as many phylogenetic branches as possible. In cell cycle research, the most interesting findings are those that apply not just in one particular cell line or model organism, but across most eukaryotes. Occasionally, mechanisms appear conserved even though the underlying genes are not. For instance, the *S. cerevisiae* Whi5[26] is not homologous to the human Rb[27] and yet both regulate CDK expression, commitment to proliferation and size homeostasis through an analogous mechanism. Thus, regulatory and dynamical abstraction can tie together different biochemical mechanism under one functional paradigm.

The main challenge of the abstract exploratory approach is ensuring that the proposed dynamical mechanisms and regulatory structures are consistent with biochemistry. This is because the approach interposes a theoretical layer between the experimental inputs and phenotypic/functional outputs which cannot be accessed directly: experiments

perturb molecules, and the effect on system dynamics is indirect. So how can the advantages of abstraction be reconciled with having appropriate empirical constraints? This can be achieved in several ways; at the most basic level, writing equations that could be consistent with biochemical processes, at least in principle, contributes to our evaluation of model reasonability. For instance, if one were interested in modelling the interaction between different oscillatory cellular phenomena, such as the cell cycle and metabolic or circadian oscillations, it would be reasonable to suggest that the individual phenomena are more appropriately modelled by relaxation oscillators as opposed to simple harmonic oscillators, because simple chemical reaction schemes can easily give rise to the former, but rarely the latter. At a second level, the interactions proposed to make up abstract models could be linked to known biochemical interactions, thus lending more credence to the assumptions of the model. Finally, direct comparisons between abstract and mechanistic models can be made and compatibility can be robustly determined by showing that the assumptions/principles of the simplified models are embedded within detailed mechanistic descriptions.

In summary, this thesis aims to develop new understanding of complex dynamical phenomena in the context of cell cycle regulation. Rather than viewing biology as a collection of enzymatic activities, I hope to show that important insight into cell physiology might come from viewing it as a collection of interconnected regulatory motifs. Although such units have been characterised in biological context previously, the novelty of the current work lies in using them as building blocks to understanding higher order functional properties that have not been hitherto explored.

1 Introduction

1.1 The cell cycle

1.1.1 Function and organisation

The cell cycle comprises a series of fundamental biochemical process that are necessary for cellular division. The precise and accurate regulation of these events is essential for the generation of viable daughter cells. In multicellular organisms, the controlled progression through the cell cycle is fundamental to correct development, while the deregulation of this functional programme may be embryonic lethal[28,29], or otherwise result in cancer development[30,31] or premature ageing[32,33].

In its most basic form, the cell cycle drives two temporally separate events: DNA replication and the segregation of the sister chromatids to the daughter cells (followed by division)[34]. This view, however, is deceptively simple: each of these events must be carried out in at least two distinct steps to ensure accuracy. DNA replication is first licensed by loading the replicative helicases onto the replication origins. During this period, any replication firing is prevented. Subsequently, the activity of the helicases and DNA polymerases is triggered, while that of the licensing factors is inhibited. Similarly, during mitosis, chromosomes are first condensed and aligned at the centre of the cell, while segregation is prevented. Once alignment is complete, the chromatids are pulled apart and eventually decondense to prepare the cell for interphase.

This kind of biphasic organisation of the two chromosomal events is absent in bacteria and in some archaea, and it underscores one of the challenges of genomic maintenance in eukaryotes: the size and number of chromosomes. In order to complete genome duplication in a timely manner, eukaryotes initiate DNA replication at numerous chromosomal loci. However, it must be ensured that each replication origin fires once and only once per generation to prevent over or under-replication of chromosomal

regions. This challenge is addressed by making licensing and firing mutually-exclusive. This is not a problem in bacteria, where only one or two replication origins are present, which may fire replication multiple times within one interdivision period. Eukaryotes most commonly have multiple chromosomes; to ensure that none of them is left behind at division, cells align their sister chromatids at the centre of the cell to account for them. Only once this step is completed does segregation happen. Last but not least, DNA replication and mitosis must themselves be mutually exclusive processes to ensure the inheritance of a complete set of chromosomes. Thus, the eukaryotic cell cycle comprises (at least) 4 biochemically distinct phases, each of which responds sensitively to numerous inputs and carries out multiple molecular processes. Conventionally, the 4 phases (Fig. 1.1) are G1 (gap), S (DNA synthesis), G2 and M (mitosis).

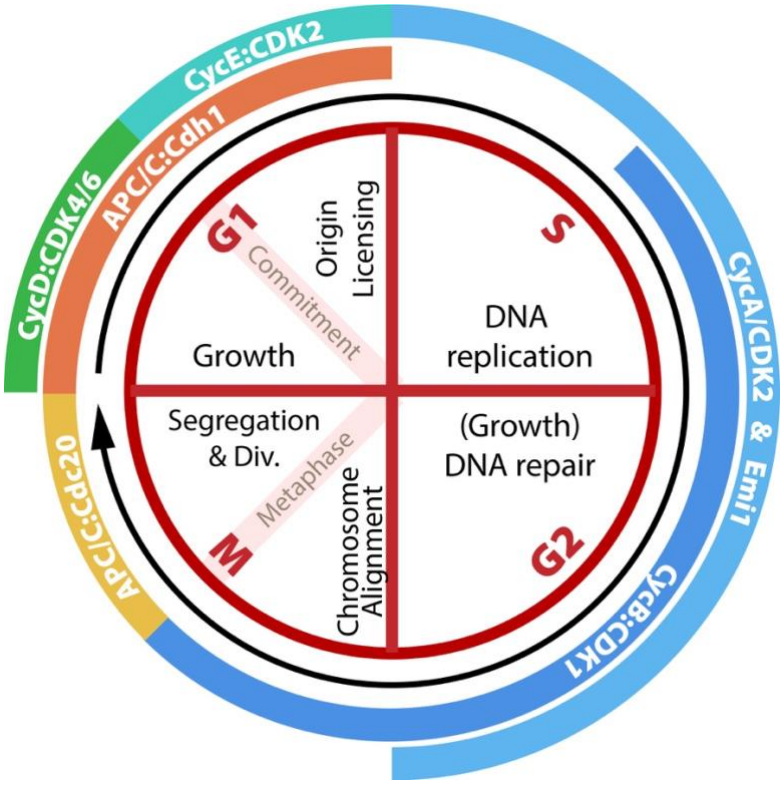

Fig. 1.1 – The organisation of the cell cycle, the phase specific events and their molecular regulators

The G1 phase is the point in the cell cycle at which the cell gathers information about its internal state and external milieu before committing to proliferation. Simultaneously, it is also the period during which origin licensing takes place. In vertebrates, this is the period in which the bulk of cellular growth takes place[26,27]. Similarly, in budding yeast this is the

main phase during which the cells increase their cytoplasmic volume (although bud growth, specifically, takes place post G1). In multicellular organisms, G1 is also the period in which extracellular signals are thought to stimulate proliferation[35,36] (although this view has been challenged recently[37]). At the same time, cells assess whether any errors have accumulated in the previous generation, either during DNA replication[38] or mitosis[39,40] and 'decide' whether commitment to proliferation, error correction, permanent arrest or apoptosis is appropriate. Finally, appropriate cellular attachment and the availability of biosynthetic precursors[41–43], such as nucleotides must also be confirmed. Once all conditions are satisfied, cells commit to DNA replication and division by crossing the 'restriction point' (in vertebrates) or Start (in yeasts).

During S-phase, the main cellular event is the triggering of template-directed synthesis of a copy of each chromosome. This is a particularly vulnerable moment for the cell, as much DNA damage can occur, due to either nucleotide misincorporation by the polymerase, collisions with chromatin obstacles (which may lead to double strand breaks), or the presence of single stranded intermediates, which are particularly susceptible to damage. This means that S-phase is also a time of careful DNA damage management, which involves the appropriate pausing of replication firing and the activation of repair pathways[44] (e.g. homologous recombination). Concomitant with replication, sister chromatid cohesion is established, through topological entrapment of the chromatin strands by cohesin[45], which later allows for the metaphasic alignment of the sisters. Simultaneously, the cell must drive histone biosynthesis[46–48] in order to appropriately package the growing DNA strands into nucleosomes. Importantly, this is also the cell cycle phase in which centriole duplication commences[49].

Following the completion of DNA replication, cells enter G2 phase. In many ways, this phase is similar to S-phase from a regulatory/signalling perspective. In most mammalian cells, this is a time in which any remaining errors that occurred during replication are corrected, or if the damage is too great, apoptosis is triggered. Nevertheless, in specific cell types, G2 has specific functions. For instance, in wild type, fast-growing fission yeast, this is the period in which most cellular growth takes place. Interestingly, G2 arrests also play an important part in vertebrate development: oocytes remain arrested at this stage

for a very long time, until progesterone signals the time for germ cell production and trigger meiosis I[50].

Mitosis is perhaps the most striking phase from a cytological perspective, as this is when the most dramatic changes in cell morphology take place. M-phase is conventionally subdivided into 4 stages, characterised by specific observable changed. In Prophase, the nuclear envelope breaks down and the chromosomes condense thanks to loop extrusion by condensin[51,52]. The centrosomes then migrate to the opposite ends of the cell, as the microtubules are rearranged to form the mitotic spindle. Simultaneously, cells lose their extracellular attachment and round up. In prometaphase, the microtubules of the mitotic spindle begin to attach to chromosome centromeres, such that the bivalents are pushed/pulled towards the cellular equator. A signalling pathway known as the "Spindle Assembly Checkpoint" is triggered by unattached kinetochores, such that progression to anaphase is prevented until all chromosomes are aligned at the metaphase plate[53]. Once this alignment process is complete, the cohesin links that hold the sister chromatids together are severed by separase, which triggers anaphase, when the chromatids are pulled apart, towards the two poles of the cell. Finally, cytokinesis is initiated, as the plasma membrane begins to constrict around the cell equator, and eventually abscission takes place. Simultaneously, the chromosomes begin to decondense, and the nuclear envelope starts to reform around them, completing telophase.

1.1.2 Global properties and dynamical paradigms

The cell cycle comprises a great diversity of biochemical processes and physiological functions. As such, one of the intellectual challenges in this field is to identify common features that facilitate a conceptually unified view through which to frame and understand the events making up the cell cycle. As the tools and techniques available for dissecting cell cycle regulation have evolved, so have the ways in which the physiology is framed.

The first attempts to systematically study cell cycle regulation relied on genetic techniques. The approach was developed by Hartwell in the 1970s and it consisted of identifying *S. cerevisiae* temperature-sensitive mutants which consistently showed defects in the cell division cycle phenotype at the restrictive temperature, as revealed by light microscopy[54]. For instance, Cdc1 mutants were judged to permanently arrest in G1, as cells accumulated at a stage where only very small buds were present. In contrast, Cdc2 mutants were shown to arrest at a later stage, prior to division. As more mutants were found in budding yeast[55] as well as fission yeast[56], a clear pattern began to emerge: the cells which could not complete a specific cell cycle phase due to the presence of a mutation would never progress to the subsequent stages. This suggested that the completion of one phase's events triggered the entry into the following phase[57]. Thus, based on this genetic view, progression through the cell cycle phases was viewed as being akin to a row of falling dominoes[58].

The cytological and, later, biochemical view provided a different perspective on the cell cycle. It is clear from observing cells under the microscope that certain events occur with regularity in each cycle: following division, in *S. cerevisiae*, a bud starts appearing after sufficient growth; subsequently, the DNA is replicated and eventually the chromatids are segregated between the 'mother' and 'daughter' cell. The approximate periodicity of these events in wild-type unperturbed cells suggested that some master regulator might orchestrate the timing of all these events, which could otherwise happen independently[57]. In agreement with this, biochemical experiments have shown that the amounts and activity of cell cycle regulators oscillate periodically in cellular extracts[59,60]. The idea of periodic events occurring without regard to the completion of specific steps was solidified by the observation of MPF oscillations in enucleated[61] or colchicine treated[60] frog eggs. This has resulted in the 'clock' view of the cell cycle[62]. This view was further solidified by experiments in Cdc4, Cdc34 or Cdc53 budding yeast mutants, which periodically initiate budding events, without completing DNA replication or initiating mitosis[63,64].

As the precise biochemical interactions driving the completion of cell cycle events and phase progression have been elucidated, new regulatory principles started to emerge. A

number of feedback motifs[65,66] in which the cell cycle regulators are engaged have been shown to lie at the foundation of most of the transitions and to be responsible for the properties identified by the early genetic and cytological experiments. The biochemical basis of these motifs and how they underpin function is the subject of the next sections. In the simplest terms, the dynamical paradigm that emerged from these argues that the cell cycle control network ensures the existence of multiple steady states, characterising each phase[67]. For the control network to transition from one phase to the next, all the phase-specific events must feed back a signal confirming completion. This accounts for the older 'dominoes' view. In addition, thanks to a property known as hysteresis, once the system has transitioned into a new phase, it cannot return to a previous one[68]. This imposed directionality ensures the orderly completion physiological events. Thus, the only allowed trajectory through the cell cycle that enables a return to the G1 state is through mitosis. Repeatedly running through this unidirectional programme results in oscillations, similarly to the previously described "clock". The simple mechanical analogy to this description is that of a series of toggle switches, whose flipping represents the cell cycle transitions.

As the details of the mitotic cycle become settled, research turns its attention to alternative variants of the cell cycle, which underpin functions beyond proliferation. Endocycles are abridged versions of the cell cycle oscillations, in which one or more phases are abrogated. They occur in a great diversity of organisms and developmental stages. Endoreplication, the repetition of DNA replication in the absence of mitosis[69], typically facilitates the increase in cellular size[70]. This may lead to several advantages, such as increased storage capacity, or an evolutionary advantage over competing species in unicellular organisms. In multicellular organisms, polyploidy has been argued to play a role in tissue regeneration[71]. In cancer development, whole genome duplication drives malignancy through oncogene amplification[72]. A process similar to endoreplication is endomitosis, in which cells complete S-phase and undergo M-phase at least partially, but do not divide.

The definition of endocycling proposed above allows not just for replicative endocycles, but also mitotic endocycles, in which multiple rounds of M-phase events may occur

without an intervening S-phase. Reductive mitosis is one such rarely occurring example, which may serve to reverse tetraploidisation[72]. In addition, this process may aid in rapidly increasing the surface area of epithelial tissue in some species[73]. Together with the role of endoreplication in increasing storage capacity, this suggests that ploidy control may provide a mechanism to fine tune the surface/volume ratio of cells. Nonetheless, the most common type of M-phase endocycle is meiosis, which generates germ cells[74]. Finally, other kinds of mitotic endocycles have been experimentally induced in various cell types[75,76]. Though they are unlikely to occur physiologically, they provide insight into cell cycle organisation and will therefore be discussed in subsequent chapters.

The endo-oscillatory property of the cell cycle is interesting from a theoretical perspective because it cannot be explained through any of the preceding dynamical paradigms. What makes studying such behaviour challenging is the fact that it emerges at global cell cycle level, and not just as a superposition of the properties of individual transitions. Thus, the aim of this thesis is to identify new dynamical paradigms through which to conceptualise the emergence of endo-oscillations and to enable their rational interrogation, from an experimental and mechanistic modelling perspective.

1.2 The biochemical regulation of the cell cycle

The checkpoints and transitions of the cell cycle are implemented by an exceedingly complex network of interacting genes and proteins[77]. At the core of this system, cyclin dependent kinases (CDKs) regulate cell cycle events by phosphorylating a great number of molecular targets which are responsible for carrying out DNA replication and mitosis[78]. As the name suggests, CDKs bind cyclins, whose availability changes as the cell progresses through the division cycle[59] (Fig. 1.1). Cyclins determine the substrate specificity of CDKs and as such, their activity. The regulation of cyclin accumulation is one of the main cell cycle regulatory strategies. In addition to the CDKs, a number of counteracting phosphatases also make a contribution to the timing of cell cycle events[79]. In this section, I discuss the biochemical mechanisms that regulate the activity of CDKs and phosphatases, and how these contribute to cycle progression and checkpoint

establishment. Unless otherwise stated, the mechanisms under consideration will be the ones applicable in mammals.

1.2.1 The control of the G1 state

Early G1 phase is characterised by the absence of CDK activity. To maintain this state, the cell employs a number of strategies (Fig. 1.2). First, Cyclins A and B are targeted for degradation by the APC/C:Cdh1 ubiquitin ligase[80,81]. Second, the transcription of Cyclins E and A is suppressed[82]. Third, a number of stoichiometric inhibitors (CKIs), in the INK4 and Cip/Kip families, inhibit CDK4/6 and CDK2 activity, respectively[83,84]. To leave G1 phase and enter S-phase, APC/C:Cdh1 activity must be suppressed, and this is initiated by the transcription factor E2F. To prevent premature entry into S phase, E2F is inhibited in G1 phase by the retinoblastoma protein (Rb), the primary agent arresting G1 cells ahead of the restriction point (RP). To pass the RP, the cell must inactivate Rb by phosphorylation [85–87], started by CycD:Cdk4/Cdk6 (CDK activities under the control of a variety of mitogens, growth factors and anti-growth factors). Rb phosphorylation releases E2F to induce the synthesis of CycE[88], CycA and Emi1[89]. CycE:CDK2 further phosphorylates Rb[90] and, together with Emi1[91,92], drives down Cdh1-dependent degradation of CycA and CycB. The irreversible inactivation of APC/C:Cdh1 marks the entry into S-phase, when Cdk2, in complex with CycE or CycA, can initiate DNA replication. As CycA:CDK2 activity becomes self-sustaining, CycE, in turn, becomes dispensable, and it is targeted for ubiquitination and degradation by the SCF pathway[93]. Further, E2F-dependent transcription is suppressed by CycA-dependent phosphorylation[94].

One of the justifications for the complexity of this pathway is to ensure the robustness and switch-like nature of the G1/S transition, as explained in the final section of this introduction. However, the main rationale for including so many CDK regulators (which are otherwise redundant for the dynamical properties of the transition) is that the pathway can respond to a great diversity of signals, which converge at CDK activity to determine the suitability of proliferation. One of the principal inputs into the G1/S control

pathway is mitogen signalling. Mitogens, such as EGF, FGF and PDGF, are extracellular signalling molecules that are produced by the neighbouring or distant tissues, which stimulate entry into the cell cycle. Typically, they exert their stimulatory effects by binding receptor tyrosine kinases, which trigger the Mitogen-Activate Protein Kinase (MAPK) cascade[95]. The downstream kinases of the pathway, such as ERK, phosphorylate transcription factors, which upregulate pro-proliferative genes. The principal targets are the D-type cyclins, which indirectly activate E2F (Fig. 1.2). One of the targets of E2F is the DNA replication origin licensing protein Cdc6[96], such that mitogens help stimulate S-phase entry by both through CDK activation and by stimulating licensing.

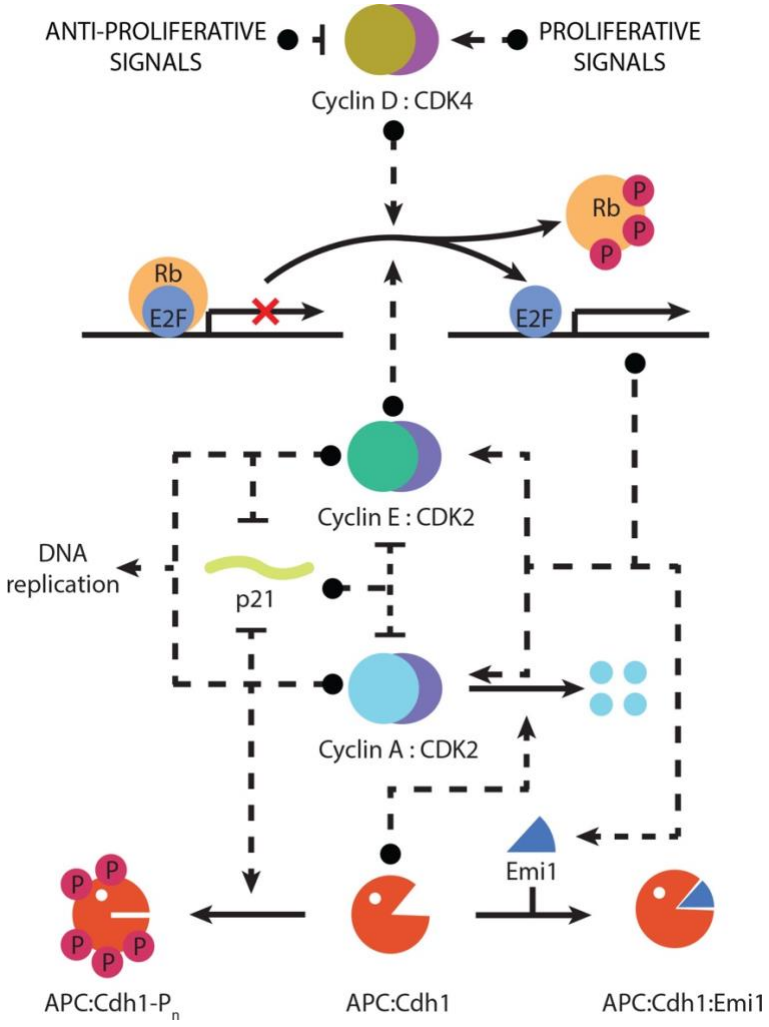

Fig. 1.2 – The molecular control pathway of the Restriction Point and G1/S transition. Black dots indicate the molecules which stimulate/inhibit some reaction, process or protein. The arrow heads indicate the proteins/processes that are being stimulated, while the bar head indicate inhibition.

The mitogen-driven stimulation of proliferation is intimately linked to growth control. Cells must control their size to maintain an appropriate balance between ploidy and

biosynthetic capacity, as well as to facilitate tissue/cell-type specific function[97]. The average size of cells in a population depends on the growth rate and the inter-division time. Since the mass accumulation rate scales with the mass itself, mammalian cells grow exponentially[98–100]. Thus, some homeostatic mechanism must counteract imbalances between the size doubling time and the cycle duration, as well as any random deviations, as might occur with asymmetric division, or noisy protein expression. It appears that one of the main strategies to achieve this involves the adaptive control of cell cycle duration. In mammals and budding yeast, the greatest variability occurs in G1 and indeed, the duration is inversely proportional to the birth size[26,27,98,99]. In mammals, this relationship seems to depend on Rb[27]. This is because a roughly constant number of molecules (proportional to the gene copy number, which doubles with DNA replication and halves at division) are present in the cell, regardless of volume. Consequently, unlike most other proteins, the concentration of Rb decreases as the cell grows. Thus, in small cells, Rb should saturate E2F molecules and prevent entry into S-phase. Nevertheless, as cells grow, a stoichiometric deficit develops and CDK2 activity starts to accumulate.

1.2.2 The regulation of DNA replication

One of the unique features of eukaryotic genomes is the existence of a plurality of DNA replication origins, unlike the prokaryotic ones, which typically have a single origin. The need for this feature is explained by the significantly larger genome size of eukaryotes and the existence of multiple chromosomes. While the concerted action of numerous replisomes during the S-phase makes the completion of DNA replication in a timely manner possible, it also introduces a significant challenge: the cells must ensure that each individual DNA fragment is replicated once and only once per cell cycle, so that each daughter cell inherits an exact copy of the genome. To address this bookkeeping conundrum, eukaryotes partition the steps needed to initiate DNA replication to two mutually exclusive periods of the cell cycle. The loading of the MCM2-7 replicative helicase (also known as origin licensing) happens exclusively in G1 phase, while the firing of replication and template-directed DNA polymerisation only happens in S-phase. As CDK activity is responsible for licensing inhibition, this ensures that relicensing is not

triggered before the completion of the cell cycle. In addition, a checkpoint mechanism prevents progression to mitosis until all DNA has been replicated.

The licensing of replication origins is inhibited by CDK activity through a variety of direct and indirect mechanisms. Subsequently, MCM helicases are only loaded during G1, when CDK activity is suppressed by the mechanisms described above (Fig. 1.2). Helicase loading is a multi-step process that requires several protein components whose availability is regulated in a cell cycle-dependent manner (Fig. 1.3). First, the origin recognition complex (ORC) is loaded onto DNA. Then, together with the licensing factors, Cdt1 and Cdc6, ORC loads two MCM helicases in opposite orientation. Cdt1 availability is restricted to G1 through at least two mechanisms. First, geminin is a stoichiometric inhibitor of Cdt1, but also a target of APC/C:Cdh1 ubiquitination,[101] such that it only accumulates post S-phase entry. Second, the ubiquitin ligase CRL4:Cdt2 is recruited to active replisomes by PCNA and targets Cdt1 for degradation in S-phase[102]. In parallel, Cdt1 is also targeted for degradation by the SCF ubiquitin ligase following S-phase entry[103]. Similarly, Cdc6 may be targeted for degradation following CDK2-dependent phosphorylation[104] and/or nuclear exclusion[105,106]. Finally, ORC and MCM proteins may be inhibited by CDK activity through a variety of mechanisms which appear cell type dependent[107,108].

Following entry into S-phase, CDK2 (and DDK, another S-phase kinase) phosphorylates the MCM complexes and some of the "firing factors", Sld2, Sld3 (Treslin in humans), Sld7, Dpb11, the GINS complex, which help recruit the replicative polymerases to the loaded helicases[107,109]. Once this process is complete, DNA polymerisation is initiated. Throughout this process, the mutual exclusivity of Cdh1 and CDK2 plays a crucial role in ensuring that licensing (G1) and replication (S) are mutually exclusive processes. The properties of the cell cycle control network that facilitate this behaviour are discussed in the later sections of the introduction and in the Results chapters.

Throughout this thesis, none of the biochemical mechanisms associated with licensing and replication will be modelled. Instead, it will be assumed that the licensing phase (G1)

is active when APC/C:Cdh1 is active. Similarly, cells will be assumed to be in the S/G2 phases after the inactivation of APC/C:Cdh1 and before the activation of CycB:CDK1.

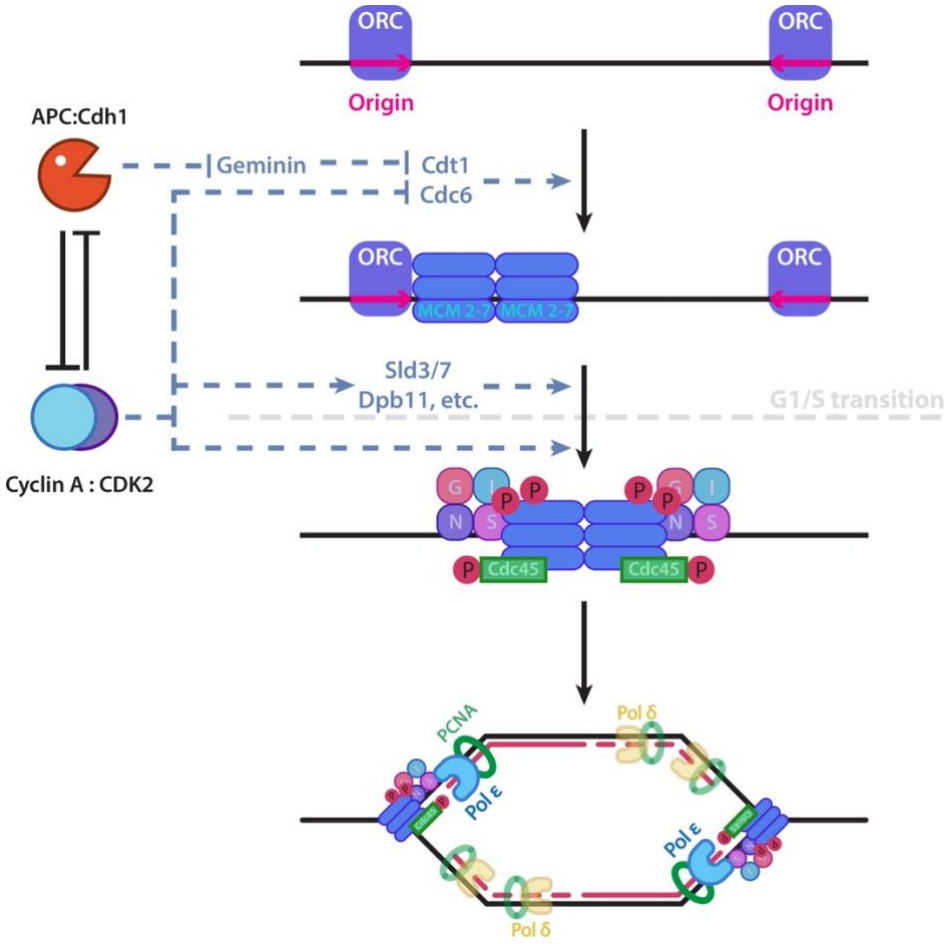

Fig. 1.3 – The regulation of DNA replication – Replication origin licensing (the loading of the MCM2-7 replicative helicase is facilitated by APC/C:Cdh1 in G1, through the protection of licensing factors. Replication firing is driven by CDK2, which phosphorylates the helicase proteins and activates the firing factors.

1.2.3 The unreplicated DNA and DNA damage checkpoint

To ensure that each daughter cell inherits a full copy of the genome, the cells must prevent entry into mitosis before the completion of DNA replication. Similarly, the genome must be free of errors. The same signalling pathway, known as the DNA damage response, ensures that cell cycle progression is delayed (or aborted altogether) unless replication is complete and all damage is resolved. The pathway is typically triggered by either double stranded breaks (potentially the most deleterious kind of DNA damage), or single stranded DNA (ssDNA)[110,111]. ssDNA is generated during numerous repair

processes, such as the nucleotide excision repair pathway, or homologous recombination, during which strand resection is one of the crucial steps[112] (Fig. 1.4). In addition, ssDNA is a natural intermediate in DNA replication, particularly on the lagging strand. Double strand breaks are typically recognised by the MRN complex[113], while ssDNA is bound by the RPA protein[114]. These proteins initiate the signalling cascade by binding and activating the kinases ATM and ATR, respectively. In turn, they activate the Chk2 and Chk1 kinases. Chk1 is primarily responsible for suppressing CDK activity by inactivating Cdc25[115]. As discussed below, this phosphatase is essential for removing the inhibitory phosphorylation of CDK1, after which the cell enters mitosis. In contrast, Chk2's primary effect is the stabilisation of the transcription factor p53[116], a major tumour suppressor gene. p53 has many targets, which include DNA repair proteins, pro-apoptotic factors and cell cycle inhibitors.

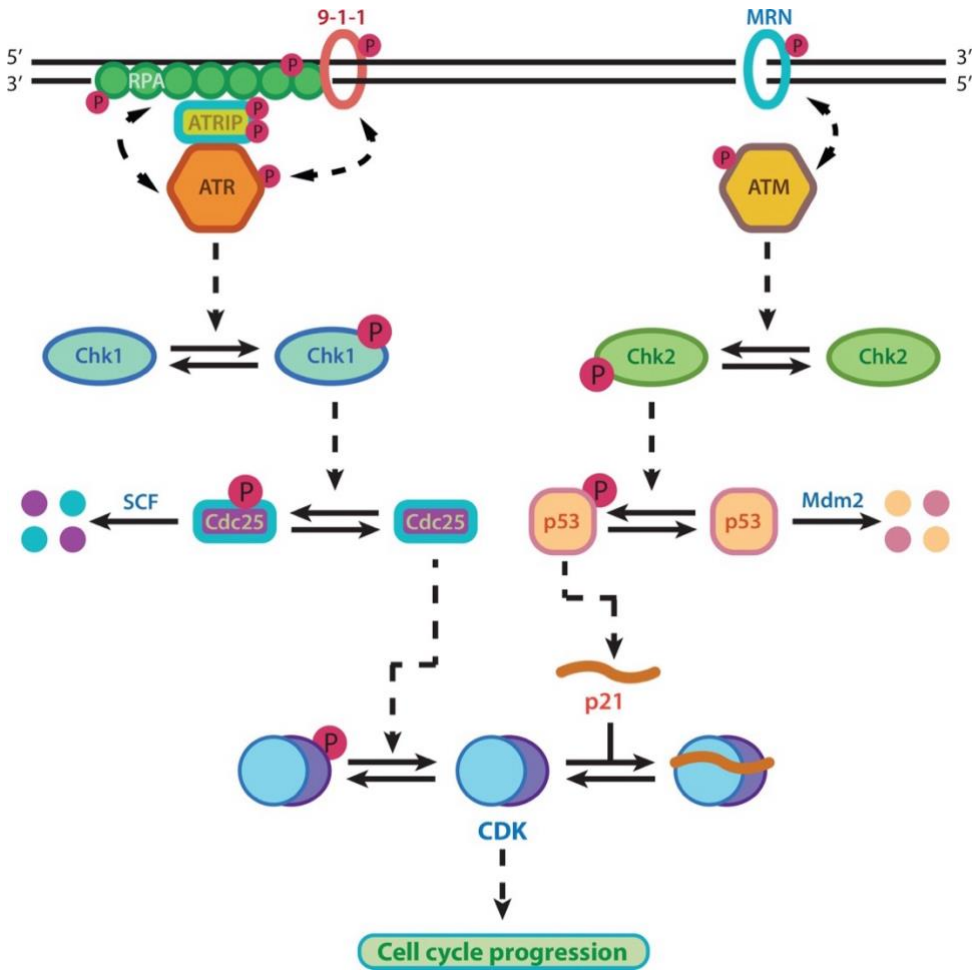

Fig. 1.4 – The DNA damage response pathway. The inputs of the DDR pathway are ssDNA, which occur naturally during replication, or as intermediates of the repair processes, and double strand breaks. These inputs activate a kinase signalling cascade, which prevents cell cycle progression by suppressing CDK activity.

The DNA damage checkpoint can also be triggered in G1 phase, to avoid initiating replication of damaged chromosomes[117]. The same signalling pathway is triggered as during S-phase. However, the downstream effectors are different. Although the Cdc25A phosphatase may play a role in the timing of the G1/S transition[118] and potentially respond to the DNA checkpoint, the main effector of the pathway is the p53 target gene, CDKN1A, coding for the CKI p21. In S-phase, this mechanism is unavailable, as p21 is targeted for degradation by CRL4:Cdt2[119].

1.2.4 The regulation of mitosis

The numerous cellular events that make up mitosis are initiated by the phosphorylation of a large number of biochemical effectors. As such, mitotic progression is regulated globally through the control of activity of kinases and phosphatases. The key players are CycB:CDK1 kinase and its counteracting phosphatase, PP2A:B55, although several other kinases, such as Aurora A/B and Plk1 (herein also referred to as Polo), control specific aspects of mitosis.

The cell is primed for entering M-phase as soon as S-phase commences, as CycA:CDK2 activates the MuvB, B-MYB and FOXM1 transcription factors for CycB expression[120]. Simultaneously during S phase, after a burst in E2F-mediated transcription, E2F is inactivated by phosphorylation by CycA- and CycB CDKs[121], which ensures that proteins needed for DNA replication are no longer expressed as cells enter mitosis. Along with CycB, Polo, an APC/C:Cdh1 substrate is also begins to accumulate. Thus, when Cdh1 activity is low (in S/G2/M), the accumulation of Polo-kinase is indirectly activated by CycA- and CycB-activated CDK[122]. At mitotic entry, Polo is activated by Aurora A[123]. In turn, Polo is responsible for phosphorylating Emi1, thereby promoting Emi1 degradation through the SCF ubiquitin-ligase[124] and leaving A-type and B-type CDKs the only remaining activities to maintain Cdh1 inactive until mitotic exit.

The G2/M transition is driven by the activation of CycB:Cdk1, central component of the mitotic control network[125] (Fig. 1.5) CycB:Cdk1 complexes undergo inhibitory tyrosine-

phosphorylation on the Cdk1 subunit by Wee1-kinase and dephosphorylation by Cdc25-phosphatases. The abrupt rise of Cdk1 activity at the onset of mitosis is triggered by the positive feedback loops between Cdk1|Wee1 (−|−) and Cdk1|Cdc25 (+|+). As explained in the subsequent sections, this regulatory motif gives rise to bistability[87,126,127], ensures the robustness of the mitotic transition and creates the opportunity for an 'unreplicated DNA' checkpoint ahead of the G2/M transition. Rising CycB:Cdk1 activity phosphorylates Greatwall-kinase (Gwl). Activated Gwl phosphorylates and activates endosulfine (ENSA), which inhibits the major phosphatase (PP2A:B55) during mitosis[128,129].

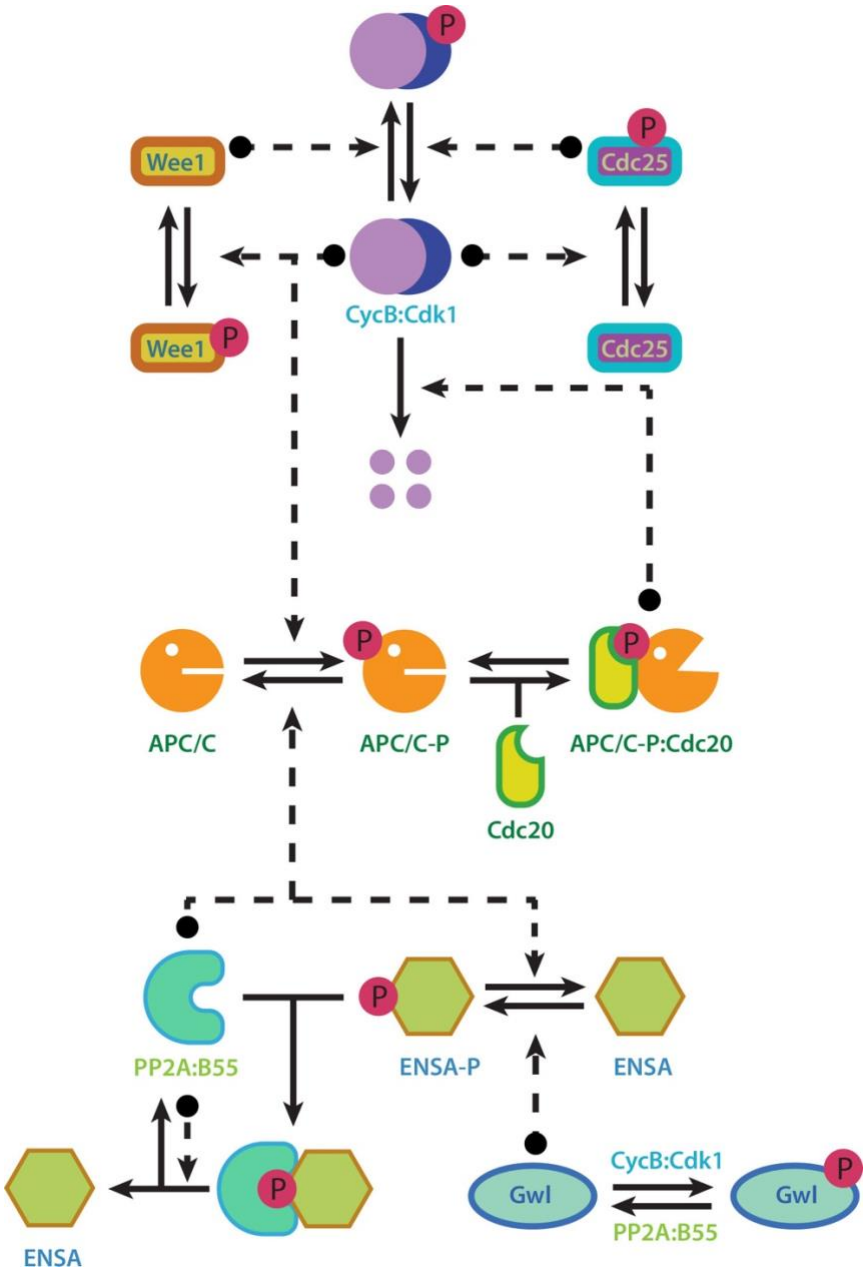

Fig. 1.5 - The molecular network controlling mitotic entry and exit.

As the balance of kinase and phosphatase activity shifts, numerous molecular targets are phosphorylated in mitosis. Nuclear envelope breakdown occurs thanks to the phosphorylation of nuclear lamins[130,131] and the nuclear pore complex[132]. Chromosome condensation is driven by the phosphorylation of condensin proteins by CDK1[133–136], which lead to chromatin compaction through loop extrusion[137]. Centrosome disjunction is promoted by Plk1, while the migration of the centrosomes to the opposite poles is driven by the Eg5 kinesin, which is activated by CDK1 and Plk1[138]. Simultaneously, Aurora B promotes the correct (amphitelic) attachment of spindle microtubules to kinetochores.

A crucial target of CycB:Cdk1 phosphorylation is APC/C. The phosphorylated ubiquitin ligase rapidly binds Cdc20, and the active complex (P-APC/C:Cdc20)[81,139,140] promotes the degradation of cyclins. However, up to the end of metaphase, only CycA is degraded. This is because the activation of the spindle assembly checkpoint by unattached kinetochores prevents the activity of APC/C towards securin and CycB in order to delay mitotic exit until all chromosomes are aligned at the metaphase plate[53]. When kinetochores are not under tension (i.e. no amphitelic attachment), Aurora B phosphorylates the NDC80 component. Then, the MPS1 kinase poly-phosphorylates KNL1 component of the kinetochore, which acts as a scaffold for the catalytic formation of the mitotic checkpoint complex (Cdc20:Mad2:BubR1:Bub3), which inhibits APC/C. Once all chromosomes are attached, APC/C:Cdc20 is activated abruptly, leading to the degradation of securin. Securin is an inhibitor of the protease separase, which cleaves cohesin, leading to the loss of sister chromatin cohesion and the segregation of chromatids towards the opposite poles of the cell[141]. The other major target of APC/C:Cdc20 is CycB; as CycB:Cdk1 activity drops, the balance between APC/C phosphorylation and dephosphorylation shifts to favour its dissociation from Cdc20 and association with dephosphorylated Cdh1. These molecular changes drive the cell back to G1 (active APC/C:Cdh1).

1.2.5 The biochemistry of endocycles

The interplay between CDKs and their antagonists is responsible for the careful ordering of cell cycle events. The licensing (G1) and replicative (S) phases occur sequentially (rather than simultaneously) thanks to the mutual antagonism between Cdk2 and Emi1, on the one hand, and APC/C:Cdh1 and CKIs, on the other hand. Similarly, mitosis and interphase follow each other, at least in part, because the mitotic kinase, Cdk1, is in mutual antagonism with Wee1, while the PP2A phosphatase is in mutual antagonism with Gwl. Further, replication and mitosis follow sequentially because Cdk2 stimulates the activation of Cdk1 and vice versa.

For the purposes of this thesis, endocycles are defined as cell cycle variants where subsets of cell cycle phases are abrogated. As phase identity is intimately linked to the activity of cell cycle regulators, their specific perturbation results in endocycles. Replicative endocycles occur when cells undergo multiple rounds of origin licensing and DNA replication without dividing, such that they become polyploid. Analogously, mitotic endocycles would occur when the cell repeatedly activates the mitotic network, without driving intervening DNA replication events.

Replicative endocycles are surprisingly diverse, with the exact biochemical mechanism and stage of cell cycle termination being dependent on the organism, cell type and developmental stage[69,70,142]. Endoreplication specifically refers to the repeated alternation of G1 and S phases, without entry into mitosis, as revealed either cytologically, or via the detection of mitotic markers, such as Ser 10 phosphorylated histone H3[143]. These cells complete their cycle and return to G1 not by activating APC/C:Cdc20, but by prematurely turning on APC/C:Cdh1[144]. It is tempting to suppose that because endoreplicating cells do not undergo anaphase, their chromosomes would be linked by cohesin rings. While some postmitotic polyploid cells have polytene chromosomes, such as in the Drosophila salivary glands[145], in many cells, cohesion of sister chromatids is lost via a Pds5-dependent mechanism[146]. This is similar to cohesin removal from chromosome arms during early mitosis, and serves to prevent errors that might arise in subsequent mitoses.

In contrast to endoreplication, in endomitosis cells enter M-phase following S/G2, but they do not complete anaphase or divide[142]. Subsequently, the nucleus might become multilobed. Occasionally, cells can become polyploid via the direct inhibition of cytokinesis. This can be achieved by disrupting the actomyosin contraction necessary for cleavage furrow ingression. Here, I do not consider this to be an endocycle, as polyploidy does not directly emerge from the perturbation of the cell cycle control network.

Replicative endocycles are ubiquitous across eukaryotic species. Starting with unicellular protists, many of these organisms show either polyploidy within one nucleus, polynucleation, or both[147]. A likely explanation for this is that increasing the number of genome copies allows the cell to grow to larger sizes, which may present a selective advantage in ecological niches where predator-prey dynamics exert significant pressure. Polyploidy is necessary when the gene copy number becomes limiting for the rate of transcription. This is exemplified in ciliates, such as Paramecium or Tetrahymena, where micronuclei hold one copy of the genome, which undergoes meiosis and is used for mating, while a large macroneucleus with hundreds of copies of each chromosome is used for transcription. The amplification of DNA in the macronucleus is driven by an endoreplication-like process, where replication origins are licensed and fired periodically without entering mitosis[148].

The most familiar example of endoreplication in a multicellular organism is the one observed in drosophila salivary glands, known for their polytene chromosomes, which show characteristic banding determined by euchromatic and heterochromatic domains[149]. Much like in the unicellular ciliates, the extra DNA copies support high rates of transcription and cellular enlargement. However, unlike typical endoreplication cycles, chromosome replication is incomplete, with heterochromatic regions being under-replicated.

In mammals, several cell types undergo replicative endocycles. Megakaryocytes rely on endomitosis to increases their size prior breaking up into platelets. The induction of endomitosis is triggered by thrombopoietin, which upregulates CycE[149]. The purpose of this may be to stimulate the G1/S transition and potentially to help complete S-phase if

mitotic cyclins are simultaneously downregulated. M-phase is prematurely terminated by APC/C:Cdh1 activation, but stoichiometric inhibitors like p21 may also play a part in inhibiting CDK activity.

Mammalian endoreplication is encountered in placental development, when trophoblast stem cells differentiate into trophoblast giant cells[150]. This is achieved by suppressing CycB:Cdk1 activity, through the upregulation of stoichiometric inhibitors, p21 and p57[151]. In addition, polyploidy can be encountered in hepatocytes. Although this can be achieved via different mechanisms, including acytokinetic mitosis, leading to binucleation, true endoreplication can also be triggered, possibly due to genotoxic stress[71].

In experimental context, endoreplication can be induced reliably in a variety of cell types and organisms, through the inhibition of the mitotic kinase[69,152–154]. As Cdk1 (or its non-mammalian homologue) is inactivated, the cell can no longer enter mitosis. Instead, after the completion of S-phase, CDK activity drops and the cell returns to the G1 state, during which origins are relicensed. As this process repeats, the cell's ploidy doubles numerous times.

Mitotic endocycles occur very rarely, if at all, in physiological contexts, as the loss of chromosomes is likely lethal. However, aside from meiosis and reductive mitosis, mitotic endocycles can be induced experimentally. In budding yeast, mitotic exit requires the release of the Cdc14 phosphatase from the nucleolus[155,156]. Preventing the return of the cell to the G1 state by expressing a non-degradable variant of Clb2 results in the periodic release of Cdc14 from the nucleolus, giving rise to Cdc14 endocycles[76]. A different type of mitotic endocycle, termed Cdc20 endocycle, can also be induced in mammalian cells. In HeLa cells, expression of the CDK1AF allele, which cannot be phosphorylated and inhibited by Wee1, results in low amplitude, high frequency oscillations in CycB levels in the absence of DNA replication or division. The dynamical basis of endocycle emergence in *S. cerevisiae* has been studied in a theoretical paper by Novak & Tyson[157]. In Chapter 2, I introduce an analogous mechanistic model of cell cycle control that aims to explain endoreplication and Cdc20 endocycles in mammalian cells[158].

1.3 Mathematical modelling, analytical tools and control motifs in cell cycle regulation

Mathematical modelling plays an essential role in the development of physiological intuition, as well as in scientific hypothesis generation and testing. This is largely because most techniques in molecular and cellular biology are *perturbative*, in the sense that they use genetic or pharmacological means to ablate or enhance the activity of biochemical factors and then measure the effect on some phenotype of interest. This provides insight into the role specific genes in biological process. However, this approach makes it difficult to establish what the minimal functional units that carry out a physiological process are. For this, *constructive* techniques, such as *in vitro* biochemical reconstitution are necessary. Recently, these approaches have been invaluable for determining the minimal set of proteins and reaction steps needed for replication origin licensing and firing[159–161]. Nevertheless, there are practical limits on the complexity of the biochemical systems that could be reconstructed *in vitro*. On example is any process that requires complex gene regulation events, such as the activation of the DNA checkpoint, in which p53-dependent transcription might play a significant part. Mathematical modelling can bridge the gap between the bottom-up approach of biochemical reconstitution and the top-down approach of genetic perturbations. In addition, modelling provides the opportunity for making precise quantitative predictions, as well as a way to quickly generate proofs of concept for putative biochemical mechanisms.

The primary modelling approach used throughout this thesis will be that of systems of coupled nonlinear ordinary differential equations (ODEs). ODEs describe the rate of change of levels or activity of some molecular species. As such, the principles of chemical kinetics will be at the heart of all research presented here. Nonlinearity is a ubiquitous property of biochemical systems, which is essential for underpinning much physiological function. Coupling such ODEs is a way to account for the role of multiple interacting genes and proteins. The remaining part of this introduction is dedicated to

explaining the basic principles of these concepts and how they are applied to understanding cell cycle properties.

1.3.1 Ordinary differential equations, rate balance plots and bifurcation diagrams

ODEs are expressions that link the rate of change (i.e. time derivative) of a dynamical variable (here, the activity of some molecular species) to a number of terms that involve functions of the variable itself and of potentially other variables that make up the system. This idea can be exemplified with respect to an important cell cycle regulator, which will be part of subsequent models, the ubiquitin ligase APC/C:Cdc20. Let us assume that APC/C can be converted between two forms, phosphorylated and dephosphorylated, according to the equilibrium APC⇌ APC-P. The phosphorylated form is bound by Cdc20 and it is active towards substrates. If the forward step is catalysed by CDK1, while the backwards one by PP2A, the following ODE can be written:

$$\frac{dAPC_P}{dt} = kp_{APC} \cdot Cdk1 \cdot (APC_T - APC_P) - kdp_{APC} \cdot PP2A \cdot APC_P \qquad (1.1)$$

The phosphorylation and dephosphorylation rates are proportional to the concentration of the two species (i.e. mass action kinetics are assumed) and the product between kinase or phosphatase activity, and the applicable rate constants (kp_{APC}, kdp_{APC}), respectively. Notice the equation assumes that the total concentration of APC (APC_T) is constant, such that the dephosphorylated concentration is equal to $APC_T - APC_P$.

In this case, the ODE can be integrated to produce an exact expression that gives the concentration of dephosphorylated Cdc20 at any point in time:

$$APC_P(t) = \frac{A}{B} + APC_{Pi} \cdot e^{-Bt}$$

Where $A = kp_{APC} \cdot Cdk1 \cdot APC_T$ and $B = kp_{APC} \cdot Cdk1 + kdp_{APC} \cdot PP2A$, while APC_{Pi} is the initial phosphorylated APC concentration. Although such integrated solutions are important for simulating the time evolution of the system of interest, no further attention will be dedicated to solving ODEs analytically, as numerical integration techniques are used throughout the thesis. The steady state response and how it is affected by variables such as Cdk1 and PP2A can be computed more readily, either analytically or using a graphical approach. First, notice that the steady state can be derived from the integrated solution; in the limit of infinite time, the exponential term vanishes such that $APC_P(t) = \frac{A}{B}$. Equivalently, the same result can be obtained by applying the definition of steady state: the value of the dynamical variable at which the rate of change is zero, $\frac{dAPC_P}{dt} = 0$, which results in an easily solvable algebraic equation.

An alternative for finding the steady state is using a rate balance plot[162]. Despite being more computationally involved, this method can provide an intuitive sense of how the steady state changes with a change in an input or parameter. The principle of the rate balance plot is that the positive and negative terms of a differential equation are plotted as functions of the dynamical variable. The value of the dynamical variable at which the two terms are equal (and the curves cross each other) represents the steady state (Fig. 1.6 left). Further, the curves of the rate balance plot can be calculated for different values of one input, such as Cdk1, in this case. By plotting the steady state as a function of the input generates a bifurcation diagram (Fig. 1.6 right). Such plots are indispensable tools for understanding the qualitative behaviour of dynamical variables and will be used throughout this thesis.

Notice that the response of APC_P to Cdk1, given ODE 1.1, is hyperbolic. This relationship is a direct consequence of the assumed linearity in phosphorylation and dephosphorylation terms. The next sections focus on the change in this response as nonlinearities are introduced.

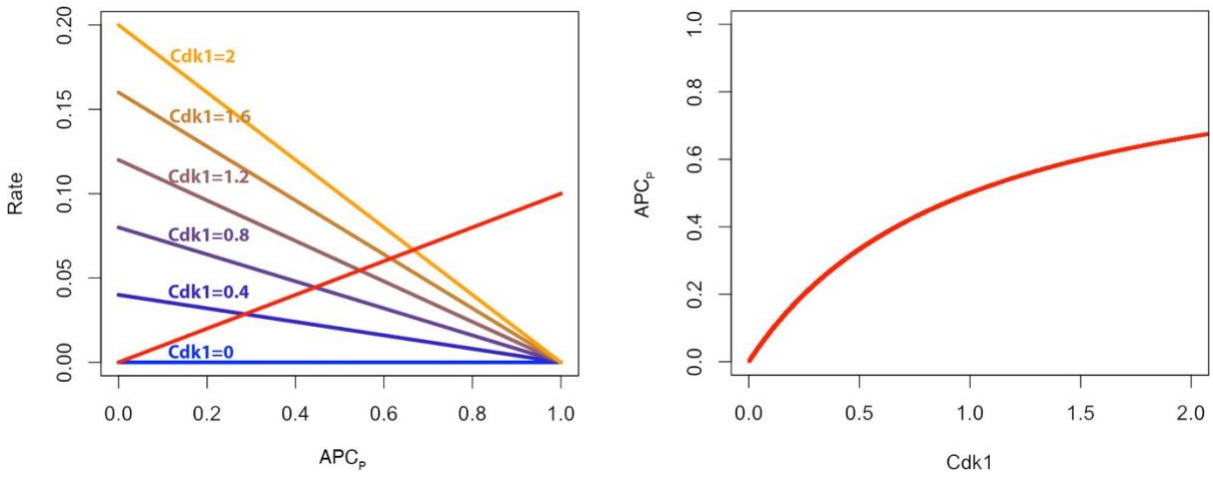

Fig. 1.6 – Steady state response of mass action phosphorylation and dephosphorylation – Left: rate balance plot for Eq. 1.1; the forward rate is plotted for different values of Cdk1, using a colour gradient that runs from blue to orange. The reverse rate is not affected by changes in the Cdk1 parameter, and is plotted as a linear function in red. Notice that as the steepness of the forward rate function increases, the change in APC_P steady state decreases, given the same increment change in Cdk1. This accounts for hyperbolic response of APC_P, as shown by the bifurcation diagram with respect to Cdk1 (Right). The parameter values are: kp_{APC}=0.1, kdp_{APC}=0.1, APC_T=1.

1.3.2 Nonlinearity. Sigmoid (hypersensitive) responses

Equation 1.1 assumes that the rate of (de)phosphorylation increases linearly with substrate concentration. However, it is conceivable that at least in some situations, the concentration of enzyme is much lower than that of the substrate. Consequently, assuming Michaelis-Menten (saturable) kinetics may be more suitable than mass action. Subsequently, ODE 1.1 can be updated:

$$\frac{dAPC_P}{dt} = kp_{APC} \cdot Cdk1 \cdot \frac{APC}{j1 + APC} - kdp_{APC} \cdot PP2A \cdot \frac{APC_P}{j2 + APC_P} \qquad (1.2)$$

Where $APC = APC_T - APC_P$, the dephosphorylated concentration, and j1, j2 are the Michaelis constants for the phosphorylation and dephosphorylation reactions, respectively. This means that the forwards and backwards reaction rates will show a hyperbolic response with respect to the Cdk1 concentration (Fig. 1.7 left). Notice that this has an interesting consequence: The steady state level of APC_P changes significantly only when Cdk1 is approximately 1, but changes very little when Cdk1 is either much greater or lower than that. Plotting the bifurcation diagram reveals that APC_P has a

sigmoid response to Cdk1 (Fig. 1.7 right). This phenomenon is known as zero-order ultrasesitivity[162], because it occurs under kinase and phosphatase saturation (i.e. the substrate concentration is much greater than the Michaelis constant), such that the rate of reaction is effectively zero-order with respect to the (de)phosphorylated APC concentration. It turns out that the steady state can be calculated analytically, according to the Goldbeter-Koshland function[163]. First, let:

$$V_1 = kp_{APC} \cdot Cdk1 \qquad V_{-1} = kdp_{APC} \cdot PP2A \qquad J1 = \frac{j1}{APC_T} \qquad J2 = \frac{j2}{APC_T}$$

Then, the Goldbeter-Koshland equilibrium is given by:

$$\frac{APC_P}{APC_T} = \frac{2 \cdot J2 \cdot V_1}{B + \sqrt{B^2 - 4 \cdot J2 \cdot V_1 \cdot (V_{-1} - V_1)}}$$

Where $B = V_{-1} - V_1 + J1 \cdot V_{-1} + J2 \cdot V_1$

This equation does not provide much intuition into the steady state response of a dynamical variable to an input. However, in this thesis, I occasionally use this function to model sigmoid responses, as an alternative to the more commonly used Hill function, particularly when the competition between a kinase and phosphatase for a substrate has a physiologically relevant effect.

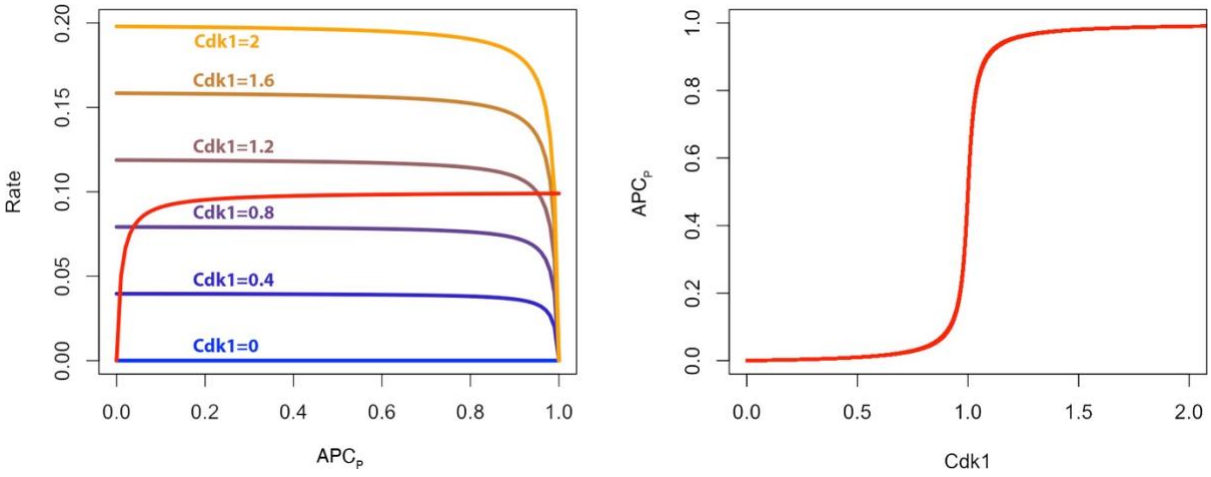

Fig. 1.7 – Steady state response of Michaelis-Menten phosphorylation and dephosphorylation – Left: rate balance plot for Eq. 1.2. Increasing Cdk1 leads to an increase in the asymptote of the forward

rate function (corresponding to Vmax). The colour coding is consistent with the previous figure. Right – APC_P vs Cdk1 bifurcation diagram, showing a sigmoid response. Parameter values: j1=j2=0.01, with the rest unchanged.

The validity of the assumption of enzyme saturation *in vivo* has been called into question[19]. This is because the concentration of many enzymes and their protein substrates can often be comparable, such that the assumption of Michaelis-Menten kinetics, that the enzyme-substrate complex concentration is much lower than that of free substrate, might not hold. Nevertheless, CDKs may in fact be an important exception to this argument. This is because CDKs have hundreds of substrates, many of which have numerous phosphorylation sites[164–166]. Thus, it is likely that CDKs are effectively saturated through the cell cycle. Indeed, many CDK substrates, including APC/C, as modelled above, respond sigmoidally to changes in kinase activity[167–169]. Consequently, the use of the GK function is at least empirically justified.

In addition to zero-order ultrasensitivity, several other mechanisms are available for generating ultrasensitive responses, such as ordered, distributive multisite phosphorylation[170,171], stoichiometric inhibition, or positive feedback[172].

1.3.3 Positive feedback and bistability

Positive feedback is a ubiquitous regulatory motif in biological systems. One of its features is the amplification of signals. In combination with ultrasensitivity, however, it gives rise to a property known as bistability, which underpins many essential physiological features of the cell cycle control network. To illustrate this point, I refer to the regulation of the mitotic kinase. As already explained, inhibitory tyrosine phosphorylation plays an important role at the G2/M transition. As such, the effect of the Wee1 kinase and Cdc25 phosphatase can be summarised by the ODE:

$$\frac{dCdk1}{dt} = (kp + kp' \cdot Cdc25) \cdot (CycB - Cdk1) - (kdp + kdp' \cdot Wee1) \cdot Cdk1 \qquad (1.3)$$

Where *kp* and *kdp* are the basal rates of phosphorylation and dephosphorylation, while *kp'* and *kdp'* the rate constants for the enzyme catalysed reactions. For consistence with previous publications[87], I refer to the total *Cdk1* (phosphorylated and dephosphorylated) pool as *CycB*. This is because CycB protein is assumed to bind to Cdk1 completely and instantaneously, while unbound Cdk1 is assumed to be inactive.

Interestingly, Cdc25 and Wee1 are activated and inactivated by Cdk1, respectively. Thus, both variables can be expressed as functions of Cdk1 activity. For simplicity, I only consider Cdc25 here and assume Wee1 is a constant. If Cdc25 exists in an equilibrium between phosphorylated and dephosphorylated forms, established by Cdk1 and some constitutive phosphatase, the steady state level of the active (phosphorylated form) is given by a hyperbolic function of Cdk1 (c.f. ODE 1.1 steady state calculation above): $Cdc25 = \frac{Cdk1}{j3+Cdk1}$. As such ODE 1.3 can be updated:

$$\frac{dCdk1}{dt} = (kp + kp' \cdot \frac{Cdk1}{j3 + Cdk1}) \cdot (CycB - Cdk1) - (kdp + kdp' \cdot Wee1) \cdot Cdk1 \quad (1.4)$$

Calculating the rate balance plot reveals that the forward rate can be approximated by a parabolic function of *Cdk1* (Fig. 1.8 left). Intriguingly, this implies that more than one steady state can be observed for some specific values of *CycB*, since two intersections of the forward and reverse rate functions can occur. However, plotting the bifurcation diagram (Fig. 1.8 right) reveals only one steady state. This conundrum can be resolved by noting that one of the steady states is unstable and therefore is not physically observable (though it can be calculated). The existence of this unusual state can be understood according to an analogy: if stable steady states correspond to local energy minima of a reaction coordinate, two such minima must logically be separated by a local maximum. In this particular case, only a local minimum (the stable state) and the maximum (the unstable state) exist.

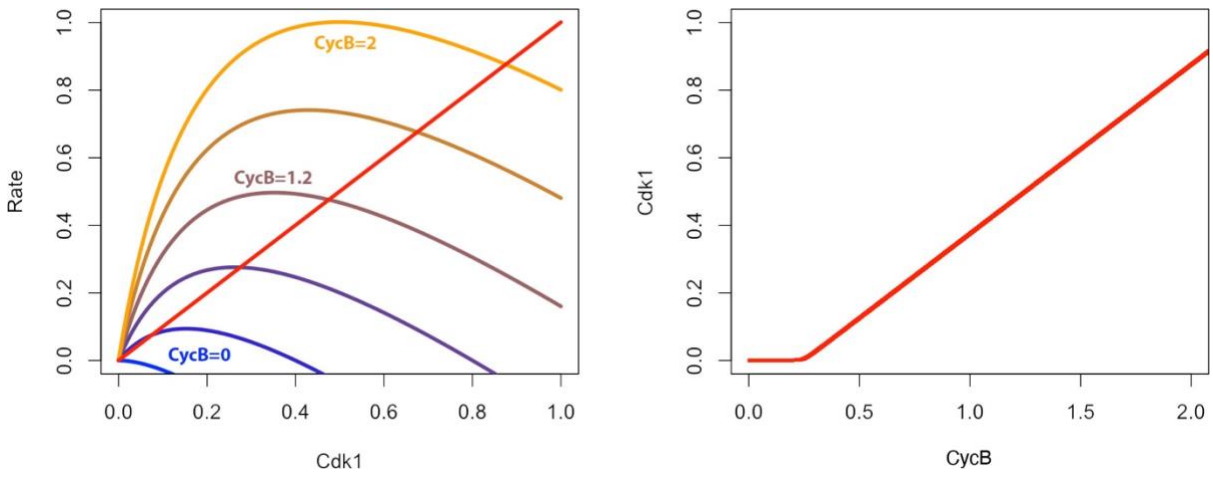

Fig. 1.8 – The equilibrium response of phosphorylation and dephosphorylation reactions, with positive feedback – Left: rate balance plot for Eq. 1.4. The forward rate is shown to vary with the value of the total Cdk1 concentration (P-ated and de-P-ated). Right – Cdk1 vs *CycB* bifurcation diagram, showing a threshold response. Parameter values: kp'=kdp'=1, kp= kdp=0.001, Wee1=1, j3=0.25.

It is tempting two ask if three steady states can be generated by an ODE, two of which are stable. On way to achieve this is to modify the forward rate to resemble a higher order polynomial, such that the forward and backward rate functions generate three intersections. For this, it can be assumed that Cdc25 is a sigmoid, rather than hyperbolic, function of Cdk1, and modelled as a Hill function:

$$\frac{dCdk1}{dt} = (kp + kp' \cdot \frac{Cdk1^n}{j3^n + Cdk1^n})(CycB - Cdk1) - (kdp + kdp' \cdot Wee1)Cdk1 \quad (1.5)$$

This approach is justified both empirically[169], and theoretically, as *Cdc25* undergoes multisite phosphorylation by *Cdk1*. The rate balance plot (Fig. 1.9 left) shows that the forward rate function is such that the resulting curve can generate three steady states in conjunction with reverse rate curve. As revealed by the bifurcation diagram (Fig. 1.9 right), this ODE gives rise to an S-shaped *Cdk1* response with respect to *CycB*. The most interesting property of this response is bistability: the existence of two distinct stable values of Cdk1 activity for the same *CycB*, separated by an unstable state. The implication of this diagram is that the state in which the system is found will depend on its history. Suppose that initially *CycB*=0. Then, as *CycB* increases, the activity of Cdk1 increases very slowly. However, once *CycB*=a, the lower steady state loses stability by merging with the unstable state at a *saddle-node bifurcation*. Subsequently, only the

upper steady state remains stable and the system is spontaneously attracted to it. This point corresponds to the sharp activation of *Cdc25*, such that *Cdk1* is dephosphorylated suddenly and its activity becomes self-sustaining. Notice that if *CycB* were to decrease, the system would not immediately revert to the lower steady state. Instead, *CycB* would have to fall below *CycB*=b. This property is known as hysteresis, and it is an essential feature of all cell cycle transitions.

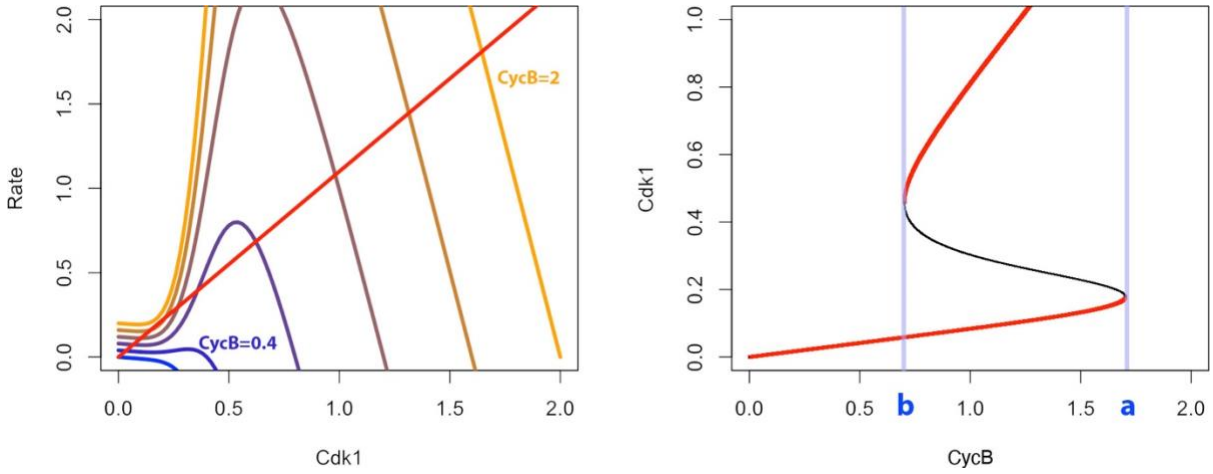

Fig. 1.9 – The equilibrium response of phosphorylation and dephosphorylation reactions, with nonlinear positive feedback – Left: rate balance plot for Eq. 1.5. For some CycB values, three intersections between the forward and backwards rate plots can be found. Right – Cdk1 vs CycB bifurcation diagram, showing a bistable response, with ON and OFF thresholds at CycB=a and CycB=b, respectively. With n=5, kp'=5, kdp'=1, kp=kdp=0.1, j3=0.5, j1= j2=0.01.

Bistability has important implications for cell cycle physiology. Most importantly, it ensures that CDK activity changes in discrete steps (assuming sufficiently long time scales), which underpins phase identity and is necessary for triggering cellular events that must be mutually exclusive[65,67,173]. Further, hysteresis ensures that cell cycle transitions are, broadly speaking, irreversible, such that the cell cycle progresses unidirectionally and deleterious events, such as rereplication, are prevented[174,175]. Both experimental and theoretical approaches have confirmed that bistable networks underpin the G2/M[87,127,176,177] and G1/S[178,179] transitions.

1.3.4 Coupled ODE systems and phase planes

In order to study the regulation of the cell cycle from a dynamical perspective, it is important to consider numerous proteins and their interactions. This can be achieved by introducing systems of coupled ODEs. In ODE 1.2, APC_P was already defined as a function of *Cdk1*. If ODE 1.5 can be rewritten such that *Cdk1* is a function of APC_P, then a system of coupled ODEs can be defined, which would allow the study of the dynamics of a more complex molecular control unit. In turn, this would enable us to study more complex molecular biological phenomena from a theoretical perspective.

Conveniently, APC/C:Cdc20 is already known to influence the activity of Cdk1, as the ubiquitin ligase can target CycB for degradation. Thus, it could be argued that CycB is a function of APC_P, noting that APC_P here refers to the phosphorylated from of APC/C, which I assume is fully and instantaneously bound and activated by the Cdc20 adaptor:

$$\frac{dCycB}{dt} = ks - (kd + kd' \cdot APC_P) \cdot CycB \tag{1.6}$$

While it is legitimate to have a system of 3 differential equations composed of ODEs 1.2, 1.5 and 1.6, the current system can be simplified by assuming that *CycB* is a much faster variable than *Cdk1* and APC_P, such that it is in pseudo-steady state with respect to the other variables. Of course, from a physiological perspective this is not justified, as protein synthesis and degradation tend to be slower than post-translational modification. As such, I will revisit this assumption in a later section. However, for the time being, I make this assumption because it allows the introduction of a new analytical tool with minimal modifications to existing equations. Thus, *CycB* is rewritten as:

$$CycB = \frac{ks}{kd \ + \ kd' \cdot APC_P}$$

Dividing the top and bottom of the fraction by *kd'*, allows us to rewrite *CycB* as $K/(K_t+APC_P)$. As such, ODE 1.5 can be expressed as:

$$\frac{dCdk1}{dt} = (kp + kp' \frac{Cdk1^n}{j3^n + Cdk1^n}) \left(\frac{K}{K_t + APC_P} - Cdk1\right) - (kdp + kdp' \cdot Wee1)Cdk1 \tag{1.7}$$

To understand the steady state behaviour of this system, the bifurcation diagrams of *Cdk1* with respect to APC_P and of APC_P with respect to *Cdk1* can be calculated and plotted on the same graph (Fig. 1.10). APC_P is still sigmoid with respect to *Cdk1*, as in figure 1.7. Equally, Cdk1 is still bistable too, but notice that the curve is Z-shaped, rather than S-shaped, since the forward rate is inversely proportional to APC_P. This plot is termed phase plane and it is an indispensable tool for understanding the stability of systems of coupled ODEs. Importantly, a system is in steady state when all variables it consists of are in steady state (i.e. when the two curves – *nullclines* – intersect each other). In this case, there are 3 steady states: two of them are stable, as they fall on the stable branches of the *Cdk1* nullcline, while the third is a saddle point, because it falls on the saddle of the *Cdk1* nullcline. In the following section, I explore how changing the parameters can affect the behaviour of the system.

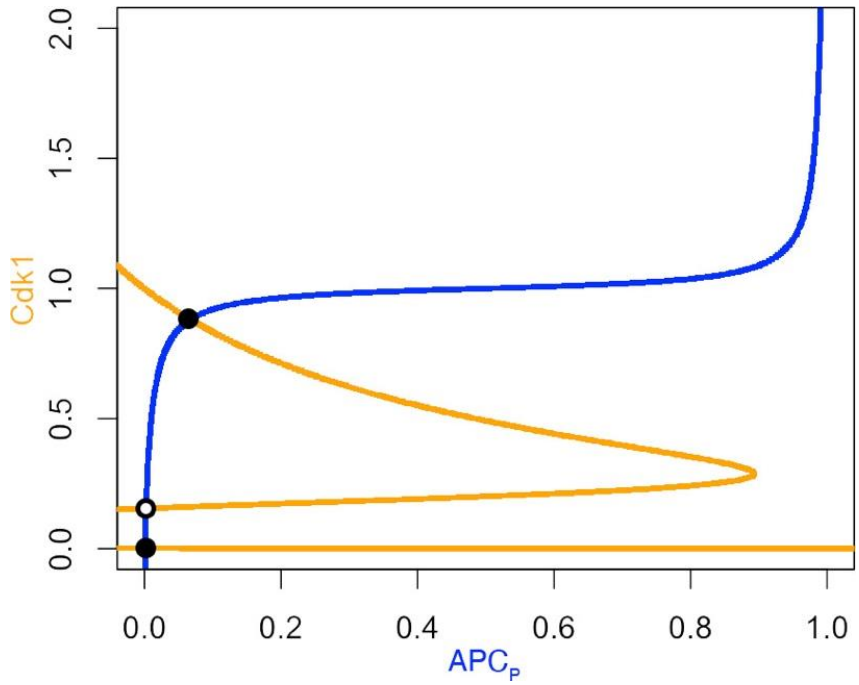

Fig. 1.10 – Cdk1 – $Cdc20_P$ phase plane – The plot is generated using equations 1.2 and 1.7, and shows that the nullclines intersect at 3 points, determining 3 steady sates. Two of these states are stable (black dots), meaning that the system can settle onto either of them, while the third state is unstable (white dot). The parameter values are: K=1, K_t=0.5, Wee1=1, kp'=kdp'=1, kp=kdp=0.001, APC_T=1, j1= j2=0.01, j3=0.25, n=5, kp_{APC}=kdp_{APC}=0.1

1.3.5 Negative feedback and oscillations

One of the features of the system introduced above is the existence of a negative feedback motif: *Cdk1* stimulates the phosphorylation of *APC*, while APC_P leads to the degradation of *CycB*, and subsequently inactivates *Cdk1*. Negative feedback can, in certain situations, act to increase the robustness of system by opposing the effect of perturbations, as might occur due to noise. More interestingly, however, negative feedback can give rise to oscillatory behaviour. The simplest case is that of delayed negative feedback. For instance, if some input triggers an antagonistic species, the delay may allow the input to accumulate to a very high level after which the antagonist is overstimulated. Consequently, the overactive inhibitor drives the input to a very low level, such that the inhibitor will eventually be suppressed. Finally, the cycle can restart with the accumulation of input. Negative feedback can be implemented by biological systems in many ways to achieve oscillations[180,181]. The main mechanism enabled by the system above and the one used throughout this thesis is that of amplified negative feedback[66]. The general principle through which amplified negative feedback oscillator is established is the coupling of a bistable switch and a negative feedback loop. Suppose that an activator is bistable (similarly to *Cdk1* here), while the inhibitor shows a hypersensitive response (c.f. APC_P). This means that the activator could rapidly switch between two states which may be either below or above the threshold for inhibitor activation. As such, the system can oscillate because when the activator is low, the inhibitor is also low, such that activator can accumulate spontaneously and trigger the positive feedback, to 'jump' to the upper steady state. Subsequently, this hyper-activates the inhibitor, which can bring the system back to baseline.

The system presented above can achieve this kind of behaviour. The only thing that prevents it from oscillating is the presence of stable steady states, which suppress the oscillation. Thus, if the unstable steady state on the saddle of the Cdk1 nullcline can be maintained while abolishing the stable steady states, then the system should oscillate spontaneously. Fortunately, this can be readily achieved by changing a few parameters,

as shown in Fig. 1.11 left. A time course simulation reveals that the system does indeed display limit cycle oscillations (Fig. 1.11 right).

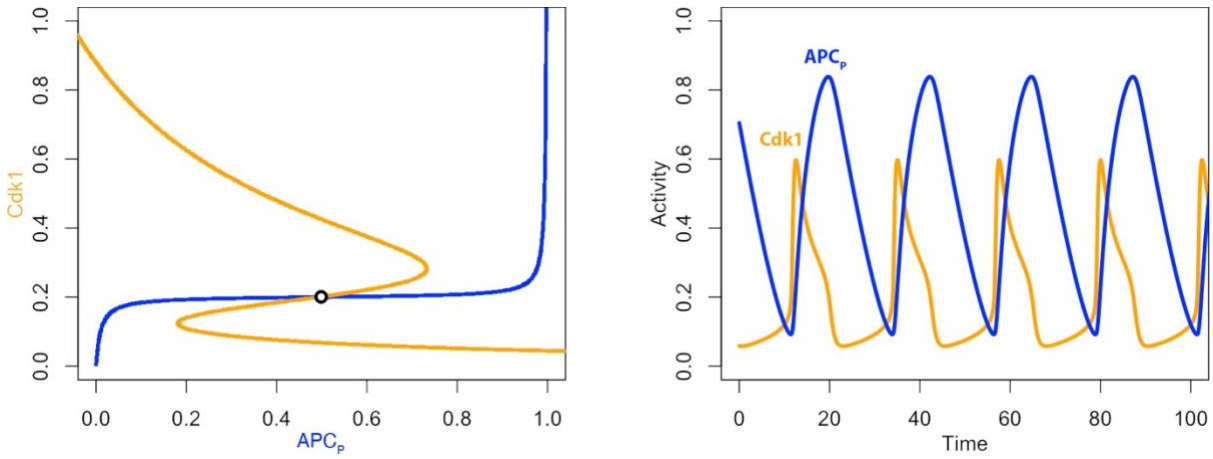

Fig. 1.11 – Amplified negative feedback oscillator dynamics – Left: Phase plane of the Cdk1-APC$_P$ system with new parameter set (kp=0.1, kdp=0.4, kp$_{APC}$=0.5, with the rest unchanged from the previous figure). The only remaining steady state is the unstable on, around which the system oscillates. Right: Time course simulation of the same system, showing periodic dynamics.

1.3.6 Reviewing dynamical assumptions

In section 1.3.4 I commented that converting *CycB* to a steady-state algebraic equation is not biologically justified, because protein synthesis and degradation cannot be expected to be faster processes than phosphorylation and dephosphorylation reactions. Nonetheless, in order to plot a phase plane, a system must consist of only 2 dynamical variables. One way to solve this issue would be to convert *Cdk1* (ODE 1.5) to a steady state algebraic equation. However, notice that this is a rather laborious task, given the nonlinear (Hill function) positive feedback term. Luckily, APC$_P$ is also a relatively fast variable, whose steady state I have already shown to be given by the Goldbeter-Koshland function. It would be tempting to suppose that the rest of the system would consist of ODEs 1.5 and 1.6. However, to be precise, ODE 1.5 must be updated as follows:

$$\frac{dCdk1}{dt} = ks + \left(kp + kp' \cdot \frac{Cdk1^n}{j3^n + Cdk1^n}\right)(CycB - Cdk1)$$
$$-(kdp - kdp' \cdot Wee1) \cdot Cdk1 - (kd + kd' \cdot APC_P) \cdot Cdk1 \qquad (1.8)$$

Notice that constant synthesis and APC/C:Cdc20-dependent degradation terms were added. These terms are essential because they account for the assumption that as the CycB protein is synthesised, it instantaneously forms a complex with Cdk1 enzyme. This complex represents the *Cdk1* variable in the model. Consequently, there ought to be no delay between the accumulation of the *CycB* and *Cdk1* dynamical variables, since they are initially identical. *Cdk1* can then be phosphorylated and inactivated (i.e. converted to the form whose quantity is given by *CycB – Cdk1*) by Wee1. Strictly speaking, without the addition of these terms, the accumulation of the *Cdk1* variable would be delayed with respect to *CycB* in a manner that depends on the dephosphorylation kinetics.

With this set-up, a phase-plane for the *Cdk1-CycB* dynamical system can be plotted (Fig. 1.12 left). Notably, the *Cdk1* nullcline still shows bistability, but the curve is S-shaped, rather than Z-shaped, because the accumulation of *CycB* favours the accumulation of the active *Cdk1* form. Similarly, the *CycB* nullcline is sigmoid, but high values of *Cdk1* reduce the steady state level of *CycB* thanks to the activation of APC/C:Cdc20. This, in essence, is the 1993 Novak & Tyson[87] view of the mitotic oscillator.

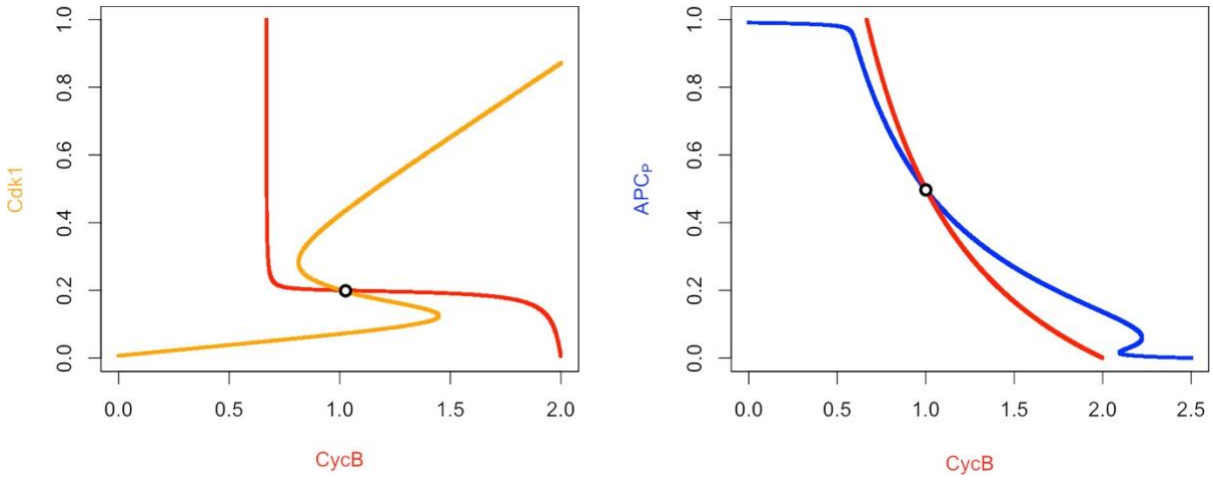

Fig. 1.12 – Alternative phase plane views of the APC-CDK1 oscillator – (left) Cdk1-CycB phase plane, under the assumption of APC_P steady state. (right) APC_P – CycB pseudo phase plane. Parameter values: ks=0.01, kd=0.005, kd'=0.01 (which correspond to the same K and K_t values as in figs. 1.10 and 1.11). All other parameters are unchanged.

For completeness, it can be asked whether there is any way to plot a CycB – APC_P phase plane, even though there is no clean way to express the Cdk1 steady state based on ODE 1.8. As a nullcline is simply the steady state response of a variable with respect to another

variable taken as a constant, it means nullclines can be plotted by calculating the bifurcation diagram of each variable of interest with respect to the other variable. Specifically, to calculate the CycB nullcline with respect to APC_P, APC_P is first turned into a constant, such that we are left with a CycB and Cdk1 system. Thus, we can calculate the steady state response of this system with respect to APC_P. A similar approach can be carried out for finding the APC_P vs CycB nullcline. Finally, both curves are plotted on the same graph to obtain a pseudo phase plane (Fig. 1.12 right). I use this approach whenever a phase plane is needed, but there is no straightforward way to compute steady state solutions for any of the dynamical variables.

1.3.7 Endo-oscillatory systems

Having established the basic principles of modelling biological control systems that will be used throughout this thesis, it is possible to return to the basic biological question that motivates this research: how can the cell cycle control network transition between the mitotic cell cycle, in which all 4 typical phases are triggered sequentially, and endocycles, in which limited subsets of phases occur periodically? I first address this question in Chapter 2, by building a mechanistic model of the mammalian cell cycle control network, which reproduces and predicts the emergence of endocycles following pharmacological or genetic perturbations. Subsequently, I aim to identify the general properties a dynamical system must satisfy in order to be able to give rise to endo-oscillations. Thus, I define an endo-oscillatory system as a multi-component dynamical system with periodic solutions, for which a subset of components can be disengaged from oscillation following parameter changes. In Chapter 3, I show such a system can consist of two mutually-inhibitory amplified negative feedback oscillators, and argue that this regulatory structure underpins the preceding mammalian model. In chapter 4, I show that a more general endo-oscillatory system can consists of a multi-stable excitable system.

2 The oscillation of mitotic kinase governs cell cycle latches in mammalian cells

2.1 Introduction

As a first step towards understanding the emergence of endo-oscillations in the mammalian cell cycle, I attempt to model the regulatory interactions that drive DNA replication and mitosis, whose perturbation might give rise to endocycles. In doing so, I hope that I can reproduce the endoreplication and Cdc20 endocycle phenotypes *in silico* (Section 1.1) and predict the conditions under which the same processes could take place in a different genetic background. Previously, mammalian endocycles have been studied in HeLa cells[75,144], which are known to suffer from aneuploidy and extensive mutations, including in cell cycle regulators, such as Rb and p53. This casts doubt on whether the experimental findings are generally applicable. Thus, an additional goal of this modelling approach is to determine whether and how equivalent phenotypes can be triggered in wild type cells and what role, if any, is played by the perturbed genes.

As a starting point for my modelling endeavour, I refer to previous attempts at modelling the cell cycle in budding yeast[157,182,183]. One of the core assumptions has been that the cell cycle represents the alternation of two states, G1 and S/G2/M, formed by the mutual antagonism between CDKs and the APC/C:Cdh1 ubiquitin ligase. Importantly, the properties of this bistable switch are such that the ON (CDK activation) and OFF (APC/C activation) transitions are driven by two different helper molecules. In the $G1_{ss}$ steady state (Fig. 2.1), APC/C:Cdh1 and CKIs are highly active and suppress CDK activity. As proliferative signals are detected, leading to the accumulation of G1-CDK activity, the CDK suppressors are inactivated, leading to the destabilisation of $G1_{ss}$ and the spontaneous attraction to the mitotic steady state M_{ss}. On the trajectory to M_{ss}, the cell drives DNA replication and chromosome condensation and alignment. Importantly, the CDK positive feedback is sufficiently strong that the bistable switch is essentially irreversible, meaning that the system cannot return to $G1_{ss}$ even if the initial stimulus is

removed. This property is the essence of the latching gate argument: the cell cannot return to the $G1_{ss}$ state without activating a different pathway, which can only be stimulated after the completion of DNA replication and the silencing of the mitotic checkpoint. The same argument applies to the return to M_{ss} after the completion of mitosis. Consequently, the latching gate mechanism accounts for the alternation of the replication licensing phase (G1) and metaphase, with replication and segregation/division happening as the cell transitions between the two states.

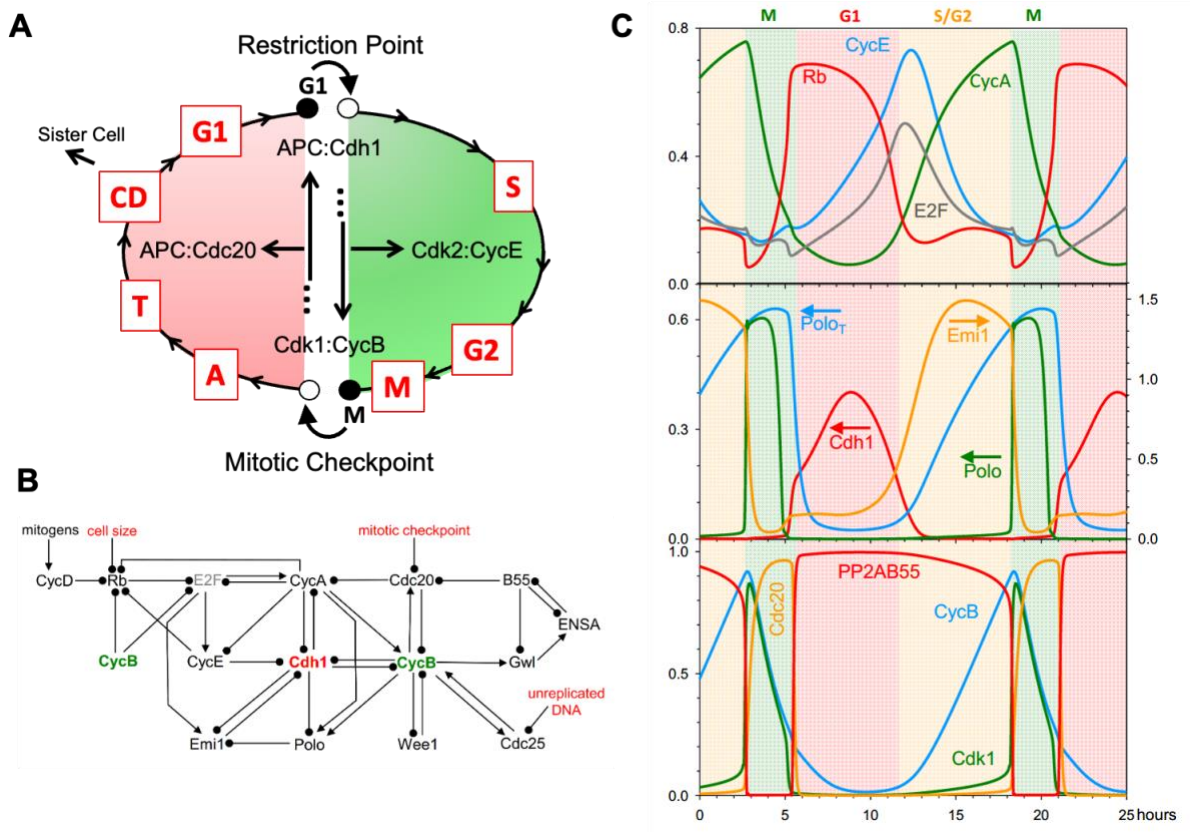

Fig. 2.1 – A model of mammalian cell cycle controls. (A) Conceptual framework. A newborn cell arrests in G1 phase (unreplicated chromosomes) at a stable steady state, denoted by the black circle labelled G1ss. Growth factors, integrated at the restriction point (RP), destabilize G1ss (white circle) and induce the cell to enter S/G2/M phase (green), replicating its chromosomes and eventually arresting in mitosis at a different stable steady state, denoted by the black circle labelled Mss, while the replicated chromosomes are coming into alignment on the mitotic spindle. When the spindle is properly assembled and all chromosomes are properly aligned, the mitotic checkpoint is lifted, destabilizing M (black circle to white circle transition) and allowing the cell to exit mitosis (red phase: M→A→T), divide (CD) and return to the G1 stable state. These events are coordinated by a complex protein interaction network, whose principal components are displayed inside the cycle. (B) An influence diagram summarizing mammalian cell cycle controls. Arrowheads indicate 'activation' or 'synthesis'; black dots indicate 'inactivation' or 'degradation'. Cdh1 and CycB play central roles in the control system. At the G1 steady state, Cdh1 and Rb are active, E2F is inactive, the levels of the cyclins (CycA, CycB, CycE and CycD) are low, as are those of Emi1 and Polo. At the M steady state, Cdh1 is inactive, and CycA, CycB and Polo are active. This diagram is converted into a set of nonlinear ordinary

differential equations in the Materials and Methods. (C) Limit-cycle oscillations of the model when all checkpoints are removed. The model ODEs are simulated numerically for the parameter values given in Table S2.1, and selected variables are plotted as functions of time (in hours). The phases of the cell cycle are colour coded: G1 (pink), S/G2 (yellow) and M (green). Notice that Rb and Cdh1 activities are high in G1 phase, CycE and E2F activities peak at the G1/S transition, Emi1 and CycA are high in G2 phase, 'Cdk1 activity' (i.e. active CycB:Cdk1) and Polo peak as the simulated cell enters mitosis, and Cdc20 peaks as the cell exits mitosis and returns to G1 phase. Meanwhile, PP2A:B55 activity is high throughout G1/S/G2 and low only when Cdk1 activity is high. Because no checkpoint controls are operational in this simulation, the cell cycle time-courses do not pause at the stable steady states (G1 and M) in A. In the middle panel, arrows indicate the corresponding y-axis for dynamic variables.

Within this framework, endocycles can be thought to occur when the central CDK-APC/C switch is perturbed such that it becomes reversible with respect to one of the 'helper' molecules that normally drives the unidirectional flipping of the switch[157]. When this happens, for instance in endoreplication cycles, the $G1_{ss}$ state can be destabilised. However, as the gate fails to latch, the cell readily 'falls back' to G1 before it is able to reach M_{ss}. This means that mitotic events are not completed, since the OFF pathway has become dispensable. As the helpers are no longer stimulated following state destabilisation, their activity wanes, leading to small amplitude oscillations.

Although this concept of the cell cycle regulation was originally presented for budding yeast, it is applicable to eukaryotic organisms in general, because B-type CDKs are a universal feature of entry into mitosis[125], and their opposition by APC/C:Cdh1 and stoichiometric CKIs is a universal feature of G1 arrest in eukaryotic cells. Here, I focus on the control system in mammalian cells. As suggested by Fig. 2.1A, the coexisting stable steady states ($G1_{ss}$ and M_{ss}) of the underlying bistable switch force the cell to follow a distinctive loop of cell-cycle events governed by two characteristic transitions: from G1 into S/G2/M as the RP is lifted, and from M into A/T/CD/G1 as the MC is lifted (Fig. 2.1A). At these transitions, the cell executes the two crucial events of the chromosome cycle: (1) passing from G1 into S/G2/M, during which the chromosomes in the cell are replicated and brought into alignment by the mitotic spindle, and (2) passing from M into A/T/CD/G1, when the sister chromatids are partitioned to two daughter cells.

These two transitions are fundamentally irreversible because of the 'latching' property of the bistable switch. Mechanistically, at the restriction point (RP), the G1 steady state becomes unstable (denoted as the black circle to white circle transition in Fig. 2.1A), and

the cell enters S/G2/M by upregulating cyclin E bound to Cdk2 (CycE:Cdk2), which promotes the rise of cyclin A bound to Cdk2 (CycA:Cdk2; involved in DNA replication) and CycB:Cdk1 (mitotic CDK activity). As the levels of CycA- and CycB-dependent kinases rise, CycE is phosphorylated and degraded by the SCF pathway (negative feedback)[93]. As CycE-dependent kinase activity drops, the control system is captured by the stable steady state M_{ss} (black circle in Fig. 2.1A). At RP, the 'G1 gate' is opened and CycE pushes the cell into S/G2/M. The negative feedback loop acts as a 'spring' to pull the gate closed, and it 'latches' at the stable M state. For the cell to divide and return to G1 phase, the silencing of mitotic checkpoint (MC) must destabilize M_{ss} (black circle to white circle transition in Fig. 2.1A), causing Cdc20-bound APC/C (APC/C:Cdc20) to polyubiquitylate/degrade both securin and CycB[184], which allows sister chromatids to separate and the cell to proceed into A and T. As CycB-dependent kinase activity drops, the APC/C dissociates from Cdc20 and binds to Cdh1[185]. The falling activity of APC/C:Cdc20 is the 'spring' that pulls the mitotic-exit gate closed and latched at the stable $G1_{ss}$ state.

Analogously to budding yeast, the irreversible 'latching' property of these gates guarantees that a proliferating cell alternates between S phase (DNA replication) and mitosis (accurate partitioning of replicated chromosomes to the two incipient daughter cells). The alternation between G1 and M is facilitated by 'helper' molecules (in mammals, a starter kinase like CycE:Cdk2 and an exit protein like APC/C:Cdc20). The helper molecules are regulated by negative feedback mechanisms that inactivate them after the transition is triggered [157,183].

The focus of this chapter is to show that this informal, verbal description of cell cycle progression is a precise mathematical consequence of the molecular interactions among the CDKs, antagonists and helpers of the mammalian cell cycle control system. The mathematical model makes interesting predictions about the appearance of 'endocycles' (e.g. periodic DNA replication without mitosis, or periodic oscillations of CycB-dependent kinase activity without DNA replication) when the latching gates at G1 and M are compromised. To validate the model's predictions, I induce both mitotic and replicative endocycles in the untransformed cell line, RPE1.

2.2 Results

2.2.1 Proposed Mechanism and Mathematical Model

To build a model of mammalian cell cycle control, I select a subset of the interactions presented in Section 1.1, as shown in Figure 2.1B. This is hardly a complete picture of the complex web of molecular interactions governing progression through the mammalian cell cycle. Any 'model' of such molecular control systems must focus solely on those interactions that are essential to the issues under consideration. In this case, I am focusing on the interactions that create and control the 'latching gates' at the G1 and M steady states, and that generate the Cdh1- and Cdc20-endocycles observed when the gates fail to latch. To probe the properties of this model, the proposed mechanism (Fig. 2.1B) is translated into a set of ordinary differential equations (ODEs), in the Methods section. Subsequently, the solutions of these ODEs are studied by numerical simulation and by analytical methods based on bifurcation theory (c.f. Section 1.2).

2.2.2 A Cell-Cycle Clock

I start the analysis of the mathematical model by numerical integration of the ODEs in the absence of checkpoint regulation at RP or MC. With appropriate choice of kinetic parameters, numerical simulations exhibit persistent limit-cycle oscillations, corresponding to an autonomous cell-cycle 'clock' (Fig. 2.1C). As expected, in G1 phase, APC/C:Cdh1 is active and unphosphorylated Rb is high. As E2F activity rises, CycE is the first E2F target to appear, because it is not degraded by Cdh1. CycE phosphorylates Cdh1 and Rb, causing their activities to drop, allowing CycA and Emi1 to rise, which are hallmarks of the G1/S transition[91,92]. The rise of CycB is delayed until CycA activates the MuvB transcription factor complex. As CycB level rises, CycB:Cdk1 is activated by the positive feedback-aided dephosphorylation of Cdk1. High CycB-dependent kinase activity activates Polo and APC/C:Cdc20, and inactivates PP2A:B55 via the Gwl-ENSA pathway. Polo activation causes degradation of Emi1 (the Cdh1 inhibitor), but Cdh1-

dependent APC/C activity remains low because high CDK activity phosphorylates Cdh1 and inhibits its association with APC/C. CycB-activated APC/C:Cdc20 maintains its activity until CycB is almost completely degraded, because the APC/C-inactivating phosphatase (PP2A:B55) is inhibited by ENSA.

2.2.3 Mapping the Cell Cycle Clock with Bifurcation Curves

The previous section illustrates that without any checkpoint control, the model of the mammalian cell cycle exhibits a limit cycle oscillation. To provide insight into this clock mechanism, I turn to bifurcation diagrams. I choose CycE and Cdc20 as bifurcation parameters, because they act as helper molecules for the G1/S and the M/G1 transitions, respectively. To characterize the state of the cell cycle control system, I choose either Cdh1 activity or the level of CycB (mitotic cyclin). Given that the changes of the two helper molecules are almost out-of-phase during the cycle (see Fig. 2.1C), I set Cdc20=0 when calculating the bifurcation diagram for CycE, and CycE=0 for the Cdc20 diagram. To be more precise, to calculate the bifurcation diagram with CycE as the parameter, I eliminate the differential equations for both d[CycE]/dt and d[Cdc20]/dt, then set [Cdc20]=0 and [CycE]=constant everywhere in the remaining ODEs. I then solve for the steady state of the remaining nonlinear ODEs as a function of the value of [CycE], using the bifurcation software AUTO as implemented in XPP[186].

The Cdh1 bifurcation diagrams (Fig. 2.2) show a Z-shaped dependence of Cdh1 steady-state activity (the red curves) on the activity of each of the helper molecules, CycE (Fig. 2.2A) and Cdc20 (Fig. 2.2B). In Fig. 2.2A, I plot Cdh1 steady-state values for both positive values of CycE (white region to the right) and negative values (grey region to the left). (Although the negative region is 'unreachable,' its significance will become apparent later). Focusing on the white region, we see that, for $0<[CycE]<0.47$, there are two coexisting, stable steady states of Cdh1 activity (on the upper and lower branches of the Z-shaped curve) separated by an intermediate branch of unstable steady states. The upper states are G1-like, and the lower states are S/G2/M-like. At [CycE]=0.47, the upper and intermediate branches merge and annihilate each other, leaving only a stable steady

state of low Cdh1 activity. [CycE]=0.47, called a 'saddle-node' bifurcation point, represents the onset of the G1/S transition. Fig. 2.2B tells a similar story. For 0<[Cdc20]<0.17, there are two coexisting, stable steady states – an M-like state (high CycB activity) and a G1-like state (low CycB activity), separated by an intermediate branch of unstable steady states. At [Cdc20]=0.17, the M-like state is annihilated at a saddle-node bifurcation point, and, for [Cdc20]>0.17, the control system must leave the M state and switch to the branch of stable, G1-like steady states.

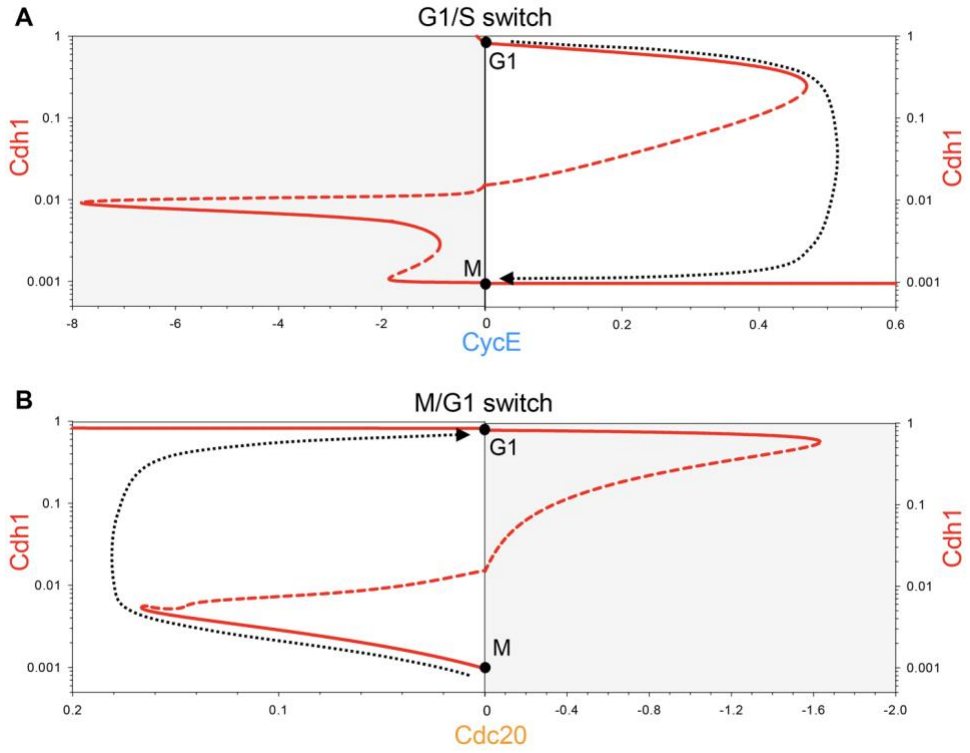

Fig. 2.2 – Bifurcation diagrams for Cdh1 activity as a function of CycE or Cdc20. (A) Steady state activity of APC/C:Cdh1 as a function of [CycE], and (B) as a function of [Cdc20]. Solid red curves: stable steady states; dashed red curves: unstable steady states; dotted black line: proposed cell cycle 'trajectory' projected onto the bifurcation diagram based on the negative feedback loops controlling CycE and Cdc20. To calculate the CycE diagram, it is assumed that [Cdc20]=0; for the Cdc20 diagram, it is assumed that [CycE]=0. The G1 and M steady states are marked by black circles. Notice that, for the CycE diagram, positive values of [CycE] are plotted to the right and negative values (shaded, which cannot be visited by the system) to the left. For the Cdc20 diagram, the positive and negative values are reversed so that the unshaded portions in panels A and B can be combined into a single panel in Fig. 2.3.

As long as the reverse transitions in both Fig. 2.2A and B occur for negative values of the switching variables, CycE and Cdc20, the G1/S and M/G1 transitions are irreversible. For instance, to leave G1 and enter S/G2/M, CycE activity must increase above 0.47 to get beyond the saddle-node bifurcation point (Fig. 2.2A). Thereafter, the trajectory drops to

the branch of lower steady states, and, as CycE is degraded (as a consequence of CycE- and CycA-dependent phosphorylation and SCF-dependent ubiquitylation), the trajectory stops at M because it can go no further. To switch back to G1 phase spontaneously, [CycE] would have fall to negative values. For this reason, spontaneous 'endocycles' are impossible, and progression through the cell cycle is an irreversible alternation between G1/S and M/G1 transitions, as suggested by the cell cycle trajectory (dotted black curves in Fig. 2.2). However, any genetic or physiological disturbances that move the 'unreachable' saddle-node bifurcation points from negative to positive values of [CycE] or [Cdc20] could potentially create endocycles (G1/S/G1/S/... or M/G1/M/G1/..., respectively).

The corresponding CycB bifurcation diagrams (Fig. S2.1) are S-shaped, mirroring the Cdh1 curve (Fig. 2.2), because Cdh1 activity and CycB levels mirror each other. When [CycE] exceeds 0.47 (Fig. S2.1A), Cdh1 becomes inactivated and CycB level increases. Given that CycE is regulated by a negative feedback loop, its level decreases after the G1/S transition, as CycB is accumulating. As CycE level falls, Cdh1 does not become reactivated, because the reactivation threshold is at a negative value of [CycE]. Both CycA (not shown) and CycB reach stable steady-state values (M) as [CycE] tends to zero.

To reactivate Cdh1, the other helper molecule, APC/C:Cdc20, must be activated above a threshold value of 0.17 (Fig. 2.2B), which leads to the degradation of both CycA and CycB (Fig. S2.1B). Because APC/C:Cdc20 activity depends upon APC/C phosphorylation by CycB:Cdk1, Cdc20 activity falls as CycB activity falls (with a slight time delay). Cdh1, on the other hand, stays active and keeps CycB at a low steady-state level (G1) after Cdc20 inactivation. CycB does not spontaneously reaccumulate, because the CycB reactivation threshold is at negative Cdc20 value (−1.6). In this way, active Cdh1 latches the gate after the cell exits mitosis.

The dotted black trajectories in Fig. 2.2 and Fig. S2.1 are 'sketched' onto the bifurcation diagrams, assuming that Cdh1 and CycB activities change very rapidly relative to the rates of change of CycE and Cdc20, respectively. Indeed, that is the case for the parameter values used to compute Fig. 2.1C, where the transitions are very abrupt (the

limit cycle has the characteristics of a 'relaxation oscillator'). However, this assumption is not necessary – the transitions could be smoother without jeopardizing the 'latching' properties of the G1/S and M/G1 transitions. These properties depend solely on (1) the bistability of the control system, (2) the saddle-node bifurcations as the helper molecule activities rise, (3) the negative feedback loops that drive back down the helper molecule activities beyond the bifurcation point, and (4) the fact that the other saddle-node bifurcation associated with the Z- or S-shaped curves lies in the unreachable region of negative helper-molecule activities.

In summary, I propose that both G1/S and M/G1 transitions in the mammalian cell cycle are governed by irreversible bistable switches ('latching gates'). To put together a picture of the whole cell cycle, I combine the two half-bifurcation diagrams calculated with CycE and Cdc20 as helper molecules (Fig. 2.3). Keep in mind that these diagrams are approximations based on reasonable simplifying assumption that the two helper molecules do not coexist, that is that Cdc20 and CycE are absent (equal to zero) on the right and left sides, respectively. The combined Cdh1 bifurcation diagram maintains the characteristic Z-shape of the Cdh1 versus CycE and Cdh1 versus Cdc20 diagrams (Fig. 2.2A). Similarly, the combined CycB bifurcation diagram (Fig. 2.3B) maintains the S-shape of the diagrams in Fig. S2.1. According to the model, opening the G1/S gate triggers the transition from G1 to the alternative M steady state and also latches the M/G1 gate by inactivating Cdh1. To open the M/G1 gate, Cdc20 must be activated (in response to successful alignment of all replicated chromosomes on the metaphase spindle); during the transition from M to G1, Cdh1 is reactivated and the M/G1 gate is locked by degrading CycB. Alternation of the two switches is guaranteed by the licensing mechanism provided by the antagonism between CycB and Cdh1. The trajectory (grey dotted line) superimposed on Fig. 2.3 is derived from the numerical simulations of the model displayed in Fig. 2.1C. Fig. 2.3 confirms that the cartoon in Fig. 2.1A is indeed a precise consequence of the molecular mechanism in Fig. 2.1B, given reasonable assumptions on the rate laws and rate constants involved in the mathematical model.

To provide further evidence for this model, I next discuss mutations that interfere with the alternation of the two switches.

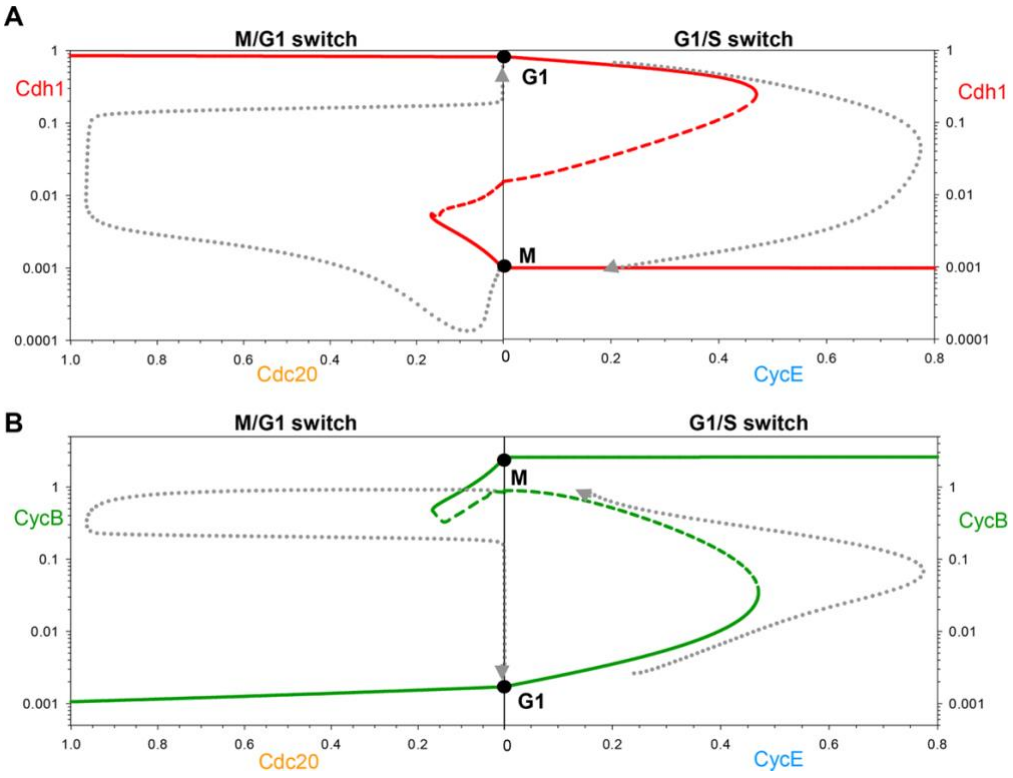

Fig. 2.3 – Two complementary views of progression through the mammalian cell cycle. (A) The changing activity of Cdh1 during progression through the mammalian cell cycle (Fig. 2.1C) is projected (grey dotted curve) onto a bifurcation diagram composed from the two panels in Fig. 2.2 (solid red curves: stable steady states; dashed red curves: unstable steady states). The negative feedback controls on CycE and Cdc20 are evident from the simulation, although they differ considerably from the proposed trajectories in Fig. 2.2. (B) CycB activity changes during the mammalian cell cycle projected onto a bifurcation diagram composed from the two panels in Fig. S2.1, with the same conventions as in panel A.

2.2.4 Endoreplication Cycles (Cdh1 Endocycles)

Mammalian cells, under certain conditions, exhibit endoreplication cycles, during which the cell undergoes multiple rounds of DNA replication without mitosis and cell division. (Under other conditions, a cell may exhibit over-replication, i.e., persistent DNA synthesis exhibiting a steady rise in DNA content.) In the context of this model, an endoreplicating cell does not visit the left sides of the diagrams in Fig. 2.3; rather it resets from G2 phase back to G1. Endoreplication can be induced in fission yeast cells by repressing synthesis of Cdc13, a major B-type mitotic cyclin[152] and in budding yeast cells by deleting five B-type cyclins (four mitotic and one S-phase cyclin)[187]. In fruit flies, both CycA and CycB are suppressed during endoreplication, which is driven by oscillating CycE-kinase activity[149]. In human cells, conditional inactivation[188] or chemical inhibition[144,189] of Cdk1 induces

discrete rounds of DNA replication without mitosis or cell division. In these endoreplicating mammalian cells, Cdh1 activity is oscillating[144,190] in the absence of any Cdc20 activation; CycB level is also oscillating, although Cdk1:CycB activity is suppressed. Therefore, endoreplication cycles are classified as Cdh1-endocycles.

These observations are consistent with the implications of the model that the irreversible nature of the G1/S switch (under normal cell cycling) requires CycB-dependent mitotic kinase activity. To illustrate this point, I have calculated the Cdh1 bifurcation diagram of the G1/S switch at different levels of Cdk1 inhibition (Fig. S2.2). The stronger Cdk1 inhibition is, the larger the Cdh1 reactivation threshold becomes. Above a critical value of Cdk1 inhibition (~25% remaining Cdk1 activity), Cdh1 can reactivate at low CycE activity, rather than relying on Cdc20 activation. Hence, Cdh1 is still bistable at low Cdk1 activity, but the G1/S switch loses its irreversible characteristic. At, say, 20% remaining Cdk1 activity, Cdh1 activity can oscillate with large amplitude as CycE activity oscillates back and forth across the two saddle-node bifurcation points (the C and ↄ 'noses' of the Z-shaped bifurcation curve).

Fig. 2.4 provides a closer view of how normal mitotic cycles are converted into Cdh1 endocycles (endoreplication cycles) as Cdk1 activity is suppressed by chemical inhibition. Mitotic cycles persist down to ~60% inhibition of CycB:Cdk1 (Fig. 2.4A), with the only effect to extend the duration of G2 phase (not shown). For 26–38% of remaining Cdk1 activity, the model predicts a G2 block, because Cdk1 is unable to self-activate through the Wee1- and Cdc25-positive feedback loops. During this G2 arrest Cdh1 is kept inactive by combined inhibition from Emi1, CycA- and CycB-bound kinases. At above 75% inhibition of Cdk1 activity, Cdh1 cannot be kept inactive, but rather Cdh1 executes large amplitude oscillations around a hysteresis loop involving the bistable G1/S switch only (Fig. 2.4B). The trajectory on the Cdh1–CycE bifurcation diagram is a projection of the simulation shown on Fig. 2.4C. During this limit cycle oscillation, the periodic appearance of CycE and CycA induces initiation of DNA replication, and the concomitant inactivation of Cdh1 could lead to the accumulation of the replication licensing inhibitor, geminin (not present in the model). Subsequent degradation of Emi1 reactivates Cdh1

and resets the endoreplicating cell back to G1, when replication origins can be relicensed for a new round of DNA replication. Therefore, the large amplitude Cdh1 oscillations are expected to drive discrete rounds of DNA replication characteristic of endoreplicating cells.

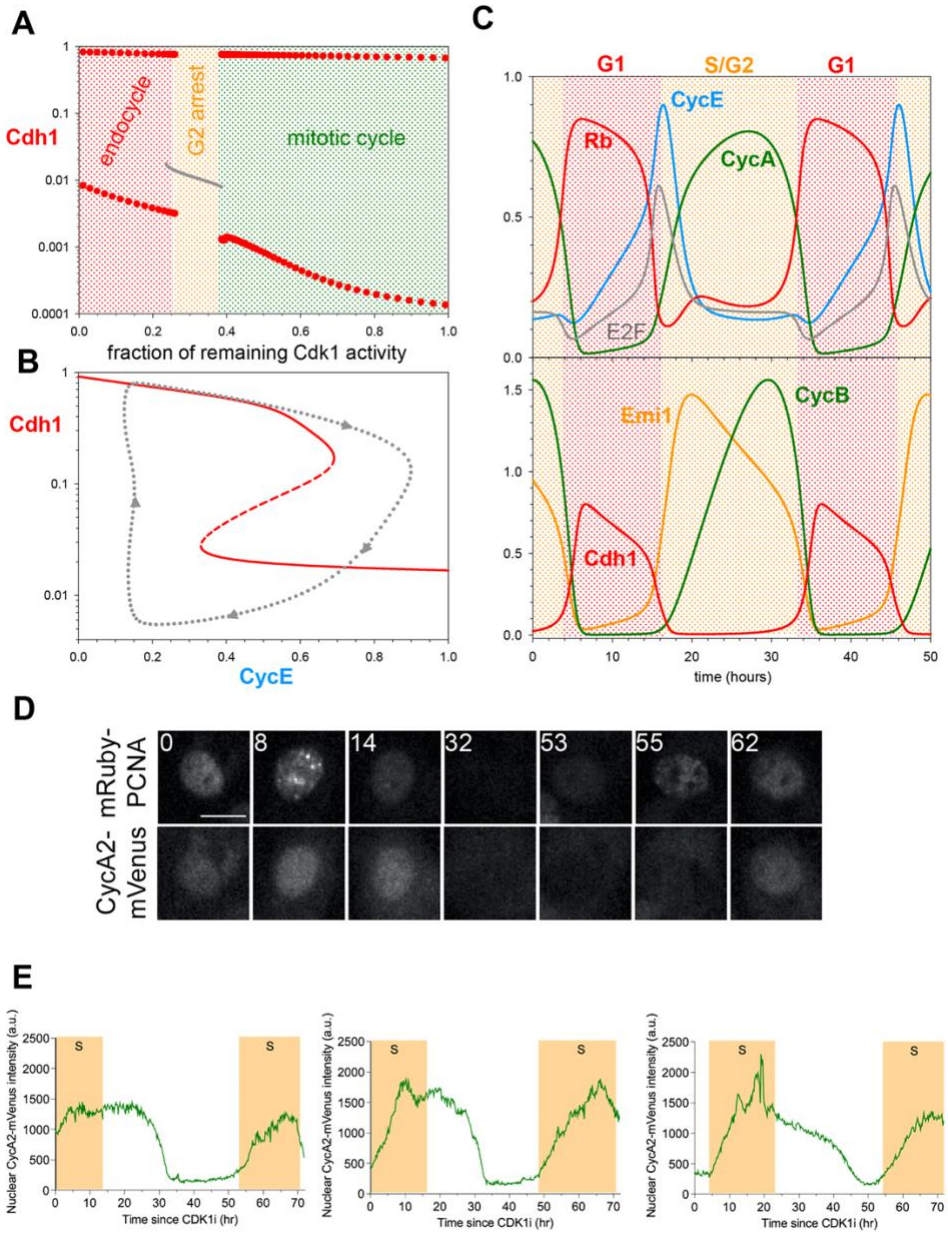

Fig. 2.4 – Cdk1 inhibition converts mitotic cycles into Cdh1 endocycles. (A) Bifurcation diagram: Cdh1 activity as a function of Cdk1 activity after chemical inhibition. Grey line: stable steady states; solid red circles: maximum and minimum excursions of Cdh1 activity during stable limit cycle oscillations. Mitotic cycles are distinguished from endoreplication cycles by the very low activity of Cdh1 (corresponding to high CycB:Cdk1 activity in mitosis). (B) Bifurcation diagram: Cdh1 activity versus CycE, for 10% remaining Cdk1 activity. As before, solid and dashed red curves indicate stable and unstable steady states, respectively; and the dotted grey line is the projection of Cdh1 limit cycle oscillations around a hysteresis loop on the bifurcation diagram. (C) Simulation of Cdh1 endocycles for 10% remaining Cdk1 activity. (D) Still images of mRuby–PCNA and CycA2–mVenus-labelled nuclei from timelapse experiments. Time shown in hours. Scale bar: 10 μm. (E) Graphs showing quantification of CycA2–mVenus in individual cells undergoing endocycles, plotted from the time of

CDK1i addition (*t*=0 h). Shaded yellow areas represent S-phase, defined by mRuby-PCNA foci. *n*=1 with four technical replicates. a.u., arbitrary units. Panels D and E, as well as the data on which they are based were authored by Alexis Barr and Ekjot Kaur.

To experimentally test these theoretical results, I collaborated with Dr. Alexis Barr and Dr. Ekjot Kaur, who first looked for endoreplication in non-transformed hTert-RPE1 (RPE1) cells after Cdk1 inhibition with the chemical inhibitor RO-3306 (Cdk1i). After 72 h treatment with Cdk1i, distinct 8n and 16n peaks were observed by flow cytometry, indicative of endoreplication (Fig. S2.3A,B). At high concentrations of Cdk1i (>7.5 μM) an increasing fraction of cells arrested in G1 (2n), presumably due to inhibition of Cdk2 at high concentrations of RO-3306, as previously reported[144]. In timelapse imaging using the mRuby–PCNA reporter to track DNA replication[191], it can be observed that endoreplication was even more prominent in 7.5 μM Cdk1i after depleting p53 from RPE1 cells using siRNA (Fig. S2.3C). Therefore, all subsequent experiments were performed under conditions of p53 depletion. To observe cell cycle dynamics in cells undergoing endocycles, timelapse imaging was used to quantify the levels of fluorescently tagged CycA2–mVenus in RPE1 cells[192] co-expressing mRuby–PCNA during treatment with Cdk1i. In the absence of Cdk1i, CycA–mVenus showed characteristic oscillations for mitotic cycles, peaking in intensity during cell rounding (mitotic entry) followed by abrupt degradation (Fig. S2.3D). In cells treated with Cdk1i, an extended G2 was observed with initially high CycA2–mVenus levels that then dropped abruptly (Fig. 2.4D,E; Fig. S2.3F). In 60% of these cells, this extended G2 was followed by a new round of DNA replication in the absence of any signs of mitosis (endoreplication, Fig. 2.4D,E; Fig. S2.3B, Movies 1 and 2). These data support the theoretical predictions.

Another way to subvert the latching gate at M is by suppressing Emi1 synthesis, as suggested by experiment[193–195]. According to the model, cells maintain their mitotic cycles up to ~40% reduction of Emi1 synthesis (Fig. S2.4A). Stronger inhibition of Emi1 synthesis leads to an abrupt reduction in the amplitude of Cdh1 and Cdk1 oscillations (Fig. S2.4A,B). For nearly complete inhibition of Emi1 synthesis, the G1/S switch stops oscillating and settles onto a stable steady state. This steady state is characterized by intermediate values of Cdh1 and CycA activities, in addition to high CycE levels. The reduced amplitude Cdh1 endocycles (caused by increased trough) and the intermediate

Cdh1 steady states are associated with continuous DNA synthesis (over-replication phenotype – when licensing and firing of replication origins are not temporally separated), based on the residual Cdh1 activity, which could maintain low levels of geminin, thereby allowing replication origin licensing and firing to proceed simultaneously.

2.2.5 Cdc20 Endocycles

Given that Cdk1 inhibition disrupts the latching property of the M gate and enables Cdh1 endocycles, it is tempting to consider the consequences of the opposite effect: sustained CycB:Cdk1 activity. Working with HeLa cells, Pomerening et al. (2008)[75] expressed an allele (Cdk1AF) for non-phosphorylatable Cdk1 subunits, which cannot be inactivated by Wee1 or Myt1 inhibitory kinases. Cdk1AF short-circuits the Cdk1 activation feedback loop operating at the G2/M transition (Fig. 2.1B). Cdk1AF-expressing cells carry out a relatively normal first mitosis, but then undergo rapid cycles of CycB accumulation and degradation at 3–6-h intervals. These fast CycB oscillations show certain resemblances to the early embryonic cell cycles of Xenopus[196]. Inspired by these experimental results, I decided to analyse the effects of weakening inhibitory Cdk1 phosphorylation in the model (Fig. 2.5). It is important to mention that the complete absence of Cdk1 inhibitory phosphorylation (Cdk1AF only) does not allow cell proliferation[197] owing to premature entry into mitosis during S phase leading to mitotic catastrophe[198].

Fig. 2.5A presents CycB versus Cdc20 bifurcation diagrams for different values of kwee, the combined activities of Wee1 and Myt1 (hereafter, simply Wee1). Decreasing Wee1 activity moves the threshold for Cdc20 inactivation (the threshold for CycB re-accumulation) to less negative values of Cdc20 (i.e. to the left in Fig. 2.5A). When Wee1 activity falls below 13%, the Cdc20 threshold for CycB re-accumulation moves to positive values of Cdc20, meaning that exit from mitosis no longer latches the cell at the G1 gate. Now the control system can oscillate around a hysteresis loop on the CycB–Cdc20 bifurcation diagram. As the inhibitory phosphorylation of Cdk1 becomes weaker, the amplitude of the Cdh1 oscillations decreases (Fig. 2.5B) and finally becomes

negligible at Wee1 activity of below 25%. In the absence of any fluctuations of Cdh1, the CycB level still shows persistent oscillations at low Wee1 activity (Fig. 2.5C). These oscillations of CycB level are exclusively driven by fluctuating activity of APC/C:Cdc20; so I call them Cdc20 endocycles. During Cdc20 endocycles, Cdh1 is kept inactive by high Emi1 levels and by strong inhibition by CycB:Cdk1 kinase (Fig. 2.5C). Given that the synthesis of both Cdh1 inhibitors is dependent on E2F activity (directly for Emi1 and indirectly – via CycA – for CycB), sustained Cdc20 endocycles require that the level of Rb must be less than the level of E2F. Indeed, these limit-cycle oscillations persist in the absence of Rb, providing an explanation for the observations by Pomerening et al. (2008) of Cdc20 endocycles in Rb-negative HeLa cells. Cdc20 endocycles can be detected in Rb-positive RPE1 cells. This evidence will be discussed after describing the role for Rb in the cell size checkpoint.

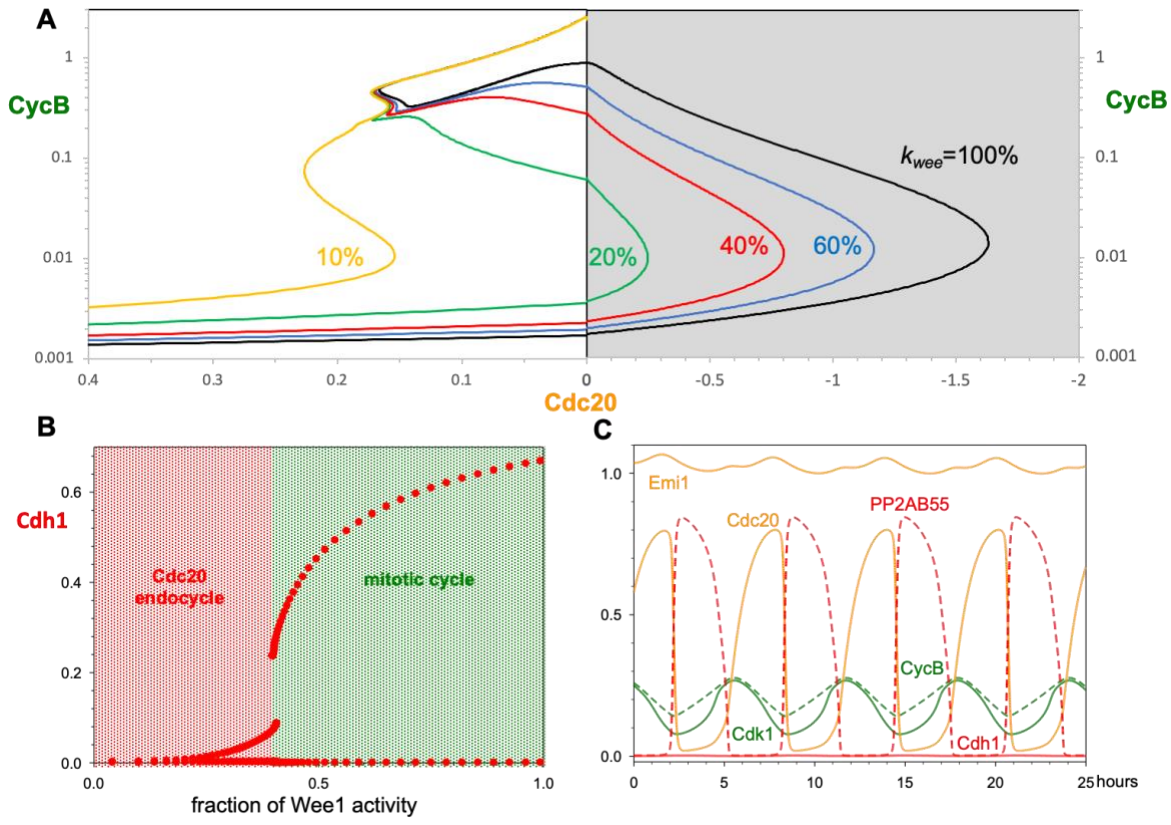

Fig. 2.5 – Inhibition of Wee1 kinase activity converts mitotic cycles into Cdc20 endocycles. (A) Bifurcation diagram: CycB activity as a function of Cdc20, for increasing inhibition of Wee1. (B) Bifurcation diagram: Cdh1 activity as a function of remaining Wee1 activity. (C) Simulated Cdc20 endocycles, for 10% Wee1 activity. The PP2AB55 trace is dashed to distinguish it from the Cdh1 trace (the solid red line at 0).

In summary, inhibition and premature activation of the mitotic kinase has opposite effects on human cell cycle switches. Cdk1 inhibition breaks the latch at the M/G1 gate and induces Cdh1 endocycles, which trigger periodic and distinct rounds of DNA replications. In contrast, in the absence of inhibitory Cdk1 phosphorylation, the G1/S latch is broken, and CycB level oscillates rapidly by the periodic activation and inactivation of Cdc20.

2.2.6 Checkpoints

Up to this point, the cell cycle control network has been treated as an oscillator, which induces cell cycle events by measuring time only. However, this underlying clock is subject to several checkpoint mechanisms that make progression through the cell cycle sensitive to a variety of important intra- and extra-cellular signals. The most important signals are (1) extracellular growth and antigrowth factors, which govern passage through the restriction point, (2) cell growth, which must be sufficient to authorize the G1/S transition, (3) DNA damage, which can block both G1/S and the G2/M transitions, (4) unreplicated DNA, which blocks mitotic entry, and (5) misaligned chromosomes, which prevent the metaphase-to-anaphase transition. These checkpoint mechanisms stop progression around the cell cycle loop (Fig. 2.3) by creating stable steady states on the upper and lower branches of the bifurcation curves near the neutral point, where both CycE and Cdc20 are absent. In this subsection, I focus on two relevant checkpoints.

The mitotic checkpoint blocks activation of Cdc20 (thereby inhibiting degradation of CycB and securin) until all chromosomes become bioriented on the mitotic spindle[53]. (Upon degradation of securin, active separase cleaves the cohesin rings that are holding sister chromatids together at bioriented centromeres, allowing the sister chromatids to be separated in anaphase). In the model, a reduction of Cdc20 activity to below ~10% normal (not shown) terminates the limit cycle oscillation of CycB and creates a stable steady state of high CycB:Cdk1 activity.

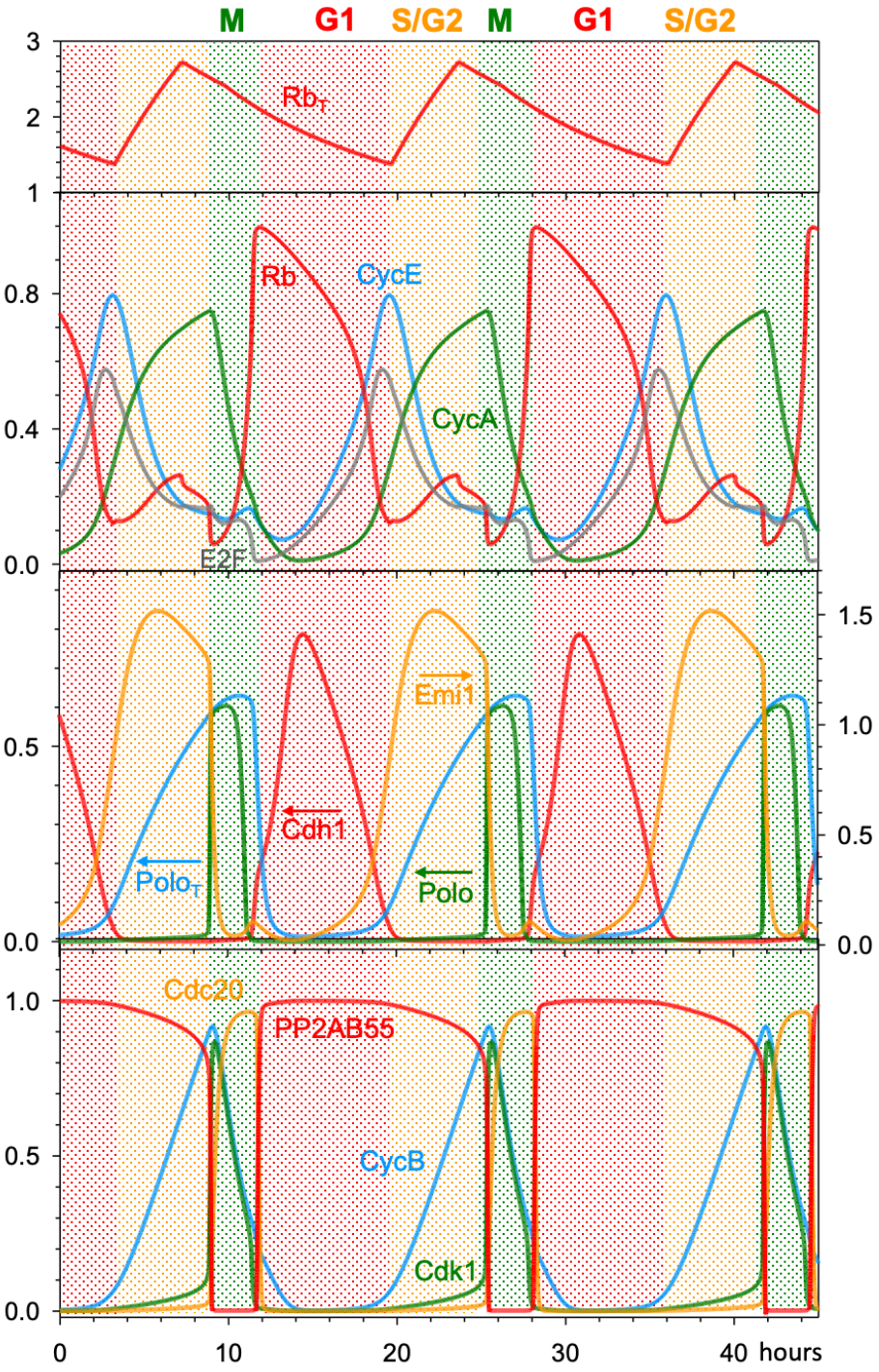

Fig. 2.6 – Growth-controlled cell cycle upon Rb dilution. The limit-cycle model is supplemented with cell cycle-regulated transcriptional control over Rb synthesis. Rb synthesis during S/G2 phase results in an increase of its concentration, followed during the remainder of the cell cycle by decreasing Rb concentration due to dilution by cell volume growth. (Notice that Rb concentration does not change during cell division). This mechanism automatically leads to two-fold fluctuations in Rb concentration when cell volume doubles over the course of a cell cycle. In the third panel, the arrow indicates that the variable is read off the right axis.

The effects of cell growth on cell cycle progression are complex and as yet not fully understood. However, it has been demonstrated that Rb plays an important role in size

control[27]. At above a certain threshold concentration, Rb inhibits the G1/S transition by blocking E2F-dependent expression of CycE, CycA and Emi1. The model is consistent with this observation because, at high Rb concentration, large amplitude mitotic oscillations of CycB become stabilized at a low, steady state concentration, which is characteristic of G1 phase (Fig. S2.5A). To illustrate the role of Rb in cell size control, I have supplemented the clock mechanism with an Rb-dilution model[27]. I assume that cells are growing linearly in volume and that the Rb synthesis rate is size-independent (proportional to the genome content) and transcriptionally regulated. Fast Rb synthesis is restricted to a 4-h-long window starting around the G1/S transition and leading to a doubling of Rb concentration; subsequently, Rb concentration is diluted out by volume growth during the remainder of the cycle (Fig. 2.6, top panel). These assumptions provide a temporal pattern for cell cycle changes in the amount of Rb molecules (Fig. S2.5B) that agrees well with the experimental data of Zatulovskiy et al. (2020)[27]. In this framework, Rb concentration (amount/volume) mirrors the cellular DNA/volume ratio and provides a possible mechanism for balanced growth and division, by adjusting the period of the cell cycle to the time required to double cell mass (Fig. S2.5A).

2.2.7 Rb-controlled Cdc20 Endocycles

Dr. Barr and Dr. Kaur have tested the possibility that constitutively active CycB:Cdk1 could induce Cdc20 endocycles in the context of size control by an Rb-dilution mechanism. The model predicts that inactivation of Wee1 after completion of mitosis induces small amplitude oscillations in CycB level, while Cdh1 is completely inhibited (Fig. 2.7A). Moreover, these Cdc20 endocycles have a period very close to the normal cycle time, because they are controlled by periodic synthesis and dilution of Rb in the following way. Cdc20 endocycles are driven by the fundamental negative feedback loop between CycB and Cdc20 (CycB:Cdk1 activates APC/C:Cdc20 and APC/C:Cdc20 degrades CycB). Given that CycB synthesis is initiated by CycA-dependent kinase and CycA is synthesized by E2F transcription factor in an Rb-dependent manner, Cdc20 endocycles (in Rb-positive cells) are controlled in part by the oscillating level of unphosphorylated Rb. Whenever unphosphorylated Rb is in stoichiometric excess over

E2F the synthesis of both CycA and CycB are on hold and the oscillation is temporarily stopped.

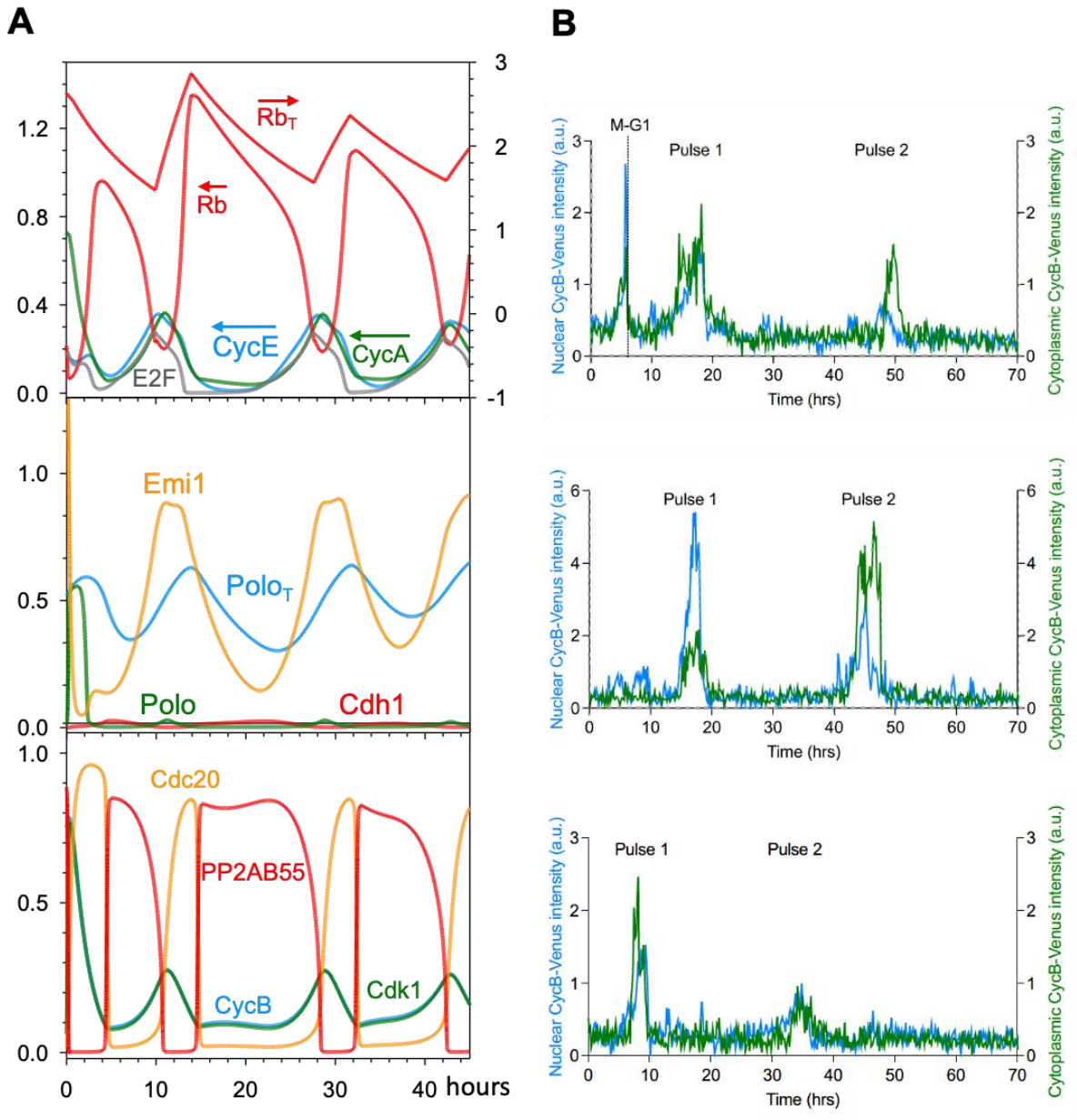

Fig. 2.7 - Cdc20 endocycles controlled by Rb dilution. (A) Numerical simulation of the growth-controlled cell cycle model with complete Wee1 inhibition (kwee=0). After exiting mitosis, CycB level shows small amplitude oscillations driven by APC/C:Cdc20 in the absence of any Cdh1 activity. Given that CycB:Cdk1 activity does not reach the mitotic threshold, both nuclear and cell division are hampered. The continuous rise in cell volume (not shown) causes an imbalance between Rb synthesis and dilution, which results in a decreasing amplitude of oscillations in Rb concentration. In the top panel, the arrow indicates that Rbtot is read off the right axis. (B) Normalised CycB1–mVenus intensity in individual cells treated with Wee1 siRNA and undergoing Cdc20 endocycles. Blue curve: nuclear CycB level in arbitrary units (a.u.); green curve: cytoplasmic CycB level, in arbitrary units. Experiment shown is n=1 and is representative of three biological repeats. Panel B, as well as the data on which it is based, was authored by Alexis Barr and Ekjot Kaur.

Using siRNA to deplete Wee1 inhibitory kinase, renders constitutively active CycB:Cdk1 complexes in Rb-positive RPE1 cells. In RPE1 cells with fluorescently tagged CycB1–mVenus[199], my collaborators used timelapse imaging to quantify CycB1 protein levels after Wee1 depletion. In control-depleted cells, CycB1–mVenus oscillates – increasing prior to mitotic entry (defined by cell rounding) and being rapidly degraded on mitotic exit (Fig. S2.6A). After Wee1 depletion by siRNA (Fig. S2.6B), cells could go through an initial early mitosis but then continue to grow in volume, becoming large, interphase-arrested cells. Despite their robust interphase arrest, cells displaying one or two bursts of CycB signal can be observed, both in the cytoplasm and in the nucleus (Fig. 2.7B; Fig. S2.6C,D, Movies 3 and 4). The rise in CycB level was not accompanied by nuclear division.

In order to show that the drop of CycB level at the end of CycB pulses is caused by APC/C:Cdc20-dependent degradation, the kinetics of CycB degradation in control- and Wee1-depleted cells were analysed by estimating the half-life (t½) of CycB1–mVenus and its specific rate of degradation (dlnCycB/dt=ln2/t½) during normal mitotic exit and in the falling phase of the CycB pulses. At mitotic exit in control cells, the half-life of CycB is ~10 min (Fig. S2.6E), consistent with a previous report[199], and its value is independent of the preceding peak of CycB. In contrast, the half-life of CycB is significantly longer and more variable in Wee1-depleted cells (Fig. S2.6E), which is a consequence of its hyperbolic (saturating) dependence on the CycB peak value (Fig. S2.6F). The peak value of CycB is a proxy for the maximum Cdk1 activity that is responsible for activating APC/C:Cdc20 in the pulses[200], and the different kinetics of CycB degradation in control- and Wee1-depleted cells is a consequence of the elimination of the abrupt activation of Cdk1 in cells depleted of Wee1. Notice, however, that, in cells treated with siRNA against Wee1, the kinetics of CycB degradation are quite similar in both M/G1 peaks (normal exit from mitosis) and in CycB pulses, suggesting that CycB degradation in the pulses, like that in normal exit from mitosis, is APC/C:Cdc20 dependent[200]. That the activation of APC/C:Cdc20 in CycB pulses is mitosis-independent is supported by the observation of a lower Cdk1AF threshold for CycB degradation than for nuclear envelope breakdown (NEBD)[201].

A similar, but less frequent, phenotype was observed with the co-depletion of Wee1 and Myt1 or inhibition of Wee1 kinase activity using the small molecule inhibitor MK1775 (Fig. S2.7A–C). The majority of these cells arrested in mitosis, which is consistent with previous observations that a complete lack of inhibitory phosphorylation is not compatible with cell proliferation[197,198].

In summary, these results support and extend the findings of Pomerening et al. (2008)[75], who first described small amplitude CycB oscillations by weakening the Cdk1 inhibitory phosphorylation in HeLa cells. In Rb-negative HeLa cells, Cdc20 endocycles behave as an autonomous oscillator[75], whereas in Rb-positive RPE1 cells, the period of Cdc20 oscillations is influenced by an Rb-mediated size control mechanism (the present work).

2.3 Discussion

2.3.1 Summary

In this chapter, I showed that a model of the mammalian cell cycle control network can reproduce the known dynamical features displayed by well-understood proteins and genes, while also supporting two types of endocycles. For this, I introduced a mathematical model of mammalian cell cycling based on a molecular network of intermediate complexity, aiming to explain the mechanistic basis of endocycling, while maintaining a level of faithfulness to the temporal profiles of regulator activities and to the roles of checkpoint mechanisms in governing progression through the mammalian cell cycle. Using bifurcation theory, I argued that the transition between wild type mitotic cycles and endocycles can be understood with reference to a toggle switch mechanism. The mutual antagonism between the protein degradation pathway initiated by APC/C:Cdh1 and its target proteins CycA, CycB and Emi1 forms the basis for this switch, in analogy to the previous proposal for yeast cells[182,183]. Indeed, hysteresis in the regulation of APC/C:Cdh1 activity is supported by experiments with mammalian cells[91].

This hypothesis is illustrated schematically in Fig. 2.1A. The bistable toggle switch (between APC/C:Cdh1 and CycB:Cdk1) is flipped 'on' (high CycB:Cdk1 activity) by CycE:Cdk2 and flipped 'off' (high APC/C:Cdh1 activity) by APC/C:Cdc20. It is found that inhibition of mitotic CycB:Cdk1 complex makes APC/C:Cdc20 dispensable for Cdh1 reactivation by disabling the 'latching' property of the mitotic steady state (M_{ss}), and converting the 'one-way' toggle switch into an autonomous oscillator regulated only by the remaining antagonistic interactions between APC/C:Cdh1 and CycA:Cdk2 plus Emi1. In the absence of mitotic CDK activity, cells are driven around a Cdh1 hysteresis loop by negative feedback regulation of the CycE:Cdk activity. The oscillations in CycE and CycA levels and their CDK activities lead to discrete rounds of DNA synthesis, analogous to yeast endoreplication cycles. This was confirmed by live-cell imaging of fluorescently tagged CycA in RPE1 cells exposed to the Cdk1 inhibitor RO3306.

2.3.2 Limitations

While the model's relative simplicity supports its methodological and conceptual tractability, it also comes at the expense of including additional molecular detail. human cell cycle model is simplified by neglecting some cell cycle regulators, including cyclin-dependent kinase inhibitors (CKIs) like p27 (CDKN1B), p21 (CDKN1A) etc. These CKIs provide an extra layer of mutual antagonism to the regulatory network (CKIs inhibit CDKs and are targeted to degradation by CDKs). There is no theoretical bottleneck to extend the model with CKIs, and this is a task for future work. For instance, p27 has a complex role in regulating the activities of CycD-bound Cdk4 and Cdk6 and CycE:Cdk2[202], thereby influencing the G1/S transition by interfering with the Rb–E2F double-negative feedback loop. p21 plays similar roles in the DNA-damage response induced by p53[203,204]. Equally, I did not model the replication origin licensing process explicitly, despite it playing a crucial role in endoreplication, as I assume it responds simply (i.e. linearly) to the activity ratio between APC/C and CDK.

Another limitation of this model is the methodology for parameter estimation. Parameters were selected so that they are broadly in line with experimentally derived

values, where known. However, in most cases, empirical kinetic and thermodynamic constants are not known with sufficient accuracy, such that they were chosen to be roughly in line with those expected for similar biochemical processes. At the same time, the parameters were fine tuned to generate dynamical behaviour that is consistent with the empirically observed endo-oscillatory properties. The justification for this approach is that, for large and complex models, experimentally derived parameters are not sufficiently accurate and precise to produce models whose behaviour mimics that of physiological systems. Consequently, future work will aim to develop the methodology for such complex model fitting and for generating the appropriate experimental data.

2.3.3 Comparison to previous modelling approaches

The proposal that G1 and M are two alternative stable steady states has first been made in the context of the budding yeast cell cycle control system[157,182,183]. Similarly to mammalian context, these alternative steady states are a consequence of double-negative feedback between B-type (Clb1–Clb5) CDKs (B-CDKs) and their antagonists (APC/C:Cdh1 and Sic1, a stoichiometric CDK inhibitor). The toggle switch concept of the yeast cell cycle has been verified by elegant experiments in budding yeast[205,206]. Recently, Novak and Tyson have shown that the toggle switch model also provides a natural explanation for two sorts of endocycles induced by perturbations of mitotic cyclin expression[157]: (1) endoreplication, where discrete rounds of DNA replication are induced by deletion of Clb1–Clb4 (the mitotic cyclins) and of Clb5 (one of the S phase cyclins)[154], and (2) Cdc14 endocycles, where periodic activation of the Cdc14 mitotic exit phosphatase occurs in the presence of a non-degradable form of the mitotic cyclin Clb2[76,207].

In yeast, Cdh1 activity oscillates during both endocycles, and it promotes the degradation of the Nrm1 transcription inhibitor and of polo kinase (Cdc5) during endoreplication and Cdc14 endocycles, respectively.

To date, numerous models of the mammalian cell cycle have also been put forward. Most of these models focus on specific cell cycle transitions, but the work of Gérard and Goldbeter[208] is particularly relevant to this work because it provides a detailed model of all phases of the mammalian cell cycle and even notes the possibility of endoreplication (Cdh1 endocycles). Pomerening et al. (2008)[75] correctly surmised that the rapid Cdc20 endocycles they observed rely on a simple negative feedback loop involving CycB, Cdk1 and Cdc20, and that these oscillations are normally overridden by a 'bistable switch' that toggles between interphase (low CycB:Cdk1 activity) and mitosis (high CycB:Cdk1 activity); but they did not back up this hypothesis with a mathematical model. To my knowledge, there are no mathematical models that account for both Cdh1 and Cdc20 endocycles in mammalian cells, or that provide a general dynamical theory of how these endocycles arise and how cells avoid their potentially deleterious consequences.

The current model can be compared to that of Tyson et al. (2001)[174], where the molecular mechanism regulating the transitions between G1 and S/G2/M phases was studied by mathematical modelling. The 2001 model focused on normal cycling (G1-S-G2-M) driven by cell growth, where the G1/S transition was controlled by a saddle-node bifurcation, but progression through S/G2/M and back to G1 was driven by an autonomous negative feedback loop (see Fig. 4 in the paper). Here, by supplementing the 2001 model with other crucial proteins and interactions, I show that the double-negative feedback loop that stabilises the G1 and M steady states is sufficiently strong to render both transitions (G1/S and M/G1) irreversible. I show that specific mutations of the feedback loops can modify the bistability range of one of the underlying switches (the G1/S or M/G1 'gate'), potentially making the transition reversible and thereby giving rise to endocycles.

2.3.4 Biological and translational relevance

The mechanism of endoreplication, suggested by the theoretical model and verified experimentally, provides a basis for understanding how whole-genome doubling (WGD) can arise during tumorigenesis. The many layers of regulation underlying the 'latching' mechanism for cell cycle progression ensure that WGD is a rare event. However, it is

estimated that up to 40% of all cancers have undergone at least one WGD event[209]. WGD can promote tumorigenesis by buffering the effects of deleterious mutations, by fostering mutations that increase cell proliferation[210–212], and – quite generally – by disrupting the genomic stability of cells[213]. By providing a mechanistic basis for how WGD can arise, the model might assist efforts to develop targeted treatments against WGD.

Endoreplication, is often induced by mutations that short-circuit mitosis by reducing or eliminating CycB-dependent kinase activity. The inverse perturbation, inducing mitosis in the presence of non-degradable CycB, generates Cdc14 endocycles in yeast cells. In mammalian cells, persistent mitotic Cdk1 activity induced by non-degradable CycB reactivates the error-correction mechanism of the mitotic checkpoint, which results in sister chromatids oscillating between the two poles (pseudo-anaphase)[214,215]. These oscillations are the consequence of tension-dependent fluctuations of Aurora B kinase activity at kinetochores. I have investigated an alternative way to disrupt the antagonistic relationship between mitotic kinase and APC/C:Cdh1 in mammalian cells, by depleting cells of Wee1 kinase, the kinase that inhibits CycB:Cdk1 activity in G2. It is found that sustained activity of CycB:Cdk1 in Wee1-depleted cells makes the CycE:Cdk dispensable for Cdh1 inactivation, because it maintains constitutive phosphorylation of Cdh1 and hence keeps it inactive. Moreover, in the absence of inhibitory phosphorylation of CycB:Cdk1, APC/C:Cdc20 is activated prematurely, which promotes early degradation of CycB and (because of the negative feedback loop between CycB and Cdc20) loss of APC/C:Cdc20 activity. Hence, although CycB:Cdk1 activity is ‘sustained’ under these conditions, the amplitude of CycB:Cdk1 oscillations is never high enough to drive the cell into mitosis or low enough to let Cdh1 make a comeback. Therefore, sustained activity of CycB:Cdk1 induces Cdc20 endocycles in the absence of Cdh1 activity, which makes the situation in human cells different from Cdc14 endocycles in yeast where Cdh1 oscillates. This dissimilarity between yeast and human cells could be a consequence of different mitotic exit phosphatases and their regulation, as well as different roles of Cdc20 and Cdh1 in the degradation of mitotic CycBs. In budding yeast, complete degradation of the Clb2 mitotic cyclin requires Cdh1, which is dephosphorylated during mitotic progression by the release of the active Cdc14 phosphatase from the nucleolus [216]. In contrast, in human cells, Cdh1 is dispensable for degradation of mitotic cyclins, and their mitotic exit

phosphatase, PP2A:B55, is kept inactive by CycB:Cdk1 via the Gwl–ENSA pathway. Despite these differences, notice that Cdc20 fluctuations induced by sustained CycB:Cdk1 activity are accompanied by large amplitude oscillations of PP2A:B55 phosphatase activity (Fig. 2.7A). This observation suggests that unregulated Cdk1 activity induces mitotic exit phosphatase endocycles in both yeast and human cells.

On the experimental front, these small amplitude oscillations in CycB level were cofirmed using live-cell imaging of RPE1 cells depleted for Wee1 by siRNA. A kinetic analysis of interphase CycB pulses suggests that the pulses are APC/C:Cdc20 dependent, consistent with the model; however, the Cdc20 dependence of the pulses still awaits direct experimental proof. Unfortunately, it was impossible to achieve efficient or sustained inhibition of Cdc20 activity, either by siRNA or by use of the APC/C inhibitors (ProTAME and APCin). The periods of CycB oscillations observed in RPE1 cells are significantly longer than those for the CycB oscillations observed by Pomerening et al. (2008)[75] in HeLa cells, which was attribute to the indirect role of an Rb-dependent size-control mechanism on the production of CycB. Importantly, Wee1 inhibitors are currently in clinical trials for cancer treatment[217]. The aim of these inhibitors is to specifically target cancer cells on the basis that only p53-mutant cancers, which rely on Wee1 to maintain the DNA damage checkpoint in G2, will be sensitive to Wee1 inhibitors[218,219]. By providing an understanding of the effects of inhibiting Wee1 in non-cancerous cells, this model might allow for a better understanding of potential side-effects of this treatment.

2.4 Materials and methods

2.4.1 Cell cycle clock model

The mathematical model presented here describes the biochemical interactions governing the mammalian cell cycle control network. It is assumed that the activity of Cyclin:CDK complexes is limited by the availability of cyclins, which strongly and rapidly bind CDKs. In early G1, cyclin expression is repressed via Rb-dependent stoichiometric

inhibition of E2F transcription factors. A fraction of total Rb (Rb_{tot}) protein is mono-phosphorylated and inactivated by CycD:CDK4/6 (the CycD parameter, here); the remaining fraction of unphosphorylated Rb_t is:

$$Rb_t = \frac{Rb_{tot}}{1 + \alpha \cdot CycD}$$

This pool of unphosphorylated Rb can be further phosphorylated by the other Cyclin:CDK complexes, such that the rate law of Rb available to inhibit E2F (i.e., Rb molecules that are unphosphorylated by any Cyclin:CDK complexes) is given by the differential equation:

$$\frac{dRb}{dt} = k_{dprb} \cdot \frac{Rb_t - Rb}{J_{rb} + Rb_t - Rb} - k_{prb} \cdot (CycE + CycA + \varepsilon \cdot Cdk1) \cdot \frac{Rb}{J_{rb} + Rb}$$

Notably, ε is a parameter that quantifies the relative activity of Cdk1. ε=1, unless it is reduced to a value 0<ε<1, to simulate Cdk1 inhibition, as indicated in the text. I am using Michaelis-Menten kinetics to describe the rates of phosphorylation ('prb') and dephosphorylation ('dprb') of Rb. Next, assuming that the Rb:E2F complex (RbE2F) is in equilibrium with the dissociated monomers, I calculate its concentration by:

$$RbE2F = \frac{BB1 - \sqrt{(BB1^2 - 4 \cdot Rb \cdot E2F_T)}}{2}$$

where $BB1 = Rb + E2F_T + K_{drbe2f}$, $E2F_T$ is the total concentration of E2F (assumed to be constant), and K_{drbe2f} is the equilibrium-dissociation constant of the complex. In addition, E2F can be independently inhibited through CDK-dependent phosphorylation:

$$\frac{dE2FP_t}{dt} = k_{pe2f} \cdot (CycA + \varepsilon \cdot Cdk1) \cdot (E2F_T - E2FP_t) - k_{dpe2f} \cdot E2FP_t$$

Consequently, the fraction of active E2F is given by:

$$E2F = (E2F_T - E2FP_t) \cdot \frac{E2F_T - RbE2F}{E2F_T}$$

Active E2F (i.e., unbound by Rb and unphosphorylated by CDKs) stimulates the transcription of a number of genes required for G1/S progression, including CycE, CycA and Emi1.

$$\frac{dCycE}{dt} = k_{scyce} \cdot E2F - (k'_{dcyce} + k''_{dcyce} \cdot CycA) \cdot CycE$$
$$\frac{dCycA}{dt} = k_{scyca} \cdot E2F - (k'_{dcyca} + k''_{dcyca} \cdot Cdc20 + k_{dcyca} \cdot Cdh1) \cdot CycA$$
$$\frac{dEmi1}{dt} = k_{semi1} \cdot E2F - (k'_{demi1} + k''_{demi1} \cdot Cdh1 + k_{demi1} \cdot Polo) \cdot Emi1$$

In addition to being regulated transcriptionally, these proteins are also targeted for degradation in specific manners, as described by the 'k_d' terms in these differential equations. CycA is a substrate of the ubiquitin ligase APC/C in complex with either Cdc20 or Cdh1; CycE is a substrate of the SCF ubiquitin ligase, after it is phosphorylated by CycA:Cdk2; and Emi1 is a target of both APC/C:Cdh1-mediated degradation and SCF-mediated degradation (after phosphorylation by Polo kinase). For these reasons, CycE—but not CycA or Emi1—accumulates in G1; in S phase, CycE is rapidly degraded in response to CycA-mediated phosphorylation; and during M phase, both CycA and Emi1 are rapidly degraded (by different pathways) and kept low throughout G1. All of these regulators cooperate to drive the inactivation of Cdh1 at the G1/S transition. The stoichiometric binding of Emi1 to Cdh1 is modelled in the same way as the binding of Rb to E2F, namely:

$$Cdh1Emi1 = \frac{BB2 - \sqrt{BB2^2 - 4 \cdot Emi1 \cdot Cdh1_{tot}}}{2}$$
$$BB2 = Emi1 + Cdh1_{tot} + K_{dc1e1}$$

The phosphorylation of Cdh1 by CycE, CycA and CycB is described by:

$$\frac{dCdh1}{dt} = k_{acdh1}(Cdh1_t - Cdh1) - (k'_{icdh1}CycE + k''_{icdh1}CycA + k_{icdh1}\,\varepsilon\,Cdk1)Cdh1$$

where $Cdh1_t$ is the Emi1-free Cdh1: $Cdh1_t = Cdh1_{tot} - Cdh1Emi1$.

As CycA accumulates, it is responsible for driving the accumulation of CycB and Polo:

$$\frac{dCycB}{dt} = k_{scycb} \cdot CycA - V_{dcycb} \cdot CycB$$

$$\frac{dPolo_T}{dt} = k'_{spolo} + k_{spolo} \cdot CycA - (k'_{dpolo} + k''_{dpolo} \cdot Cdh1) \cdot Polo_T$$

with V_{dcycb} being a degradation rate function that depends on Cdc20 and Cdh1:

$$V_{dcycb} = k'_{dcycb} + k''_{dcycb} \cdot Cdc20 + k_{dcycb} \cdot Cdh1.$$

Nevertheless, as the CycB:Cdk1 complex accumulates, it is initially inactivated by Wee1-dependent phosphorylation; the active, dephosphorylated form is denoted as Cdk1:

$$\frac{dCdk1}{dt} = k_{scycb} \cdot CycA + V_{25} \cdot (CycB - Cdk1) - V_{wee} \cdot Cdk1 - V_{dcycb} \cdot Cdk1$$

The net rate of accumulation of the dephosphorylated CycB:Cdk1 complex depends on the rate functions for the Wee1 kinase and Cdc25 phosphatase reactions:

$$V_{wee} = k'_{wee} + k_{wee} \cdot (1 - YMEP) \quad \text{and} \quad V_{25} = k'_{25} + k_{25} \cdot YMEP$$

where YMEP is a Goldbeter-Koshland function for the tyrosine-modifying enzymes:

$$YMEP = GK(k'_{pyme} \cdot CycA + k_{pyme} \cdot \varepsilon \cdot Cdk1, k_{dpyme}, J_{yme}, J_{yme})$$

The GK function depends on the activities of CycA, Cdk1 and a constitutive phosphatase, denoted by the constant parameter k_{dpyme}. The GK function was defined in section 1.2.2.

Together, CycA and Cdk1 also lead to the activation of Polo and Greatwall kinases:

$$\frac{dPolo}{dt} = (k'_{apolo} \cdot CycA + k''_{apolo} \cdot \varepsilon \cdot Cdk1) \cdot \frac{Polo_T - Polo}{J_{polo} + Polo_T - Polo} - k_{ipolo} \cdot \frac{Polo}{J_{polo} + Polo}$$

$$\frac{dpGwl}{dt} = k_{CdkGwl} \cdot \varepsilon \cdot Cdk1 \cdot (Gw_{tot} - pGwl) - (k'_{ppx} + k_{B55Gwl} \cdot PP2AB55) \cdot pGwl$$

In addition, Gwl is dephosphorylated by the PP2A:B55 phosphatase. In its active, phosphorylated form, Gwl phosphorylates ENSA (pENSAt), which leads to the formation of an inhibitory complex with the PP2A:B55 phosphatase.

$$\frac{dpENSA_t}{dt} = k_{GwENSA} \cdot pGwl \cdot (ENSA_{tot} - pENSA_t) - k_{catB55} \cdot Complex$$

Where $Complex = B55_{tot} - PP2AB55$, $B55_{tot}$ being the total concentration of B55, assumed to be constant. The dissociation of the complex is favoured by the PP2A:B55-dependent dephosphorylation of pENSA:

$$\frac{dPP2AB55}{dt} = (k_{diss} + k_{catB55}) \cdot Complex - k_{ass} \cdot (pENSA_t - Complex) \cdot (B55_{tot} - Complex)$$

Finally, when the ratio of Cdk1 and PP2AB55 increases sufficiently, Cdc20 is activated, leading to the degradation of mitotic cyclins:

$$\frac{dCdc20}{dt} = k_{acdc20} \cdot \varepsilon \cdot Cdk1 \cdot (1 - Cdc20) - k_{icdc20} \cdot PP2AB55 \cdot Cdc20$$

2.4.2 Size control model

The rate of cell volume growth is assumed to be constant (see Fig. 1K in Zatulovskiy et al. 2020[27]):

$$\frac{dV}{dt} = \mu$$

and volume is halved at cell division when Cdk1 drops below 0.7. In order to model size-controlled cycling, the total Rb concentration is converted from a constant to a dynamic variable, where the rate of synthesis in concentration units is inversely proportional to the volume:

$$\frac{dRb_{tot}}{dt} = \frac{k_{srb}}{V} - (k_{drb} + \mu) \cdot Rb_{tot}$$

The rate of Rb synthesis (k_{srb}) is assumed to change in a cell cycle dependent manner. During G1, k_{srb} is very small ($0.02h^{-1}$), which means that the amount of total Rb protein is roughly constant, given a sufficiently long (~ 30h) half-life (k_{drb} = 0.023 h^{-1}). Consequently, the protein concentration depends on the cellular volume at this stage, or in other words, the rate of change of Rb_{tot} concentration depends on the rate of volume growth, μ. Nevertheless, the amount of Rb must be replenished during each cycle; to this end, I assume that Rb expression is turned on (k_{srb} = 0.1 h^{-1}) after S-phase entry (when CycA > 0.3) for a fixed duration (4 h), ensuring that a fixed amount of protein is expressed during each cycle. This amount corresponds to a doubling of the Rb number of molecules present in early G1.

2.4.3 Parameter selection

The parameters used in the context of this model were chosen so that the simulations are in broad qualitative agreement with experimental data and with the existing understanding of cell cycle biochemistry and dynamics. In practice, this means that, for instance, rate constant for ‘fast’ reactions (such as binding and phosphorylation) are greater than those of ‘slow’ ones, such as protein synthesis and degradation. Beyond the

application of such biochemically sensible heuristics, the parameters were set in such a way that makes the simulations broadly consistent with the available data and intuition. It is important to note that applying some statistical algorithm to parameter selection does not necessarily yield more 'objective' estimates, for reasons broadly outlined in the preface. In brief, in order to carry out a statistical fitting, some error function must be minimised. The choice of such functions (e.g. coefficient of determination, root mean square error, mean absolute error etc.) is generally arbitrary, and is typically decided based on the qualitative agreement between models and data. Nevertheless, with particularly complex models as the one herein, there is typically no single parameter set that minimises the error – instead, many (potentially infinite) parameter sets can be found to locally minimise the error function[220].

In other contexts, it is possible to use kinetic and thermodynamics constants from *in vitro* experiments. However, it is notable that such constants may not apply to *in vivo* contexts, because many intracellular properties differ from those in a test tube. Finally, all experimentally measured constants are not absolute values, but rather come with a certain degree of uncertainty. If a model were constructed bottom-up from such individual measurements, the compounded error would be so great so as to make the model unusable. Consequently, the iterative process of qualitative model refinement implemented here is appropriate for the purposes of summarising knowledge of cell cycle regulation, interpreting experimental results and making qualitative predictions.

Importantly, the process of validating the model and its qualitative assumptions is not affected by the algorithm for parameter selection. Specifically, as detailed in the Results section, the model has been subjected to numerous perturbations, which reproduce the effects of mutations or gene knock-down procedures.

2.4.4 Computation

Solutions to the system of differential equations introduced above have been calculated numerically, using the XPPAUT software package with the 'Stiff' integration method. The

XPPAUT code is provided in Supplementary Information. The numerical values of the parameters are provided in Table S1, unless otherwise stated.

2.4.5 Bifurcation diagram calculation

Bifurcation diagrams of the system were calculated using the AUTO extension of XPP. Given the assumption that there is no significant activity overlap between the two helper molecules, CycE and Cdc20, the differential equations describing the two species were replaced by parameters with the same name. Thus, to plot the bifurcation diagrams with respect to CycE, Cdc20 was set to zero, and the steady state solutions of the system were calculated for a range of CycE values. Cdc20 bifurcation diagrams were calculated analogously.

2.4.6 Experimental methods

The experimental methods are available in Appendix 1.

Acknowledgements

The content of this chapter has been peer reviewed and published at the Journal of Cell Science[158]. The full author list is: Calin-Mihai Dragoi, Ekjot Kaur, Alexis R. Barr, John J. Tyson, Béla Novák. The experimental work has been carried out by ARB and EK.

3 From Dominoes and Clocks to Newton's Cradle: the cell cycle as two mutually inhibitory oscillators

3.1 Introduction

The previous chapter introduced a model of the mammalian cell cycle, which focused on reproducing endocycling and checkpoint phenomena. At its core, the model argued that the cell cycle can be conceptualised as consisting of two alternating phases. In G1 APC/C:Cdh1 is active, leading to the degradation of cyclins and geminin, which allows the assembly of pre-replicative complexes on replication origins. – In S/G2/M, CDK activity inhibits Cdh1, drives DNA replication and initiates mitosis. The succession of the two phases underpins the homeostatic mechanism whereby genome replication takes place once and only once per cell cycle, ensuring that each cell inherits exactly one copy of each of the chromosomes that make up the diploid genome. In order to ensure these physiological requirements are fulfilled, several dynamical properties must be met: the progression of the cell cycle phases must be unidirectional and irreversible, to avoid pathological changes in ploidy. The two phases must be mutually exclusive, to prevent the simultaneous licensing and firing of origins, which would lead to over-replication. Some reversible mechanism whereby the progression of the cell cycle can be stalled at various points in response to a diversity of signals must exist, to ensure that both the internal and external conditions are suitable for proliferation. In the absence of such triggers, the cell cycle should behave as an autonomous 'limit cycle' oscillator. Finally, as shown by pharmacological and genetic experiments, the progression of the G1 and S/G2/M phases can be decoupled, such that some small amplitude oscillation can, in principle, exist around each of these individual phases.

The formerly discussed model has shown that a subset of interactions in the regulatory network controlling the mammalian proliferative programme is sufficient for the emergence of these properties. Nevertheless, the high level of molecular detail assumed by the model, with the intention of accurately reproducing experimental phenotypes,

obscures the features that are strictly necessary for the establishment of such behaviour. Therefore, a minimal system that can recapitulate each of the properties mentioned above must be identified, to establish *how* these properties emerge and not just that they do. The necessity of this approach is highlighted by the fact that work on the budding yeast cell cycle has revealed analogous regulation[221]. Therefore, it is likely that the dynamical basis of endocycling is a ubiquitous property of the cell cycle control network across eukaryotes and hence, identifying general control principles is an essential step in understanding a fundamental biological process.

In this chapter, I address this challenge by taking a bottom-up approach with respect to the generation of dynamical properties, such as cell cycle transition irreversibility, endo-oscillatory behaviour and checkpoint triggering. To do so, I assume that the cell cycle control network comprises two oscillatory modules, which drive DNA replication and division, respectively. The mutual antagonism of components regulating these two modules ensures that genome replication and segregation/division follow each other sequentially. Nevertheless, this mechanism provides a simple explanation for the generation of endocycles, as a consequence of the arrest of one oscillator. Arguably, this system allows the introduction of a new paradigm of cell cycle regulatory dynamics, which builds on and extends previous analogies, such as the dominoes and the clocks (Section 1.1.2). In this chapter I propose that the cell cycle can be thought of in analogy to Newton's Cradle.

3.1.1 The cell cycle control network comprises S-phase and M-phase oscillators

If the assumption that two mutually regulated oscillators drive DNA replication and mitosis is correct, then the network proposed in the previous chapter should already contain regulatory motifs that can give rise to limit cycle oscillations, such as amplified negative feedback loops (Section 1.3.5). To show that is the case, the influence diagram in Fig. 2.1B can be rearranged to highlight the relevant interactions. Instead of focusing on the APC/C:Cdh1 – Cdk1:CycB switch, which gives rise to the top-down, latching-gate perspective on the dynamical processes that distinguish mitotic cycles from endocycles,

I group the regulators according to whether their role is mainly relevant to replication or mitosis. Thus, figure 3.1 can be plotted, where the G1/S regulators are displayed on the top row, while the G2/M ones are present on the bottom one. The interactions between CDKs and APC/C allow the two modules to interact.

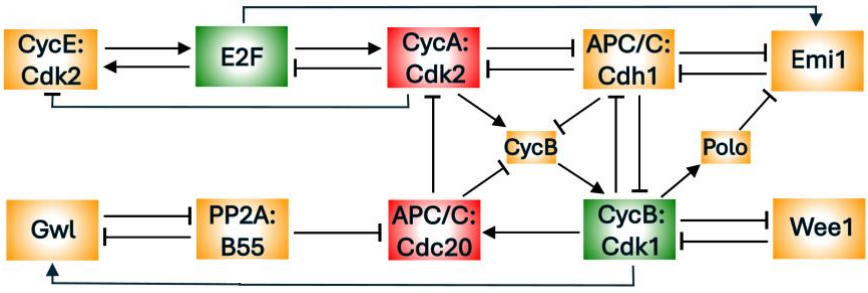

Figure 3.1 – A simplified, rearranged diagram of the cell-cycle regulatory network. Cdk2:CycA and Cdk1:CycB are the cyclin-dependent kinases that initiate DNA synthesis and mitosis, respectively. They are both involved in double-negative feedback loops with the ubiquitin ligase, APC/C:Cdh1, creating two bistable switches that control the transitions from G1 to S and from M back to G1. The network has many other positive feedback loops (+ + or − −) and negative feedback loops (+ −, + + −, etc.) that are conducive to bistable switches and periodic oscillations.

Our depiction of the eukaryotic cell cycle control system in Fig. 3.1 identifies two analogous subsystems, an S-phase control module and an M-phase control module, that regulate the activities of Cdk2:CycA and Cdk1:CycB, respectively. At the core of each module is a negative feedback loop (NFL): in the S-phase module, Cdk2:CycA inactivates its transcription factor, E2F[94], while in the M-phase module, Cdk1:CycB activates APC/C:Cdc20, which targets cyclin B for degradation[200]. An NFL, which is a necessary attribute of all biochemical oscillators[66], is composed of (at least) two components, which can be called the activator (e.g., E2F) and the inhibitor (e.g., Cdk2:CycA). Another common feature of the two modules is that, in each case, both the activator and the inhibitor are amplified by positive or double-negative feedback loops (PFL or DNFL). In the S-phase module, E2F (the activator) induces the synthesis of CycE, while CycE activates E2F by inactivating its repressor Rb (not shown). Similarly, Cdk2:CycA (the inhibitor) hyper-phosphorylates and inactivates its antagonist, APC/C:Cdh1. In the M-phase module, the activator Cdk1:CycB inhibits its inhibitory kinase, Wee1. On the other side, the inhibitor APC/C:Cdc20 is amplified by the DNFL between PP2A:B55 and Gwl [40], which can flip the inhibitory role of APC/C:Cdc20 between ON and OFF states.

According to Novak & Tyson[66], these network motifs, termed activator-inhibitor amplified negative feedback oscillators, give rise to robust and highly tunable oscillations.

This analysis shows that my presumption that two nonlinear oscillators drive the events of the cell cycle is reasonable. Thus, I first propose a 'toy' model of the double-oscillator hypothesis in terms of two symmetric, nonlinear, second-order oscillators coupled by mutual inhibition. I show that the emerging 'activity handover' between the two oscillators is sufficient to explain the alternation of S- and M-phase events observed during mitotic cycles. Subsequently, I show that permanent arrest of one oscillator may leave the other one intact, giving rise to endocycles. Lastly, I show that the double-oscillator hypothesis is perfectly consistent with the latching-gate view. After analysing the toy model, I return to the full model (Fig. 3.1, Fig. 2.1B) and show, using pseudo-phase plane analysis and bifurcation diagrams, that the CDK—APC/C mechanism known to operate in mammalian cells displays all the same qualitative features as the minimal model of four ODEs.

3.2 Results

3.2.1 A double-oscillator motif illustrates the endo-oscillatory characteristics of the cell cycle

<u>The basic oscillator Ω_1</u>

To begin building-up the double-oscillator motif, I first design a simple oscillator, Ω_1, based on two components, an activator (A_1) and an inhibitor (I_1) locked in a doubly amplified negative feedback loop (Fig. 3.2A). Strictly speaking, the double amplification is not required for oscillations: a single positive feedback loop per oscillator can yield qualitatively similar results. Nonetheless, in order to highlight the similarity of Ω_1 to the cell cycle control system (Fig. 3.1), I elect to add positive feedback to both the activator

and the inhibitor. Hence, the dynamical system Ω_1 consists of two nonlinear differential equations:

$$\frac{dA_1}{dt} = k'_{sa1} + k_{sa1}\frac{A_1^q}{L_a^q(1+rI_1)+A_1^q} - (k'_{da1} + k_{da1}\cdot A_2)\cdot A_1 \quad (3.1a)$$

$$\frac{dI_1}{dt} = k'_{si1}\cdot A_1 + k_{si1}\frac{I_1^p}{L_i^p + I_1^p} - (k'_{di1} + k_{di1}\cdot C_1)\cdot I_1 \quad (3.1b)$$

The synthesis of A_1 is autocatalytic, according to a Hill function, and inhibited by I_1, which increases the effective binding constant, $L_a{}^q(1+rI_1)$. The degradation of A_1 is promoted by A_2, the activator of the other module (Ω_2), which I take as a constant for now. The synthesis of I_1 is also autocatalytic, while its degradation is stimulated by a checkpoint component (C_1).

I start the analysis with an isolated system Ω_1, when both A_2 and C_1 are set to zero. The phase plane of this system reveals a backwards N-shaped nullcline for A_1 and an S-shaped nullcline for I_1 (Fig. 3.2B). The two nullclines intersect at an unstable steady state, and the system exhibits limit cycle oscillations (Fig. 3.2B,C).

Next, I study the effect of increasing the value of A_2. As shown in Fig. 3.2D, increasing A_2 to 0.25 squashes down the A_1-nullcline. This makes sense because both A_2 and I_1 inhibit A_1, so, when A_2 increases, a lower activity of I_1 is needed to inactivate A_1. In this case (A_2 = 0.25), the nullclines intersect in three steady states, but only the leftmost steady state (marked with a black dot) is stable. I call this stable steady state the *latched state* and A_2 the latching parameter. When the latched state exists, the dynamical system is attracted to it, suppressing oscillations and maintaining both A_1 and I_1 inactive.

To see how the system changes over a range of values of the latching parameter, I plot a bifurcation diagram (Fig. 3.2E), which shows the steady state value of A_1 as a function of A_2. The plot reveals that for sufficiently small values of A_2, A_1 oscillates with large amplitude. As A_2 increases, oscillations arrest abruptly due to the appearance of the latched state at a SNIC (*saddle node on invariant circle*) bifurcation point. The SNIC bifurcation ensures that the Ω_1 oscillator is robustly arrested as the latching parameter

increases. (Another possible scenario is that Ω_1 undergoes a Hopf bifurcation between oscillations and a latched state, as shown in Fig. S3.1. In this case, there are two different latched states with intermediate and low A_1 activity.)

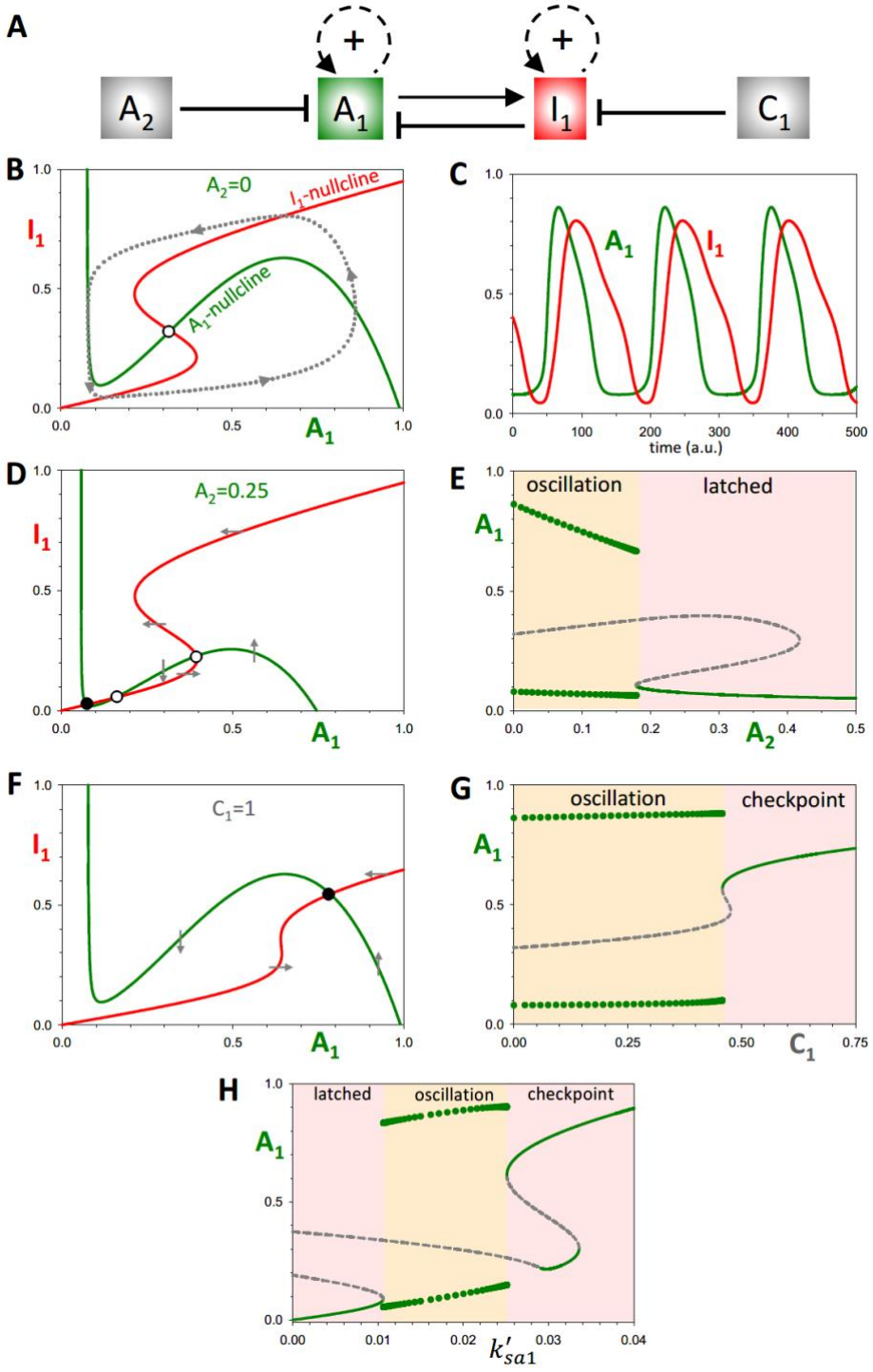

Figure 3.2 – The dynamical properties of the single oscillator, Ω1. (A) Influence diagram of the single oscillator network. A1 and I1 are the activator and inhibitor of Ω1; A2 is the 'latching' parameter and C1 the 'checkpoint' parameter. (B) Phase plane of the Ω1 system in the basal oscillating state.

Parameter values in the Material and Methods. The two nullclines intersect at an unstable steady state (o), surrounded by a limit cycle oscillation (dotted line). (C) Time course simulation of the limit cycle oscillation. (D) Phase plane for A2 = 0.25. The downward translation of the A1 nullcline results in three steady states: an unstable node (o), a saddle point (o), and a stable 'latched' state (●). The latched state arrests the oscillation at low activities of A1 and I1. (E) Bifurcation diagram of A1 with respect to the latching parameter, A2, showing the abrupt arrest of the oscillation at a SNIC bifurcation. (F) Phase plane for the checkpoint arrested system, when C1 = 1. The system arrests at a new stable steady state (●) with high A1 activity. (G) Bifurcation diagram of A1 with respect to the checkpoint parameter, C1, showing the abrupt arrest of the oscillation through a SNIC bifurcation. (H) Bifurcation diagram, A1 versus basal synthesis rate, k'sa1. On bifurcation diagrams: solid green lines, stable steady states; grey dashed lines, unstable steady states; green circles, amplitude of limit cycle oscillations.

Lastly, I study the effects of increasing the checkpoint signal. Because C_1 increases the rate of degradation of I_1, as C_1 increases, the activation of I_1 by A_1 becomes more difficult; hence, the shift of the I_1 nullcline to higher values of A_1 (Fig. 3.2F). This shift generates a new stable steady state; i.e., a *checkpoint*. Unlike the latched state, A_1 activity is high when the checkpoint is active (Fig. 3F). The bifurcation diagram, A_1 versus C_1 (Fig. 3G), shows that increasing the checkpoint signal causes the system's oscillation to be arrested at a SNIC bifurcation.

Figure 3.2H illustrates an interesting relation among the latched, oscillatory and checkpoint states. Both the latched and checkpoint states arise from SNIC bifurcations at opposite ends of the oscillatory region. The latch arrests Ω_1 at low values of A_1 whereas the checkpoint arrests Ω_1 at high values of A_1.

The coupled-oscillator system $\Omega_1\Omega_2$

I create a coupled-oscillator system by duplicating the Ω_1 oscillator as Ω_2 with dynamic variables A_2 and I_2, and coupling them (Fig. 3.3A) by assuming that A_1 promotes A_2 degradation in the same way that A_2 regulates A_1 in Eq. (3.1A). Time-course simulations confirm that the components of Ω_1 and Ω_2 oscillate out of phase (Fig. 3.3B), comparable to the out-of-phase oscillations of the S- and M-modules of the cell cycle. The oscillatory regime is surrounded by latched and checkpoint states in case of $\Omega_1\Omega_2$ coupled oscillators as well (Fig. 3.3C).

To understand the mechanism that enables this sequential, unidirectional triggering of the two oscillators, I consider the phase plane of each individual oscillator at different points in the overall cycle (Fig. 3.3D). As a starting point, I suppose that A_2 is large enough to put Ω_1 in the latched state with A_1 small, ensuring that Ω_2 is unlatched and able to oscillate freely. Consequently, A_2 increases, followed by I_2, followed by an abrupt drop in A_2. As the repression on A_1 is relieved, the Ω_1 oscillator is unlatched, A_1 increases, A_2 drops further, and Ω_2 is latched. Finally, the activity of A_1 falls, in consequence of negative feedback from I_1, which unlatches and Ω_2, allowing A_2 to increase and complete the cycle.

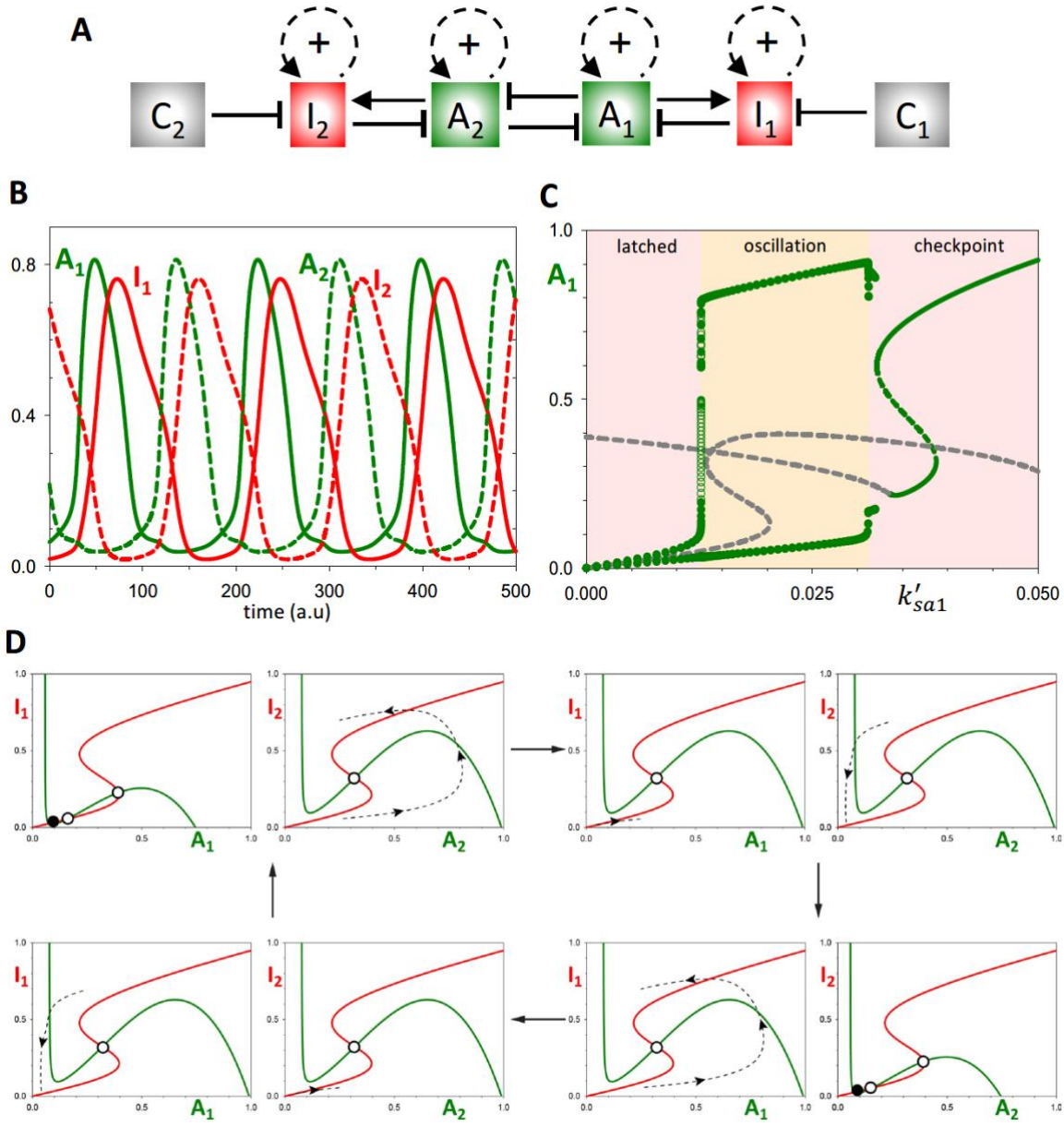

Figure 3.3 – Mutual inhibition of Ω_1 and Ω_2 results in out-of-phase oscillations. (A) Influence diagram of the $\Omega_1\Omega_2$ double-oscillator network. **(B)** Time course simulation showing the strict alternation of Ω_1 and Ω_2 components. **(C)** Bifurcation diagram, A_1 versus basal synthesis rate, k'_{sa1}. **(D)** Phase plane views of the state of the Ω_1 and Ω_2 systems at different time points in the coupled oscillation. Notice that, when the level of either activator exceeds ~0.2 (see Fig. 3.2E), the other oscillator is latched. When the level of the activator in play falls below this threshold, the other activator unlatches and begins to accumulate.

Within this framework, it is inevitable that an endocycle arises when a perturbation arrests one of the oscillators in the latched position, allowing the other to cycle periodically. For instance, suppose the suppression of Ω_1 by Ω_2 increases; say, by increasing k_{da1} (the second-order rate constant for A_2-dependent degradation of A_1). Figure 3.4B illustrates the Ω_2 endocycle when k_{da1} = 0.7. Bifurcation diagrams (Fig. 3.4C,D) reveal that these endocycles arise via a global bifurcation at $k_{da1} \approx 0.57$, where the amplitude of Ω_1 oscillations drops precipitously, while the Ω_2 oscillator presses on uninterrupted. An Ω_2 endocycle could alternatively be generated by silencing the Ω_1 oscillator internally, e.g., by decreasing the rate of A_1 accumulation.

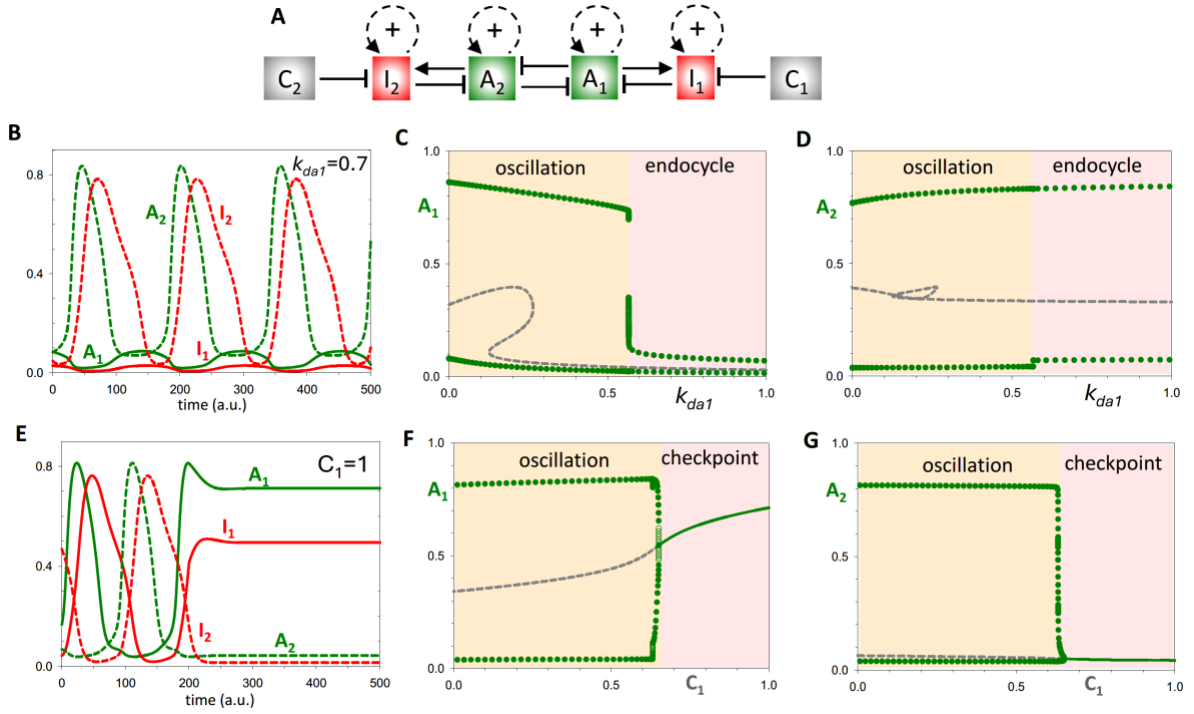

Figure 3.4. The response of the $\Omega_1\Omega_2$ double-oscillator to perturbations. (A) Influence diagram of the $\Omega_1\Omega_2$ double-oscillator network. **(B)** Time-course simulation after increasing the strength of A_2 inhibition on A_1 (k_{da1}=0.25 → 0.7), which leads to an abrupt transition to endo-oscillations. **(C,D)** Bifurcation diagrams illustrating the effects of k_{da1} on the amplitude of the oscillations. While k_{da1}>0.57 completely suppresses the inherent oscillation of Ω_1, it has little effect the Ω_2 oscillation. **(E)** Time-

course simulation after increasing the checkpoint parameter C_1=0 → 1, which arrests both oscillators. **(F,G)** Bifurcation diagrams show an abrupt transition between oscillatory and checkpoint regimes. Ω_1 arrests with high activity of A_1, while Ω_2 arrests in its latched state.

Unlike the case of an endocycle (Fig. 3.4C,D), increasing the checkpoint signal (C_1) on Ω_1 arrests both oscillators, as it should (Fig. 3.4E). By raising the value of C_1, the checkpoint prevents the accumulation of I_1, such that A_1 cannot be down-regulated. Consequently, Ω_1 arrests with a high level of A_1 (its checkpoint state) and Ω_2 arrests in its latched state. The bifurcation diagrams, A_1 and A_2 versus C_1 (Fig. 3.4F,G), show that both oscillators are suppressed at a Hopf bifurcation. Endocycles, on the other hand, arise when one oscillator is arrested in its latched state (low level of activator), allowing the other oscillator to oscillate freely (endocycle).

3.2.2 The double-oscillator motif displays the latching-gate property

The latching-gate hypothesis frames cell cycle control as a bistable switch between a G1-state of high APC/C:Cdh1 activity and an S/G2/M-state of high Cdk1:CycB activity. The G1/S transition is driven by a 'helper' protein (Cdk2:CycE) and the M/G1 transition by a different helper protein (APC/C:Cdc20). A similar view of the double-oscillator model is afforded by the bifurcation diagrams for A_1 in dependence on I_1 and I_2 as helper molecules (Fig. 3.5B). As expected, the mutual antagonism between A_1 and A_2 gives rise to a bistable switch: when $(I_1, I_2) \approx (0, 0)$, there are two alternative, stable steady states: at $(A_1, A_2) \approx (1, 0)$ and at $(A_1, A_2) \approx (0, 1)$. Notice that increasing I_1 flips A_1 OFF, but then the mutual antagonism locks Ω_1 in its OFF state, $A_1 \approx I_1 \approx 0$ and $A_2 \approx 1$. The only way to get A_1 back to its ON state is by increasing I_2. By symmetry, the same argument holds for flipping A_2 ON and OFF. In this manner, the double oscillator executes the full oscillation simulated in Fig. 3.3B. Notice that, although the mutual antagonism between A_1 and A_2 permits a stable steady state at $(A_1, A_2) \approx (0.5, 0.5)$, the cell cycle trajectory never visits this state.

Here, I return to the more realistic mechanism of the mammalian cell cycle control network in Chapter 2 and Fig. 3.1. As discussed previously, the mechanism consists of two modules for S-phase control and M-phase control, and each module has the features of a doubly amplified, negative feedback loop. Furthermore, the two modules are linked

by robust mutual antagonism between APC/C:Cdh1 and Cdk1:CycB. In the previous chapter, I proposed a biochemical kinetic model of this mechanism and probed its global dynamics. There, the antagonism between APC/C:Cdh1 and Cdk1:CycB was left intact; here, I begin by breaking the interaction between APC/C:Cdh1 and Cdk1:CycB, in order to analyse the properties of the uncoupled modules and gain understanding of how they influence each other.

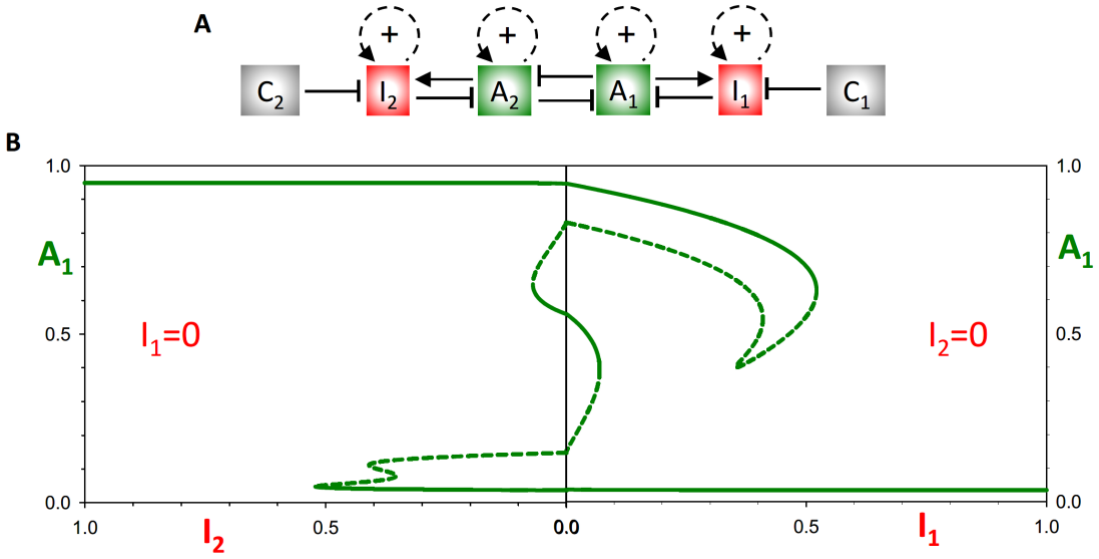

Figure 3.5. The latching-gate perspective. (A) Influence diagram of the Ω1Ω2 double-oscillator network. (B) Bifurcation diagrams. (Right panel) A1 vs I1 for I2=0. As I1 increases, A1 flips irreversibly from ON to OFF. (Left panel) A1 vs I2 for I1=0. As I2 increases, A1 flips irreversibly from OFF to ON. When A1 is ON, A2 is OFF, and vice versa, because of the antagonism between A1 and A2.

3.2.2 The mammalian mechanistic model subsumes the double oscillator motif

To analyse the S-module, I redefine the activity of Cdk1:CycB as a parameter, instead of a dynamic variable (Fig. 3.6A). Consequently, any effect of the S-module on the M-module is eliminated, as CycA:Cdk1 and APC/C:Cdh1 can no longer influence Cdk1:CycB. Likewise, the level and activity of all the components in the mitotic module remain constant. When Cdk1:CycB activity is zero, the activities of APC/C:Cdc20 and Gwl-kinase are low, while those of B55:PP2A and Wee1 are high. Hence, it is possible to analyse the dynamical properties of the S-module in isolation. To this end, I analyse the system by 'pseudo-phase plane' methods, as explained in the Materials & Methods.

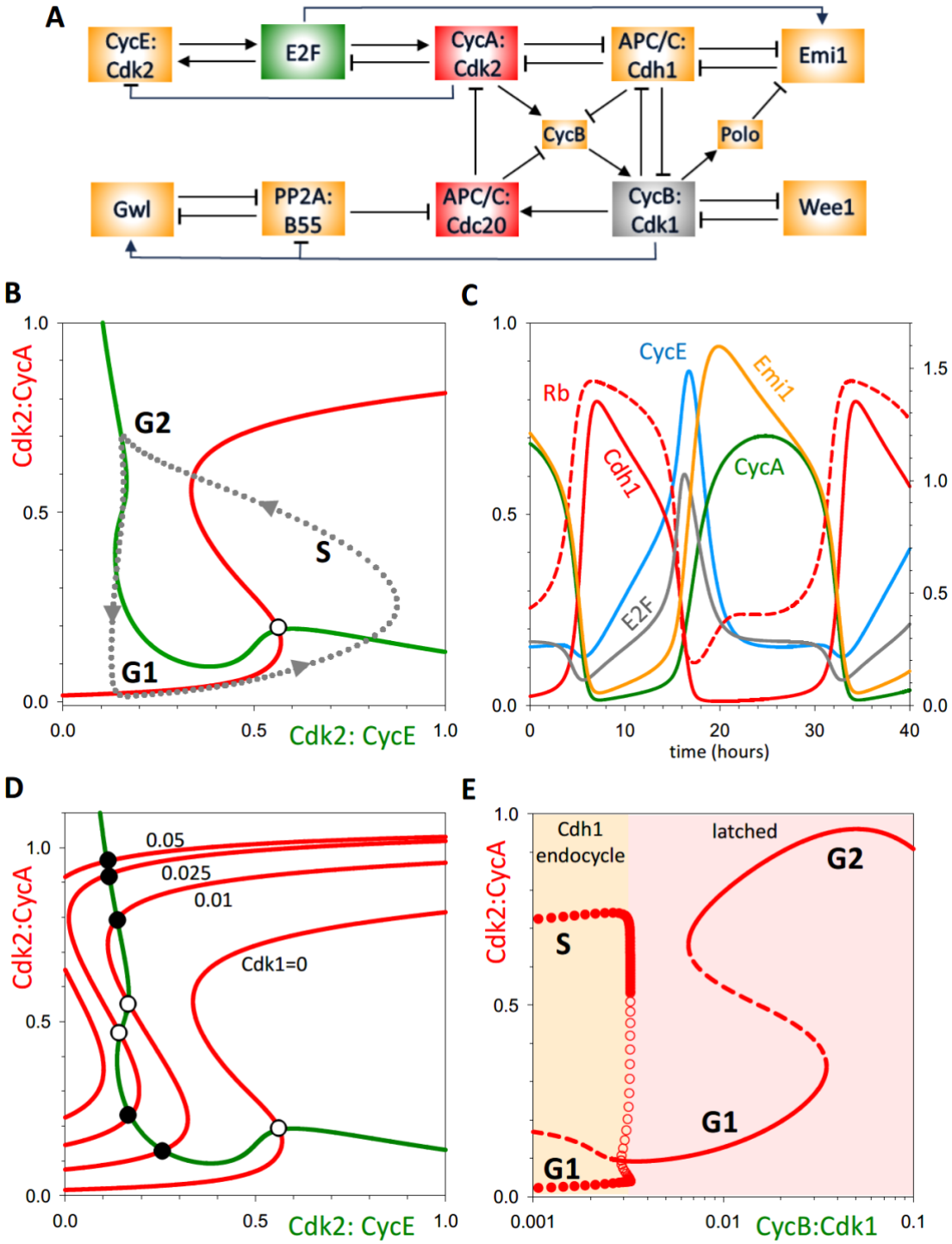

Figure 3.6 – The dynamical properties of the S-phase (Cdh1) oscillator. (A) Influence diagram of the system, highlighting the conversion of Cdk1:CycB from a dynamical variable to a parameter (grey box). **(B)** Pseudo-phase plane, Cdk2:CycA versus Cdk2:CycE, exhibits the characteristic features of a doubly amplified negative feedback oscillator. The unstable steady state (o) is surrounded by a stable limit cycle (dashed line is a projection of the time course simulation in panel C). **(C)** Time course simulation. **(D)** Pseudo-phase plane showing the emergence of a stable steady state of Cdk2:CycA activity, as the value of the Cdk1:CycB parameter increases. The stable steady state corresponds to arrest of the S-phase module. **(E)** Bifurcation diagram (Cdk2:CycA activity versus Cdk1:CycB parameter value) showing that a Cdh1-endocycle (endoreplication) emerges abruptly, through a subcritical Hopf bifurcation, when Cdk1:CycB activity falls below a threshold ~0.0035. In addition, G1- and G2-arrested states are observed at higher values of Cdk1:CycB.

In Fig. 3.6B, I plot pseudo-nullclines in the (Cdk2:CycE, Cdk2:CycA) phase plane. Cdk2:CycA is the inhibitor of the S-module oscillator. I use Cdk2:CycE as the 'activator' of this module because I assume pseudo-steady state kinetics for the binding/dissociation of the Rb:E2F complex, which results in an algebraic equation for E2F as a function of Cdk2:CycE. The Cdk2:CycE nullcline is backwards N-shaped, and the Cdk2:CycA nullcline is S-shaped; analogous to the Ω_1 oscillator in Fig. 3.2B. The intersection of the nullclines is an unstable steady state, surrounded by a stable limit cycle. The full time-course of oscillations of the S-phase module (in isolation) is shown on Fig. 3.6C. As the switching on and off of APC/C:Cdh1 activity is essential to these oscillations, I refer to the S-phase module as a 'Cdh1-endocycle.' Because Cdk2:CycA is oscillating with negligible Cdk1:CycB activity, these oscillations constitute endoreplication cycles (repeated rounds of DNA synthesis without mitosis).

In order to understand the coupling between the S-phase and M-phase modules, I now show how increasing the Cdk1:CycB parameter affects the Cdh1-oscillator (Fig. 3.6D, E). Since Cdk1:CycB regulates both the activator (E2F) and inhibitor (CycA) of the negative feedback loop, both nulllclines are affected as the value of Cdk1:CycB is increased. Nevertheless, at small Cdk1:CycB values the most relevant changes occur on the Cdk2:CycA-nullcline. Notice how increasing Cdk1 activity shifts the S-shaped nullcline to the left, making the system bistable, thereby converting the unstable steady state into a stable one, as indicated by the filled circle (Fig. 3.6D). At higher activity of Cdk1:CycB the lower steady states disappear through a saddle-node bifurcation and only the upper stable steady state remains. A more detailed picture about the effect of Cdk1:CycB on the Cdh1-oscillator is given by the bifurcation diagram in Fig. 3.6E, which shows that the large amplitude CycA oscillations are terminated by a sub-critical Hopf-bifurcation before the system enters into the bistable regime. For Cdk1 activity > 0.04, the system leaves the bistable regime, and only a high CycA-activity (G2) state remains. This dynamic behaviour resembles the situation observed for the toy-model (Suppl. Fig. S3.1).

A similar approach can be taken to analyse the mitotic module. For this, I turn the activity of APC/C:Cdh1 into a parameter (indicated by the grey rectangle in Fig. 3.7A), which eliminates its regulation by Cdk2:CycA and Cdk1:CycB. Setting APC/C:Cdh1 to zero (i.e.

the system cannot be arrested in G1) and plotting the pseudo-phase plane for Cdk1:CycB and APC/C:Cdc20 (Fig. 3.7B) reveals nullclines consistent with the mitotic module being an activator-inhibitor-double-amplified negative feedback oscillator. As expected, this system displays limit cycle behaviour (Fig. 3.7C). Increasing the activity of APC/C:Cdh1 arrests these oscillations through a SNIC bifurcation (Fig. 3.7D,E). Again, this is consistent with the hypothesis that the mutual antagonism of the two modules is at the heart of their alternating oscillations. Nevertheless, it must be noted that by setting APC/C:Cdh1 constant, the mitotic modules still receives fluctuating inputs from Cdk2:CycA in the S-phase module. This is caused by APC/C:Cdc20-dependent degradation of CycA, while Cdk2:CycA is responsible for activation of CycB synthesis. To show that the mitotic control module can indeed behave as an autonomous oscillator, I also convert Cdk2:CycA to a parameter. Time course and phase plane analysis reveals the expected properties of the double amplified negative feedback oscillator are still present (Suppl. Fig. S2).

3.3 Discussion

This chapter has presented an argument for framing the cell cycle regulatory network as a pair of oscillating modules under mutually antagonistic regulation, with one of the units controlling the replication origin licensing process and the other, DNA replication and division. At the core of each oscillator lies a bistable switch that introduces hysteresis and makes the progression through each phase irreversible, and a negative feedback motif which drives periodic switching between the two steady states, giving rise to limit cycle behaviour. Each oscillator responds to changes in a latching parameter (the activity of the analogous species in the other oscillator) and a checkpoint parameter: when either of these inputs crosses a particular threshold, the oscillation ceases through the generation of a stable steady state. Though dynamically similar, the two stimuli arrest the oscillator in different states: the former forces the bistable switch to remain in the ‘off’ state, while the latter maintains the main component of the switch in a state of high activity.

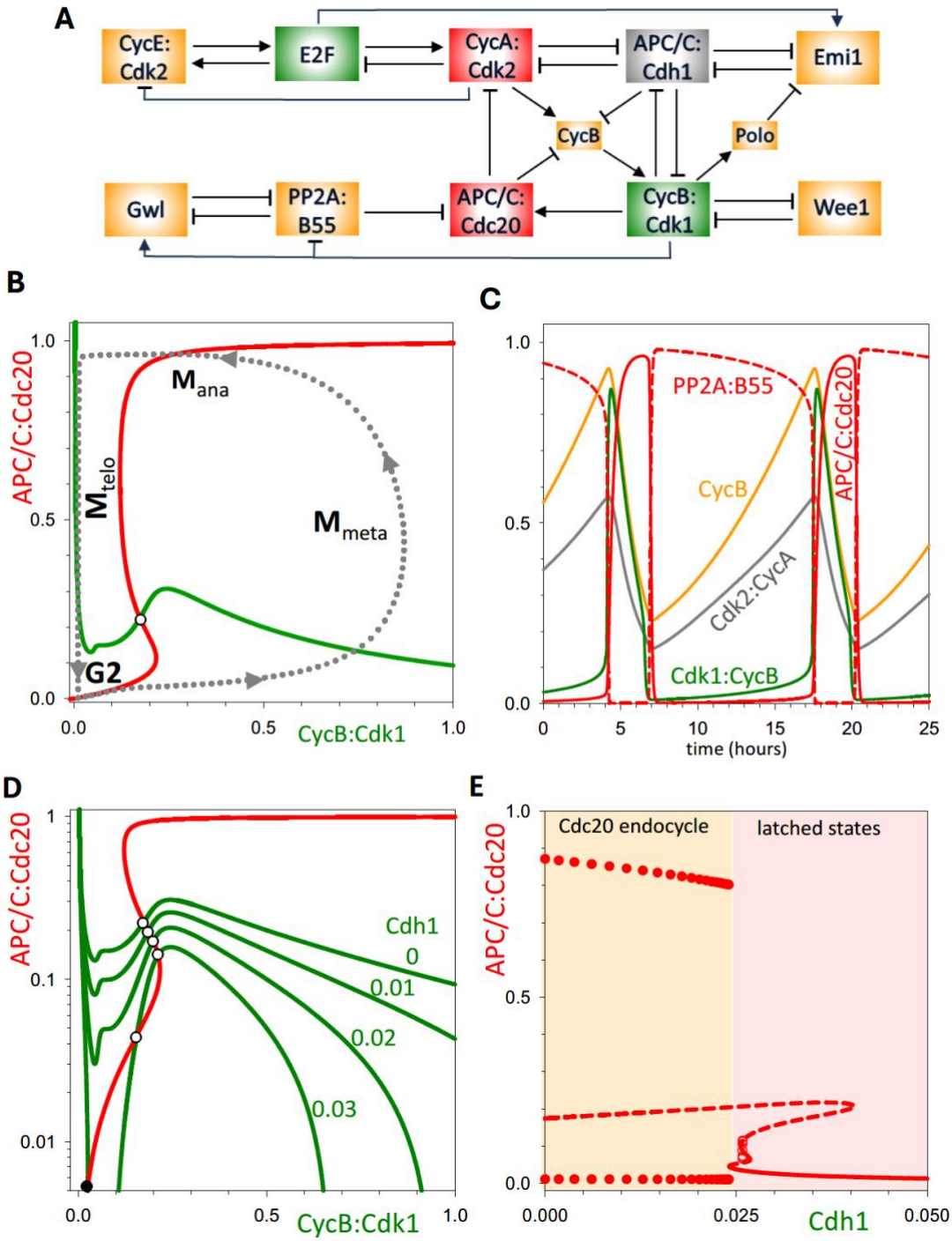

Figure 3.7. The dynamical properties of the M-phase (Cdc20) oscillator. (A) Influence diagram of the system, highlighting the conversion of Cdk1:CycB from a dynamical variable to a parameter (grey box). **(B)** Pseudo-phase plane, APC/C:Cdc20 versus Cdk1:CycB, exhibits the characteristic features of a doubly amplified negative feedback oscillator. A stable limit cycle (dashed line is a projection of the time course simulation in panel C). **(C)** Time course simulation. **(D)** Pseudo-phase plane showing the emergence of a stable steady state of APC/C:Cdc20 activity, as the value of the APC/C:Cdh1 parameter increases. The stable steady state corresponds to arrest of the M-module. **(E)** Bifurcation diagram (APC/C:Cdc20 activity versus Cdh1 parameter value) showing that a Cdc20-endocycle emerges abruptly, through a SNIC bifurcation, when APC/C:Cdh1 activity falls below a threshold ~0.025.

It is relevant to ask why there should be two nonlinear oscillators, rather than a series of steady states and one oscillator that brings the system back into the G0/G1 at the end of mitosis. It is possible that this phenomenon is an inevitable consequence of the requirements of eukaryotic DNA replication and origin licensing: in order to prevent over-replication, the licensing phase (from late M to G1/S) and replicative phase (S to G2/M) must never overlap and therefore should be self-limiting. Hence negative feedback must be in place. Of course, this negative feedback will lead to oscillations, since the licensing and replicative are delineated by a bistable switch, which helps prevent over- or under-replication.

The existence of these two mutually-regulated oscillators allows for the possibility of decoupling one of them and the generating an endocycle. This suggests a novel analogy for cell cycle dynamics.

3.3.1 Newton's cradle

I propose that the alternating oscillation of S- and M-modules (and $\Omega_1\Omega_2$ oscillators) is analogous to the dynamics of Newton's cradle (Fig. 3.8A), a mechanical device used to illustrate the conservation of momentum and other aspects of Newtonian physics. When one of the outer pendula is set in motion, the device executes an alternating sequence of half-swings of both outer pendula. Clearly, the two outer pendula can be associated with the S- and M-modules ($\Omega_1\Omega_2$ oscillators) of the cell cycle control system. By plotting pseudo-phase planes for the individual Ω_1 and Ω_2 oscillators (Fig. 3.8B), I illustrate the parallel symmetries between Newton's cradle and my toy coupled-oscillator model of the cell cycle. The only steady state showing up on each of these phase planes corresponds to the latched state of both oscillators, where both activator and inhibitor levels are low. In Newton's cradle, these steady states correspond to low potential energy positions of the outer spheres, where they are in contact with the other stationary spheres. Once an outer sphere reaches the low point of its oscillation, its momentum is transferred to the other outer sphere. In case of the double-oscillator, reaching one of these latched states causes a release of the other activator from inhibition and drives the

system to the other pseudo-phase plane (Fig. 3.8B). In this way, the motion of Newton's cradle resembles the alternation of S phase and M phase during the mitotic cycle of eukaryotic cells. As with endocycles, when the oscillators' coupling is perturbed by blocking the swinging of an outer sphere, the other outermost pendulum oscillates independently as a consequence of elastic collisions with the stationary inner spheres (Fig. 3.9A,B).

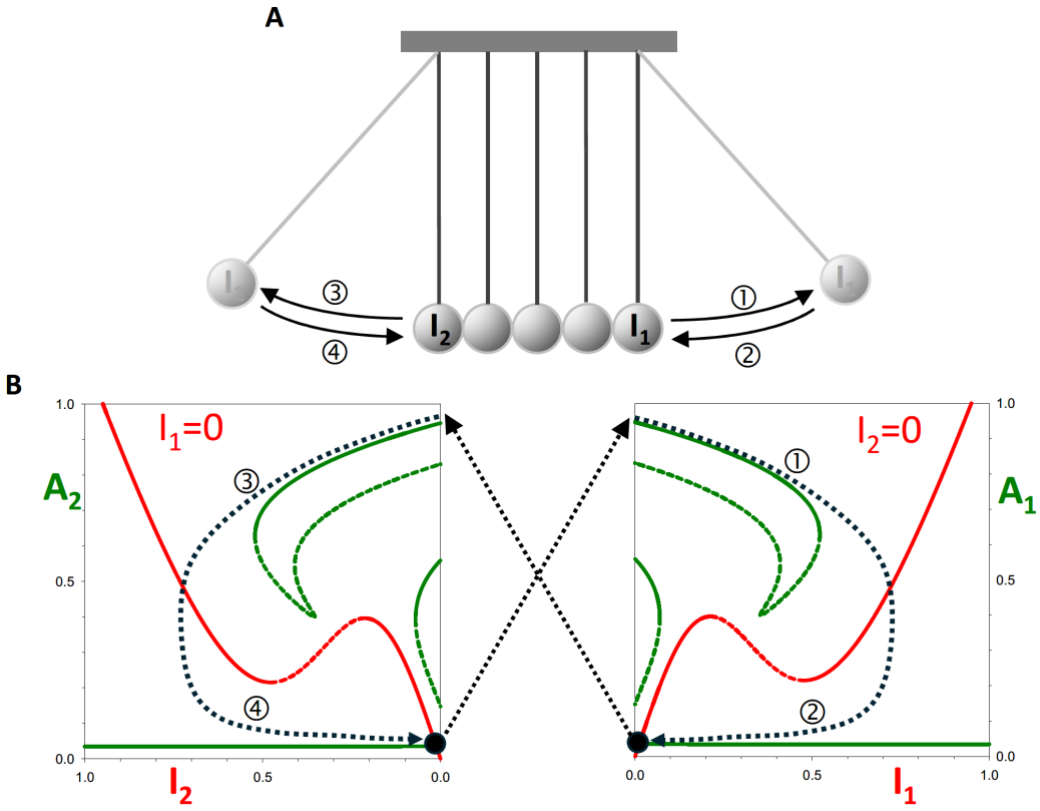

Figure 3.8 – The Newton's cradle analogy to the double oscillator system. (A) Newton's cradle (see youtube video). **(B)** Pseudo-phase planes for A_1-I_1 (right panel) and for A_2-I_2 (left panel), and schematic cell cycle trajectory (dotted line). Starting from $A_1 \approx 1$ and $I_1 \approx A_2 \approx I_2 \approx 0$, as I_1 increases A_1 switches OFF, which allows A_2 to switch ON, bringing the trajectory to $A_2 \approx 1$ and $I_2 \approx A_1 \approx I_1 \approx 0$, completing one-half of the cycle.

Because the double-oscillator model executes limit cycle oscillations in the absence of checkpoints, it is consistent with older clock models (and clock-shop models) of the cell cycle. Furthermore, checkpoints can be seamlessly integrated into the model, easily aligning it with older falling-dominoes and newer latching-gates views of cell cycle controls. Within Newton's cradle analogy, a checkpoint would correspond to catching one of the pendula in a state of high potential energy, thereby preventing oscillations of both outer spheres (Fig. 3.9C,D). When the checkpoint is released (the sphere is

dropped), the normal cycle picks up where it left off. Thus, I suggest that my linked oscillators framework builds on the classical metaphors of cell cycle dynamics and expands them to account elegantly for perturbations leading to endocycles.

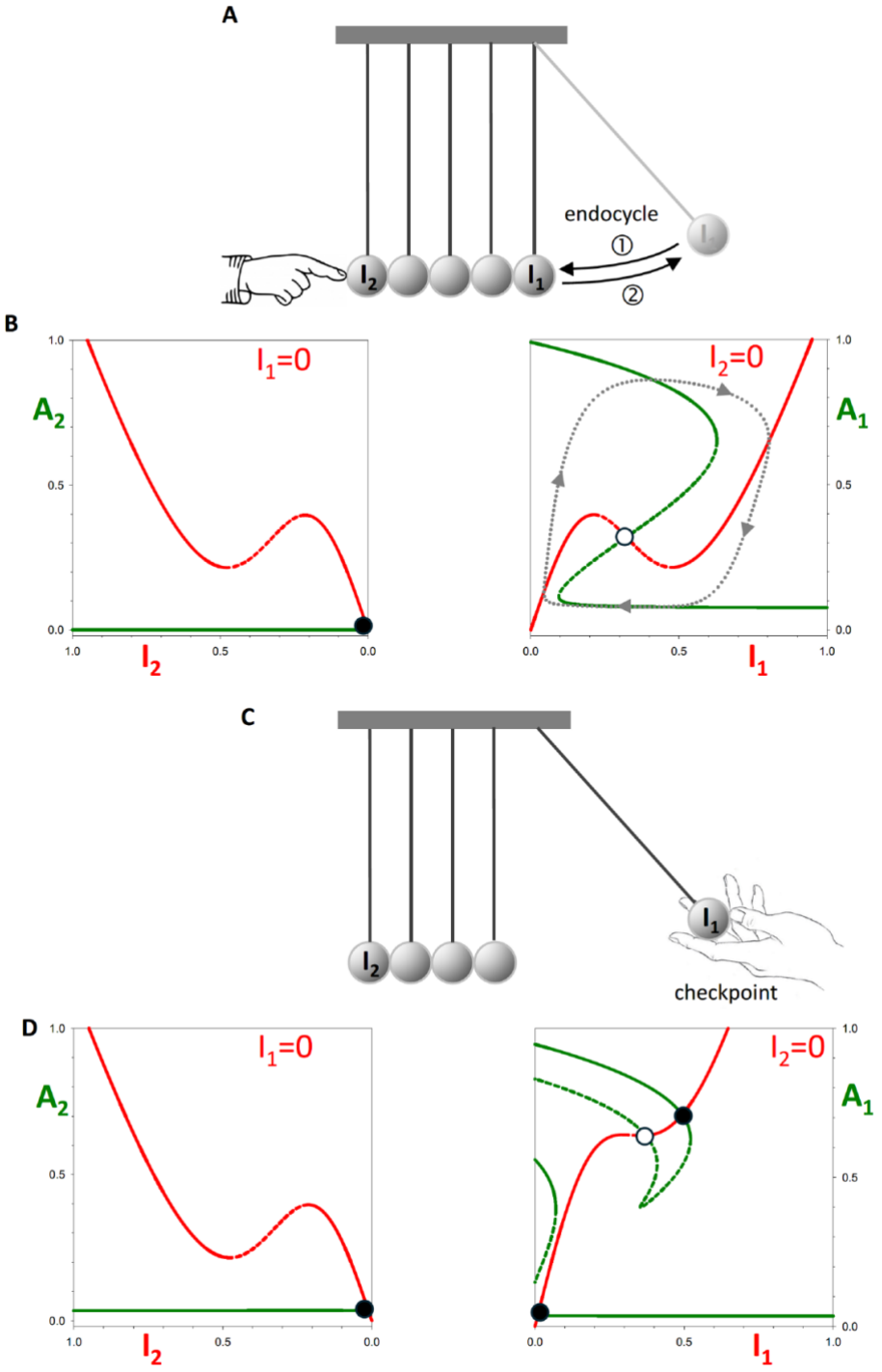

Figure 3.9: Newton's cradle analogy to double oscillator perturbations. (A) Outline of Newton's cradle dynamics when the movement of one of the outer spheres is prevented by an external counteracting force. The free-running pendulum continues to swing as a consequence of elastic collisions with the stationary spheres. **(B)** Ω_1 endocycle pseudo-phase planes, with k_{sa2}'=0, showing that the A_2-I_2 system is permanently latched, while the A_1-I_1 system displays the dynamical properties

of a free-running, double-amplified negative feedback oscillator. **(C)** Preventing the return of an oscillating sphere to the equilibrium position prevents the system's oscillation until the sphere is released. **(D)** Checkpoint pseudo-phase planes, with C_1=1, showing that the generation of a high A_1 stable steady state prevents oscillations by keeping the A_2-I_2 system in the latched position permanently.

3.4 Material and methods

3.4.1 A doubly amplified negative feedback oscillator

I model a doubly amplified negative feedback oscillator by a pair of nonlinear ordinary differential equations (ODE), Eqs. 3.1a and 3.1b, describing the kinetics of Activator-1 (A_1) and Inhibitor-1 (I_1) accumulation and degradation with parameter values in Table 3.1 (Appendix 2).

The model was implemented in freely available software XPPAUT (https://sites.pitt.edu/~phase/bard/bardware/xpp/xpp.html). The 'ode' file Fig2_FigS1.ode (Appendix 2) can be used with XPPAUT to reproduce the time-course simulations (panels C), phase plane diagrams (panels B,D,F) and one-parameter bifurcation diagrams (panels E,G,H) in Figure 3.2 and Suppl. Fig. S3.1.

3.4.2 Two coupled doubly amplified negative feedback oscillators

A second copy (A_2 and I_2) of the doubly amplified NFL was coupled to the first by mutual inhibition, yielding a system of four ODEs:

$$\frac{dA_1}{dt} = k'_{sa1} + k_{sa1}\frac{A_1^q}{L_{a1}^q(1+rI_1)+A_1^q} - (k'_{da1} + k_{da1}\cdot A_2)\cdot A_1 \qquad (3.1a)$$

$$\frac{dI_1}{dt} = k'_{si1}\cdot A_1 + k_{si1}\frac{I_1^p}{L_{i1}^p + I_1^p} - (k'_{di1} + k_{di1}\cdot C_1)\cdot I_1 \qquad (3.1b)$$

$$\frac{dA_2}{dt} = k'_{sa2} + k_{sa2}\frac{A_2^q}{L_{a2}^q(1+rI_2)+A_2^q} - (k'_{da2} + k_{da2}\cdot A_1)\cdot A_2 \qquad (3.2a)$$

$$\frac{dI_2}{dt} = k'_{si2} \cdot A_2 + k_{si} \frac{I_2^p}{L_{i2}^p + I_2^p} - (k'_{di2} + k_{di2} \cdot C_2) \cdot I_2 \qquad (3.2b)$$

The file Fig3B_Fig4.ode can be used to reproduce the time-course simulations on Fig. 3.3B and Fig. 3.4B,E and the one-parameter bifurcation diagrams on Fig. 3.4C,D,F,G.

Pseudo-nullclines are calculated using the capacity of XPPAUT to plot one-parameter bifurcation diagrams for a reduced set of ODEs. First, the dynamic variable chosen as the bifurcation parameter is removed from the system of ODEs and treated as a parameter. Next, for the A_1-I_1 pseudo-phase plane, I_1 is also converted to a parameter (and similarly for the A_2-I_2 pseudo-phase plane) and a one-parameter bifurcation diagram for the A_1 steady state as a function of I_1 is calculated with the remaining ODEs to plot the pseudo-nullcline for $dA_1/dt = 0$. To calculate the pseudo-nullcline for $dI_1/dt = 0$, the roles of A_1 and I_1 are reversed. The file Fig5_Fig8B.ode calculates the one-parameter bifurcation diagram (i.e., the pseudo-nullcline) of A_1 as a function of I_1.

3.4.3 Adaptation of the mammalian model from chapter 2

To illustrate the double oscillator behaviour of the cell cycle control network, the mammalian model of Chapter 2 was used with slight changes to four parameter values. In the file Fig6.ode, both CycB and Cdk1 are converted to parameters, so that it can be used to simulate the oscillatory time-course of endoreplication cycles (Fig. 3.6C). Fig6.ode also supports calculation of the Cdk2:CycA bifurcation diagram (Fig. 3.6E) after setting the initial value of the Cdk1 bifurcation parameter to 0.1 in the parameter list. The Cdk2:CycE and Cdk2:CycA pseudo-nullclines in Fig. 3.6B,D phase planes can be calculated by overlaying two one-parameter bifurcation diagrams. To plot the Cdk2:CycA pseudo-nullcline, CycE is converted to a constant and used as a bifurcation parameter to calculate the CycA steady state values ($CycA_{ss}$). To plot the CycE pseudo-nullcline, CycE is used as the variable and CycA as the bifurcation parameter in a one-parameter bifurcation diagram calculation.

To calculate the Cdc20-endocycles on Fig. 3.7, Cdh1 was converted from an ODE to parameter in Fig7_FigS2.ode. This file supports calculation of the one-parameter bifurcation diagram of Fig. 3.7E after setting the initial value of the bifurcation parameter (Cdh1) to 0.05. The limit cycle oscillation at Cdh1=0 can be captured by setting the time of integration to the period of the oscillation (13.35 hours). The pseudo-nullclines for Cdk1:CycB (Cdk1 in the ode file) and for APC/C:Cdc20 are calculated as one-parameter bifurcation diagram after converting Cdc20 or both CycB and Cdk1 into parameters. The file Fig7_FigS2.ode can also be used to calculate all the panels in Suppl. Fig. S2 after setting CycA=0.4 as a parameter using a similar procedure.

Acknowledgements

The material in this has been peer-reviewed and published at Mathematical Biosciences[222].

4 The wheel of Fortune: The cell cycle as a tetra-stable excitable system

4.1 Introduction

The double oscillator framework can explain the emergence of endocycles, both in principle and in the context of a mechanistic model of the mammalian cell cycle control network. Its simplicity makes it an attractive conceptual tool by which to reason about the organisation of the cell cycle and to make qualitative predictions on the effect of molecular perturbations. Nevertheless, before taking its assumptions at face value, the model must be subjected to more stringent verification. This, however, can be a very resource intensive process, so it is necessary to identify the most promising theoretical frameworks first. Thus, a complementary approach is to tackle the problem from multiple theoretical angles and appraise the strengths and limitations of different models which produce broadly consistent dynamical outcomes in response to known perturbations. In the current context, it may first be asked whether a system of two mutually inhibitory oscillators is the only one that can generate endo-oscillatory behaviour. If it is, then it must underpin endocycles *in vivo*. If it is not, a different framework can be found. Second, if the double oscillator solution to the endo-oscillation problem is not unique, it must be ascertained whether the alternative solutions present any advantages. Such advantages may, in principle, lead the new model to supplant the previous framework as the organisational basis of the cell cycle.

The first question can be addressed by analysing a previous model of cell cycle endo-oscillations. In 2022, Novak and Tyson introduced the latching gate hypothesis for the first time, to rationalise the dynamics of endocycles in a model of the budding yeast cell cycle control network[157]. The model is based on a simple set of biochemical interactions. At its core, it consists of several mutually inhibitory species: on the one hand, the cyclin:CDK complexes, denoted by ClbS and ClbM, and on the other hand, by their negative regulators, the ubiquitin ligase APC/C:Cdh1 and the stoichiometric inhibitor Sic1. These interactions give rise to a bistable switch determining the quiescent state (G1), characterised by reduced CDK activity, and the replication/division state (S-G2-M),

when CDK activity is high. In addition, two helper molecules – appropriately connected to the core network through other regulators – drive the flipping of the APC/C-CDK switch through negative feedback. MBF is a transcription factor determining the accumulation of ClbS and with it, the G1/S transition. Cdc14 is a phosphatase opposing CDK-dependent phosphorylation, which is responsible for APC/C reactivation and mitotic exit. The authors showed that the APC/C-CDK1 bistable switch is irreversible with respect to each helper molecule, such that in order to complete a cell cycle oscillation, both helpers must be engaged sequentially.

Within this framework, an endocycle occurs when the switch is rendered reversible with respect to one of the helpers. The constitutive inhibition of the mitotic kinase, ClbM, makes the switch reversible with respect to MBF, giving rise to endoreplication. This is because the mitotic network is no longer activated, which means that cells cannot initiate division and Cdc14 activity becomes dispensable for CDK inactivation, leading to its disengagement from oscillation. In contrast, expressing non-degradable mitotic cyclin means that cells cannot establish G1 robustly, which prevents the licensing of DNA replication origins and with it, S-phase, giving rise to a type of mitotic endocycle, termed 'Cdc14 endocycle'[76,223]. The Cdc14 phosphatase is sequestered in the nucleolus for most of the cell cycle and is only released between anaphase and cytokinesis. In Cdc14 endocycles, the phosphatase can be released more than once without the cell dividing and returning to G1.

As a description of the cell cycle control network, this model is rather simplified. It assumes a Cdc20, Pds1, Clb5 triple mutant genetic background. A drawback of this simplifying assumption is that the Cdc14 endocycles have not been tested in such an *S. cerevisiae* strain[76]. Despite concerns over the physiological applicability of this model, it represents an interesting case study of an endo-oscillatory system. Intriguingly, this regulatory architecture gives rise to endo-oscillations **without** being based on the "Newton's Cradle" framework, as shown in the Results section. This is interesting, because both the budding yeast model and the mammalian model in Chapter 2 started from the same premise: the latching gate hypothesis. This shows the double oscillator

framework is not *necessarily* responsible for the emergence of endocycles *in vivo*, but that it shares features with other endo-oscillatory systems.

It is now possible to address the second question: whether this framework could represent an improvement over "Newton's Cradle". A benchmark for this could be set by considering the limitations of the double oscillator model. First, it can only explain a subset of the endocycles that have been observed: endoreplication and Cdc20 endocycles. While the same framework could account for other endocycles (Cdc14 and meiosis), it could not easily explain endomitosis. As explained in Section 1.2.5, endomitosis occurs when cells complete S-phase and enter mitosis, but do not complete anaphase and divide. Second, the double oscillator framework can only account for two checkpoints: the G1 and spindle assembly checkpoints. At least one other checkpoint exists in the form of the DNA damage (or G2) checkpoint, which represses CDK1 through Cdc25 downregulation and p21 accumulation (Section 1.2.3), preventing mitotic entry. Clearly, the stripped-down double oscillator framework could not account for this, because inhibiting the activator of the mitotic module leads to endoreplication[222] (Chapter 3), instead of an arrest.

The checkpoint limitation could be resolved by arguing that the double oscillator is just an overly simplistic version of the cell cycle control network and the extra properties can be obtained by introducing a few complications to "Newton's cradle" framework. In the mammalian model (Chapter 2), the G2 checkpoint is explained by noting that CDK1 activity is needed for E2F phosphorylation and inactivation. In the double oscillator context, this interaction would be modelled as A_2--|I_1. Thus, incomplete activation of the mitotic activator forces the replicative oscillator to arrest in an unusual state where the inhibitor (E2F) is high and the activator (APC/C:Cdh1) is low, which does not correspond to either the latched or checkpoint state as defined in the previous chapter. However, to my knowledge, there is no evidence to suggest this interaction is necessary for the establishment of the DNA damage checkpoint. A new framework may be able to dispense with such disputable assumptions.

To address these problems, I introduce a generalised version of the Novak & Tyson (2022) endo-oscillatory framework, based on 4 pseudo-steady states corresponding to G1, S, G2 and metaphase, instead of 2 pseudo-steady states, corresponding to G1 and S/G2/M. I then show that in either framework, an endocycle occurs when one (or more) of the pseudo-steady states loses stability. Thus, while the 2-state model can account for replicative and mitotic endocycles, the 4-state model can additionally account for endomitosis and well as several other hypothetical endocycles. In addition, the 4-state model can generate 4 distinct types of checkpoint arrest at the transition between any two phases. Finally, I argue that an intuitive mechanical analogy of this system is a "wheel of fortune" with 4 sectors (i.e. "prizes"), corresponding to each cell cycle phase. An endocycle is then understood as the removal of a barrier between two sectors, while a checkpoint can be imagined as the strengthening of a barrier.

4.2 Results

4.2.1 A minimal latching gate system: two pseudo-oscillators linked by a bistable switch

The latching gate view of the cell cycle represents a top-down perspective on the dynamics of endo-oscillatory systems studied so far. Nevertheless, as shown in the previous chapter, while the latching gate signature phase plane provides an indication of endo-oscillatory behaviour, it does not provide a sufficient mechanistic explanation for the emergence of endocycles. Thus, to understand how endocycles are determined in the Novak & Tyson (2022) paper[157], I take a constructive approach, through which I show all conditions that must be satisfied in order to develop a system with qualitatively identical properties, while making a minimal number of assumptions.

As the latching gate hypothesis is premised on the existence of an irreversible bistable switch, I build a core module consisting of 3 species (A, B, B') engaged in non-linear positive and double-negative feedback (Fig. 4.1A). A and B are mutually activatory, while A and B' are mutually repressive. Although a single positive network is sufficient, I chose

to include two of them for symmetry reasons and to highlight the similarity to the yeast network. Next, two helper molecules (C and C') are introduced to establish negative feedback loops that drive the flipping of the bistable switch. A activates C indirectly through B, while C inactivates A. Anti-symmetrically, A inactivates C' through B', while C' activates A. In addition, two delay molecules, D and D' ensure that the activity of the helpers does not overlap. This delay makes pseudo-phase plane analysis possible, and is important for generating robust endocycles. For a more detailed discussion of the role of delay in this framework, see Fig. S4.1.

This verbal description of interactions is formalised as a system of coupled nonlinear differential equations. Subsequently, a time course simulation can be calculated (Fig. 4.1B). It is immediately apparent that the activity of A/B and B' alternates similarly to the G1 and S/G2/M phases of the cell cycle. The transition between these two phases is driven by the accumulation of the helper molecules. C flips the A switch off and triggers the activation of B', while C' flips the A switch on. As each state of the switch triggers its own inactivation, this system displays limit cycle oscillations.

It is possible to analyse the dynamical properties of this system with reference to a pair of pseudo phase planes (PPP, c.f. Section 1.3.6). To achieve this, the nullclines (i.e. steady state values) of each of the helper molecules are plotted against A and vice versa, for a fixed value of the other helper molecule (Fig. 4.1C). Setting C'=0 for the AC PPP and C=0 for AC' PPP reveals the characteristic features of the latching gate system. The dynamical variable A shows irreversible bistability with respect to both helper molecules. A is activated by increasing values of C' and inactivated by increasing values of C. Equally, A inactivates C' and activates C. Thus, two negative feedback loops are established. Following the dotted black line (the projection of the time course on the pseudo phase plane) shows how this system evolves in time. Starting at the stable pseudo steady state SS', where A is high and both helpers are zero, C begins to accumulate. As C increases past a threshold value ($C \cong 6$), A is inactivated, and it stops stimulating C. Subsequently, the AC system reaches the pseudo-steady state SS. Nevertheless, the system does not arrest, as B' is high (since A no longer suppresses it), which stimulates C'. As C' accumulates, A is gradually activated, until it reaches another threshold (around C'=7),

at which it abruptly turns on thanks to positive feedback. As B' is simultaneously turned off, C' wanes and the system returns to the SS' state.

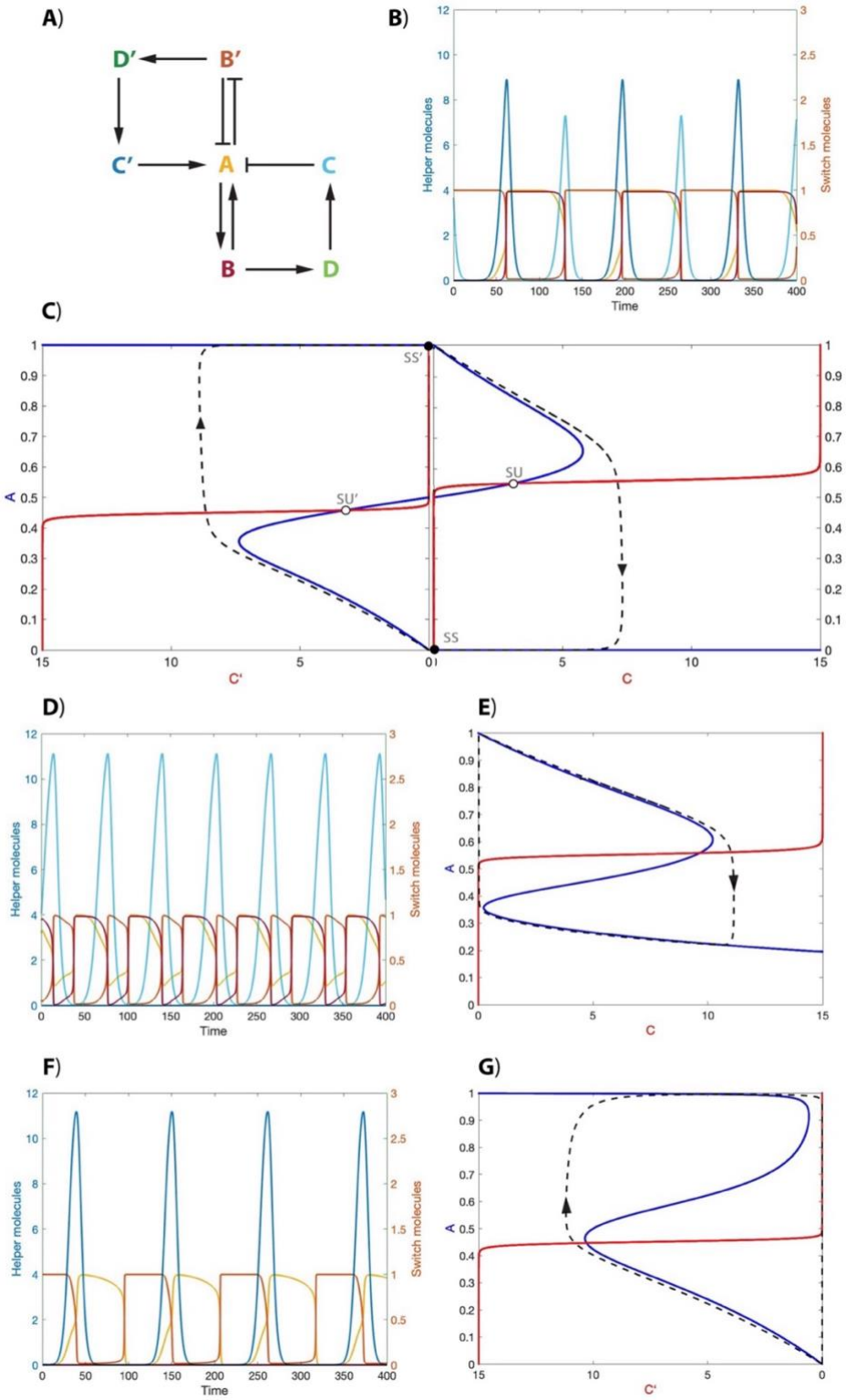

Fig. 4.1 – The dynamics of the minimal latching gate system – (A) Influence diagram of the mixed negative feedback oscillator with delay. (B) Time course simulation. Note that the curves' colour coding matches panel A. 'Helper molecules' refers to C and C'; 'Switch molecules' refers to A, B and B'. (C) The systems pseudo phase planes. The left PPP assumes C=0, while the right PPP assumes

C’=0. The time course projection is plotted in black dashed lines. The black circles represent stable pseudo-steady states. The white circles denote unstable states. (D) C endocycle time course, for ksa=0.75. (E) AC pseudo phase plane, for ksa=0.75. (F) C’ endocycle time endocycle, for B’tot=0. (G) AC’ pseudo phase plane, for B’tot=0.

The premise of the latching gate hypothesis is that endocycles can be generated by rendering the core bistable switch reversible with respect to one helper molecule, while retaining the oscillatory behaviour generated by the amplified negative feedback motif. Increasing the basal rate of A synthesis, *ksa*, renders the C’ helper unnecessary for A activation. This means that A can initiate its positive feedback as long as C is absent. The kinetics of the system are such that the switch now spends an insufficient amount of time in the low A state for D’ and subsequently C’, to accumulate to appreciable levels. This generates the C endocycle (Fig. 4.1D). As expected, the A switch can be shown to be reversible with respect to C on a pseudo phase plane (Fig. 4.1E). It is important to note that although the features of the phase plane are consistent with an amplified negative feedback oscillator, the delay variable D makes a significant contribution to the oscillation amplitude (c.f. Fig. S4.1D,E). Analogously, a C’ endocycle can be generated by removing all B from the system (i.e. the parameter Btot=0) (Fig. 4.1F,G).

It is possible to show that the dynamics of this system and that of the budding yeast cell cycle model proposed by Novak & Tyson are equivalent by plotting bifurcations diagrams that reveal similar transitions between mitotic cycles and endocycles (Fig. S4.2A-D) and by comparing the system wiring directly (Fig. S4.2E). The main conclusion of this section is that though the pseudo phase plane offers a way to ‘diagnose’ endo-oscillatory systems by revealing the latching gate features, it does not provide a full mechanistic explanation for how they emerge. In this case, the introduction of delay variables is essential for robust, high-amplitude endocycles. Nevertheless, the introduction of delay does not change the steady state properties of the switch and helper variables and therefore, there is no change in the PPP. As such, the PPP view can be misleading and must be interpreted carefully. In essence, the mitotic cycle oscillation may rely on the amplified negative feedback motif (Fig. 4.1C, Fig. S4.1C), but the endocycle cannot be explained on this basis, because the helper and switch molecules do not always intersect on the unstable branch of the switch molecule (Fig. 4.1G), which is normally a prerequisite of limit cycles. Thus, under the current formulation and that of the 2022

Novak & Tyson model, the endocycle is necessarily a delayed negative feedback oscillator. In the following sections, to get a different perspective on how the endocycle is generated, I plot a different set of phase planes and attempt to model endocycles through a different strategy.

4.2.2 Towards a generalised endo-oscillatory system: a different perspective on the latching gates

To begin identifying a general endo-oscillatory framework that can account for more than two cell cycle phases I introduce a new phase plane view of the system (Fig. 4.2A). Rather than looking at two half-phase planes, involving one switch and one helper variable, in which the system oscillates, I choose to look at the core system (ABB') in isolation and explain the effect of the helpers. Since only 2 variables can be plotted on a 2D plane, it is only possible to analyse either the AB or AB' phase plane. I focus on the AB' phase plane only, as the AB view is equivalent. A is bistable (S-shaped) with respect to B', while B' is sigmoid with respect to A. The shape of the A nullcline is explained by the fact that B' inactivates A, but A is also engaged in nonlinear positive feedback through B. The shape of the B' nullcline is explained by the fact that B' is modelled as a Hill function of A. This system is overall bistable, because the nullclines intersect at two stable nodes (High A/Low B', and Low A/High B'). These states correspond to two cell cycle phases: G1 and S/G2/M. On its own, this system cannot oscillate – it can only arrest in one of the two stable states. However, this is where the two helper variables come in. The helpers act as 'forces' that 'push' the system out of the basin of attraction of the state in which it is arrested. Subsequently, the system is spontaneously attracted to the other state. The role of the delay variables is to allow sufficient accumulation of C and C' to push the system over the threshold of the opposite state. Thus, when the core system engages both helpers and their delay variables, the system oscillates between the two states. Notice that thanks to hysteresis, the system goes from the OFF state to the ON state and *vice versa* via different paths.

Endocycles occur when one of the two core states loses stability, and the system becomes monostable (Fig. 4.2B). When this happens, the helper associated with the state that lost stability can no longer be activated. Nevertheless, the system is not arrested, because other state can still trigger the activation of the remaining helper. This excites the core system to position of higher potential, after which it relaxes spontaneously back to the stable steady state. Once this happens, the helper can start accumulating again, driving the oscillation forward. Again, note the importance of delay between the flipping of the swich module and helper activation: without it, the helper would not accumulate sufficiently to push the core system out of its equilibrium position.

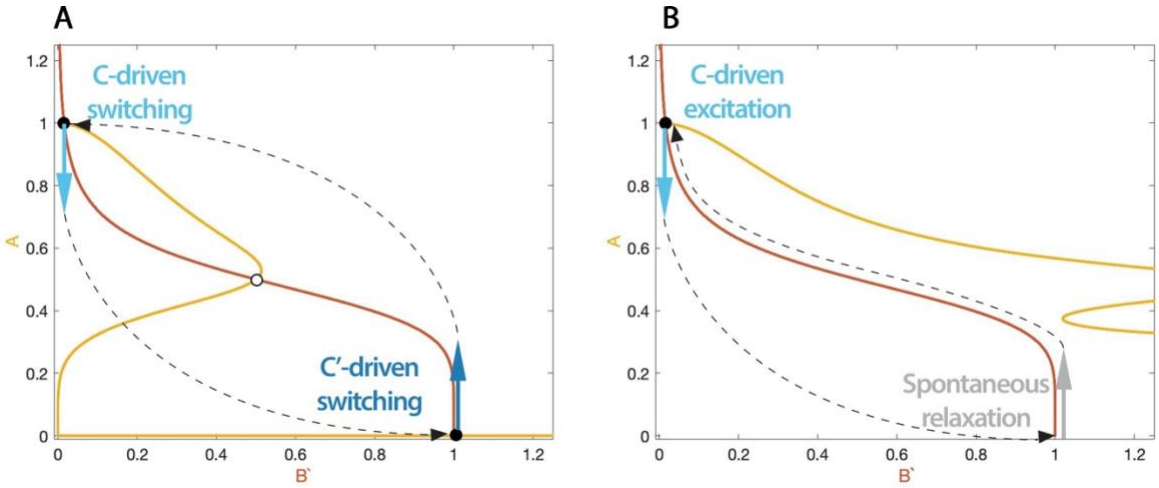

Fig. 4.2 – The latching gate system viewed from switch variables' perspective – (A) The phase plane of the AB' core system. The dashed lines represent sketches of the system's trajectory under the action of the helper molecules, C and C' (B) The phase plane of the AB' core system, characteristic of the C endocycle, with *ksa*=0.8.

4.2.3 A tetra-stable, double-amplified negative feedback core

The new phase plane perspective on the latching gate system introduced in the previous section can be easily generalised to more steady states, or in other words, cell cycle phases. All that needs to be done is to shape the nullclines so that more stable pseudo-steady states are present and applicable helper molecules are introduced for each individual state. Suppose that both dynamical variables on the phase plane of the core system were amplified by nonlinear positive feedback (Fig. 4.3A). Then, both variables would be bistable with respect to each other, and it would be possible to generate 4 intersections of the stable branches, to give rise to 4 stable steady states, which I name

G1, S, G2 and a metaphase (Fig. 4.3B), for reasons detailed in the Discussion. In addition, 4 saddle points are present at the intersections of stable branches with saddles, which can be loosely seen as the 'thresholds' for the cell cycle phase transitions $Th_{G1/S}$, $Th_{S/G2}$, $Th_{G2/Meta}$, $Th_{Meta/G1}$. The notion of phase threshold can be more rigorously understood as the boundary of the basin of attraction of a stable node (i.e. cell cycle phase), which includes the saddle points (Fig. S4.3). Finally, an unstable point (pOsc), at the intersection of the two nullclines' saddles, is also present (discussed below).It is easy to imagine that this system could oscillate with fixed period if some helper variable were activated by each stable steady state, and in turn, pushed the core system over the threshold, into the next state. For instance, if the system were in the G1 state, the helper could force the transition to the S state by driving an increase in the core variable A.

Analogous to the notion of endocycle in the previous section, in this system, an endocycle is triggered if a parameter change can be introduced, such that one or more stable steady states (i.e. phases) is abolished. In Fig. 4.3C, a change in the parameter *jdA* (see Section 4.4.2) moves the activation threshold of the A nullcline to a more positive value. Subsequently, the G1 state is lost through a saddle-node bifurcation (Fig. 4.3E), as it merges with the saddle point $Th_{G1/S}$. When this happens, the system is automatically attracted to the next steady state in line. Further, as the two core dynamical variables are modelled symmetrically, any subset of the steady states can be eliminated through an analogous perturbation. This property makes this system a very versatile tool, which can generate up to 15 endocycles (whether they have a physiological correspondent or not). For example, in Fig. 4.3D both the G1 and S states are eliminated, corresponding to a mitotic endocycle.

Notice that the two core variables are in negative feedback relation, with A activating B, and B inhibiting A. Thus, since both variables are engaged in non-linear positive feedback, they could determine a limit cycle oscillator, provided no stable steady states were present to block the oscillation. This is why the intersection of the nullclines' saddles is termed pseudo-oscillator (pOsc). This property is a crucial feature of this system, as it is this oscillatory potential that helps drive the system forward, to the next phase in line, during an endocycle, when the appropriate helper molecule cannot be engaged.

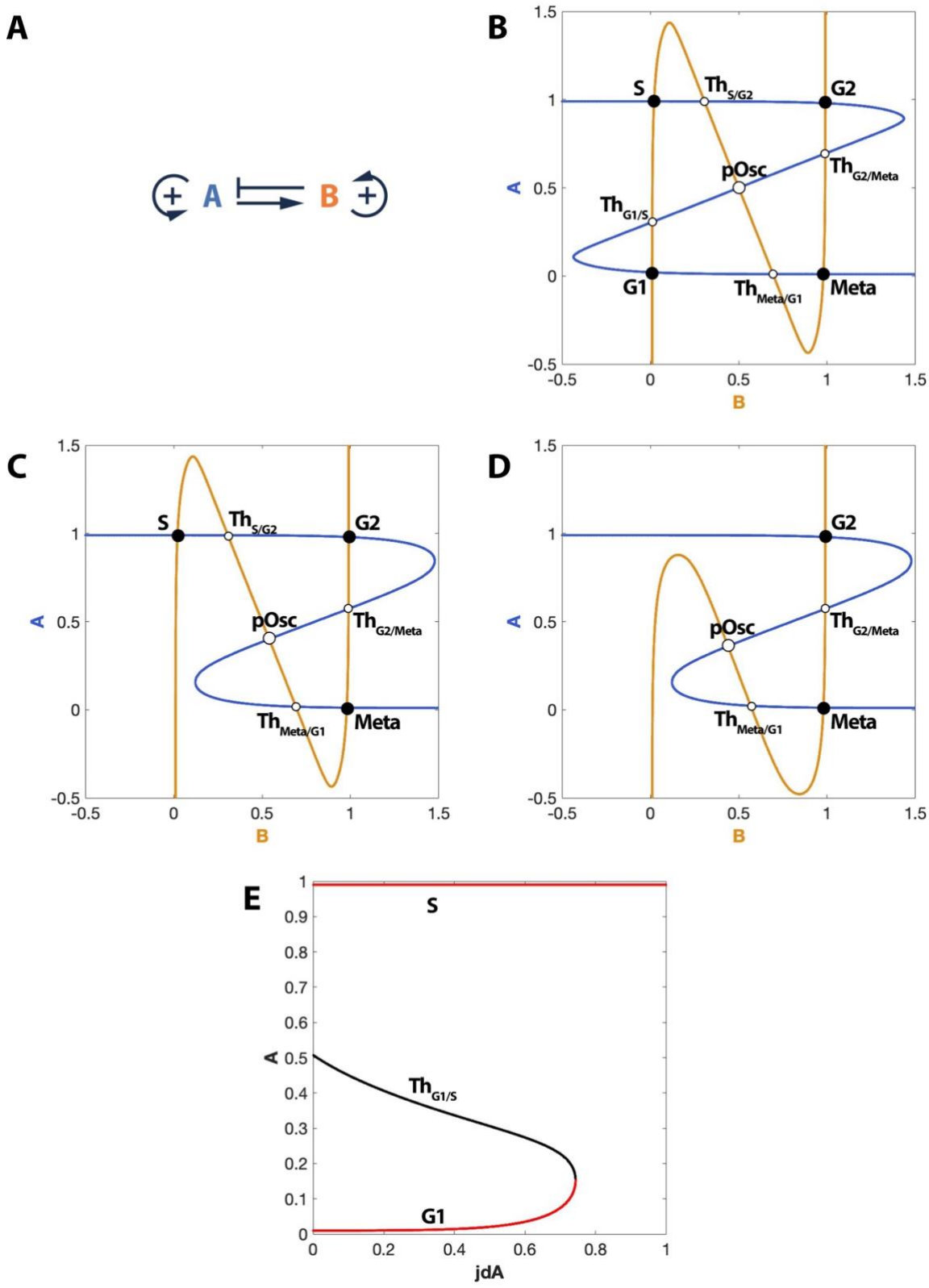

Fig. 4.3 – A tetra-stable core system – (A) Influence diagram of the core system. (B) Phase plane for the basal AB core system. (C) Phase plane for the core system with *jdA*=0.8, where the G1 state is eliminated. (D) Phase plane for the core system with *jdA*=0.8 and *jdB*=0.8, where the G1 and S states are eliminated. (E) Bifurcation diagram of A with respect to the *jdA* parameter. Bifurcation diagram legend: red denotes stable steady states and black denotes saddle and unstable points.

4.2.4 The excitatory module: helper-driven negative feedback pseudo-oscillators

The helper molecules drive state switching for the core module. For this to be achieved correctly, the activity of the helpers must be triggered only when the core module is in the appropriate state. Specifically, the helper of the G1/S transition (H1) must only be activated when the system is in the G1 state. Similarly, the S/G2 helper (H2) is to be activated when the system is in the S state and so on. Since each state is characterised by a different level of A and B activity, these activities will regulate each helper differently. For instance, since the G1 state is characterised by low A and low B activity, it follows that H1 must be suppressed in any state where either A or B is high. Therefore, A and B inhibit H1 (Fig. 4.4A). In contrast, since the S state differs from the G1 state by having high activity of A, it follows that H1 drives the state transition by activating A. With this wiring in mind, it is possible to analyse the properties of the excitatory module, which comprises a helper molecule and the core variable it regulates, as well as the second core variable, taken as a parameter, because it remains constant over the course of the transition. Here, I analyse H1-A module, but all other excitatory modules behave completely analogously, thanks to the symmetry of the system.

I plot the H1-A phase plane when B=0 (Fig. 4.4B). The A nullcline shows bistability, thanks to nonlinear positive feedback, which is consistent with A being bistable at B=0 on the core module phase plane (Fig. 4.3B). As expected from the positive effect of H1, only the higher A activity branch is stable for high H1 values. Notice that the H1 variable is also positive feedback-regulated, which renders its nullcline bistable as well. Thus, given the negative feedback between A and H1, the intersection of the nullclines' saddles gives rise to an unstable steady state, which has the potential to generate oscillations [66], and it is thus termed $pOsc_{H1}$. However, notice that the oscillation is blocked by the presence of a stable steady state, which corresponds to the S state of the core module. Thus, in essence, the excitatory module provides a path from the G1 state to the S state that bypasses the barrier imposed by $Th_{G1/S}$ in the core system plane.

Contrast this setup to that of the latching gate model in Fig. 4.1C. In that case, a delay in the activation of the helpers was introduced by interposing slow dynamical variables between the core regulators' (ABB') activation and that of the two helpers, C and C', in

order to generate high amplitude endocycles. The nonlinear auto-amplification of H1 obviates the need for explicit delay, reducing the number of dynamic variables of the system, while still enabling the generation of high-amplitude helper (pseudo)-oscillations. In addition, this modification improves the tunability of the oscillator[224] and is more likely to be consistent with the biochemical organisation of the cell cycle.

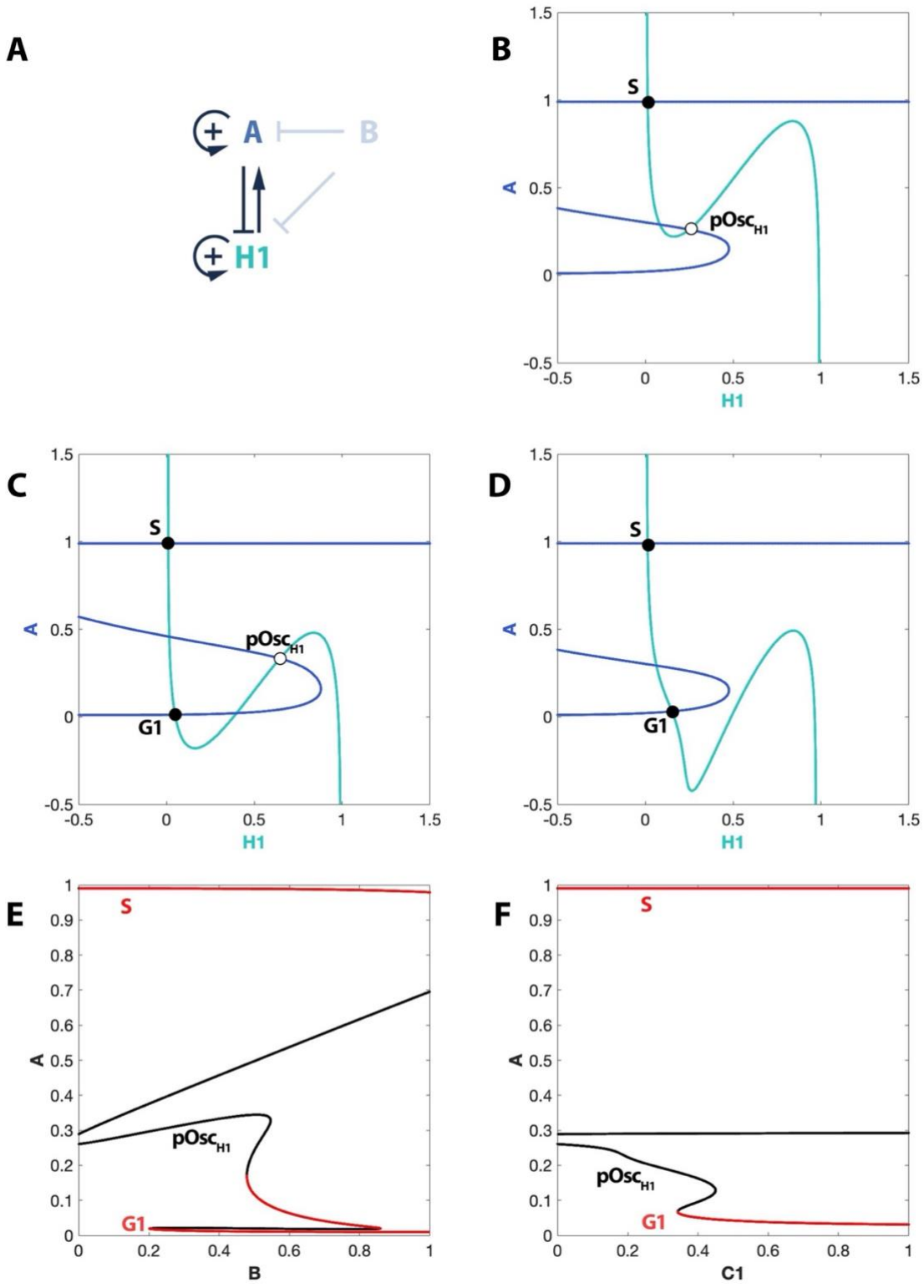

Fig. 4.4 – The dynamical properties of the excitatory module – (A) Influnce diagram for the excitatory module associated with the G1 state. H1 and A are dynamical variables here, while B (light grey) is taken as a parameter. (B) Phase plane of the excitatory module with B=0. (C) Phase plane with B=0.4. (D) Phase plane with the checkpoint parameter C1=1. (E) Bifurcation diagram of A with respect to the parameter B. (F) Bifurcation diagram of A with respect to the checkpoint parameter C1.

It is possible to note how the activity of the excitatory module changes when the core module is in different states. When A is high, H1-A system immediately reaches the S-state and therefore there is no other change in H1 levels. However, when B increases, a new stable steady state appears (G1) at low H1 and A values, as the inhibitory effect of B lowers the A activity necessary for H1 inactivation, such that the H1 nullcline undergoes a downward translation (Fig. 4.4C). Without this effect, the H1 variable could start accumulating prematurely, when the system reaches the Meta state (high B, low A).

Any other perturbation that prevents the activation of H1 will have a similar effect as increasing B. This property allows the introduction of checkpoints – arrests of the systems' oscillation of indefinite duration in response to a particular stimulus. C1 is a parameter that favours the inactivation of H1. If C1 is high, the G1 stable steady state is present on the H1-A phase plane regardless of B activity (Fig. 4.4D), such that H1 helper cannot aid the core system in bypassing the $Th_{G1/S}$ barrier and the overall oscillation is prevented until C1 parameter drops again. Bifurcation diagrams of the H1-A module with respect to either B (Fig. 4.4E) and C1 (Fig. 4.4F) show that the G1 state emerges through a saddle-node bifurcation as the parameters increase past a certain threshold (approx. 0.2 and 0.35, respectively), suggesting that the arrest is brought about abruptly and robustly.

4.2.5 The dynamics of the complete mitotic oscillation

The system proposed must be able to oscillate autonomously and pass through all the states of the core module in sequence to be an accurate model of the cell cycle. For this, the helper variable H2, H3 and H4 are introduced in analogy to H1 (Fig. 4.5A). H2 must accumulate in the S-state, when A is high and B is low. Consequently, H2 is activated by A and inhibited by B. In turn, H2 drives the activation of B, to take the system to G2. In G2, both A and B are high and stimulate H3. For the system, to transition to the Metaphase

state, A must be inactivated, which is the function carried out by H3. Note that this preserves the negative feedback of the H3-A excitatory module, which is anti-symmetric to the H1-A module analysed in detail previously. Finally, the H4-B module is anti-symmetric with H2-B.

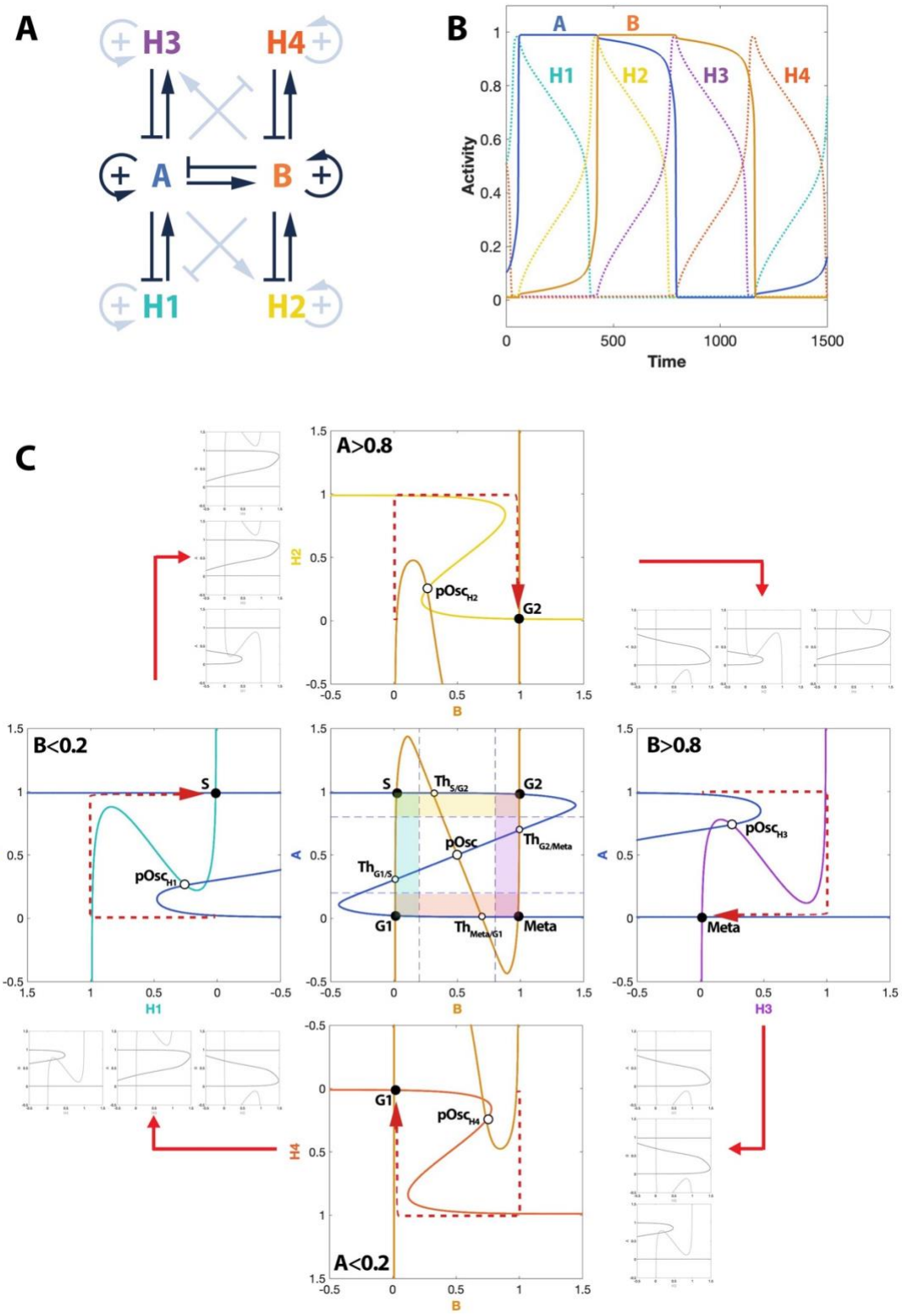

Fig. 4.5 – The dynamics of the complete mitotic oscillator – (A) Influence diagram. (B) Time course simulation. (C) The oscillation trajectory through projections of the 6-dimensional phase space. The central panel is the phase plane of the core model when all helpers are zero. The coloured regions represent the portions of the phase plane where each helper is active, bounded by the 0 and 1 values of each core variable. The phase planes on the periphery show each excitatory module at each phase of the core system. The enlarged, coloured phase planes correspond to the helpers driving the particular transitions, while the adjacent small grey panels show the state of the other excitatory modules at the same time. The dotted red arrows indicate the calculated trajectory on each helper's phase plane.

Plotting a time-course simulation of this system (Fig. 4.5B) reveals that oscillations occur as expected. First, H1 accumulates, and A follows in quick succession. When the S state has been reached, H1 activity drops and H2 increases. This takes the system to G2, as B activity increases sharply. Then, H2 drops and H3 accumulates, leading to the removal of A. Finally, Meta is reached and H3 is replaced by H4, which the system back to G1. The whole system dynamics can be illustrated by plotting the trajectory of the system through 2D sections of the phase space (Fig. 4.5C). Specifically, it is possible to see how each helper gets activated sequentially as the core changes state. This simplified view suggests that each of the helpers provides a path for the system to transition spontaneously from one state's basin of attraction to another one's without encountering any barrier. As each excitatory module is placed in an orthogonal plane to that of the core, the helpers essentially make the system 'jump' over the barriers between states.

A different, but equally valid, perspective looks at how the core is affected when each helper is active (Fig. 4.6). The familiar picture of the tetra-stable core system (Fig. 4.3B) is only applicable when all helpers are zero. However, when the helpers are active (i.e. during transitions), the properties of the core's phase plane change. For instance, during the G1/S transition (Fig. 4.6 bottom-left), H1=1 and the G1 state disappears. Subsequently, the core is spontaneously attracted to the S state. After H2 accumulates, S vanishes (Fig. 4.6 top-left) and the system 'falls' to G2, and so on. Of course, neither of these scenarios is strictly true, as the system is not confined to these well-defined sections through the phase space. Nevertheless, these approximate pictures serve as an aid to the intuition.

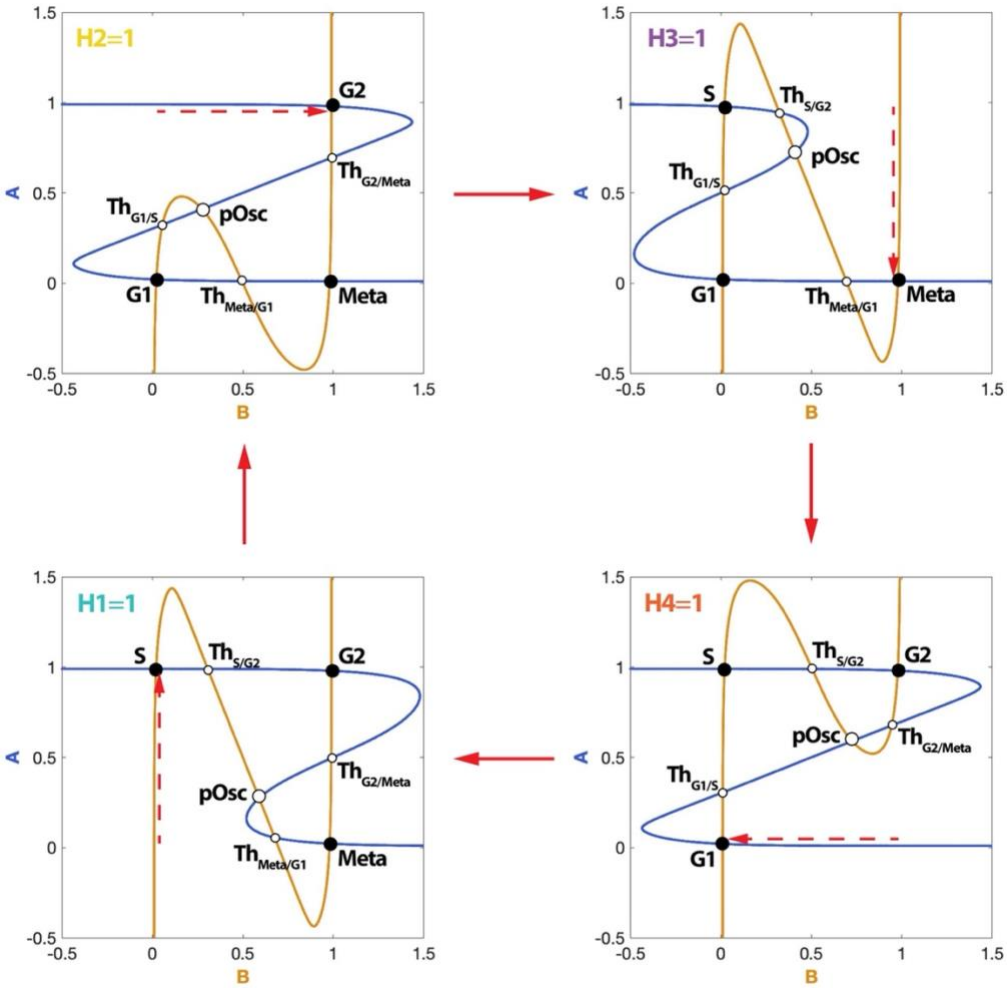

Fig. 4.6 – An alternative view of the oscillator's dynamics – the plot shows the sequence of changes to the core phase plane as each helper is activated. When each helper is sufficiently active, the state that led to its activation loses stability via a saddle-node bifurcation and the system is attracted to the next stable steady state in line.

4.2.6 Endocycle dynamics

I have previously defined endocycles formally as perturbed periodic solutions of a dynamical system from which some component is disengaged. As already explained (Fig. 4.3C,D), the core system can be perturbed via single parameter changes to abolish any of the 4 stable steady states, independently of each other. This is done by changing the *jdA, jsA, jdB and jsB* parameters, which control the position of the ON and OFF thresholds of the A and B nullclines. When a stable steady state is lost, the core system can bypass the activation of the helper, thanks to the loss of the barrier for entry into the next state. Because the helpers are modelled as slower variables than the core variables, they cannot accumulate to an appreciable extent under such conditions. In other words, the

helper affected by the loss of state stability is disengaged from oscillation, such that an endocycle emerges. This idea is illustrated as a time course simulation in Fig. 4.7A, where *jdB*=1 and the S-state is suppressed, such that H2 only accumulates to a very limited extent. Indeed, any two (or more) states can be suppressed giving rise to new types of endocycles. In Fig. 4.7B, both *jsB* and *jdB* are set to 1, such that S and Meta are suppressed and neither H2 nor H4 accumulates.

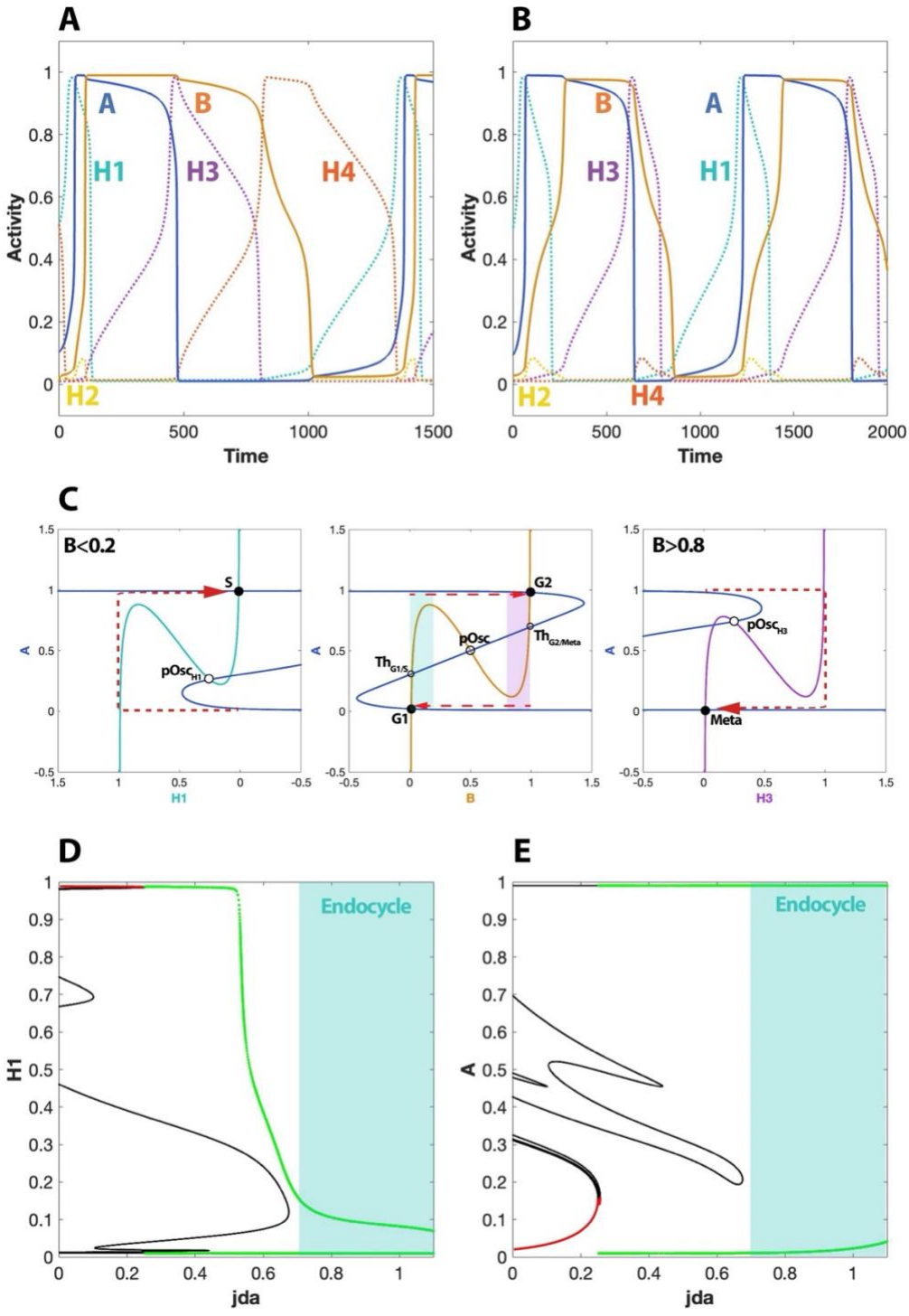

Fig. 4.7 – Endocycle dynamics – (A) Time course simulation for *jdB*=1, showing H2 disengagement from oscillation. (B) Time course simulation for *jdB=jsB*=1, showing H2 and H4 disengagement from oscillation. (C) Phase plane view of the *jdB=jsB*=1 perturbation. The G1/S and G2/Meta transitions are driven by excitatory modules (shown by left and right panels), while the S/G2 and Meta/G1 transitions are spontaneous for the core. (D) H1 vs *jdA* bifurcation diagram showing the dramatic loss of amplitude in H1 oscillation with *jdA* increase. (E) A vs *jdA* bifurcation diagram showing virtually no change in A amplitude with *jdA* increase. Bifurcation diagram legend: red denotes stable steady states, black denotes saddle and unstable points, and green denotes oscillation amplitude.

This endocycle can be visualised on the projections through the phase space (Fig. 4.7C), in analogy to Fig. 4.5C. The G1/S and G2/Meta transitions take place in the plane of the excitatory modules, under the action of H1 and H3, respectively. In contrast, the S/G2 and Meta/G1transitions take place spontaneously, in the AB core phase plane.

The transition between the mitotic cycle and endocycles can be tracked by plotting a bifurcation diagram of a helper with respect to the parameter that leads to the loss of stability of the corresponding core system state. In Fig. 4.7D, H1 is plotted with respect *jdA*, which shows that once jdA increases past approx. 0.6, the amplitude of H1 oscillation drops dramatically. In this context, endocycles can be defined as a drop in amplitude below 15% of the unperturbed oscillation. This only counts for the helper molecule targeted by the state – the amplitude of the other species is virtually unchanged (Fig. 4.7E). Note that this is analogous to the endocycle transition observed in the original budding yeast latching gate model (Fig. S4.1D).

4.2.7 The latching gate perspective on the 4-state system

The reason for introducing the core view of the endo-oscillatory system (Fig. 4.2) was that the latching gate perspective did not seem easy to generalise to more than two cell cycle phases. Now that a general form of that system exists, it is tempting to investigate what it looks like from the latching gate perspective. In Fig. 4.1C, two pseudo phase planes of the core variable A with respect to each helper were necessary to illustrate each system transition. Extrapolating, for a 4-state system, four phase planes will be necessary to depict all transitions. For this, the H1-A and H3-A phase planes are appended similarly to the AC and AC' pseudo phase planes (Fig. 4.8). In the top panel of Fig. 4.8, starting at the point where both H1 and H3 are zero and A is inactive, the system evolves naturally

toward the S state (the latched state), via the spontaneous accumulation of the H1 helper. However, the system cannot return to G1 right away through the accumulation of H3. This is because in the absence of active core variable B, the H3-A excitatory module is locked up in the G2 state. Thus, for the system to progress, assume B has increased to 1 (Fig. 4.8 bottom panel). This results in a downward translation of the H3 nullcline, which generates the $pOsc_{H3}$ unstable state and the loss of the G2 state. Now, the system can progress spontaneously to Meta (the second latched state). Of course, to return to G1, B has to be inactivated. Naturally, to fully describe the dynamics of the system, a similar pair of phase planes can be generated for the H2-B and H4-B. However, as that view is fully analogous to Fig.4.8, the plot is redundant.

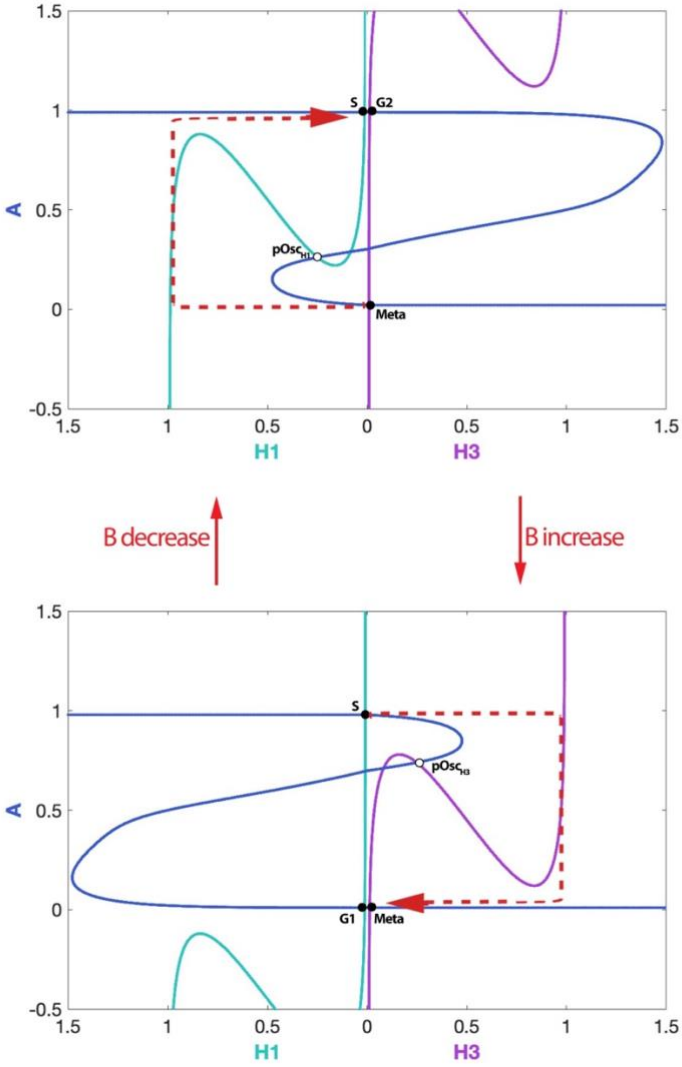

Fig. 4.8 – Latching gate view of the transitions in the core variable A – In the top panel, the latching gate perspective shows that, when the core variable B is inactive, the H1-A system drives the G1/S transition. From the perspective of A, the state reached is identical to G2. Nevertheless, the cycle cannot be completed, unless B accumulates and the G2 state loses stability. As shown in the bottom

panel, the H3-A system can complete bring the system to the Meta state, which from the perspective of A is identical to G1. The cycle is complete once B is eliminated.

4.3 Discussion

4.3.1 The Wheel of Fortune and its relation to the mammalian cell cycle

In this chapter, I have analysed and extended a novel type of endo-oscillatory system that may account for the emergence of endocycles in physiological context. In essence, this system frames the cell cycle as a series of stable pseudo steady states (on short time scales), which are normally insulated by the presence of 'high-energy barriers'. On longer time scales, each state generates a 'force' mediated by the so-called 'helper molecules' which facilitate crossing the barrier into the next state.

In this framework, an endocycle emerges when the 'barrier' between two states is eliminated and state transitions occur spontaneously, without the accumulation of the 'force-generating helper'. In contrast, a checkpoint can be understood as a process which opposes the generation of the helper 'force', such that the system is prevented from crossing the barrier into the next state. Notice that, at an intimate dynamical level, checkpoints and endocycles appear to be opposite processes, which is a feature shared by the "Newton's cradle" model where latching and checkpoint triggering are opposite states at the level of the individual oscillator.

An important question is whether this system is consistent with biochemical organisation of the cell cycle control network. Conspicuously, the A and B core variables in this framework correspond to the levels of the main cyclins driving DNA replication and mitosis, Cyclin A and B (Fig. 4.9). In G1, the levels of both CycA and CycB are kept low through degradation by APC/C:Cdh1. The system is pushed into S-phase by E2F-mediated CycA transcription. In this context, E2F corresponds to the first helper (H1) in the minimal model. In late S-phase, CycA:CDK2 helps activate the FoxM1 (H2) transcription factor, which triggers the accumulation of CycB, marking entry in G2 phase. The activation of the Cdc25 phosphatase, following the resolution of residual DNA

damage from S-phase leads to the activation of the CycB:CDK1 complex, which drives entry into mitosis. One of the targets activated by CDK1 is the ubiquitin ligase APC/C:Cdc20. Until the resolution of the spindle assembly checkpoint, this complex is in mitotic checkpoint complex form (H3), active towards CycA, but not CycB, establishing the 'Metaphase' state of the minimal model. Finally, the resolution of the mitotic checkpoint leads to the formation of active APC/C:Cdc20 (H4), which degrades CycB and brings the cell back to G1. While this simplistic description of cell cycle regulators and their interactions is largely consistent with the model proposed here, it is important to remark that the central negative feedback between A and B is not present directly between CycA and CycB, but rather it is mediated by the helpers (Fig. 4.9 green and red interactions). To conclusively establish whether this cell cycle control architecture can behave like the minimal model, or whether it can be updated to more closely resemble it, a mechanistic model must be built.

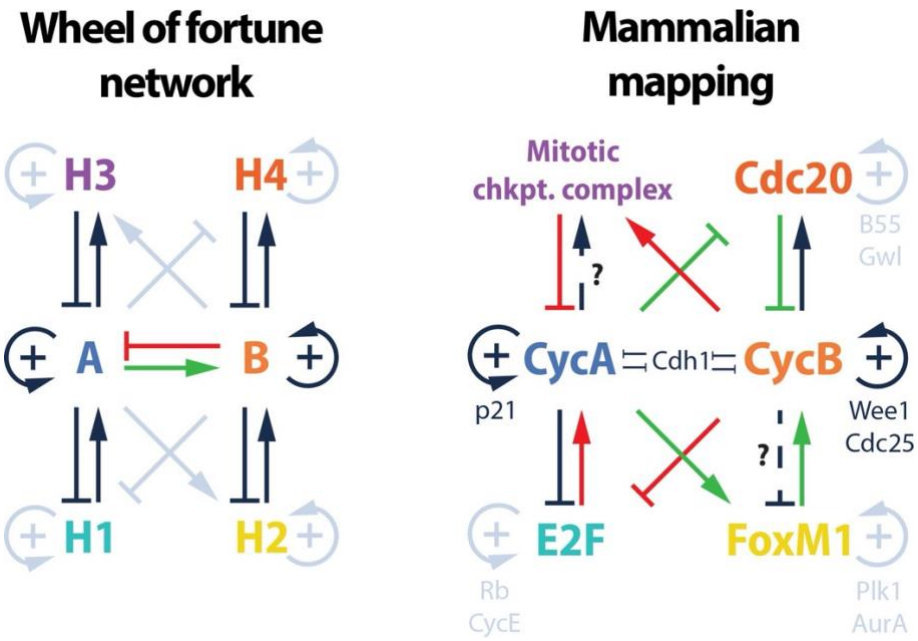

Fig. 4.9 – Putative mapping of the mammalian cell cycle control network to the 4-state excitable system

The properties of this system favour a new mechanical analogy to the mitotic cell cycle: a wheel of fortune with 4 equal sectors, corresponding to the cell cycle phases (Fig. 4.10). Between each sector, a peg is placed that prevents spinning unless sufficient force is applied to pull the indicator arrow's spring. In cell cycle context, this 'force' is generated by the helper variables, which dictate cyclin synthesis and degradation. Thus, an

endocycle occurs if one or more pegs is removed, such that spinning across one or more sectors is unhindered and does not require extra force. Equally, a checkpoint acts as force which opposes that of the helper variable (e.g. Rb opposes E2F to establish a G0 arrest and prevent the G1/S transition). I note that there is no stochastic element to this system, despite the potential implication of the name.

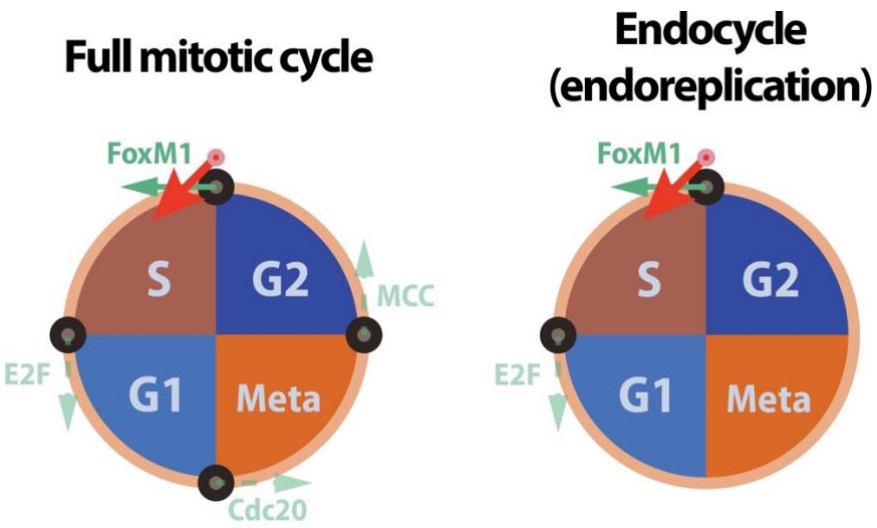

Fig. 4.10 – The "Wheel of fortune" analogy of the cell cycle endo-oscillatory system – The left-side schematic indicates that each cell cycle phase corresponds to one of the prizes of the wheel of fortune. The red arrow indicates the state of the core system. Pegs are present between the sectors, which prevent the spinning of the wheel unless sufficient force is applied. The helper molecules provide the required force. The right-side schematic corresponds to the cell cycle perturbations that give rise to endoreplication. The pegs between G2/Meta and Meta/G1 are removed, such that the wheel only requires the activation of helpers to progress after G1 and S phases.

Physiological endocycles can be seen as the suppression of different combinations of states. For instance, endoreplication occurs when the cell returns to G1 phase right after the completion of DNA replication. Therefore, endoreplication corresponds to the suppression of the G2 and Meta states. In contrast, endomitosis is similar to endoreplication, but the cell initiates mitotic events, without completing cytokinesis. This might correspond to the suppression of the Meta state only. In meiosis, the cell undergoes two divisions without intervening DNA replication; this endocycle might then correspond to the suppression of the G1 and S states. In Cdc20 endocycles, Cyclin B pulses are observed in the absence of either DNA replication or cell division. This could be consistent with a situation in which only the G2 state is stable.

4.3.2 “Newton’s Cradle” and the “Wheel of Fortune”

“Newton’s cradle” and the “Wheel of fortune” are dynamically distinct, despite being similar on the surface. In the case of “Newton’s cradle”, endocycles are driven by entirely autonomous oscillators. In the context of the full mitotic cycle, one oscillator temporarily arrests the other, to ensure the ordering of their firing. In the “Wheel of fortune” context, the system is not made up of individual autonomous oscillators. Instead, the function of the system relies of amplified negative feedback modules, which are nonetheless only ‘pseudo-oscillators’ as, in isolation, they give rise to stable steady states, not limit cycle oscillators. The oscillation emerges at the systems level, through unidirectional transitions between pseudo-stable steady states driven by the action of pseudo-oscillators. Therefore, in this framework, endocycles are not driven by a simple, autonomous, amplified negative feedback oscillator, but through the selective decoupling of pseudo-oscillators from the overall higher level, emergent oscillator.

The two dynamical frameworks introduced in this thesis demonstrate that at least two different regulatory strategies are available for the generation of endo-oscillatory behaviour. In spite of their differences, both strategies appear broadly consistent with the organisation of the cell cycle regulatory network. This raises the question of which of these models is likely to be a more accurate representation of cell cycle dynamics, and highlights the challenge of discriminating between theoretical models when highly complex experimental systems are concerned. Indeed, the problem is further complicated by the fact that either framework may not be universal and instead, different species drive endocycles with different underlying control networks.

The principal aim of future research is to provide experimental verification for the theoretical models proposed herein. One of the challenges is to discriminate between the “Newton’s cradle” and the “Wheel of fortune” frameworks. This is a challenging task, because many of the model’s dynamical features are, by definition, identical. However, one of the key differences is the change in oscillatory dynamics of different regulators in response to perturbations that lead to endo-oscillations. Specifically, the signature feature of “Newton’s cradle” dynamics is the abrupt suppression of one oscillator as a

specific perturbation threshold is reached (Fig. 3.4). This effect is underpinned by a global bifurcation of the overall system, which relies on the arrest of one of the oscillators at a SNIC bifurcation. The consequence of this property is critical slowing down, which implies that the period of oscillation near the bifurcation point approaches infinity. This has two implications at experimental level. First, if the strength of perturbation can be varied incrementally (such as through careful dosing of a pharmacological inhibitor), then a sharp change in the probability of oscillation of the module of interest could be observed. For instance, remember that Wee1 inhibition triggers Cdc20 endocycles. If the assumptions of the "Newton's cradle" model apply, we would expect to see a very sharp transition in the probability of mitotic cycle oscillation vs. endo-oscillation given a very narrow in inhibitor dosing. Second, due to critical slowing down, the period of oscillation is expected to increase very abruptly close to the bifurcation threshold (i.e. the critical concentration of inhibitor at which endocycles begin to emerge). This behaviour is in sharp contrast to that observed for the "Wheel of fortune" (Fig. 4.7). In this model, when the appropriate perturbation is induced, the oscillation amplitude of the targeted Helper diminishes gradually with the change of bifurcation parameter (i.e. inhibitor concentration). Thus the two models should be distinguished on the basis of the inhibitor dose-response curve properties.

Finally, it can be asked whether either control system provides any physiological advantages to the cell. It is immediately apparent that the "Wheel of fortune" framework provides more flexibility to implement checkpoints that guard cell cycle phase transitions. This likely is an important aspect in cells where very stringent regulation of proliferation is necessary, such as in multicellular organisms with complex developmental pathways and/or susceptibility to cancer. In contrast, "Newton's cradle" appears more intimately linked to the fundamental processes of the cell cycle – DNA replication and mitosis – and simultaneously appears less optimised for stringent computation of proliferative decisions. In addition, the fact that the transitions between mitotic cycles and endocycles happen very sharply given a change in a relevant input, suggests that the double oscillator might be a more robust architecture in cell types that customarily rely on processes such as endoreplication. It is conceivable that the gradual

transitions predicted by the “Wheel of fortune” carry the risk of over or under replication, or incomplete mitosis.

4.3.3 Insight into Cdc14 endocycles

The analysis of the latching gate system introduced by Novak and Tyson[157] and its extension to the 4-state “Wheel of fortune” system sheds new light on the results of Lu and Cross[76]. In their paper from 2010, the authors introduce the Cdc14 endocycle by demonstrating oscillations of Cdc14 phosphatase localisation to and outside the nucleolus in the presence of non-degradable Clb2, which prevents complete mitotic exit and the re-entry into G1. They claim that the Cdc14 endocycle is likely driven by a CDK-independent oscillator. This was countered by Novak and Tyson in 2022[157], using a mechanistic modelling approach, through the introduction of the latching gate hypothesis. The current theoretical investigation further refines the findings of these two papers. On the one hand, the “Wheel of Fortune” framework demonstrates that a completely autonomous limit cycle oscillator is not *necessary* for driving the endocycle. Instead, it is possible that the Cdc14-Cdh1-Cdc5 negative feedback loop, which Lu and Cross claim contributes to the endocycle, may give rise to a pseudo-oscillator, as defined above. Subsequently, changes in activity within the Cdk network may required, be they reduced in amplitude, for the endocycle to emerge. On the other hand, the latching gate hypothesis (i.e. the presence of a simple, irreversible, bistable switch coupled to two negative feedback loops) is not *sufficient* to explain robust, high amplitude endocycles – for this, further amplification or delays are necessary, which suggests that Lu and Cross correctly identified the importance of the Cdc14-Cdh1-Cdc5 negative feedback loop.

It is interesting to note that the authors of the experimental paper recorded the period of the Cdc14 endocycle as a function of non-degradable Clb2. In essence, the level of Clb2 can be thought of as a bifurcation parameter in the context of a model (c.f. Fig. S4.2), which allows the investigation of the transition between mitotic cycles and endocycles. In figure S5 of their paper, Lu and Cross show the frequency of Cdc14 oscillation increases roughly linearly with Clb2 concentration and then plateaus. This smooth

transition between mitotic cycles and endocycle is consistent with the “Wheel of Fortune” mechanism (Fig. 4.7, Fig. S4.2). If “Newton’s cradle” had underpinned the biological system, the frequency would have been expected to drop to zero at the boundary between mitotic cycles and Cdc14 endocycles, due to critical slowing down. Thus, at least for this particular experimental setup, the “Wheel of fortune” is the endo-oscillatory framework supported by evidence.

4.4 Materials and Methods

4.4.1 The two-state endo-oscillatory system

The minimal endo-oscillatory system based on the 2022 Novak & Tyson budding yeast model is constructed around a bistable core system. For the main component of this switch, A, it is assumed that the total concentration (A_{tot}) is fixed and that species can be converted between two forms: an active one (denoted by A) and an inactive one ($A_{tot} - A$). The conversion to the active form is stimulated linearly by C’ and nonlinearly by B and similarly, the inactivation is stimulated linearly by C and nonlinearly by B’:

$$\frac{dA}{dt} = \left(ksa + ksa' \cdot \text{C'} + \text{ksa"} \cdot \frac{B^p}{Jab^p + B^p}\right) \cdot (A_{tot} - A) - \left(kda + kda' \cdot C + kda" \cdot \frac{B'^p}{Jab^p + B'^p}\right) \cdot A \quad (4.1.1)$$

Where *ksa, ksa’, ksa”, kda, kda’, kda”,* are rate constants, with the basal rates of conversion (*ksa, kda*) being zero unless otherwise stated. *Jab* is the threshold level of B and B’ for the regulation of A and *p* is the applicable Hill exponent.

B and B’ are activated and inactivated, respectively, by A and assumed to be in steady state:

$$B = ndb + B_{tot} \frac{A^l}{Jb^l + A^l} \quad (4.1.2)$$

$$B' = ndb' + B'_{tot}\frac{Jb^l}{Jb^l + A^l} \quad (4.1.3)$$

B_{tot} and B'_{tot} are constants quantifying the total concentration of the two regulators, *Jb* is the threshold for regulation by A and *l* is a Hill exponent. *ndb* and *ndb'* are the non-degradable *B* and *B'*; these parameters are normally zero, but can be increased to generate endocycles.

The delay molecules are activated with simple mass-action kinetics by B and B', as stated by the ODEs:

$$\frac{dD}{dt} = ksd \cdot B - kdd \cdot D \quad (4.1.4)$$

$$\frac{dD'}{dt} = ksd' \cdot B' - kdd' \cdot D' \quad (4.1.5)$$

Where *ksd, kdd, ksd', kdd'* are rate constants. In turn, D and D' regulate the helper molecules C and C' nonlinearly:

$$\frac{dC}{dt} = ksc \cdot \frac{D^n}{Jc^n + D^n} - kdc \cdot C \quad (4.1.6)$$

$$\frac{dC'}{dt} = ksc' \cdot \frac{D'^n}{Jc^n + D'^n} - kdc' \cdot C' \quad (4.1.7)$$

Where *ksc, kdc, ksc', kdc'* are rate constants, *Jc* is the threshold for regulation by D and D', and *n* is a Hill exponent.

The parameter values are available in Table 4.1 (Appendix 3)

4.4.2 The four-state endo-oscillatory system

The core system consists of two dynamical variable, A and B, defined according to 2 ODEs. Each equation describes the symmetric conversion of each species between two forms: an active one (e.g. A), and an inactive one (e.g. 1-A).

$$\frac{dA}{dt} = (ksa \cdot AC_A + ksa') \cdot (1 - A) - (kda \cdot AC_{1-A} + kda') \cdot A \quad (4.2.1)$$

$$\frac{dB}{dt} = (ksb \cdot AC_B + ksb') \cdot (1 - B) - (kdb \cdot AC_{1-B} + kdb') \cdot B \quad (4.2.2)$$

Both the positive and the negative terms of each equation contain a non-linear 'auto-catalytic' (AC) function, which provides the coupling of the two variables. The form of these expressions is that of a Hill function whose threshold of activation depends on the opposite dynamical variable. Thus, A stimulates its own activation, but is opposed by B, as the threshold of the Hill function increases linearly with B:

$$AC_A = \frac{A^p}{(jsA + jA' \cdot B)^p + A^p} \quad (4.2.3a)$$

Similarly, the inactive form of A, denoted by *1 – A*, is also self-stimulated, but opposed by *1 – B* (i.e. stimulated by *B*).

$$AC_{1-A} \frac{(1 - A)^p}{\left(jdA + jA' \cdot (1 - B)\right)^p + (1 - A)^p} \quad (4.2.4a)$$

Thus, *B* inhibits *A* through both terms. This seemingly cumbersome description is necessary for rendering the dynamical system fully symmetrical and greatly simplifies the model further down the line. The auto-catalytic functions of B are treated similarly, but note that A stimulates the conversion of B to the active form:

$$AC_B = \frac{B^q}{\left(jsB + jB' \cdot (1 - A)\right)^q + B^q} \quad (4.2.5a)$$

$$AC_{1-B} = \frac{(1 - B)^q}{(jdB + jB' \cdot A)^q + (1 - B)^q} \quad (4.2.6a)$$

The helper variable *H1* is modelled in analogy to *A* and *B*, such that *H1* is present in two forms: active (*H1*) and inactive (*1 – H1*). The conversion of between terms is done at basally (rate constants *ksh1'* and *kdh1'*) and autocatalytically. In addition, a checkpoint term is present ($kch \cdot C1$), which favours H1 conversion to the inactive form with mass action kinetics:

$$\frac{dH1}{dt} = (ksh \cdot AC_{H1} + ksh')(1 - H1) - (kdh \cdot AC_{1-H1} + kdh' + kch \cdot C1)H1 \qquad (4.2.7)$$

The autocatalytic terms show that the activation of *H1* is inhibited by both *A* and *B*, as *H1* accumulation is triggered when both A and B are inactive:

$$AC_{H1} = \frac{H1^r}{(jsH \ + \ jH' \cdot A \ + \ jH" \cdot B)^r \ + \ H1^r} \qquad (4.2.8)$$

$$AC_{1-H1} = \frac{(1 - H1)^r}{(jdH \ + \ jH' \cdot (1 - A) \ + \ jH" \cdot (1 - B))^r \ + \ (1 - H1)^r} \qquad (4.2.9)$$

All other helpers are modelled analogously, except *A* and *B* terms are replaced by (*1 – A*) and (*1 – B*), and *vice versa*, if *A* or *B* activate the helper instead of inhibiting it. For example, H2 is activated by *A* and inhibited by *B*. Thus, its auto-catalytic functions are modelled as (changes in bold):

$$AC_{H2} = \frac{H2^r}{(jsH \ + \ jH' \cdot (\mathbf{1} - \boldsymbol{A}) \ + \ jH" \cdot B)^r \ + \ H2^r} \qquad (4.2.10)$$

$$AC_{1-H2} = \frac{(1 - H2)^r}{(jdH \ + \ jH' \cdot \boldsymbol{A} + \ jH" \cdot (1 - B))^r \ + \ (1 - H2)^r} \qquad (4.2.11)$$

To link the helpers to the core variables, the core's auto-catalytic functions are updated to:

$$AC_A = \frac{A^p}{(jsA \ + \ jA' \cdot B \ + \ \boldsymbol{ksah \cdot H3})^p + \ A^p} \qquad (4.2.3b)$$

$$AC_{1-A} \frac{(1 - A)^p}{(jdA \ + \ jA' \cdot (1 - B) \ + \ \boldsymbol{ksah \cdot H1})^p + \ (1 - A)^p} \qquad (4.2.4b)$$

$$AC_B = \frac{B^q}{(jsB \ + \ jB' \cdot (1 - A) + \ \boldsymbol{ksah} \cdot \boldsymbol{H4})^q + \ B^q} \qquad (4.2.5b)$$

$$AC_{1-B} = \frac{(1 - B)^q}{(jdB \ + \ jB' \cdot A + \ \boldsymbol{ksah} \cdot \boldsymbol{H2})^q + \ (1 - B)^q} \qquad (4.2.6b)$$

As such, *H1* activates *A* and *H3* inactivates it. Similarly, *H2* activates *B* and *H3* inactivates it.

The parameter values are available in Table 4.2 (Appendix 3)

5 General Discussion

5.1 Summary

Cell cycle dynamics has been the subject of extensive theoretical research for over three decades. Broadly, the aims of this research have been two-fold: on the one hand, to provide a link between biochemical mechanisms and phenomenology, and on the other hand, to develop frameworks that explain the properties of cell cycle transitions and oscillations from a regulatory perspective.

Comparatively little attention has been given to the global organisation of the cell cycle, and the properties that emerge when multiple phases are affected simultaneously by the perturbation of a single molecular species. Conversely, it has not been previously addressed whether the cell cycle is the simple juxtaposition of ordered, but otherwise isolated, phase transitions, or whether any higher-level phenomena can occur due to the interplay between different phase-specific events. The current work attempts to address this gap by considering the problem of endocycle emergence through the lens of control systems theory. To this end, I have developed a mechanistic model of the mammalian cell cycle control network, which predicts the triggering of endocycles following pharmacological and genetic perturbations. Subsequently, based on this and other mechanistic models, I introduced two endo-oscillatory dynamical frameworks. These models aimed to unify the paradigms of cell cycle unidirectionality, irreversibility, checkpoint triggering and endocycling.

The mechanistic model reproduces the temporal behaviour of cell cycle regulators in a way that is consistent with previous observations and predicts that perturbing the activity of the mitotic kinase (CDK1) can generate two types of endocycles. Reducing the activity of CDK1 prevents entry into mitosis, without preventing the periodic activation of the regulators that drive DNA replication, suggesting that this perturbation may lead to endoreplication. Further, CDK1 overactivation, through the suppression of its inhibitory kinase (Wee1), leads to the periodic accumulation/activation of mitotic regulators,

without inducing DNA replication. These oscillations were termed Cdc20 endocycles. At the same time, this model includes a mechanism for G1 size checkpoint triggering and allows for the introduction of DNA damage and spindle assembly checkpoints.

The model's predictions have been tested in RPE1 cells, by inducing the two types of endocycles through pharmacological and genetic perturbations. By treating cells with a CDK1 inhibitor, it was shown that endoreplication can be triggered. Similarly, by suppressing the activity of the CDK1 negative regulator, Wee1, through RNA interference, it was shown that Cyclin B levels can oscillate in the absence of DNA replication, consistent with the induction of Cdc20 endocycles.

While this model shows that the known interactions within the cell cycle control network can reproduce these qualitatively distinct dynamical behaviours, its complexity obscures the regulatory principles that underpin the transition to endocycles. Thus, my subsequent work aimed to identify the necessary and sufficient conditions that enable a dynamical system to transition between oscillatory modes that engage different subsets of components.

The "Newton's cradle" model assumes that the cell cycle is regulated by two autonomous, but mutually inhibitory oscillators, controlling replicative (i.e. G1/S) and mitotic (G2/M) events, respectively[222]. This network structure ensures the strict alternation of G1/S and G2/M events of the mitotic cycle. Nevertheless, silencing one oscillator still allows the second one to run independently, giving rise to an endocycle. As either oscillator can be silenced, two types of endocycles can be generated. Arresting the mitotic oscillator leads to endoreplication. Suppressing the replicative oscillator leads to repeated activation of the mitotic network, as it occurs twice in meiosis, or repeatedly in Cdc20 endocycles. The framework also allows for the introduction of checkpoints by arresting one oscillator in a state that holds the second oscillator in the latched position.

At the core of the "Wheel of fortune" network, there are two dynamical variables, giving rise to two bistable switches. Together, these switches give rise to 4 pseudo-steady states, corresponding to cell cycle phases. To drive the progression through these phases

and give rise to oscillations, 4 helper variables are activated by each of the states, respectively, and subsequently help 'push' the core system into the next steady state in line. Notably, this system can be perturbed to abolish any of the 4 phases. For this, a parameter change can be introduced that moves either threshold of either bistable switch, such that the applicable steady state (i.e. cell cycle phase) is abolished. When this happens, the system is automatically attracted to the next steady state in sequence and phase progression does not require the activation of the transition variable. Equally, the characteristic cellular events of the phase would no longer be triggered. Thus, endoreplication occurs when the G2 and metaphase states are abolished. Meiosis takes place when G1 and S are suppressed. Finally, endomitosis should be observed when the metaphase state (after which cytokinesis is triggered) is abolished. Importantly, the "Wheel of fortune" system can be perturbed such that any helper molecule can be prevented from accumulating, allowing for the establishment of 4 different checkpoints, unlike "Newton's Cradle", in which only 2 are possible.

5.2 Conclusions

The biochemical interaction networks that regulate proliferation are so complex as to be intractable to the unaided intuition. To circumvent this problem, I aimed to explain the properties of the cell cycle on the basis of hierarchies of control motifs, such as bistable switches and oscillators, as opposed to biochemical reactions. These regulatory structures give rise to complex dynamical behaviour, which matches that of the cell cycle. In this context, endocycles are primarily of methodological interest: they are complex dynamical phenomena, which are particularly suited to a control theoretical approach. Predicting and explaining them represents a touchstone of our cell biological understanding.

The primary conclusion of this abstract approach is that the cell cycle must comprise multiple oscillatory units in order to account for endocycles. Although the presence of multiple negative feedback loops with oscillatory potential has been previously recognised[225], their physiological significance has been largely unquestioned. It is now

apparent that these limit cycle (pseudo-) oscillators underpin physiological functions relevant in development, or in pathological processes, such as malignant transformation. The conservation and ubiquity of both mitotic and replicative endocycles across distant taxonomic groups, even when the biochemical components of the relevant pathways are not themselves conserved, argues that these dynamical features play fundamental roles in the operation of the cell cycle.

This work has an important corollary about the nature of physiological function. For nearly a century, the primary paradigm that has dominated biological research is that function is a consequence of the structure and biochemical properties of proteins and nucleic acids. However, the work herein highlights a different perspective: within a control pathway, any single amino acid that makes up the constituent proteins could be modified, yet function could persist. Indeed, biochemical details are in many ways dispensable; what matters is a subset of regulatory interactions that emerge from the biochemistry. Therefore, physiological properties exist 'on top of' the biochemistry, and although they practically depend on it, they logically operate according to a set of principles that does not involve those of Biochemistry. Thus, as the complexity of biological processes that make the subject of scientific research continues to increase, it will be fruitful to consider the role of regulatory motifs as a matter of course.

5.3 Limitations

The work presented herein uses an abstract and theoretical approach to reason about the organisation of the cell cycle control network. This has yielded two frameworks whose dynamics are analogous to those of two simple mechanical systems, allowing for a simple way to rationally interrogate a very complex molecular system. However, experimental validation of these theories is still pending. Such verification is fraught with challenges. First, the abstract models cannot be tested directly, as the dynamics of regulators cannot be directly perturbed. Instead, mechanistic models must be developed on the basis of these frameworks. Subsequently, the necessary perturbations that are supposed to trigger endocycles must be introduced in vivo. This comes with a

series of challenges, such as the emergence of phenomena that mask the endo-oscillatory behaviour. This may occur due to redundancies in the biological control network, which likely makes cell cycle function more robust to perturbation than assumed by the current simplified approach. Further, checkpoint mechanisms are likely to prevent the potentially deleterious endo-oscillations. Nevertheless, further insight and validation could come from the study of naturally occurring endocycles.

5.4 Future directions

To establish whether either of the endo-oscillatory architectures are indeed at the core of cell cycle regulation, future work will also aim to produce and test mechanistic models that apply to a range of eukaryotes, such as fission yeast and plants. It is, however, important to investigate not just whether the cell cycle architecture is conserved, but how it may have emerged on evolutionary scale. This is a complex task, because a highly developed Cyclin:CDK system was seemingly present in the last eukaryotic common ancestor[226], but no homologous genes have been identified in the closest prokaryotic "relatives" of eukaryotes, the archaea. Nevertheless, an underappreciated fact is that other cell cycle regulators certainly predate the archaeal/eukaryotic divergence. For instance, a DNA replicative oscillator (whose existence is presupposed by "Newton's Cradle" model) may have existed in archaea, as necessary components (e.g. the E2F transcriptions factor and the ORC1/Cdc6 licensing factors) are present is some phyla[227]. Further identifying such modules may lend credence to the existence of the regulatory modules assumed by the minimal models I proposed. Subsequently, it may be possible to show whether Cyclin:CDKs developed as a means to organise these autonomous systems driving fundamental events of the proliferative program.

Understanding the emergence of endocycles has potentially significant implications for disorders involving cellular over-proliferation, such as malignancy. On the one hand, endoreplication may play an important role in cancer development and prognosis[228]. Selectively targeting this process may impact clinical outcome[229]. In addition, given the potentially deleterious effect of endocycles, the pharmacological induction of this

phenotype may represent a new strategy for synthetic lethal approaches. Indeed, existing cancer therapeutics, such as Wee1 inhibitors already have the potential to give rise to such endocycles. Leveraging this property may have a favourable impact clinical in a therapeutic window with fewer side effects.

References

1. Dreyer, J. L. E. *Tycho Brahe : A Picture of Scientific Life and Work in the Sixteenth Century*. (Adam & Charles Black, Edinburgh, 1890).
2. Fusti, R. & Gilbert, J. History and philosophy of science through models: Some challenges in the case of 'the atom'. *Int J Sci Educ* **22**, 993–1009 (2000).
3. F.R.S., J. J. T. M. A. XL. Cathode Rays. *The London, Edinburgh, and Dublin Philosophical Magazine and Journal of Science* **44**, 293–316 (1897).
4. Joseph John Thomson. *The Corpuscular Theory of Matter*. (Scribner's Sons, 1907).
5. Gegier H. and Marsden Ernest. On a diffuse reflection of the α-particles. *Proc. R. Soc. Lond. A* **82**, 495–500 (1909).
6. Rutherford, E. The Scattering of α and β Particles by Matter and the Structure of the Atom. *Philos. Mag* **6**, 21.
7. Bohr, N. I. On the constitution of atoms and molecules. *The London, Edinburgh, and Dublin Philosophical Magazine and Journal of Science* **26**, 1–25 (1913).
8. Saigusa, T., Tero, A., Nakagaki, T. & Kuramoto, Y. Amoebae anticipate periodic events. *Phys Rev Lett* **100**, 018101 (2008).
9. Boussard, A. *et al.* Adaptive behaviour and learning in slime moulds: the role of oscillations. *Philosophical Transactions of the Royal Society B* **376**, (2021).
10. Crick, F. Central Dogma of Molecular Biology. *Nature 1970 227:5258* **227**, 561–563 (1970).
11. Ptashne, Mark. A genetic switch : phage lambda revisited. 154 (2004).
12. Laubichler, M. D. & Wagner, G. P. How Molecular is Molecular Developmental Biology? A Reply to Alex Rosenberg's Reductionism Redux: Computing the Embryo. *Biol Philos* **16**, 53–68 (2001).
13. Page, C. C., Moser, C. C., Chen, X. & Dutton, P. L. Natural engineering principles of electron tunnelling in biological oxidation–reduction. *Nature 1999 402:6757* **402**, 47–52 (1999).
14. Jeffery, C. J. Protein moonlighting: what is it, and why is it important? *Philosophical Transactions of the Royal Society B: Biological Sciences* **373**, (2018).
15. González-Arzola, K. *et al.* New moonlighting functions of mitochondrial cytochrome c in the cytoplasm and nucleus. *FEBS Lett* **593**, 3101–3119 (2019).
16. Cheng, M. *et al.* The p21Cip1 and p27Kip1 CDK 'inhibitors' are essential activators of cyclin D-dependent kinases in murine fibroblasts. *EMBO J* **18**, 1571–1583 (1999).
17. Turnbull, M. G. Underdetermination in science: What it is and why we should care. *Philos Compass* **13**, e12475 (2018).
18. Akaike, H. Information Theory and an Extension of the Maximum Likelihood Principle. *Biogeochemistry* **1998**, 199–213 (1998).
19. Kim, J. K. & Tyson, J. J. Misuse of the Michaelis–Menten rate law for protein interaction networks and its remedy. *PLoS Comput Biol* **16**, e1008258 (2020).
20. Xie, S., Swaffer, M. & Skotheim, J. M. Eukaryotic Cell Size Control and Its Relation to Biosynthesis and Senescence. *Annu Rev Cell Dev Biol* **38**, 291–319 (2022).
21. Sterner, B. & Lidgard, S. Objectivity and Underdetermination in Statistical Model Selection. *Br J Philos Sci* (2024) doi:10.1086/716243.

22. Fodor, J. A. Special sciences (or: The disunity of science as a working hypothesis). *Synthese* **28**, 97–115 (1974).
23. Koskinen, R. Multiple realizability as a design heuristic in biological engineering. *Eur J Philos Sci* **9**, 1–15 (2019).
24. Antebi, Y. E. *et al.* Combinatorial Signal Perception in the BMP Pathway Article Combinatorial Signal Perception in the BMP Pathway. *Cell* **170**, 1184-1185.e24 (2017).
25. Purvis, J. E. & Lahav, G. Encoding and Decoding Cellular Information through Signaling Dynamics. *Cell* **152**, 945 (2013).
26. Schmoller, K. M., Turner, J. J., Kõivomägi, M. & Skotheim, J. M. Dilution of the cell cycle inhibitor Whi5 controls budding-yeast cell size. *Nature* **526**, 268–272 (2015).
27. Zatulovskiy, E., Zhang, S., Berenson, D. F., Topacio, B. R. & Skotheim, J. M. Cell growth dilutes the cell cycle inhibitor Rb to trigger cell division. *Science (1979)* **369**, 466–471 (2020).
28. De Klein, A. *et al.* Targeted disruption of the cell-cycle checkpoint gene ATR leads to early embryonic lethality in mice. *Current Biology* **10**, 479–482 (2000).
29. Berthet, C. *et al.* Combined Loss of Cdk2 and Cdk4 Results in Embryonic Lethality and Rb Hypophosphorylation. *Dev Cell* **10**, 563–573 (2006).
30. Hanahan, D. & Weinberg, R. A. Hallmarks of cancer: The next generation. *Cell* **144**, 646–674 (2011).
31. Matthews, H. K., Bertoli, C. & de Bruin, R. A. M. Cell cycle control in cancer. *Nature Reviews Molecular Cell Biology 2021 23:1* **23**, 74–88 (2021).
32. Kumari, R. & Jat, P. Mechanisms of Cellular Senescence: Cell Cycle Arrest and Senescence Associated Secretory Phenotype. *Front Cell Dev Biol* **9**, 645593 (2021).
33. López-Otín, C., Blasco, M. A., Partridge, L., Serrano, M. & Kroemer, G. Hallmarks of aging: An expanding universe. *Cell* **186**, 243–278 (2023).
34. Morgan, D. O. *The Cell Cycle: Principles of Control (Primers in Biology)*. *Cell Division* vol. 2 (Sinauer Associates, Inc., 2007).
35. Zetterberg, A. & Larsson, O. Kinetic analysis of regulatory events in G1 leading to proliferation or quiescence of Swiss 3T3 cells. *Proc Natl Acad Sci U S A* **82**, 5365–5369 (1985).
36. Pardee, A. B. A restriction point for control of normal animal cell proliferation. *Proc Natl Acad Sci U S A* **71**, 1286–1290 (1974).
37. Min, M., Rong, Y., Tian, C. & Spencer, S. L. Temporal integration of mitogen history in mother cells controls proliferation of daughter cells. *Science* **368**, 1261 (2020).
38. Yang, H. W., Chung, M., Kudo, T. & Meyer, T. Competing memories of mitogen and p53 signalling control cell-cycle entry. *Nature 2017 549:7672* **549**, 404–408 (2017).
39. Fulcher, L. J., Sobajima, T., Batley, C., Gibbs-Seymour, I. & Barr, F. A. MDM2 acts as a timer reporting the length of mitosis. *bioRxiv* 2023.05.26.542398 (2024) doi:10.1101/2023.05.26.542398.
40. Meitinger, F. *et al.* Control of cell proliferation by memories of mitosis. *Science (1979)* **383**, 1441–1448 (2024).
41. Cuyàs, E., Corominas-Faja, B., Joven, J. & Menendez, J. A. Cell cycle regulation by the nutrient-sensing mammalian target of rapamycin (mTOR) pathway. *Methods Mol Biol* **1170**, 113–144 (2014).

42. Köberlin, M. S. *et al.* A fast-acting lipid checkpoint in G1 prevents mitotic defects. *Nature Communications 2024 15:1* **15**, 1–17 (2024).
43. Bohnsack, B. L. & Hirschi, K. K. Nutrient regulation of cell cycle progression. *Annu Rev Nutr* **24**, 433–453 (2004).
44. Ciccia, A. & Elledge, S. J. The DNA Damage Response: Making it safe to play with knives. *Mol Cell* **40**, 179 (2010).
45. Uhlmann, F. & Nasmyth, K. Cohesion between sister chromatids must be established during DNA replication. *Current Biology* **8**, 1095–1102 (1998).
46. Armstrong, C., Passanisi, V. J., Ashraf, H. M. & Spencer, S. L. Cyclin E/CDK2 and feedback from soluble histone protein regulate the S phase burst of histone biosynthesis. *Cell Rep* **42**, 112768 (2023).
47. Armstrong, C. & Spencer, S. L. Replication-dependent histone biosynthesis is coupled to cell-cycle commitment. *Proc Natl Acad Sci U S A* **118**, e2100178118 (2021).
48. Nelson, D. M. *et al.* Coupling of DNA Synthesis and Histone Synthesis in S Phase Independent of Cyclin/cdk2 Activity. *Mol Cell Biol* **22**, 7459 (2002).
49. Fu, J., Hagan, I. M. & Glover, D. M. The Centrosome and Its Duplication Cycle. *Cold Spring Harb Perspect Biol* **7**, a015800 (2015).
50. Nebreda, A. R. & Ferby, I. Regulation of the meiotic cell cycle in oocytes. *Curr Opin Cell Biol* **12**, 666–675 (2000).
51. Ganji, M. *et al.* Real-time imaging of DNA loop extrusion by condensin. *Science (1979)* **360**, 102–105 (2018).
52. Gibcus, J. H. *et al.* A pathway for mitotic chromosome formation. *Science (1979)* **359**, (2018).
53. Musacchio, A. The Molecular Biology of Spindle Assembly Checkpoint Signaling Dynamics. *Current Biology* **25**, R1002–R1018 (2015).
54. Hartwell, L. H., Culotti, J. & Reid, B. Genetic Control of the Cell-Division Cycle in Yeast, I. Detection of Mutants. *Proc Natl Acad Sci U S A* **66**, 352 (1970).
55. Hartwell, L. H., Culotti, J., Pringle, J. R. & Reid, B. J. Genetic control of the cell division cycle in yeast. *Science (1979)* **183**, 46–51 (1974).
56. Nurse, P., Thuriaux, P. & Nasmyth, K. Genetic control of the cell division cycle in the fission yeast Schizosaccharomyces pombe. *Mol Gen Genet* **146**, 167–178 (1976).
57. J. M. Mitchison. *The Biology of the Cell Cycle*. (Cambridge Univ. Press, New York, 1972).
58. Murray, A. W. & Kirschner, M. W. Dominoes and Clocks: the Union of Two Views of the Cell Cycle. *Science (1979)* **246**, 614–621 (1989).
59. Evans, T., Rosenthal, E. T., Youngblom, J., Distel, D. & Hunt, T. Cyclin: a protein specified by maternal mRNA in sea urchin eggs that is destroyed at each cleavage division. *Cell* **33**, 389–396 (1983).
60. Gerhart, J., Wu, M. & Kirschner, M. Cell cycle dynamics of an M-phase-specific cytoplasmic factor in Xenopus laevis oocytes and eggs. *J Cell Biol* **98**, 1247–1255 (1984).
61. Wasserman, W. J. & Smith, L. D. The cyclic behavior of a cytoplasmic factor controlling nuclear membrane breakdown. *J Cell Biol* **78**, (1978).
62. Sheehan, M. A. *et al.* Dominoes and Clocks: the Union of Two Views of the Cell Cycle. *Science (1979)* **246**, 614–621 (1989).

63. Mathias, N. *et al.* Cdc53p acts in concert with Cdc4p and Cdc34p to control the G1-to-S-phase transition and identifies a conserved family of proteins. *Mol Cell Biol* **16**, 6634–6643 (1996).
64. Haase, S. B. & Reed, S. I. Evidence that a free-running oscillator drives G1 events in the budding yeast cell cycle. *Nature 1999 401:6751* **401**, 394–397 (1999).
65. Tyson, J. J., Chen, K. C. & Novak, B. Sniffers, buzzers, toggles and blinkers: Dynamics of regulatory and signaling pathways in the cell. *Curr Opin Cell Biol* **15**, 221–231 (2003).
66. Novák, B. & Tyson, J. J. Design principles of biochemical oscillators. *Nature Reviews Molecular Cell Biology 2008 9:12* **9**, 981–991 (2008).
67. Tyson, J. J., Csikasz-Nagy, A. & Novak, B. The dynamics of cell cycle regulation. *BioEssays* **24**, 1095–1109 (2002).
68. Tyson, J. J. & Novak, B. Regulation of the Eukaryotic Cell Cycle: Molecular Antagonism, Hysteresis, and Irreversible Transitions. *J Theor Biol* **210**, 249–263 (2001).
69. Porter, A. C. G. Preventing DNA over-replication: A Cdk perspective. *Cell Div* **3**, 1–10 (2008).
70. Lee, H. O., Davidson, J. M. & Duronio, R. J. Endoreplication: polyploidy with purpose. *Genes Dev* **23**, 2461–2477 (2009).
71. Wang, M. J., Chen, F., Lau, J. T. Y. & Hu, Y. P. Hepatocyte polyploidization and its association with pathophysiological processes. *Cell Death & Disease 2017 8:5* **8**, e2805–e2805 (2017).
72. Storchova, Z. & Pellman, D. From polyploidy to aneuploidy, genome instability and cancer. *Nature Reviews Molecular Cell Biology 2004 5:1* **5**, 45–54 (2004).
73. Chan, K. Y. *et al.* Skin cells undergo asynthetic fission to expand body surfaces in zebrafish. *Nature 2022 605:7908* **605**, 119–125 (2022).
74. Marston, A. L. & Amon, A. Meiosis: cell-cycle controls shuffle and deal. *Nature Reviews Molecular Cell Biology 2004 5:12* **5**, 983–997 (2004).
75. Pomerening, J. R., Ubersax, J. A. & Ferrell, J. E. Rapid Cycling and Precocious Termination of G1 Phase in Cells Expressing CDK1AF. *Mol Biol Cell* **19**, 3426 (2008).
76. Lu, Y. & Cross, F. R. Periodic Cyclin-Cdk Activity Entrains an Autonomous Cdc14 Release Oscillator. *Cell* **141**, 268–279 (2010).
77. Kohn, K. W. Molecular interaction map of the mammalian cell cycle control and DNA repair systems. *Mol Biol Cell* **10**, 2703–2734 (1999).
78. Malumbres, M. & Barbacid, M. Mammalian cyclin-dependent kinases. *Trends Biochem Sci* **30**, 630–641 (2005).
79. Nilsson, J. Protein phosphatases in the regulation of mitosis. *Journal of Cell Biology* **218**, 395–409 (2019).
80. Nasmyth, K. At the heart of the budding yeast cell cycle. *Trends Genet* **12**, 405–412 (1996).
81. Kramer, E. R., Scheuringer, N., Podtelejnikov, A. V., Mann, M. & Peters, J. M. Mitotic regulation of the APC activator proteins CDC20 and CDH1. *Mol Biol Cell* **11**, 1555–1569 (2000).
82. Steven Zhang, H., Postigo, A. A. & Dean, D. C. Active transcriptional repression by the Rb-E2F complex mediates G1 arrest triggered by p16INK4a, TGFbeta, and contact inhibition. *Cell* **97**, 53–61 (1999).

83. Stein, G. H., Drullinger, L. F., Soulard, A. & Dulić, V. Differential Roles for Cyclin-Dependent Kinase Inhibitors p21 and p16 in the Mechanisms of Senescence and Differentiation in Human Fibroblasts. *Mol Cell Biol* **19**, 2109 (1999).
84. Besson, A., Dowdy, S. F. & Roberts, J. M. CDK Inhibitors: Cell Cycle Regulators and Beyond. *Dev Cell* **14**, 159–169 (2008).
85. Narasimha, A. M. *et al.* Cyclin D activates the Rb tumor suppressor by mono-phosphorylation. *Elife* **3**, (2014).
86. Ezhevsky, S. A. *et al.* Hypo-phosphorylation of the retinoblastoma protein (pRb) by cyclin D:Cdk4/6 complexes results in active pRb. *Proc Natl Acad Sci U S A* **94**, 10699–10704 (1997).
87. Novak, B. & Tyson, J. J. Numerical analysis of a comprehensive model of M-phase control in Xenopus oocyte extracts and intact embryos. *J Cell Sci* **106 (Pt 4)**, 1153–1168 (1993).
88. Ohtani, K., Degregori, J. & Nevins, J. R. Regulation of the cyclin E gene by transcription factor E2F1. *Proc Natl Acad Sci U S A* **92**, 12146 (1995).
89. Hsu, J. Y., Reimann, J. D. R., Sørensen, C. S., Lukas, J. & Jackson, P. K. E2F-dependent accumulation of hEmi1 regulates S phase entry by inhibiting APC(Cdh1). *Nat Cell Biol* **4**, 358–366 (2002).
90. Zarkowska, T. & Mittnacht, S. Differential phosphorylation of the retinoblastoma protein by G1/S cyclin-dependent kinases. *J Biol Chem* **272**, 12738–12746 (1997).
91. Cappell, S. D. *et al.* EMI1 switches from being a substrate to an inhibitor of APC/CCDH1 to start the cell cycle. *Nature* **558**, 313–317 (2018).
92. Cappell, S. D., Chung, M., Jaimovich, A., Spencer, S. L. & Meyer, T. Irreversible APC(Cdh1) Inactivation Underlies the Point of No Return for Cell-Cycle Entry. *Cell* **166**, 167–180 (2016).
93. Clurman, B. E., Sheaff, R. J., Thress, K., Groudine, M. & Roberts, J. M. Turnover of cyclin E by the ubiquitin-proteasome pathway is regulated by cdk2 binding and cyclin phosphorylation. *Genes Dev* **10**, 1979–1990 (1996).
94. Xu, M., Sheppard, K.-A., Peng, C.-Y., Yee, A. S. & Piwnica-Worms, H. Cyclin A/CDK2 binds directly to E2F-1 and inhibits the DNA-binding activity of E2F-1/DP-1 by phosphorylation. *Mol Cell Biol* **14**, 8420–8431 (1994).
95. Wei, Z. & Liu, H. T. MAPK signal pathways in the regulation of cell proliferation in mammalian cells. *Cell Research 2002 12:1* **12**, 9–18 (2002).
96. Yan, Z. *et al.* Cdc6 is regulated by E2F and is essential for DNA replication in mammalian cells. *Proc Natl Acad Sci U S A* **95**, 3603 (1998).
97. Ginzberg, M. B., Kafri, R. & Kirschner, M. On being the right (cell) size. *Science (1979)* **348**, (2015).
98. Cadart, C. *et al.* Size control in mammalian cells involves modulation of both growth rate and cell cycle duration. *Nature Communications 2018 9:1* **9**, 1–15 (2018).
99. Varsano, G., Wang, Y. & Wu, M. Probing Mammalian Cell Size Homeostasis by Channel-Assisted Cell Reshaping. *Cell Rep* **20**, 397–410 (2017).
100. Ginzberg, M. B. *et al.* Cell size sensing in animal cells coordinates anabolic growth rates and cell cycle progression to maintain cell size uniformity. *Elife* **7**, (2018).
101. McGarry, T. J. & Kirschner, M. W. Geminin, an Inhibitor of DNA Replication, Is Degraded during Mitosis. *Cell* **93**, 1043–1053 (1998).

102. Abbas, T. & Dutta, A. CRL4Cdt2: master coordinator of cell cycle progression and genome stability. *Cell Cycle* **10**, 241–249 (2011).
103. Li, X., Zhao, Q., Liao, R., Sun, P. & Wu, X. The SCF(Skp2) ubiquitin ligase complex interacts with the human replication licensing factor Cdt1 and regulates Cdt1 degradation. *J Biol Chem* **278**, 30854–30858 (2003).
104. Coverley, D., Pelizon, C., Trewick, S. & Laskey, R. A. Chromatin-bound Cdc6 persists in S and G2 phases in human cells, while soluble Cdc6 is destroyed in a cyclin A-cdk2 dependent process. *J Cell Sci* **113 (Pt 11)**, 1929–1938 (2000).
105. Delmolino, L. M., Saha, P. & Dutta, A. Multiple mechanisms regulate subcellular localization of human CDC6. *J Biol Chem* **276**, 26947–26954 (2001).
106. Petersen, B. O., Lukas, J., Sørensen, C. S., Bartek, J. & Helin, K. Phosphorylation of mammalian CDC6 by Cyclin A/CDK2 regulates its subcellular localization. *EMBO J* **18**, 396–410 (1999).
107. Diffley, J. F. X. Quality control in the initiation of eukaryotic DNA replication. *Philosophical Transactions of the Royal Society B: Biological Sciences* **366**, 3545–3553 (2011).
108. Diffley, J. F. X. Regulation of early events in chromosome replication. *Current Biology* **14**, R778–R786 (2004).
109. Araki, H. Cyclin-dependent kinase-dependent initiation of chromosomal DNA replication. *Curr Opin Cell Biol* **22**, 766–771 (2010).
110. Harper, J. W. & Elledge, S. J. The DNA damage response: ten years after. *Mol Cell* **28**, 739–745 (2007).
111. Sulli, G., Di Micco, R. & Di Fagagna, F. D. A. Crosstalk between chromatin state and DNA damage response in cellular senescence and cancer. *Nature Reviews Cancer 2012 12:10* **12**, 709–720 (2012).
112. Sancar, A., Lindsey-Boltz, L. A., Ünsal-Kaçmaz, K. & Linn, S. Molecular mechanisms of mammalian DNA repair and the DNA damage checkpoints. *Annu Rev Biochem* **73**, 39–85 (2004).
113. Uziel, T. *et al.* Requirement of the MRN complex for ATM activation by DNA damage. *EMBO J* **22**, 5612 (2003).
114. Shiotani, B. & Zou, L. ATR signaling at a glance. *J Cell Sci* **122**, 301–304 (2009).
115. Zeng, Y. *et al.* Replication checkpoint requires phosphorylation of the phosphatase Cdc25 by Cds1 or Chk1. *Nature 1998 395:6701* **395**, 507–510 (1998).
116. Kastenhuber, E. R. & Lowe, S. W. Putting p53 in context. *Cell* **170**, 1062 (2017).
117. Bartek, J. & Lukas, J. Pathways governing G1/S transition and their response to DNA damage. *FEBS Lett* **490**, 117–122 (2001).
118. Blomberg, I. & Hoffmann, I. Ectopic Expression of Cdc25A Accelerates the G1/S Transition and Leads to Premature Activation of Cyclin E- and Cyclin A-Dependent Kinases. *Mol Cell Biol* **19**, 6183 (1999).
119. Barr, A. R. *et al.* DNA damage during S-phase mediates the proliferation-quiescence decision in the subsequent G1 via p21 expression. *Nature Communications 2017 8:1* **8**, 1–17 (2017).
120. Fischer, M., Schade, A. E., Branigan, T. B., Müller, G. A. & DeCaprio, J. A. Coordinating gene expression during the cell cycle. *Trends Biochem Sci* **47**, 1009–1022 (2022).

121. Bertoli, C., Skotheim, J. M. & De Bruin, R. A. M. Control of cell cycle transcription during G1 and S phases. *Nat Rev Mol Cell Biol* **14**, 518 (2013).
122. Vigneron, N., Stroobant, V., Ferrari, V., Abi Habib, J. & Van den Eynde, B. J. Production of spliced peptides by the proteasome. *Mol Immunol* **113**, 93–102 (2019).
123. Seki, A., Coppinger, J. A., Jang, C. Y., Yates, J. R. & Fang, G. Bora and Aurora A Cooperatively Activate Plk1 and Control the Entry into Mitosis. *Science* **320**, 1655 (2008).
124. Hansen, D. V., Loktev, A. V., Ban, K. H. & Jackson, P. K. Plk1 regulates activation of the anaphase promoting complex by phosphorylating and triggering SCFbetaTrCP-dependent destruction of the APC Inhibitor Emi1. *Mol Biol Cell* **15**, 5623–5634 (2004).
125. Nurse, P. Universal control mechanism regulating onset of M-phase. *Nature 1990 344:6266* **344**, 503–508 (1990).
126. Pomerening, J. R., Sontag, E. D. & Ferrell, J. E. Building a cell cycle oscillator: hysteresis and bistability in the activation of Cdc2. *Nature Cell Biology 2003 5:4* **5**, 346–351 (2003).
127. Sha, W. *et al.* From the Cover: Hysteresis drives cell-cycle transitions in Xenopus laevis egg extracts. *Proc Natl Acad Sci U S A* **100**, 975 (2003).
128. Mochida, S., Maslen, S. L., Skehel, M. & Hunt, T. Greatwall phosphorylates an inhibitor of protein phosphatase 2A that is essential for mitosis. *Science* **330**, 1670–1673 (2010).
129. Gharbi-Ayachi, A. *et al.* The substrate of Greatwall kinase, Arpp19, controls mitosis by inhibiting protein phosphatase 2A. *Science* **330**, 1673–1677 (2010).
130. Peter, M., Nakagawa, J., Dorée, M., Labbé, J. C. & Nigg, E. A. In vitro disassembly of the nuclear lamina and M phase-specific phosphorylation of lamins by cdc2 kinase. *Cell* **61**, 591–602 (1990).
131. Ward, G. E. & Kirschner, M. W. Identification of cell cycle-regulated phosphorylation sites on nuclear lamin C. *Cell* **61**, 561–577 (1990).
132. Terasaki, M. *et al.* A new model for nuclear envelope breakdown. *Mol Biol Cell* **12**, 503–510 (2001).
133. Abe, S. *et al.* The initial phase of chromosome condensation requires Cdk1-mediated phosphorylation of the CAP-D3 subunit of condensin II. *Genes Dev* **25**, 863 (2011).
134. Murphy, L. A. & Sarge, K. D. Phosphorylation of CAP-G is required for its chromosomal DNA localization during mitosis. *Biochem Biophys Res Commun* **377**, 1007–1011 (2008).
135. Kimura, K., Hirano, M., Kobayashi, R. & Hirano, T. Phosphorylation and activation of 13S condensin by Cdc2 in vitro. *Science* **282**, 487–490 (1998).
136. Robellet, X. *et al.* A high-sensitivity phospho-switch triggered by Cdk1 governs chromosome morphogenesis during cell division. *Genes Dev* **29**, 426 (2015).
137. Paul, M. R., Hochwagen, A. & Ercan, S. Condensin action and compaction. *Curr Genet* **65**, 407 (2018).
138. Ong, J. Y., Bradley, M. C. & Torres, J. Z. Phospho-regulation of mitotic spindle assembly. *Cytoskeleton* **77**, 558–578 (2020).
139. Qiao, R. *et al.* Mechanism of APC/CCDC20 activation by mitotic phosphorylation. *Proc Natl Acad Sci U S A* **113**, E2570–E2578 (2016).

140. Garrido, D. *et al.* Cyclin B3 activates the Anaphase-Promoting Complex/Cyclosome in meiosis and mitosis. *PLoS Genet* **16**, e1009184 (2020).
141. Wirth, K. G. *et al.* Separase: a universal trigger for sister chromatid disjunction but not chromosome cycle progression. *J Cell Biol* **172**, 847–860 (2006).
142. Zielke, N., Edgar, B. A. & DePamphilis, M. L. Endoreplication. doi:10.1101/cshperspect.a012948.
143. Hendzel, M. J. *et al.* Mitosis-specific phosphorylation of histone H3 initiates primarily within pericentromeric heterochromatin during G2 and spreads in an ordered fashion coincident with mitotic chromosome condensation. *Chromosoma* **106**, 348–360 (1997).
144. Ma, H. T., Tsang, Y. H., Marxer, M. & Poon, R. Y. C. Cyclin A2-Cyclin-Dependent Kinase 2 Cooperates with the PLK1-SCFβ-TrCP1-EMI1-Anaphase-Promoting Complex/Cyclosome Axis To Promote Genome Reduplication in the Absence of Mitosis. *Mol Cell Biol* **29**, 6500 (2009).
145. Pauli, A. *et al.* Cell-Type-Specific TEV Protease Cleavage Reveals Cohesin Functions in Drosophila Neurons. *Dev Cell* **14**, 239–251 (2008).
146. Stormo, B. M. & Fox, D. T. Interphase cohesin regulation ensures mitotic fidelity after genome reduplication. *Mol Biol Cell* **30**, 219 (2019).
147. Zhang, X. *et al.* Timing and characteristics of nuclear events during conjugation and genomic exclusion in Paramecium multimicronucleatum. *Mar Life Sci Technol* **4**, 317–328 (2022).
148. Yin, L., Gater, S. T. & Karrer, K. M. A developmentally regulated gene, ASI2, is required for endocycling in the macronuclear anlagen of Tetrahymena. *Eukaryot Cell* **9**, 1343–1353 (2010).
149. Edgar, B. A. & Orr-Weaver, T. L. Endoreplication cell cycles: more for less. *Cell* **105**, 297–306 (2001).
150. Ullah, Z., Lee, C. Y., Lilly, M. A. & DePamphilis, M. L. Developmentally programmed endoreduplication in animals. *Cell Cycle* **8**, 1501 (2009).
151. Ullah, Z., Kohn, M. J., Yagi, R., Vassilev, L. T. & DePamphilis, M. L. Differentiation of trophoblast stem cells into giant cells is triggered by p57/Kip2 inhibition of CDK1 activity. *Genes Dev* **22**, 3024–3026 (2008).
152. Hayles, J., Fisher, D., Woollard, A. & Nurse, P. Temporal order of S phase and mitosis in fission yeast is determined by the state of the p34cdc2-mitotic B cyclin complex. *Cell* **78**, 813–822 (1994).
153. Ma, H. T., Tsang, Y. H., Marxer, M. & Poon, R. Y. C. Cyclin A2-Cyclin-Dependent Kinase 2 Cooperates with the PLK1-SCFβ-TrCP1-EMI1-Anaphase-Promoting Complex/Cyclosome Axis To Promote Genome Reduplication in the Absence of Mitosis. *https://doi.org/10.1128/MCB.00669-09* **29**, 6500–6514 (2023).
154. Simmons Kovacs, L. A. *et al.* Cyclin-dependent kinases are regulators and effectors of oscillations driven by a transcription factor network. *Mol Cell* **45**, 669 (2012).
155. Visintin, R., Hwang, E. S. & Amon, A. Cfi1 prevents premature exit from mitosis by anchoring Cdc14 phosphatase in the nucleolus. *Nature* **398**, 818–823 (1999).
156. Shou, W. *et al.* Exit from Mitosis Is Triggered by Tem1-Dependent Release of the Protein Phosphatase Cdc14 from Nucleolar RENT Complex. *Cell* **97**, 233–244 (1999).

157. Novak, B. & Tyson, J. J. Mitotic kinase oscillation governs the latching of cell cycle switches. *Current Biology* **32**, 2780-2785.e2 (2022).
158. Dragoi, C.-M., Kaur, E., Barr, A. R., Tyson, J. J. & Novák, B. The oscillation of mitotic kinase governs cell cycle latches in mammalian cells. *J Cell Sci* (2024) doi:10.1242/JCS.261364.
159. Kurat, C. F., Yeeles, J. T. P., Patel, H., Early, A. & Diffley, J. F. X. Chromatin Controls DNA Replication Origin Selection, Lagging-Strand Synthesis, and Replication Fork Rates. *Mol Cell* **65**, 117–130 (2017).
160. Yeeles, J. T. P., Deegan, T. D., Janska, A., Early, A. & Diffley, J. F. X. Regulated eukaryotic DNA replication origin firing with purified proteins. *Nature 2015 519:7544* **519**, 431–435 (2015).
161. Yeeles, J. T. P., Deegan, T. D., Janska, A., Early, A. & Diffley, J. F. X. Regulated eukaryotic DNA replication origin firing with purified proteins. *Nature 2015 519:7544* **519**, 431–435 (2015).
162. Ferrell, J. E. & Ha, S. H. Ultrasensitivity Part I: Michaelian responses and zero-order ultrasensitivity. *Trends Biochem Sci* **39**, 496 (2014).
163. Goldbeter, A. & Koshland, D. E. An amplified sensitivity arising from covalent modification in biological systems. *Proc Natl Acad Sci U S A* **78**, 6840–6844 (1981).
164. Fisher, D., Krasinska, L., Coudreuse, D. & Novák, B. Phosphorylation network dynamics in the control of cell cycle transitions. *J Cell Sci* **125**, 4703–4711 (2012).
165. Holt, L. J. *et al.* Global analysis of cdk1 substrate phosphorylation sites provides insiqhts into evolution. *Science (1979)* **325**, 1682–1686 (2009).
166. Kõivomägi, M. *et al.* Multisite phosphorylation networks as signal processors for Cdk1. *Nat Struct Mol Biol* **20**, 1415–1424 (2013).
167. Yang, Q. & Ferrell, J. E. The Cdk1-APC/C cell cycle oscillator circuit functions as a time-delayed, ultrasensitive switch. *Nat Cell Biol* **15**, 519–525 (2013).
168. Kim, S. Y. & Ferrell, J. E. Substrate competition as a source of ultrasensitivity in the inactivation of Wee1. *Cell* **128**, 1133–1145 (2007).
169. Trunnell, N. B., Poon, A. C., Kim, S. Y. & Ferrell, J. E. Ultrasensitivity in the Regulation of Cdc25C by Cdk1. *Mol Cell* **41**, 263–274 (2011).
170. Gunawardena, J. Multisite protein phosphorylation makes a good threshold but can be a poor switch. *Proc Natl Acad Sci U S A* **102**, 14617–14622 (2005).
171. Kapuy, O., Barik, D., Domingo Sananes, M. R., Tyson, J. J. & Novák, B. Bistability by multiple phosphorylation of regulatory proteins. *Prog Biophys Mol Biol* **100**, 47–56 (2009).
172. Ferrell, J. E. & Ha, S. H. Ultrasensitivity Part II: Multisite phosphorylation, stoichiometric inhibitors, and positive feedback. *Trends Biochem Sci* **39**, 556 (2014).
173. Verdugo, A., Vinod, P. K., Tyson, J. J. & Novak, B. Molecular mechanisms creating bistable switches at cell cycle transitions. *Open Biol* **3**, (2013).
174. Tyson, J. J. & Novak, B. Regulation of the Eukaryotic Cell Cycle: Molecular Antagonism, Hysteresis, and Irreversible Transitions. *J Theor Biol* **210**, 249–263 (2001).
175. Novák, B. & Tyson, J. J. Mechanisms of signalling-memory governing progression through the eukaryotic cell cycle. *Curr Opin Cell Biol* **69**, 7–16 (2021).

176. Kamenz, J., Gelens, L. & Ferrell, J. E. Bistable, Biphasic Regulation of PP2A-B55 Accounts for the Dynamics of Mitotic Substrate Phosphorylation ll Bistable, Biphasic Regulation of PP2A-B55 Accounts for the Dynamics of Mitotic Substrate Phosphorylation. *Current Biology* **31**, 794–808 (2021).
177. Mochida, S., Rata, S., Hino, H., Nagai, T. & Novák, B. Two Bistable Switches Govern M Phase Entry. *Current Biology* **26**, 3361–3367 (2016).
178. Novák, B. & Tyson, J. J. A model for restriction point control of the mammalian cell cycle. *J Theor Biol* **230**, 563–579 (2004).
179. Yao, G., Lee, T. J., Mori, S., Nevins, J. R. & You, L. A bistable Rb–E2F switch underlies the restriction point. *Nature Cell Biology 2008 10:4* **10**, 476–482 (2008).
180. Jiménez, A., Lu, Y., Jambhekar, A. & Lahav, G. Principles, mechanisms and functions of entrainment in biological oscillators. *Interface Focus* **12**, (2022).
181. Purcell, O., Savery, N. J., Grierson, C. S. & Di Bernardo, M. A comparative analysis of synthetic genetic oscillators. *J R Soc Interface* **7**, 1503–1524 (2010).
182. Chen, K. C. *et al.* Kinetic analysis of a molecular model of the budding yeast cell cycle. *Mol Biol Cell* **11**, 369–391 (2000).
183. Tyson, J. J. & Novak, B. Temporal organization of the cell cycle. *Curr Biol* **18**, (2008).
184. Peters, J. M. The anaphase promoting complex/cyclosome: a machine designed to destroy. *Nat Rev Mol Cell Biol* **7**, 644–656 (2006).
185. Hagting, A. *et al.* Human securin proteolysis is controlled by the spindle checkpoint and reveals when the APC/C switches from activation by Cdc20 to Cdh1. *J Cell Biol* **157**, 1125–1137 (2002).
186. Ermentrout, B. Simulating, Analyzing, and Animating Dynamical Systems. *Simulating, Analyzing, and Animating Dynamical Systems* (2002) doi:10.1137/1.9780898718195.
187. Haase, S. B., Winey, M. & Reed, S. I. Multi-step control of spindle pole body duplication by cyclin-dependent kinase. *Nat Cell Biol* **3**, 38–42 (2001).
188. Itzhaki, J. E., Gilbert, C. S. & Porter, A. C. G. Construction by gene targeting in human cells of a 'conditional' CDC2 mutant that rereplicates its DNA. *Nature Genetics 1997 15:3* **15**, 258–265 (1997).
189. Gravells, P., Tomita, K., Booth, A., Poznansky, J. & Porter, A. C. G. Chemical genetic analyses of quantitative changes in Cdk1 activity during the human cell cycle. *Hum Mol Genet* **22**, 2842–2851 (2013).
190. Laronne, A. *et al.* Synchronization of interphase events depends neither on mitosis nor on cdk1. *Am Soc Cell BiolA Laronne, S Rotkopf, A Hellman, Y Gruenbaum, ACG Porter, M BrandeisMolecular biology of the cell, 2003•Am Soc Cell Biol* **14**, 3730–3740 (2003).
191. Zerjatke, T. *et al.* Quantitative Cell Cycle Analysis Based on an Endogenous All-in-One Reporter for Cell Tracking and Classification. *Cell Rep* **19**, 1953–1966 (2017).
192. Mansfeld, J., Collin, P., Collins, M. O., Choudhary, J. S. & Pines, J. APC15 drives the turnover of MCC-CDC20 to make the spindle assembly checkpoint responsive to kinetochore attachment. *Nat Cell Biol* **13**, 1234–1243 (2011).
193. Di Fiore, B. & Pines, J. Emi1 is needed to couple DNA replication with mitosis but does not regulate activation of the mitotic APC/C. *J Cell Biol* **177**, 425–437 (2007).
194. Machida, Y. J. & Dutta, A. The APC/C inhibitor, Emi1, is essential for prevention of rereplication. *Genes Dev* **21**, 184–194 (2007).

195. Barr, A. R., Heldt, F. S., Zhang, T., Bakal, C. & Novák, B. A Dynamical Framework for the All-or-None G1/S Transition. *Cell Syst* **2**, 27 (2016).
196. Dasso, M. & Newport, J. W. Completion of DNA replication is monitored by a feedback system that controls the initiation of mitosis in vitro: studies in Xenopus. *Cell* **61**, 811–823 (1990).
197. Gupta, M., Trott, D. & Porter, A. C. G. Rescue of a human cell line from endogenous Cdk1 depletion by Cdk1 lacking inhibitory phosphorylation sites. *J Biol Chem* **282**, 4301–4309 (2007).
198. Szmyd, R. *et al.* Premature activation of Cdk1 leads to mitotic events in S phase and embryonic lethality. *Oncogene 2018 38:7* **38**, 998–1018 (2018).
199. Collin, P., Nashchekina, O., Walker, R. & Pines, J. The spindle assembly checkpoint works like a rheostat rather than a toggle switch. *Nature Cell Biology 2013 15:11* **15**, 1378–1385 (2013).
200. Kraft, C. *et al.* Mitotic regulation of the human anaphase-promoting complex by phosphorylation. *EMBO Journal* **22**, 6598–6609 (2003).
201. Gavet, O. & Pines, J. Progressive Activation of CyclinB1-Cdk1 Coordinates Entry to Mitosis. *Dev Cell* **18**, 533–543 (2010).
202. Guiley, K. Z. *et al.* P27 allosterically activates cyclin-dependent kinase 4 and antagonizes palbociclib inhibition. *Science (1979)* **366**, (2019).
203. Brugarolas, J. *et al.* Inhibition of cyclin-dependent kinase 2 by p21 is necessary for retinoblastoma protein-mediated G1 arrest after γ-irradiation. *Proc Natl Acad Sci U S A* **96**, 1002–1007 (1999).
204. He, G. *et al.* Induction of p21 by p53 following DNA damage inhibits both Cdk4 and Cdk2 activities. *Oncogene* **24**, 2929–2943 (2005).
205. López-Avilés, S., Kapuy, O., Novák, B., Nature, F. U.- & 2009, undefined. Irreversibility of mitotic exit is the consequence of systems-level feedback. *nature.comS López-Avilés, O Kapuy, B Novák, F UhlmannNature, 2009•nature.com*.
206. Cross, F., Archambault, V., ... M. M.-M. biology of the & 2002, undefined. Testing a mathematical model of the yeast cell cycle. *Am Soc Cell BiolFR Cross, V Archambault, M Miller, M KlovstadMolecular biology of the cell, 2002•Am Soc Cell Biol* **13**, 52–70 (2002).
207. Manzoni, R. *et al.* Oscillations in Cdc14 release and sequestration reveal a circuit underlying mitotic exit. *Journal of Cell Biology* **190**, 209–222 (2010).
208. Gérard, C. & Goldbeter, A. Temporal self-organization of the cyclin/Cdk network driving the mammalian cell cycle. *Proc Natl Acad Sci U S A* **106**, 21643–21648 (2009).
209. Bielski, C. M. *et al.* Genome doubling shapes the evolution and prognosis of advanced cancers. *Nature Genetics 2018 50:8* **50**, 1189–1195 (2018).
210. Dewhurst, S. M. *et al.* Tolerance of whole-genome doubling propagates chromosomal instability and accelerates cancer genome evolution. *Cancer Discov* **4**, 175–185 (2014).
211. López, S. *et al.* Interplay between whole-genome doubling and the accumulation of deleterious alterations in cancer evolution. *Nature Genetics 2020 52:3* **52**, 283–293 (2020).
212. Quinton, R. J. *et al.* Whole-genome doubling confers unique genetic vulnerabilities on tumour cells. *Nature 2021 590:7846* **590**, 492–497 (2021).

213. Fujiwara, T. *et al.* Cytokinesis failure generating tetraploids promotes tumorigenesis in p53-null cells. *Nature 2005 437:7061* **437**, 1043–1047 (2005).
214. Wolf, F., Wandke, C., Isenberg, N. & Geley, S. Dose-dependent effects of stable cyclin B1 on progression through mitosis in human cells. *EMBO Journal* **25**, 2802–2813 (2006).
215. Vázquez-Novelle, M. D. *et al.* Cdk1 inactivation terminates mitotic checkpoint surveillance and stabilizes kinetochore attachments in anaphase. *Curr Biol* **24**, 638–645 (2014).
216. Bardin, A. J. & Amon, A. MEN and SIN: what's the difference? *Nature Reviews Molecular Cell Biology 2001 2:11* **2**, 815–826 (2001).
217. Gorecki, L., Andrs, M., Cancers, J. K.- & 2021, undefined. Clinical candidates targeting the ATR–CHK1–WEE1 axis in cancer. *mdpi.comL Gorecki, M Andrs, J KorabecnyCancers, 2021•mdpi.com* (2021) doi:10.3390/cancers13040795.
218. Hirai, H. *et al.* Small-molecule inhibition of Wee1 kinase by MK-1775 selectively sensitizes p53-deficient tumor cells to DNA-damaging agents. *Mol Cancer Ther* **8**, 2992–3000 (2009).
219. Otto, T. & Sicinski, P. Cell cycle proteins as promising targets in cancer therapy. *Nature Reviews Cancer 2017 17:2* **17**, 93–115 (2017).
220. Lang, P. F., Penas, D. R., Banga, J. R., Weindl, D. & Novak, B. Reusable rule-based cell cycle model explains compartment-resolved dynamics of 16 observables in RPE-1 cells. *PLoS Comput Biol* **20**, e1011151 (2024).
221. Novak, B. & Tyson, J. J. Mitotic kinase oscillation governs the latching of cell cycle switches. *Current Biology* (2022) doi:10.1016/J.CUB.2022.04.016.
222. Dragoi, C.-M., Tyson, J. J. & Novák, B. Newton's cradle: Cell cycle regulation by two mutually inhibitory oscillators. *Math Biosci* **377**, 109291 (2024).
223. Cross, F. R. Two Redundant Oscillatory Mechanisms in the Yeast Cell Cycle. *Dev Cell* **4**, 741–752 (2003).
224. Tsai, T. Y. C. *et al.* Robust, tunable biological oscillations from interlinked positive and negative feedback loops. *Science (1979)* **321**, 126–139 (2008).
225. Gérard, C. & Goldbeter, A. A skeleton model for the network of cyclin-dependent kinases driving the mammalian cell cycle. *Interface Focus* **1**, 24–35 (2011).
226. Medina, E. M., Turner, J. J., Gordân, R., Skotheim, J. M. & Buchler, N. E. Punctuated evolution and transitional hybrid network in an ancestral cell cycle of fungi. *Elife* **5**, (2016).
227. Cezanne, A., Foo, S., Kuo, Y.-W. & Baum, B. The Archaeal Cell Cycle. *Annu Rev Cell Dev Biol* (2024) doi:10.1146/ANNUREV-CELLBIO-111822-120242.
228. Liu, P., Wang, L. & Yu, H. Polyploid giant cancer cells: origin, possible pathways of formation, characteristics, and mechanisms of regulation. *Front Cell Dev Biol* **12**, 1410637 (2024).
229. Zhang, X. *et al.* Targeting polyploid giant cancer cells potentiates a therapeutic response and overcomes resistance to PARP inhibitors in ovarian cancer. *Sci Adv* **9**, (2023).

Appendix 1: Supplementary material for Chapter 2

Table 2.1: Kinetic parameters of the mammalian cell model. Rate constants (*k's*) have a dimension of h^{-1} while other parameters are dimensionless.

CycE synthesis/degradation	k_{scyce}=1.5, k_{dcyce}'=0.6, k_{dcyce}"=1.5
CycA synthesis/degradation	k_{scyca}=0.45, k_{dcyca}'=0.045, k_{dcyca}"=0.75, k_{dcyca}=3.75
E2F phosphorylation/dephosphorylation	$E2F_T$=1, k_{dpe2f}=0.3, k_{pe2f}=1.5, K_{drbe2f}=0.001
Rb phosphorylation/dephosphorylation	J_{Rb}=0.1, k_{prb}=15, k_{dprb}=10.5, α=1, CycD=1
Emi1 synthesis/degradation	k_{semi1}=1.5, k_{demi1}'=0.15, k_{demi1}"=4.5, k_{demi1}=7.5, K_{dc1e1}=0.01
CycB synthesis/degradation	k_{scycb}=0.3, k_{dcycb}'=0.06, k_{dcycb}"=0.75, k_{dcycb}=3.75
CycB dephosphorylation (CDK1)	k_{pyme}'=0, k_{pyme}=30, k_{dpyme}=6, J_{yme}=0.1, k_{25}'=0.45, k_{25}=15, k_{wee}'=0.15, k_{wee}=15
Cdh1 phosphorylation	$Cdh1_{tot}$=1, k_{acdh1}=15, k_{icdh1}'=15, k_{icdh1}"=30, k_{icdh1}=6000
Cdc20 phosphorylation	k_{icdc20}=15, k_{acdc20}=3, ε=1, SAC=1
Polo synthesis/degradation	k_{spolo}'=0.15, k_{spolo}=0, k_{dpolo}'=0.15, k_{dpolo}"=15
Polo phosphorylation	k_{apolo}'=4.5, k_{apolo}"=15, k_{ipolo}=7.5, J_{polo}=0.01
ENSA phosphorylation	k_{GwENSA}=15, $ENSA_{tot}$=4, k_{catB55}=15
Gwl phosphorylation	k_{ppx}'=6, k_{CdkGwl}=30, k_{B55Gwl}=60, Gw_{tot}=1
PP2A:B55 – ENSA complex formation	$B55_{tot}$=1, k_{ass}=7500, k_{diss}=4.5
Rbtot synthesis/degradation	k_{srb}=0.02 or 0.1, k_{drb}=0.023
Volume growth rate	μ=0.0385

XPPAUT code for simulation of the mammalian cell cycle model.

```
# XPPAut model for the human cell cycle
# Differential equations
CycE' = kscyce*E2F - (kdcyce' + kdcyce"*CycA)*CycE
CycA' = kscyca*E2F - (kdcyca' + kdcyca"*Cdc20 + kdcyca*Cdh1)*CycA
E2FPt' = kpe2f*(CycA+eps*Cdk1)*(E2FT - E2FPt) - kdpe2f*E2FPt
Rb' = kdprb*(Rbt-Rb)/(Jrb+Rbt-Rb) - kprb*(CycE+CycA+eps*Cdk1)*Rb/(Jrb+Rb)
Emi1' = ksemi1*E2F - (kdemi1' + kdemi1"*Cdh1 + kdemi1*Polo)*Emi1
CycB' = kscycb*CycA - Vdcycb*CycB
Cdk1' = kscycb*CycA + V25*(CycB - Cdk1) - Vwee*Cdk1 - Vdcycb*Cdk1
Cdh1' = kacdh1*(Cdh1t-Cdh1) - (kicdh1'*CycE+kicdh1"*CycA+kicdh1*eps*Cdk1)*Cdh1
Cdc20' = kacdc20*eps*Cdk1*(1-Cdc20) - kicdc20*PP2AB55*Cdc20
PoloT' = kspolo' + kspolo*CycA - (kdpolo' + kdpolo"*Cdh1)*PoloT
Polo' = (kapolo'*CycA + kapolo"*eps*Cdk1)*(PoloT-Polo)/(Jpolo+PoloT-Polo)-kipolo*Polo/(Jpolo+Polo)
pENSAt' = kGwENSA*pGwl*(ENSAtot - pENSAt) - kcatB55*Complex
pGwl' = (kCdkGwl'*CycA+kCdkGwl*eps*Cdk1)*(Gwtot - pGwl) - (kppx' + kB55Gwl*PP2AB55)*pGwl
PP2AB55' = (kdiss + kcatB55)*Complex-kass*(pENSAt-Complex)*(B55tot-Complex)
# Algebraic equations
Rbt = Rbtot/(1 + alpha*CycD)
BB1 = Rb + E2FT + Kdrbe2f
RbE2F = (BB1 - sqrt(BB1^2 - 4*Rb*E2FT))/2
E2F = (E2FT-E2FPt)*(E2FT-RbE2F)/E2FT
BB2 = Emi1 + Cdh1tot + Kdc1e1
Cdh1Emi1 = (BB2 - sqrt(BB2^2 - 4*Emi1*Cdh1tot))/2
Cdh1t = Cdh1tot - Cdh1Emi1
YMEP = GK(kpyme'*CycA+kpyme*eps*Cdk1,kdpyme,Jyme,Jyme)
V25 = k25' + k25*YMEP
Vwee = kwee' + kwee*(1 - YMEP)
Vdcycb = kdcycb' + kdcycb"*Cdc20 + kdcycb*Cdh1
Complex = B55tot-PP2AB55
# Auxiliary variables
aux E2F = (E2FT-E2FPt)*(E2FT-RbE2F)/E2FT
aux Cdh1t = Cdh1tot - Cdh1Emi1
# Goldbeter-Koshland function
GB(arg1,arg2,arg3,arg4) = arg2-arg1+arg2*arg3+arg1*arg4
GK(arg1,arg2,arg3,arg4) = 2*arg1*arg4/(GB(arg1,arg2,arg3,arg4)+sqrt(GB(arg1,arg2,arg3,arg4)^2-4*(arg2-
arg1)*arg1*arg4))
# Parameter values
p kscyce=1.5, kdcyce'=0.6, kdcyce"=1.5
p kscyca=0.45, kdcyca'=0.045, kdcyca"=0.75, kdcyca=3.75
p Rbtot=1.75, JRb=0.1, kprb=15, kdprb=10.5, alpha=1, CycD=1
p E2FT=1, kdpe2f=0.3, kpe2f=1.5, Kdrbe2f=0.001
p ksemi1=1.5, kdemi1'=0.15, kdemi1"=4.5, kdemi1=7.5, Kdc1e1=0.01
p Cdh1tot=1, kacdh1=15, kicdh1'=15, kicdh1"=30, kicdh1=6000
p kscycb'=0, kscycb=0.3, kdcycb'=0.06, kdcycb"=0.75, kdcycb=3.75
p kpyme'=0, kpyme=30, kdpyme=6, Jyme=0.1, k25'=0.45, k25=15, kwee'=0.15, kwee=15
p kicdc20=15, kacdc20=3, eps=1, SAC=1
p kspolo'=0.15, kspolo=0, kdpolo'=0.15, kdpolo"=15
p kapolo'=4.5, kapolo"=15, kipolo=7.5, Jpolo=0.01
p ENSAtot=4, B55tot=1, kass=7500, kdiss=4.5, kcatB55=15
p kGwENSA=15, kppx'=6, kCdkGwl'=0, kCdkGwl=30, kB55Gwl=60, Gwtot=1
# XPP settings
@ METH=stiff,XLO=0,XHI=50,YLO=0,YHI=1.6,total=50,dt=0.05,XP=time
@ NPLOT=8,YP=CycE,YP2=CycA,YP3=Emi1,YP4=CycB,YP5=Cdk1,YP6=Cdh1,YP7=Cdc20,YP8=Rb
done
```

Supplementary figures:

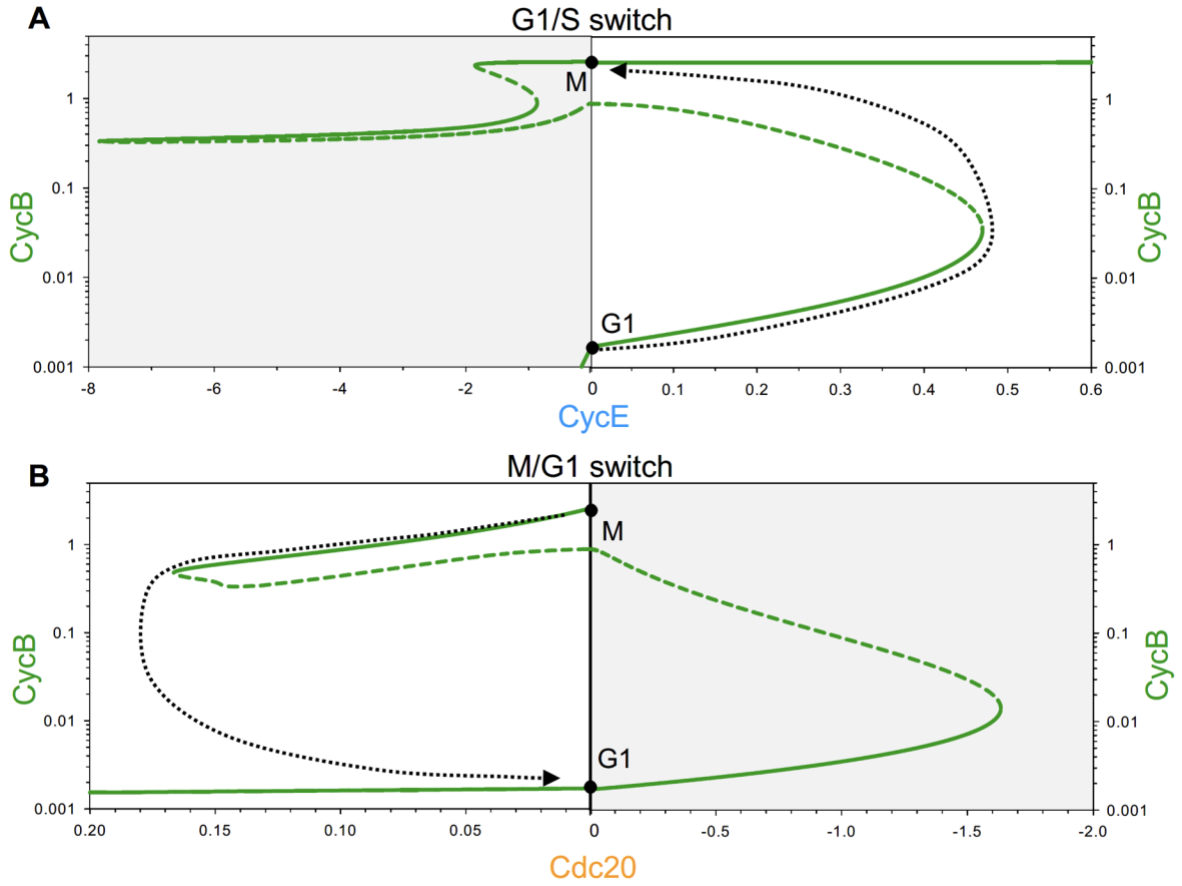

Figure S2.1. Bifurcation diagrams for CycB level as a function of CycE or Cdc20. Related to Figure 2.2. See details in Fig. 2.2.

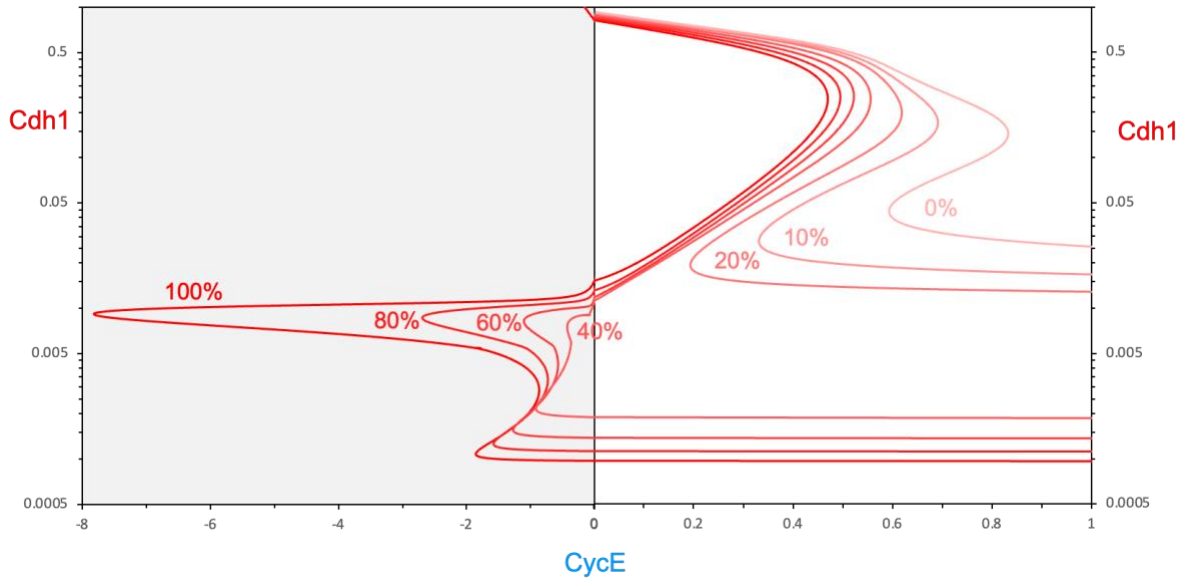

Figure S2.2. Bifurcation diagrams that account for Cdh1 endocycles. Related to Figure 2.4. Cdh1 vs CycE bifurcation curves for increasing inhibition of Cdk1 activity. Percentage refers to level of Cdk1 activity remaining, i.e., 100% means full activity, 0% is

no activity. If Cdk1 activity is < 25%, the gate at **M** (CycE = 0, Cdh1 low) fails to latch. As CycE level drops, Cdh1 will spontaneously reactivate.

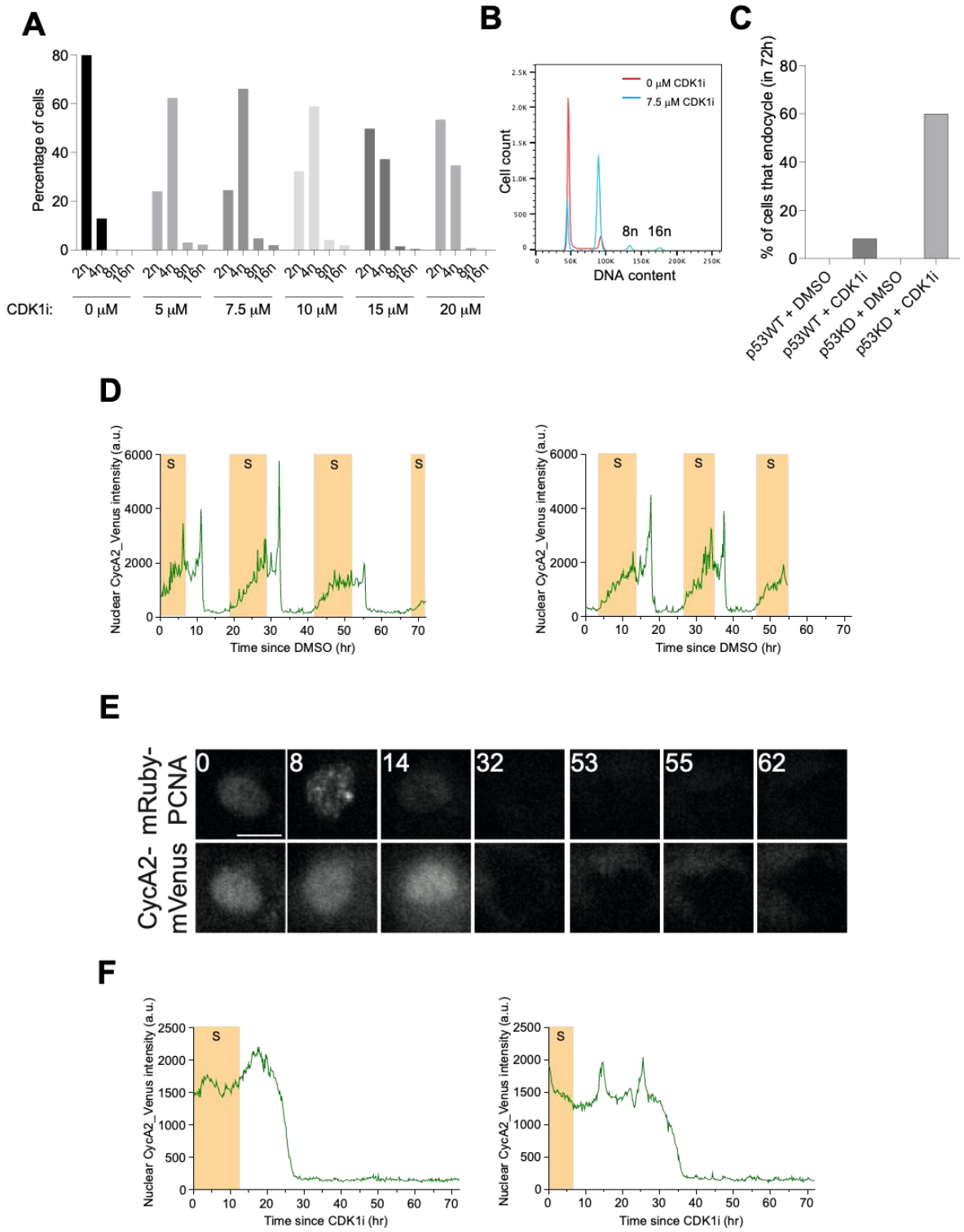

Figure S2.3. Cdk1 inhibition-induced endoreplication (Cdh1 endocycles). Related to Figure 2.4. (A) The percentage of cells of different ploidy, as quantified by flow cytometry, after treatment with different doses of the Cdk1i, RO-3306, for 72 h. Discrete 8n and 16n peaks are characteristic of endoreplication. **(B)** FACS plot of RPE1 cells treated with DMSO (0 μm CDK1i) or 7.5 μm of CDK1i for 72 h. Discrete 8n and 16n peaks

are visible indicative of endoreplication. **(C)** The percentage of cells undergoing at least one endocycle in the 72 h imaging window in each condition. WT is wild-type p53. KD is p53 knockdown by siRNA. **(D)** Fluctuations of CycA2-mVenus during mitotic cycles in the presence of vehicle (DMSO). **(E)** CycA2-mVenus in individual cells that do not undergo endocycles. Still images of mRuby-PCNA and CycA2-mVenus labelled nuclei from timelapse experiments. Time shown in hours. Scale bar is 10 μm**. (F)** Graphs showing quantification of CycA2-mVenus, plotted from the time of CDK1i addition (t = 0 h). Shaded yellow areas represent S phase, as defined by mRuby-PCNA foci. Each time trace represents one cell. This behaviour was confirmed across 4 separate experiments (technical repeats). This figure and the data on which it is based, was authored by Alexis Barr and Ekjot Kaur.

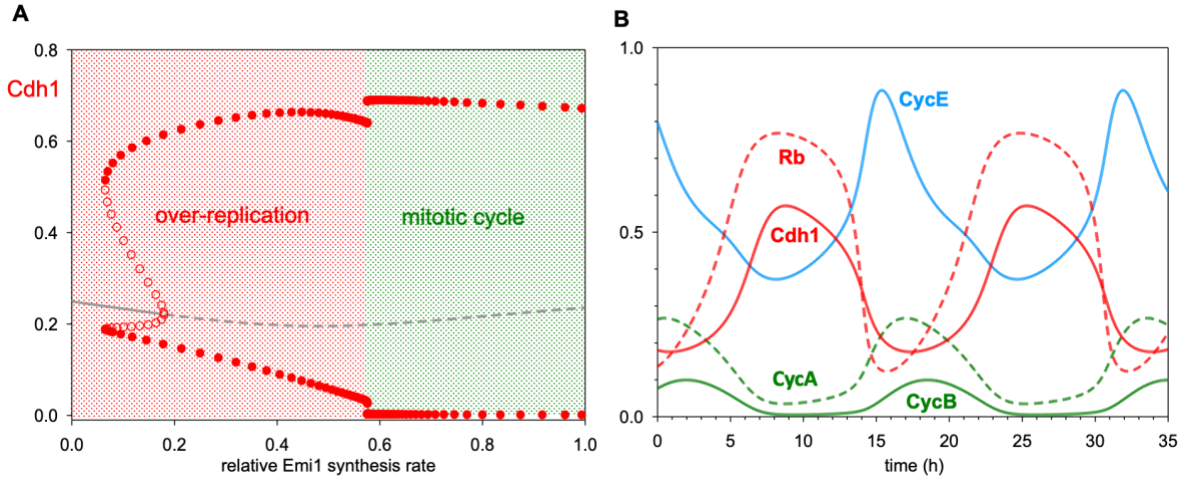

Figure S2.4. Down-regulation of Emi1 synthesis converts mitotic cycles into over-replication cycles. Related to Figure 2.4. (**A**) Bifurcation diagram: Cdh1 activity as a function of the relative synthesis rate of Emi1. Solid (dashed) gray line: stable (unstable) steady states; solid (open) red circles: maximum and minimum excursions of Cdh1 activity during stable (unstable) limit cycle oscillations. Notice that Cdh1 axis is linear compared to logarithmic on Fig. 2.4A. (**B**) Simulation of Cdh1 endocycles for 90% suppression of Emi1 synthesis. Cdh1 activity never drops very low, so (presumably) replication origins are continuously relicensed, and DNA synthesis proceeds continuously rather than in discrete rounds of replication.

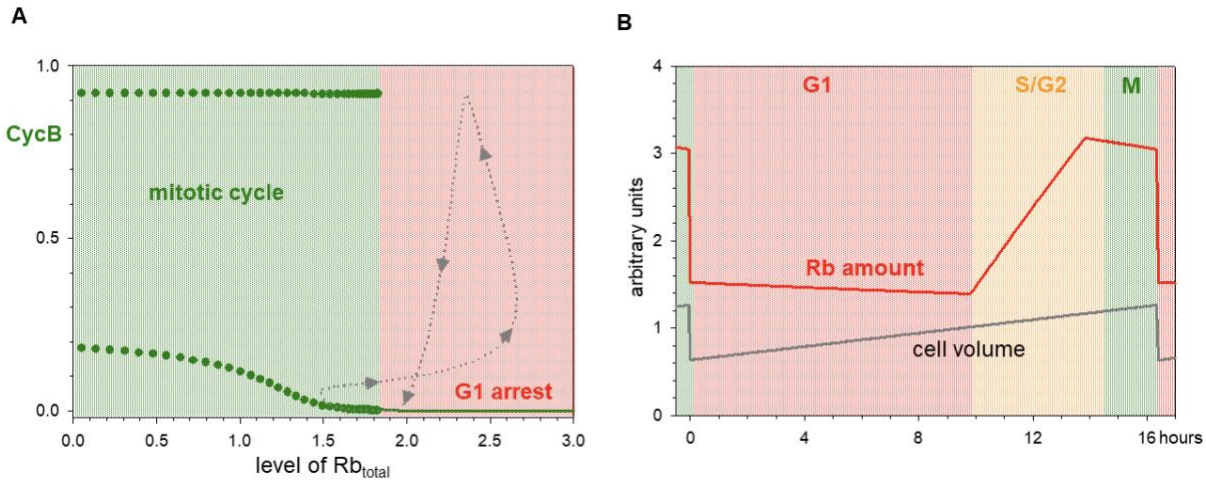

Figure S2.5. Checkpoint mechanisms convert spontaneous cell-cycle oscillations into conditional cycles, contingent on execution of certain events. Related to Figure 2.6. (A) Bifurcation diagram (CycB vs concentration of Rb_{total}) for the cell-growth checkpoint (G1/S transition). Solid green lines: stable steady states; solid green circles: maximum and minimum activity of CycB on a limit-cycle oscillation (spontaneous mitotic cycles). The dashed gray line is the conditional cell cycle, contingent on [Rb_{total}] dilution by cell growth (movement from right to left) and the doubling of total Rb amount (movement from left to right) when the *retinoblastoma* protein is synthesized in S phase. The limit cycles arise at a 'homoclinic saddle-loop' bifurcation at [Rb_{total}] ≈ 1.83. **(B)** Temporal changes of Rb amount and cell volume during the cell cycle in the simulation of Figure 2.6.

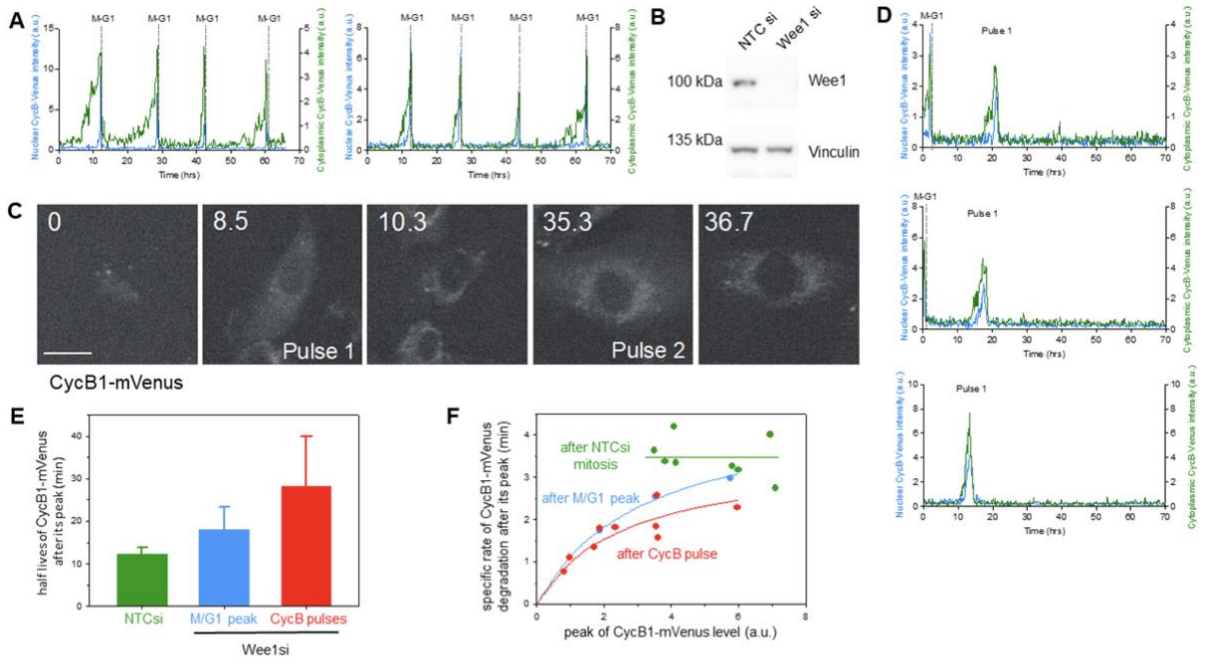

Fig. S2.6. Cdk1:CycB induces Cdc20-endocycles in the absence of Wee1. Related to Fig. 7. (**A)** Normalised CycB1-mVenus intensity in individual cells treated with control siRNA and undergoing normal mitotic cycles. **(B)** Western blot for Wee1 in Non-targeting control (NTC) and Wee1-siRNA treated cells. Vinculin is used as a loading control. **(C)** Still images of hTert-RPE1 CycB1-mVenus labelled cells from timelapse experiments. Wee1 was depleted by siRNA 6 h prior to the start of filming (t = 0 h). The cell displays two interphase pulses of CycB1-mVenus expression in the absence of further mitoses. Time shown in hours. Scale bar is 10 μm. **(D)** Normalised CycB1-mVenus intensity in individual cells treated with Wee1 siRNA with one pulse only, plotted from the time of timelapse start (t = 0 h). For A, C and D, n=1 is shown representative of three biological repeats. **(E)** Half-life (min) of CycB1-mVenus after its peak intensity value. **(F)** Specific rate of CycB1-mVenus degradation (min-1) in single cells as a function of preceding CycB1-mVenus intensity peak. For NTC siRNA treated cells the solid line represent the mean vale. In case of Wee1 siRNA treated cells the solid lines are calculated by fitting a hyperbole (spec.rate=a*CycB/(b+CycB) by least square regression. Panels A-D and the data on which they are based, were authored by Alexis Barr and Ekjot Kaur.

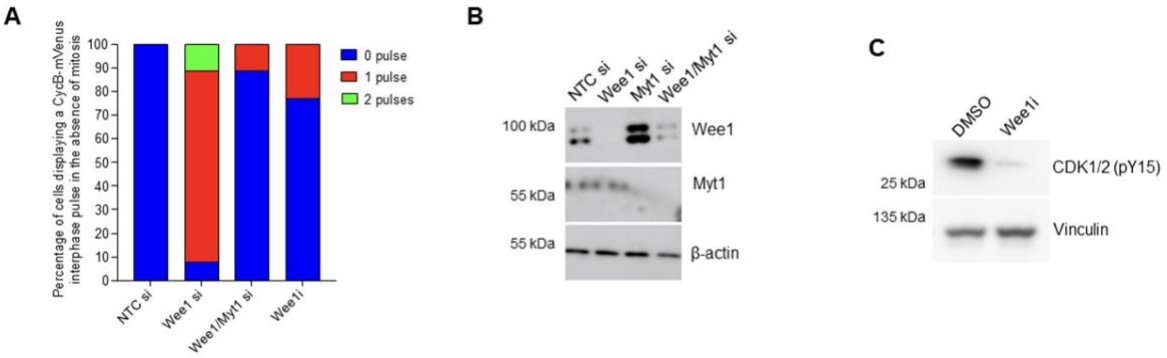

Fig. S2.7. Cdc20 endocycles are weakened in the complete absence of inhibitory Cdk1 phosphorylation. Related to Fig. 7. (A) Graph to show comparison of Wee1 depleted cells to Wee1/Myt1 co-depleted cells and Wee1 inhibitor (Wee1i, 2.5 μM) treated cells. Wee1/Myt1 and Wee1i treated cells display fewer CycB1-mVenus oscillations than Wee1 only depleted cells. **(B)** Western blot showing co-depletion of Wee1 and Myt1. β-actin is used as a loading control. **(C)** Western blot showing reduction in CDK Y15 phosphorylation after treatment with 2.5 μM Wee1i for 2 h. Vinculin is used as a loading control. This figure and the data on which it is based, was authored by Alexis Barr and Ekjot Kaur.

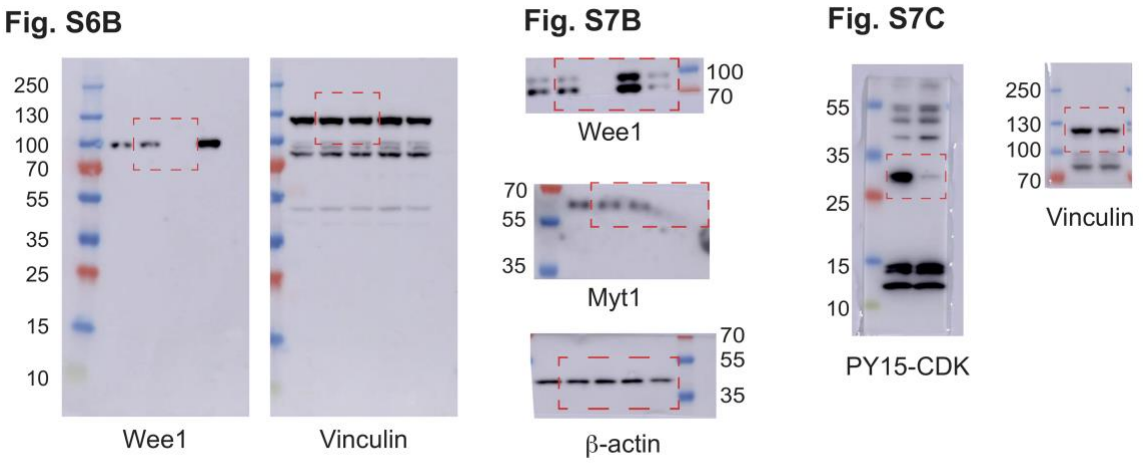

Fig. S2.8. Uncropped western blots. This figure and the data on which it is based, was authored by Alexis Barr and Ekjot Kaur.

Experimental methods

As all experiments were carried out by Dr. Alexis Barr and Dr. Ekjot Kaur, the experimental methods are not reproduced here. However, they are available as part of our joint publication at the Journal of Cell Science[158].

Appendix 2: Supplementary material for chapter 3

Table 3.1 – Numerical values of parameters in the two coupled doubly amplified negative feedback oscillators.

Parameter	Description	Value
k'_{sa1} and k'_{sa2}	Constitutive synthesis rates of A_1 and A_2	0.015
k_{sa1} and k_{sa2}	Autocatalytic synthesis rates of A_1 and A_2	0.185
L_{a1}^{q} and L_{a2}^{q}	Hill coefficients (raised to the power q) of autocatalytic synthesis of A_1 and A_2	0.01
q	Hill exponent of autocatalytic synthesis of A_1 and A_2	3
r	Inhibition of A_1 and A_2 synthesis by I_1 and I_2	25
k'_{da1} and k'_{da2}	Constitutive degradation rate constants of A_1 and A_2	0.2
k_{da1} and k_{da2}	Second order rate constants of A_1 and A_2 degradation	0.25
k'_{si1} and k'_{si2}	Constitutive synthesis rates of I_1 and I_2	0.05
k_{si1} and k_{si2}	Autocatalytic synthesis rates of I_1 and I_2	0.1
L_{i1}^{p} and L_{i2}^{p}	Hill coefficients (raised to the power p) of autocatalytic synthesis of I_1 and I_2	0.07
p	Hill exponent of autocatalytic synthesis of I_1 and I_2	3
k'_{di1} and k'_{di2}	Constitutive degradation rate constants of I_1 and I_2	0.15
k_{da1} and k_{da2}	Second order rate constants of I_1 and I_2 degradation	0.05

Supplementary figures

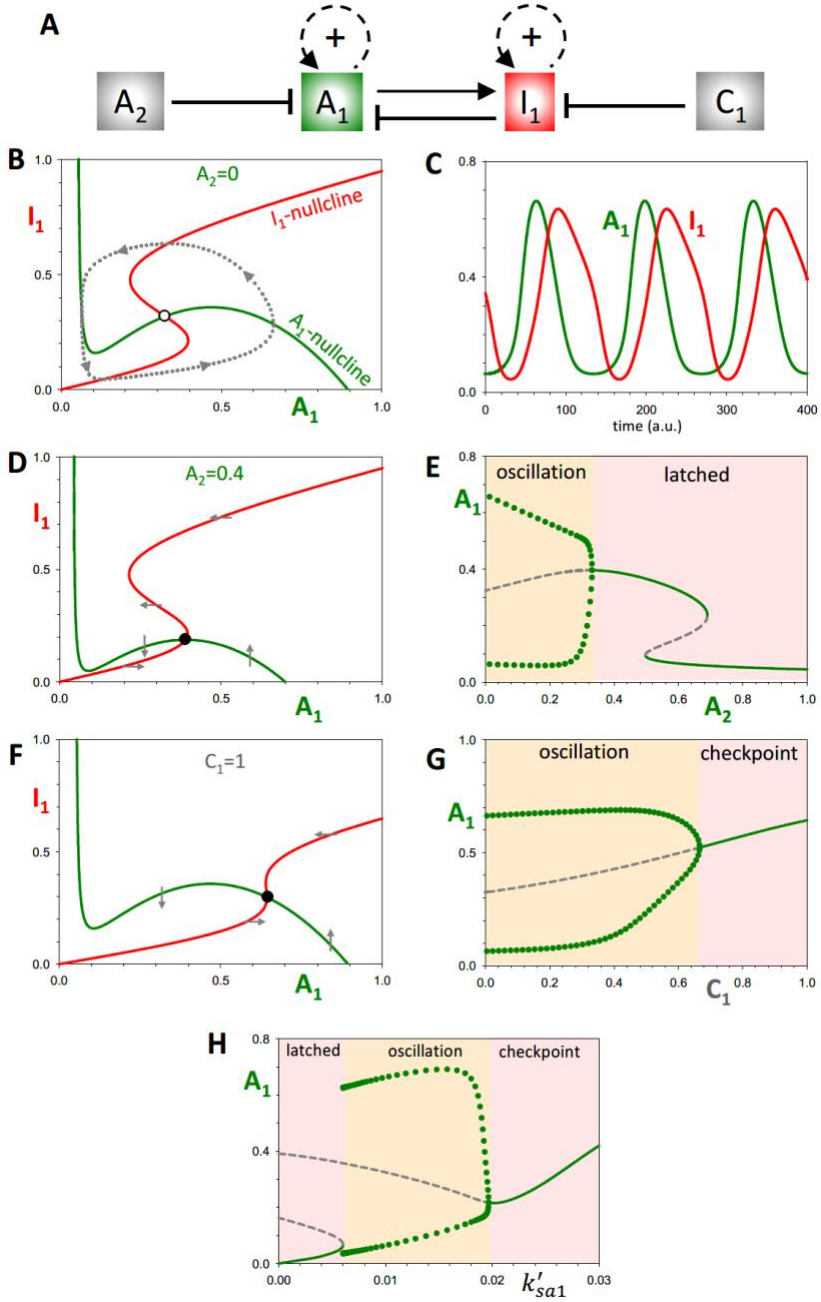

Figure S3.1: The dynamical properties of the single oscillator, Ω_1, with an alternative parameter set. **(A)** Influence diagram of the single oscillator network (identical to Fig. 3.4). **(B)** Phase plane of the *alternative* Ω_1 system in the basal oscillating state (see Fig2_FigS1.ode file). As in Fig. 3.4, there is a unique unstable steady state (on the saddles of the two nullclines), surrounded by a limit cycle oscillation. **(C)** Time course simulation. **(D)** Phase plane of the *alternative* Ω_1 system, when $A_2 = 0.4$. Notice that, as a result of the shift in the A_1 nullcline, the unstable steady state is converted to a stable steady state, on the lower stable branch of the Inhibitor nullcline and the upper stable branch of the Activator. **(E)** Bifurcation diagram of A_1 with respect to the latching parameter, A_2, showing that oscillations are generated at a Hopf bifurcation, as opposed to a SNIC (Fig. 3.4E). Notice this is similar to the response of the S-phase module to changing Cdk1:CycB activity (Fig. 3.2E). **(F)** Phase plane for the checkpoint arrested *alternative* Ω_1 system, assuming $C_1 = 1$. Observe that the shift in the I_1 nullcline has resulted in the oscillator unstable steady state being converted to a stable steady state, on the lower stable branch of I_1 and upper stable branch of A_1. **(G)** Bifurcation diagram of A_1 with respect to the checkpoint parameter, C_1, showing that oscillations are generated at a Hopf bifurcation. **(H)** Bifurcation diagram of A_1 with respect to the basal synthesis rate, k_{sa}'. The plot reveals that checkpoint triggering and latching are symmetric effects from the perspective of the *alternative* Ω_1.

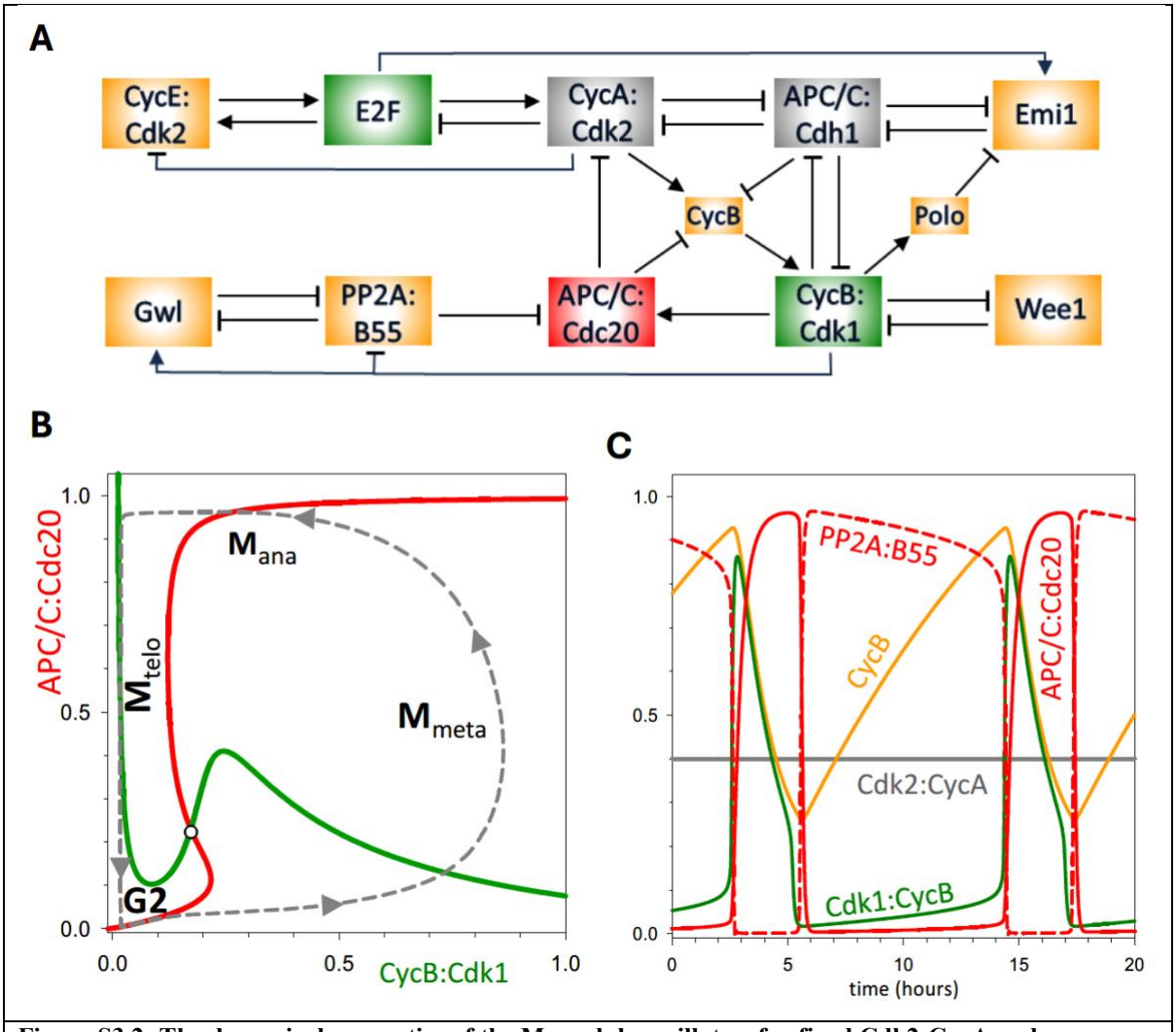

Figure S3.2: The dynamical properties of the M-module oscillator, for fixed Cdk2:CycA and APC/C:Cdh1 input. (A) Influence diagram of the system, highlighting the conversion of APC/C:Cdh1 and Cdk2:CycA from dynamical variables to parameters (grey boxes). **(B)** Phase plane plotting APC/C:Cdc20 against Cdk1:CycB, assuming Cdh1 = 0, CycA = 0.4, showing that the G2/M has intrinsic oscillatory activity in the absence of any dynamical input from the S-phase module. **(C)** The corresponding time course simulation.

Supplementary ode files

Fig2_FigS1.ode

```
# A model for doubly amplified negative feedback oscillator
# A1=Acfivator-1, I1=Inhibitor-1, A2=Acfivator-2
# Differential equations
dA1/dt = ksa' + ksa*A1^q/(La^q*(1 + r*I1) + A1^q) - (kda' + kda*A2)*A1
dI1/dt = ksi'*A1 + ksi*I1^p/(Li^p + I1^p) - (kdi' + kdi*C1)*I1
# Parameter values
p A2=0,C1=0,ksa'=0.015,ksa=0.185,kda'=0.2,kda=0.25,La^q=0.01,r=25,q=3
p ksi'=0.05,ksi=0.1,Li^p=0.07,kdi'=0.15,kdi=0.05,p=3
# parameter changes for Fig.S1: ksa'=0.01,ksa=0.19,kda=0.1,La^q=0.1,r=5,q=2
# Fig.3: the period of the oscillation is 154.8 min at A2=0 & ksa'=0.015
# XPPAUT settings
@ nmesh=400,TOTAL=1000,dt=0.5,METH=sfiff,XP=A1,YP=I1,XLO=0,XHI=1,YLO=0,YHI=1
@ NTST=150,NMAX=1000000,NPR=10000,DS=-0.01,BOUNDS=200
@ DSMAX=0.001,DSMIN=0.0001,PARMIN=-1,PARMAX=1,AUTOVAR=A1
@ AUTOXMIN=0,AUTOXMAX=0.5,AUTOYMIN=0,AUTOYMAX=1
done
```

Fig3B_Fig4.ode

```
# Two doubly amplified negative feedback oscillators with mutual inhibition
# A1=Acfivator-1, I1=Inhibitor-1, A2=Acfivator-2, I2=Inhibitor-2
# Differential equations
dA1/dt = ksa' + ksa*A1^q/(La^q*(1 + r*I1) + A1^q) - (kda' + kda1*A2)*A1
dI1/dt = ksi'*A1 + ksi*I1^p/(Li^p + I1^p) - (kdi' + kdi*C1)*I1
dA2/dt = ksa' + ksa*A2^q/(La^q*(1 + r*I2) + A2^q) - (kda' + kda*A1)*A2
dI2/dt = ksi'*A2 + ksi*I2^p/(Li^p + I2^p) - (kdi' + kdi*C2)*I2
# Parameter values
p kda1=0.25,C1=0,ksa'=0.015,ksa=0.185,kda'=0.2,kda=0.25,La^q=0.01,r=25,q=3
p ksi'=0.05,ksi=0.1,Li^p=0.07,kdi'=0.15,kdi=0.05,p=3,C2=0
# the period of the oscillation is 154.8 (at kda1=0) and 154.9 (at kda1=1)
# Initial conditions
init A1=1,I1=0,A2=0,I2=1
# XPPAUT settings
@ TOTAL=500,dt=0.5,METH=stiff,XLO=0,XHI=500,YLO=0,YHI=1
@ nplot=4,XP=t,YP1=A1,YP2=I1,YP3=A2,YP4=I2
@ NTST=150,NMAX=1000000,NPR=10000,DS=0.01,BOUNDS=200
@ DSMAX=0.001,DSMIN=0.0001,PARMIN=0,PARMAX=1,AUTOVAR=A1
@ AUTOXMIN=0,AUTOXMAX=1,AUTOYMIN=0,AUTOYMAX=1
done
```

Fig5_Fig8B.ode

```
# Figure 5 & Figure 8B
# Calculafion of pseudo-nullclines for
# two doubly amplified negafive feedback oscillators with mutual inhibifion
# A1=Acfivator-1, I1=Inhibitor-1, A2=Acfivator-2, I2=Inhibitor-2
# Differenfial equafions
dA1/dt = ksa' + ksa*A1^q/(La^q*(1 + r*I1) + A1^q) - (kda' + kda*A2)*A1
# dI1/dt = ksi'*A1 + ksi*I1^p/(Li^p + I1^p) - (kdi' + kdi*C1)*I1
dA2/dt = ksa' + ksa*A2^q/(La^q*(1 + r*I2) + A2^q) - (kda' + kda*A1)*A2
# dI2/dt = ksi'*A2 + ksi*I2^p/(Li^p + I2^p) - (kdi' + kdi*C2)*I2
# Parameter values
p I1=0,I2=0,ksa'=0.015,ksa=0.185,kda'=0.2,kda=0.25,La^q=0.01,r=25,q=3,C1=0
p ksi'=0.05,ksi=0.1,Li^p=0.07,kdi'=0.15,kdi=0.05,p=3,C2=0
# Inifial condifions
init A1=1, A2=0
# XPPAUT seftings
@ TOTAL=500,dt=0.5,METH=sfiff,XP=t,YP=A1
@ XLO=0,XHI=500,YLO=0,YHI=1
@ NTST=150,NMAX=1000000,NPR=10000,DS=0.001,BOUNDS=200
@ DSMAX=0.001,DSMIN=0.0001,PARMIN=-20,PARMAX=1,AUTOVAR=A1
@ AUTOXMIN=0,AUTOXMAX=1,AUTOYMIN=0,AUTOYMAX=1
done
```

Fig6.ode

```
# Model for the human cell cycle and endoreplicafion cycle
# Differenfial equafions
CycE' = kscyce' + kscyce"*E2F - (kdcyce' + kdcyce"*CycA)*CycE
CycA' = kscyca' + kscyca"*E2F - (kdcyca' + kdcyca"*Cdc20 + kdcyca*Cdh1)*CycA
E2FPt' = kpe2f*(CycA+eps*Cdk1)*(E2FT - E2FPt) - kdpe2f*E2FPt
Rb' = kdprb*(Rbt-Rb)/(Jrb+Rbt-Rb) - kprb*(CycE+CycA+eps*Cdk1)*Rb/(Jrb+Rb)
Emi1' = ksemi1' + ksemi1"*E2F - (kdemi1' + kdemi1"*Cdh1 + kdemi1*Polo)*Emi1
# CycB' = kscycb' + kscycb*CycA - Vdcycb*CycB
# Cdk1' = kscycb' + kscycb*CycA + V25*(CycB - Cdk1) - Vwee*Cdk1 - Vdcycb*Cdk1
Cdh1' = kacdh1*(Cdh1t-Cdh1) - (kicdh1'*CycE+kicdh1"*CycA+kicdh1*eps*Cdk1)*Cdh1
Cdc20' = kacdc20*eps*Cdk1*(1-Cdc20) - kicdc20*PP2AB55*Cdc20
PoloT' = kspolo' + kspolo*CycA - (kdpolo' + kdpolo"*Cdh1)*PoloT
Polo' = (kapolo'*CycA + kapolo"*eps*Cdk1)*(PoloT-Polo)/(Jpolo+PoloT-Polo)-kipolo*Polo/(Jpolo+Polo)
pENSAt' = kGwENSA*pGwl*(ENSAtot - pENSAt) - kcatB55*Complex
pGwl' = (kCdkGwl'*CycA+kCdkGwl*eps*Cdk1)*(Gwtot - pGwl) - (kppx' + kB55Gwl*PP2AB55)*pGwl
PP2AB55' = (kdiss + kcatB55)*Complex-kass*(pENSAt-Complex)*(B55tot-Complex)
# CycB represents the sum of inacfive and acfive Cdk1:CycB dimers, while Cdk1 refers to the acfive ones only
# Algebraic equafions
Rbt = Rbtot/(1 + alpha*SK)
BB2 = Rb + E2FT + Kdrbe2f
Comp2 = (BB2 - sqrt(BB2^2 - 4*Rb*E2FT))/2
E2F = (E2FT-E2FPt)*(E2FT-Comp2)/E2FT
BB1 = Emi1 + Cdh1tot + Kdc1e1
Comp1 = (BB1 - sqrt(BB1^2 - 4*Emi1*Cdh1tot))/2
Cdh1t = Cdh1tot - Comp1
YMEP = GK(kpyme'*CycA+kpyme*eps*Cdk1,kdpyme,Jyme,Jyme)
V25 = k25' + k25*YMEP
Vwee = kwee' + kwee*(1 - YMEP)
Vdcycb = kdcycb' + SAC*kdcycb"*Cdc20 + kdcycb*Cdh1
Complex = B55tot-PP2AB55
# Goldbeter-Koshland funcfion
```

```
GB(arg1,arg2,arg3,arg4) = arg2-arg1+arg2*arg3+arg1*arg4
GK(arg1,arg2,arg3,arg4) = 2*arg1*arg4/(GB(arg1,arg2,arg3,arg4)+sqrt(GB(arg1,arg2,arg3,arg4)^2-4*(arg2-
arg1)*arg1*arg4))
# Parameter values
p Cdk1=0, kscyce'=0, kscyce"=1.5, kdcyce'=0.6, kdcyce"=1.5
p kscyca'=0, kscyca"=0.45, kdcyca'=0.045, kdcyca"=0.75, kdcyca=3.75
p Rbtot=1.75, JRb=0.1, kprb=15, kdprb=10.5, alpha=1, SK=1
p E2FT=1, kdpe2f=0.3, kpe2f=1.5, Kdrbe2f=0.001
p ksemi1'=0, ksemi1"=1.5, kdemi1'=0.18, kdemi1"=3, kdemi1=7.5, Kdc1e1=0.0175
p Cdh1tot=1, kacdh1=15, kicdh1'=15, kicdh1"=30, kicdh1=6000
p kscycb'=0, kscycb=0.3, kdcycb'=0.06, kdcycb"=0.75, kdcycb=3.75
p kpyme'=0, kpyme=30, kdpyme=6, Jyme=0.1, k25'=0.45, k25=15, kwee'=0.15, kwee=15
p kicdc20=15, kacdc20=3, eps=1, SAC=1
p kspolo'=0.15, kspolo=0, kdpolo'=0.15, kdpolo"=15
p kapolo'=0, kapolo"=15, kipolo=7.5, Jpolo=0.01
p ENSAtot=4, B55tot=1, kass=7500, kdiss=4.5, kcatB55=15
p kGwENSA=15, kppx'=6, kCdkGwl'=0, kCdkGwl=30, kB55Gwl=60, Gwtot=1
### XppAut SETTINGS
@ Method=sfiff, Total=40, Bounds=100, Dt=0.5, tol=1e-5
@ nplot=4,XP=fime,YP=Rb,YP2=CycE,YP3=CycA,YP4=Cdh1,Xlo=0,Xhi=40,Ylo=0,Yhi=1
@ NTST=150,NMAX=1000000,NPR=10000,DS=-0.01,BOUNDS=200
@ DSMAX=0.01,DSMIN=0.001,PARMIN=0,PARMAX=2, AUTOVAR=CycA
@ AUTOXMIN=0,AUTOXMAX=0.1,AUTOYMIN=0,AUTOYMAX=1
done
```

Fig7_FigS2.ode

```
# Model for the human cell cycle and Cdc20-endocycle
# Differenfial equafions
CycE' = kscyce' + kscyce"*E2F - (kdcyce' + kdcyce"*CycA)*CycE
CycA' = kscyca' + kscyca"*E2F - (kdcyca' + kdcyca"*Cdc20 + kdcyca*Cdh1)*CycA
E2FPt' = kpe2f*(CycA+eps*Cdk1)*(E2FT - E2FPt) - kdpe2f*E2FPt
Rb' = kdprb*(Rbt-Rb)/(Jrb+Rbt-Rb) - kprb*(CycE+CycA+eps*Cdk1)*Rb/(Jrb+Rb)
Emi1' = ksemi1' + ksemi1"*E2F - (kdemi1' + kdemi1"*Cdh1 + kdemi1*Polo)*Emi1
CycB' = kscycb' + kscycb*CycA - Vdcycb*CycB
Cdk1' = kscycb' + kscycb*CycA + V25*(CycB - Cdk1) - Vwee*Cdk1 - Vdcycb*Cdk1
# Cdh1' = kacdh1*(Cdh1t-Cdh1) - (kicdh1'*CycE+kicdh1"*CycA+kicdh1*eps*Cdk1)*Cdh1
Cdc20' = kacdc20*eps*Cdk1*(1-Cdc20) - kicdc20*PP2AB55*Cdc20
PoloT' = kspolo' + kspolo*CycA - (kdpolo' + kdpolo"*Cdh1)*PoloT
Polo' = (kapolo'*CycA + kapolo"*eps*Cdk1)*(PoloT-Polo)/(Jpolo+PoloT-Polo)-kipolo*Polo/(Jpolo+Polo)
pENSAt' = kGwENSA*pGwl*(ENSAtot - pENSAt) - kcatB55*Complex
pGwl' = (kCdkGwl'*CycA+kCdkGwl*eps*Cdk1)*(Gwtot - pGwl) - (kppx' + kB55Gwl*PP2AB55)*pGwl
PP2AB55' = (kdiss + kcatB55)*Complex-kass*(pENSAt-Complex)*(B55tot-Complex)
# CycB represents the sum of inacfive and acfive Cdk1:CycB dimers, while Cdk1 refers to the acfive ones only
# Algebraic equafions
Rbt = Rbtot/(1 + alpha*SK)
BB2 = Rb + E2FT + Kdrbe2f
Comp2 = (BB2 - sqrt(BB2^2 - 4*Rb*E2FT))/2
E2F = (E2FT-E2FPt)*(E2FT-Comp2)/E2FT
BB1 = Emi1 + Cdh1tot + Kdc1e1
Comp1 = (BB1 - sqrt(BB1^2 - 4*Emi1*Cdh1tot))/2
Cdh1t = Cdh1tot - Comp1
YMEP = GK(kpyme'*CycA+kpyme*eps*Cdk1,kdpyme,Jyme,Jyme)
V25 = k25' + k25*YMEP
Vwee = kwee' + kwee*(1 - YMEP)
Vdcycb = kdcycb' + SAC*kdcycb"*Cdc20 + kdcycb*Cdh1
Complex = B55tot-PP2AB55
# Goldbeter-Koshland funcfion
GB(arg1,arg2,arg3,arg4) = arg2-arg1+arg2*arg3+arg1*arg4
GK(arg1,arg2,arg3,arg4) = 2*arg1*arg4/(GB(arg1,arg2,arg3,arg4)+sqrt(GB(arg1,arg2,arg3,arg4)^2-4*(arg2-
arg1)*arg1*arg4))
# Parameter values
```

```
p Cdh1=0, kscyce'=0, kscyce"=1.5, kdcyce'=0.6, kdcyce"=1.5
p kscyca'=0, kscyca"=0.45, kdcyca'=0.045, kdcyca"=0.75, kdcyca=3.75
p Rbtot=1.75, JRb=0.1, kprb=15, kdprb=10.5, alpha=1, SK=1
p E2FT=1, kdpe2f=0.3, kpe2f=1.5, Kdrbe2f=0.001
p ksemi1'=0, ksemi1"=1.5, kdemi1'=0.18, kdemi1"=3, kdemi1=7.5, Kdc1e1=0.0175
p Cdh1tot=1, kacdh1=15, kicdh1'=15, kicdh1"=30, kicdh1=6000
p kscycb'=0, kscycb=0.3, kdcycb'=0.06, kdcycb"=0.75, kdcycb=3.75
p kpyme'=0, kpyme=30, kdpyme=6, Jyme=0.1, k25'=0.45, k25=15, kwee'=0.15, kwee=15
p kicdc20=15, kacdc20=3, eps=1, SAC=1
p kspolo'=0.15, kspolo=0, kdpolo'=0.15, kdpolo"=15
p kapolo'=0, kapolo"=15, kipolo=7.5, Jpolo=0.01
p ENSAtot=4, B55tot=1, kass=7500, kdiss=4.5, kcatB55=15
p kGwENSA=15, kppx'=6, kCdkGwl'=0, kCdkGwl=30, kB55Gwl=60, Gwtot=1
### XppAut SETTINGS
@ Method=sfiff,Total=25,Bounds=100,Dt=0.1,tol=1e-5,Xplot=fime,YPlot=Cdk1,Xlo=0,Xhi=25,Ylo=0,Yhi=1
@ NTST=150,NMAX=1000000,NPR=10000,DS=0.01,BOUNDS=200
@ DSMAX=0.01,DSMIN=0.001,PARMIN=-1,PARMAX=1, AUTOVAR=Cdk1
@ AUTOXMIN=0,AUTOXMAX=0.05,AUTOYMIN=0,AUTOYMAX=1
done
```

Appendix 3: Supplementary material for Chapter 4

Table 4.1 – Numerical values of parameters in the two pseudo-oscillator model

A kinetic constants	ksa=0, ksa'=0.1, ksa"=2, kda=0, kda'=0.1, kda"=2
A regulatory parameters	Atot=1, o=2, Jab=0.5
B/B' steady state	Btot=B'tot=1, JB=0.5, l=6
Nondegradable B/B'	ndb = ndb' = 0 (but changed as needed)
Helper molecule (C/C') kinetic const.	ksc=kscp=0, ksc'= kscp'=7.5, kdc=kdcp=0.5
Helper molecule regulatory param.	JC=0.65, n=40
Delay molecule (D/D') kinetic const.	ksd=ksd'=0.01, kdd=kdd'=0.01

Table 4.2 – Numerical values of parameters in the four pseudo-oscillator model

A kinetic constants	ksa=1, kda=1, ksa'=0.01, kda'=0.01
A auto-catalytic function parameters	jsA=0.5, jdA=0.5, jA'=0.5, p=8
B kinetic constants	ksb=1, kdb=1, ksb'=0.01, kdb'=0.01
B auto-catalytic function parameters	jsB=0.5, jdB=0.5, jB'=0.5, q=8
Helper kinetic constants	ksh=0.5, kdh=0.5, ksh'=0.005, kdh'=0.005
Helper auto-catalytic function param.	jsH=0.8, jdH=0.35, jH'=0.5, jH"=0.5, r=8
Switch Helper-dependent regulation	ksah=0.5
Checkpoint parameters	c1=0 (variable), kdh=0.01

The two delay pseudo-oscillator model

```
dA/dt = (ksa + ksa'*Cp + ksa"*B^o/(JAB^o + B^o))*(Atot-A) - (kda + kda'*C +
kda"*Bp^o/(JAB^o + Bp^o))*A
dC/dt = ksc + ksc'*D^n/(JC^n+D^n) - kdc*C
dCp/dt = kscp + kscp'*Dp^n/(JC^n+Dp^n) - kdcp*Cp
dD/dt = ksd*B - kdd*D
dDp/dt = ksd'*Bp - kdd'*Dp

Bp = ndB' + B'tot*JB^l/(JB^l + A^l)
B = ndB + Btot*A^l/(JB^l + A^l)
Aux Bp = ndB' + B'tot*JB^l/(JB^l + A^l)
Aux B = ndB + Btot*A^l/(JB^l + A^l)

p ksa=0, ksa'=0.1, ksa"=2, kda=0, kda'=0.1, kda"=2
p Atot=1, o=2, JAB=0.5
p ksc=0, ksc'=7.5, kdc=0.5, JC=0.65, n=40
p kscp=0, kscp'=7.5, kdcp=0.5
p ksd=0.01, kdd=0.01
p ksd'=0.01, kdd'=0.01
p ndB=0, Btot=1, JB=0.5, l=6
p ndB'=0, B'tot=1

# XPP settings
@ METH=stiff, XLO=0, XHI=40, YLO=0, YHI=1, NMESH=400, total=400, dt=0.1
@ XP=t, YP=A
@ NTST=150,NMAX=1000000,NPR=10000,DS=-0.001,BOUNDS=200
@ DSMAX=0.001,DSMIN=0.0001,PARMIN=-0.1,PARMAX=1, AUTOVAR=A
@ AUTOXMIN=0,AUTOXMAX=1,AUTOYMIN=0,AUTOYMAX=1
done
```

The four pseudo-oscillator model

```
#ksa moves on threshold, ksa' moves off threshold

dA/dt = (ksa*A^p/((jsA + jA'*B + ksah1*H3)^p + A^p) + ksa')*(1-A) - (kda*(1-A)^p/((jdA + jA'*(1-B) + ksah1*H1)^p + (1-A)^p) + kda')*A
dB/dt = (ksb*B^q/((jsB + jB'*(1-A) + ksah1*H4)^q + B^q) + ksb')*(1-B) - (kdb*(1-B)^q/((jdB + jB'*A  + ksah1*H2)^q + (1-B)^q) + kdb')*B

dH1/dt = (ksh1*H1^r/((jsH1 + jH1'*A + jH1"*B)^r + H1^r) + ksh1')*(1-H1) - (kdh1*(1-H1)^r/((jdH1 + jH1'*(1-A) + jH1"*(1-B))^r + (1-H1)^r) + kdh1' + kdh1c1*C1)*H1
dH2/dt = (ksh1*H2^r/((jsH1 + jH1'*(1-A) + jH1"*B)^r + H2^r) + ksh1')*(1-H2) - (kdh1*(1-H2)^r/((jdH1 + jH1'*A + jH1"*(1-B))^r + (1-H2)^r) + kdh1')*H2
dH3/dt = (ksh1*H3^r/((jsH1 + jH1'*(1-A) + jH1"*(1-B))^r + H3^r) + ksh1')*(1-H3) - (kdh1*(1-H3)^r/((jdH1 + jH1'*A + jH1"*B)^r + (1-H3)^r) + kdh1')*H3
dH4/dt = (ksh1*H4^r/((jsH1 + jH1'*A + jH1"*(1-B))^r + H4^r) + ksh1')*(1-H4) - (kdh1*(1-H4)^r/((jdH1 + jH1'*(1-A) + jH1"*B)^r + (1-H4)^r) + kdh1')*H4

p c1=0, kdh1c1=0.01

p ksa=1, kda=1, ksa'=0.01, kda'=0.01, jsA=0.5, jdA=0.5, jA'=0.5, p=8
p ksb=1, kdb=1, ksb'=0.01, kdb'=0.01, jsB=0.5, jdB=0.5, jB'=0.5, q=8

p ksah1=0.5

p ksh1=0.5, kdh1=0.5, ksh1'=0.005, kdh1'=0.005, jsH1=0.8, jdH1=0.35, jH1'=0.5, jH1"=0.5, r=8


### XppAut SETTINGS
@ nmesh=400, TOTAL=10000, dt=0.5, METH=stiff
@ XP=b, YP=a, XLO=-0.5, XHI=1.5, YLO=-0.5, YHI=1.5
@ NTST=1500,NMAX=1000000,NPR=100000,DS=-0.01,BOUNDS=200
@ DSMAX=0.01,DSMIN=0.001,PARMIN=-2,PARMAX=1, AUTOVAR=x1
@ AUTOXMIN=0,AUTOXMAX=1,AUTOYMIN=0,AUTOYMAX=1
done
```

Supplementary figures

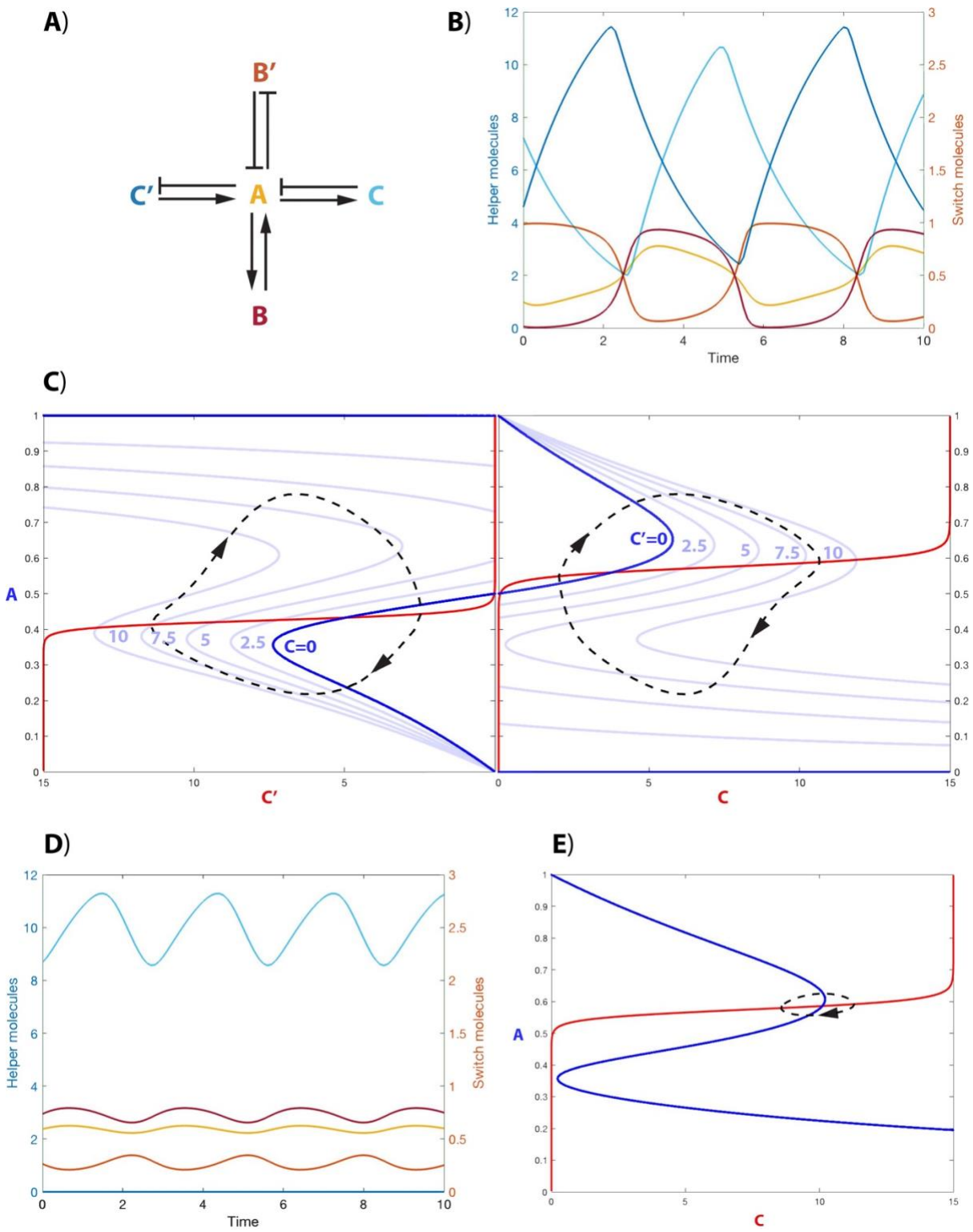

Fig. S4.1 – The dynamics of the minimal latching gate system without delay – (A) influence diagram (B) Time course simulation of the oscillator. Note that the curves' colour coding matches panel A. 'Helper molecules' refers to C and C'; 'Switch molecules' refers to A, B and B'. (C) The AC and AC' pseudo phase planes of the system. The black dashed line is the projection of the integrated solution on the AC and AC' planes. The integrated solution does not follow the calculated steady states (bark

blue and red) because it is not true that the C and C' are mutually exclusive. Pseudo nullclines are plotted for different values of C and C' on the AC' and AC planes (light blue), respectively, to provide a better sense of how movement on these planes is determined. (D) C endocycle time course, for ksa=0.75. Notice that without delay in C accumulation, the amplitude of the endocycle is minimal. (E) AC pseudo phase plane, for ksa=0.75

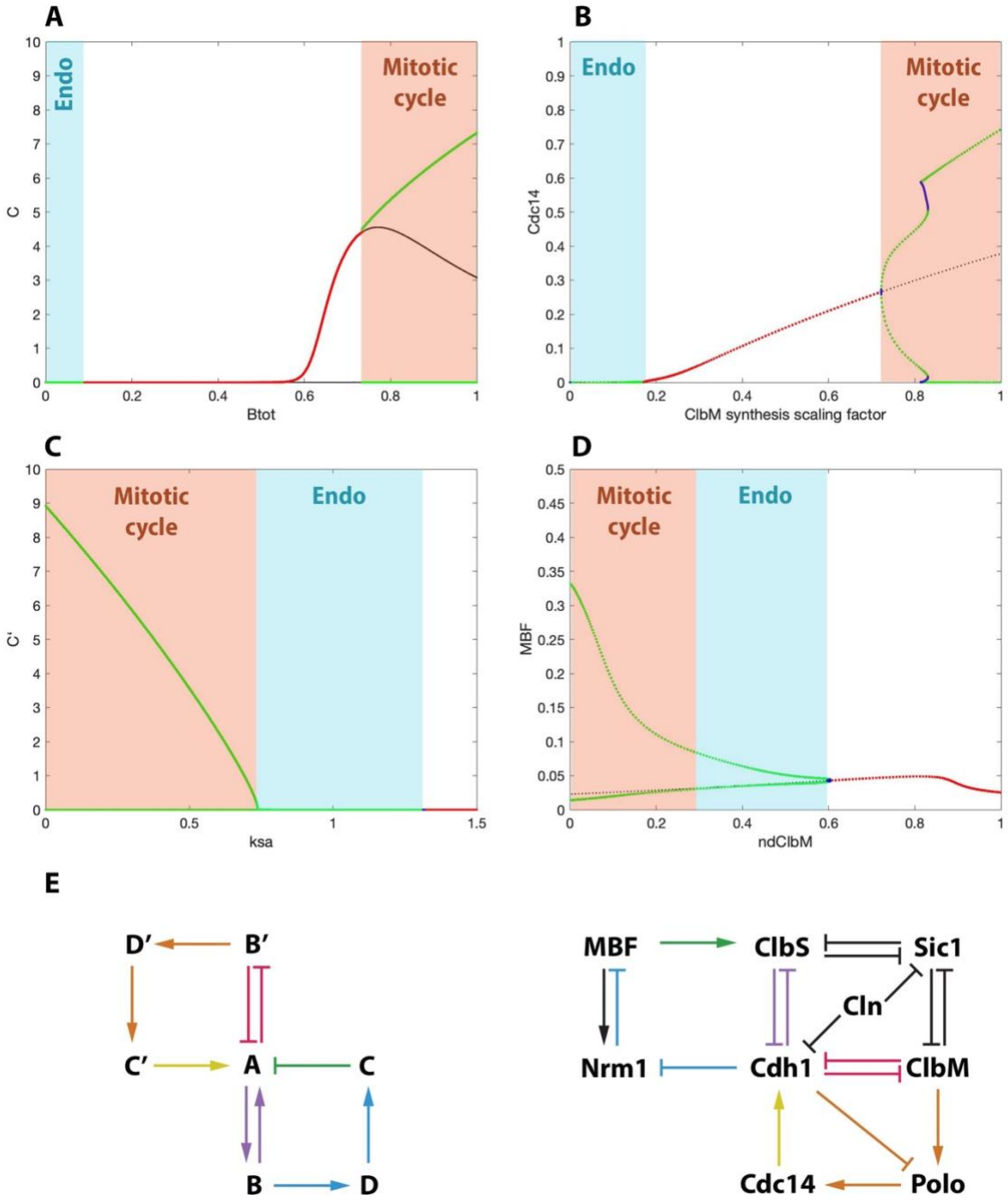

Fig. S4.2 – The basis of the transition to endocycles and the comparison of the minimal and *S. cerevisiae* models – Bifurcation diagrams for the delay mixed negative feedback oscillator showing (A) C with respect to Btot, (C) C' with respect to ksa, and for the budding yeast model showing (B) Cdc14 vs the rate of ClbM synthesis rate, as a percentage of the basal and auto-stimulated expression rate constants, and (D) MBF vs the concentration of nondegradable ClbM. (E) Comparison of the minimal and yeast network connectivity, showing the former is embedded in the latter.

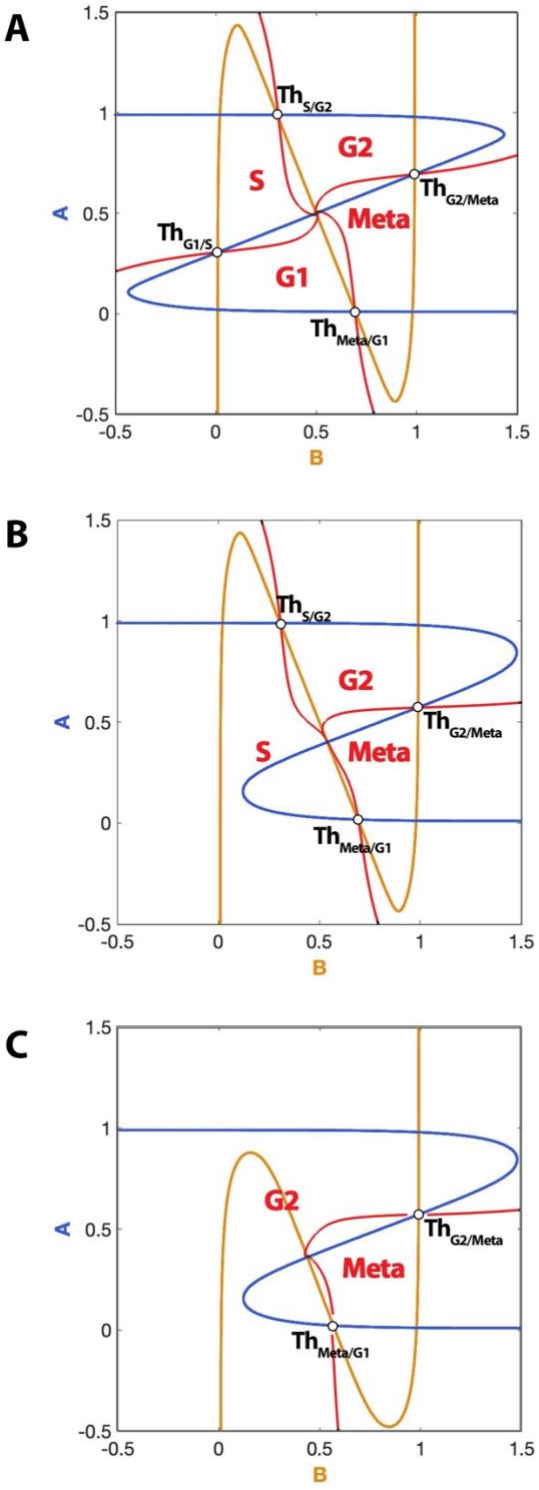

Fig. S4.3 – The basins of attraction of the stable steady states in the core model – The boundaries of the basins of attraction are drawn is red for (A) the basal system, (B) the system perturbed with *jdA*=0.8 (G1 suppressed) and (C) the system perturbed with *jdA=jdB*=0.8 (G1 and S suppressed)